Analysis of metabolic feedbacks regulating c-MYC

Inaugural-Dissertation
to obtain the academic degree
Doctor rerum naturalium (Dr. rer. nat.)

submitted to the Department of Biology, Chemistry and Pharmacy
of Freie Universität Berlin

by

Dipl.-Ing. Nadine Royla
from Leipzig

2018

Diese Arbeit wurde unter Anleitung von Dr. Stefan Kempa am Max-Delbrück-Center für Molekulare Medizin zwischen Februar 2014 und 2018 angefertigt. Das Forschungsprojekt wurde in enger Kooperation mit Francesca Romana Dejure und ihrem Betreuer Prof. Dr. Martin Eilers von der Julius-Maximilian Universität Würzburg bearbeitet.

1. Gutachter: Dr. Stefan Kempa
2. Gutachterin: Prof. Dr. Petra Knaus

Datum der Disputation: 22.05.2018

Acknowledgments

After an intensive period of four years, today is the day – this note of thanks will complete my journey as a PhD student.

I would like to thank the entire Kempa Lab for being such a great team to work with. Everyone of you has contributed to this dissertation in one or the other way. More important is the fact that all of you made me really like to come to work every single day independently of my motivation or frustration level. Thank you for that!
I would like to acknowledge my supervisor Dr. Stefan Kempa – for the opportunity to work in his lab, for his guidance and support throughout the project and for teaching me more than once that data interpretation is a process that requires time and bit of meditation. Additionally, I would like to thank Christin Zasada for sharing her data analysis, experimental and cooking skills as well as for her company during late night shifts and weekend working days. I also would like to acknowledge Guido Mastrobuoni for finally setting up the nucleotide method with me; after we found no further reasons to postpone it. I further like to thank Jenny and Alina for supporting me on the benchside in stressful times and for preparing the most beautiful western blots.

Furthermore, I would like to acknowledge my cooperation partners for contributing with experimental expertise, know-how and fruitful comments. I especially thank Francesca Romana Dejure and Prof. Dr. Martin Eilers for the great collaboration on the project. I would like to acknowledge Christine Kocks and Anastasiya Boltengagen for helping me with the smFISH experiments, as well as Raphaela Fritsche for providing her expertise on the Bio-Plex system.

I would also like to express my thanks to Prof. Dr. Petra Knaus for final discussions and supervision. Furthermore, I would like to thank all the diligent thesis readers. Without you - Christin, Martin, Birte, Guido, Henning, Tobias and Fardad - this thesis would contain many more typos and commas as well as terribly long sentences.

Abschließend möchte ich ein großes Dankeschön an meine Familie richten. Ihr lehrtet mich, das Leben nie ganz zu ernst zunehmen und dennoch in den wichtigen Momenten mit der richtigen Ernsthaftigkeit zu handeln. Dafür und für eure stetige Untersützung in allen Lebenslagen danke ich euch.

Rule no. 2. MYC Does Everything.

William P. Tansey

Summary

The *c-MYC* (*MYC*) proto-oncogene is frequently activated in human cancer. Deregulated expression of MYC induces transcriptional imbalance, thereby driving a constitutive cell growth program that renders cancer cells dependent on the non-essential amino acid glutamine for survival, inducing 'glutamine addiction'.

The thesis focused on MYC's role as a nexus in metabolic re-programming by addressing the concept of glutamine addiction. We analyzed how limitations on external glutamine supply control MYC protein expression and thereby affecting MYC as a major regulator of cell growth, metabolism and apoptosis. Extensive time-resolved studies examining MYC regulation at various omics levels by the application of molecular biological, biochemical and mass spectrometry-based approaches allowed us to add another layer of information to MYC's complex regulatory network.

Contrary to MYC's known function to regulate glutamine metabolism, we revealed MYC protein expression to be controlled by glutamine availability as a feedback mechanism in various cancer cell lines. We showed that the suppression of MYC protein expression in the absence of glutamine is mediated by its 3'-untranslated region (3'-UTR), which senses glutamine-dependent changes in adenosine nucleotide levels. The metabolic feedback protects cells from lethal glutamine addiction, while the activation of ectopic MYC in the absence of glutamine causes RNA polymerase II stalling and induces MYC-driven apoptosis. The concept of glutamine addiction has been described in experimental systems, that are predominantly based on the use of MYC transgenes, which usually lack the regulatory regions of the mRNA. Thus, this study underscores the need to include regulatory sequences into transgenes in *in vivo* and *in vitro* studies.

We provided evidence that the MYC feedback is regulated at the post-transcriptional level, but is unlikely mediated by mRNA re-localization or mRNA decay via microRNAs. We identified several *MYC* 3'-UTR binding proteins as possible mediators. The most promising are currently evaluated for their role in the glutamine-mediated MYC regulation by siRNA screen.

We speculated that the transcriptional stress caused by a disruption of the 3'-UTR-mediated feedback might sensitize MYC-driven tumors to pro-apoptotic therapies. However, we found evidence that the inhibition of glutaminase, a common therapeutic approach to starve glutamine-addicted tumors, cannot suppress MYC protein expression. Accordingly, glutaminase inhibition might not be a suitable tool for novel combinatorial treatments, that induce synthetic lethality on the principle of glutamine addiction.

We suppose that glutamine-utilizing transaminases might compensate for the inhibition of glutaminase. The majority of glutamine-converting transaminases are essential for *de novo* nucleotide biosynthesis. This bilateral function of transaminases might account for the double-sided MYC regulation via glutamine and adenosine-derived nucleotides.

Zusammenfassung

Die Deregulierung des Onkogens *c-MYC* (*MYC*) trägt maßgeblich zur Entstehung einer Vielzahl humaner Tumore bei. Onkogenes MYC bedingt die Umstrukturierung metabolischer Prozesse und schafft somit die Voraussetzungen für ein unkontrolliertes Zellwachstum. In Folge dieser Umstrukturierung benötigen Krebszellen Glutamin, eine nicht-essentielle Aminosäure, um fortan zu überleben.

Ziel dieser Arbeit war es, die Rolle des Transkriptionsfaktors MYC in der metabolischen Umprogrammierung, die zur sogenannten Glutaminabhängigkeit führt, zu charakterisieren. Im Rahmen dieser Aufgabestellung untersuchten wir mittels zeitaufgelöster Studien, basierend auf der Kombination molekularbiologischer, biochemischer und massenspektrometrischer Methoden, wie sich der Entzug von Glutamin auf die Regulation von MYC auswirkt.

Die erzielten Ergebnisse zeigen, dass endogene MYC Proteinlevel durch die Verfügbarkeit von Glutamin reguliert werden. Wir beobachteten, dass die 3'-untranslatierte Region (3'-UTR) der *MYC* mRNA essentiell für die glutaminvermittelte Regulierung ist. Weiterhin zeigten wir, dass glutaminbedingte Veränderungen in Adenosinnukleotidleveln von der *MYC* 3'-UTR wahrgenommen werden. Dieser metabolische Kontrollmechanismus schützt Krebszellen unter Glutaminmangel vor MYC-induzierter Apoptose durch Hemmung der MYC Proteinexpression. Wir postulieren, dass dieser Mechanismus Probleme der Transkription bei niedrigen Nukleotidspiegeln verhindert, nachweisbar durch einen globalen Transkriptionsstopp auf Grund fehlender Rekrutierung der RNA Polymerase II. Die induzierte exogene MYC Expression unter Glutaminmangel hebt diese Blockade auf und führt zu MYC-induziertem Zelltod.

Der metabolische Feedback-Mechanismus wurde bislang übersehen, da Untersuchungen zur Glutaminabhängigkeit zumeist auf dem Einsatz von *MYC* Transgenen basieren, die die 3'-UTR nicht beinhalten. Demnach sollten regulatorische Regionen zukünftig bei der Gestaltung von Transgenen berücksichtigt werden.

Wir fanden Hinweise darauf, dass der glutaminabhängige MYC Kontrollmechanismus post-translational reguliert wird, jedoch weitestgehend unabhängig vom Abbau oder der Translokalisation der *MYC* mRNA stattfindet. Derzeitig werden die von uns identifizierten *MYC* 3'-UTR bindenden Proteine mittels eines siRNA Screens auf ihre mögliche Beteiligung evaluiert.

Wir vermuten, dass eine kombinierte therapeutisch induzierte Störung des Kontrollmechanismus und der Glutaminverstoffwechslung zu transkiptionellem Stress führt, welcher Krebszellen – basierend auf dem Konzept der Glutaminabhängigkeit – in die MYC-induzierte Apoptose treibt. Unter dieser Annahme untersuchten wir die MYC Proteinexpression in Abhängigkeit von Glutaminaseinhibitoren, konnten jedoch keine Beeinträchtigung feststellen. Wir postulieren, dass glutamineverstoffwechselnde Transaminasen wesentlich zu dieser Beobachtung beitragen. Viele dieser Transaminasen sind essentiell für den Nukleotidstoffwechsel und bedingen so möglicherweise MYCs bilaterale Regulation durch Glutamin und Adenosin.

Contents

List of Figures

List of Tables

List of Abbreviations

General abbreviations

2',5'-dd-Ado	2',5'-dideoxy adenosine
AREs	Adenosine/uridine (AU)-rich elements
AUBPs	ARE binding proteins
bHLHZip	Basic region/helix-loop-helix/leucine zipper
BPTES	Bis-2-(5-phenylacetamido-1,3,4-thiadiazol-2-yl)ethyl sulfide
BSA	Bovine serum albumin
C968	Compound 968
CCM	Central carbon metabolism
cDNA	Complementary DNA
CDR	Coding region instability determinant
CDS	Coding sequence
C_t	Threshold cycle value
DMαKG	Dimethyl α-ketoglutarate
DMEM	Dulbeccos modified eagle medium
DMFum	Dimethyl fumarate
DMMal	Dimethyl malate
DMSuc	Dimethyl succinate
DON	6-Diazo-5-oxo-L-norleucine
Dox	Doxycycline
DTT	Dithiothreitol
E-boxes	Enhancer boxes
EDTA	Ethylenediaminetetraacetic acid
ELISA	Enzyme-linked immunosorbant assays
ER	Estrogen receptor
ESI	Electrospray ionization
ETC	Electron transport chain
EV	Empty vector
FBS	Fetal bovine serum
GC	Gas chromatography
HRP	Horseradish peroxidase
IRES	Internal ribosome entry site
LC	Liquid chromatography
mESC	Mouse embryonic stem cells
MIF	Mass isotopic fingerprints
miRNA	MicroRNAs
mRNA	Messenger RNA
mRNPs	Messenger ribonucleoprotein complexes
MS	Mass spectrometry
MYC	c-MYC
NAC	N-acetyl cysteine
OHT	4-Hydroxytamoxifen
OXPHOS	Oxidative phosphorylation
PBS	Phosphate buffered saline
PCR	Polymerase chain reaction
PKAi	PKAi, 14-22 Amide
PMSF	Phenylmethylsulfonyl fluoride

Enzymes

GLUT	Glucose transporter
GMPS	Guanosine monophosphate synthetase
GOT	Oxaloacetate transaminase
GPT	Glutamate pyruvate transaminase
GS	Glutathione synthetase
GSK-3β	Glycogen synthase kinase 3β
HAT	Histone acetyltransferase
HK2	Hexokinase 2
HuR	Human antigen R
HuR-CP1	HuR cleavage product
Ig	Immunoglobin
IMPDH2	Inosine-5'-monophosphate dehydrogenase 2
LDHA	Lactate dehydrogenase A
MAPK	Mitogen-activated protein kinase
MDH2	Malate dehydrogenase 2
mTORC	mTOR complex
NADSYN	NAD synthetase
NME1	Nucleoside diphosphate kinase A
NQO1	NAD(P)H dehydrogenase 1
PAICS	Phosphoribosylaminoimidazole carboxylase
PGD	Phosphogluconate dehydrogenase
PGK1	Phosphoglycerate kinase 1
PHGDH	Phosphoglycerate dehydrogenase
PK	Pyruvate kinase
PKA	Protein kinase A
PKFM	Phosphofructokinase
PKM	Pyruvate kinase M
PP1CB	Serine/threonine-protein phosphatase
PPAT	Phosphoribosyl pyrophosphate amidotransferase
PRPS2	Phosphoribosyl pyrophosphate synthetase 2
PSAT	Phosphoserine aminotransferase
RNAPII	RNA polymerase II
RRM2	Ribonucleoside-diphosphate reductase
SCD	Stearoyl-CoA desaturase
SCF	Skp, Cullin, F-box containing complex
SHMT2	Serine hydroxymethyltransferase
TCF/LEF	T-cell factor/lymphoid enhancer factor
TIAR	TIA-1 related protein
TKT	Transketolase
TPI1	Triosephosphate isomerase
TS	Thymidylate synthase
TTP	Tristetraprolin

Metabolites

αKG	α-Ketoglutarate
Acetyl-CoA	Acetyl coenzyme A
Adenylosuc	Adenylosuccinate
Ado	Adenosine
AICAR	5-Aminoimidazole-4-carboxamide ribonucleotide
AIR	5-Aminoimidazole ribonucleotide
Ala	Alanine
Asn	Asparagine
Asp	Aspartate
CAIR	4-carboxy-5-aminoimidazole ribonucleotide
cAMP	Cyclic AMP
Cit	Citrate

Cys .... Cysteine
Cyt .... Cytidine
DHAP .... Dihydroxyacetone phosphate
E .... Glutamate
F6P .... Fructose 6-phosphate
FAICAR .... N-Formylaminoimidazole 4-carboxamide ribonucleotide
FGAM .... Formylglycineamidine ribonucleotide
FGAR .... Formylglycineamide ribonucleotide
Fum .... Fumarate
GAR .... Glycineamide ribonucleotide
Glc .... Glucose
GlcN6P .... Glucosamine 6-phosphate
Gln .... Glutamine
Glu .... Glutamate
Guo .... Guanosine
IMP .... Inosine monophosphate
Lac .... Lactate
Mal .... Malate
NaAD .... Nicotinic acid adenine dinucleotide
OAA .... Oxaloacetate
OMP .... Orotidine 5-monophosphate
PRPP .... Phosphoribosyl pyrophosphate
Pyr .... Pyruvate
Q .... Glutamine
SAICAR .... N-succinylo-5-aminoimidazole-4-carboxamide ribonucleotide
Suc .... Succinate
Thd .... Thymidine
Urd .... Uridine
XMP .... Xanthosine monophosphate

1. Introduction

1.1. Systems biology in cancer research

Cancer is a complex disease. In 2000 Hannahan and Weinberg specified the complexity by defining the six hallmarks of cancer - resisting cell death, sustaining proliferative signaling, evading growth suppressors, activating invasion and metastasis, inducing angiogenisis and enabling replicative immortality [Hanahan and Weinberg, 2000]. Eleven years later they expanded their concept by adding the features of avoiding immune destruction, deregulating cellular energetics, genome instability, and mutation- and tumor-promoting inflammation [Hanahan and Weinberg, 2011]. It became clear that the tumor cell has to be considered an interactive network of biological functions.

Cells randomly acquire mutations throughout life. These mutations can be either selective neutral or beneficial as they confer cell growth and survival advantages [Martincorena et al., 2017]. Cancer develops as a consequence of clonal selection for cells that have sequentially accumulated advantageous mutations, so called driver mutations. A typical tumor exhibits two to eight driver mutations, while the selective neutral mutations, termed passenger mutations, occur more frequently [Vogelstein et al., 2013]. Each small genetic alteration has extensive effects on the molecular characteristic of a cell by affecting levels of DNA, RNA, proteins and metabolites [Werner et al., 2014]. Considering the multitude of mutations that occur in a tumor cell, cancer is a complex adaptive system with emerging properties at various levels that cause multivariate dysregulations within the molecular network [Kreeger and Lauffenburger, 2009]. Thus, cancer systems biology aims to understand the complexity of the disease via the combination of empirical, mathematical and computational tools that enable the integrative analysis of networks [Werner et al., 2014].

1.1.1. Impact of metabolism on different omics layers

Traditionally, cancer studies focused on the examination of individual mutations with a distinct phenotype as guided by the central dogma of molecular biology [Crick, 1970]. The concept implies the unidirectional flow of information from genes to proteins via transcripts. The linear logic was questioned by the discovery that proteins and metabolites, the functional units subsequent of the dogma, can loop back and regulate transcriptional as well as translational processes (*figure* 1.1A) [Buescher and Driggers, 2016].

On the one hand, metabolism provides building blocks in form of nucleotides and amino acids to build up DNA, RNA and proteins. These processes are highly energy-consuming and thereby once more dependent on metabolism, which assures the sufficient supply of energy carriers such as ATP and GTP. On the other hand, metabolites allosterically control the activity of enzymes that act on distinct regulatory levels [Buescher and Driggers, 2016]. For example, the activity of the 5' adenosine monophosphate-activated protein kinase (AMPK) is dependent on the competitive binding of the metabolites AMP and ATP [Wegner et al., 2015]. In case the cellular energy state is low, AMP binds to the regulatory domain of AMPK, which leads to a conformational change of the protein resulting in its phosphorylation and thereby activation. The dominant presence of ATP reverts the conformational change and dephosphorylates the kinase leading to its inactivation [Wegner et al., 2015].

Furthermore, the translation of messenger RNA (mRNA) is regulated by metabolites. The RNA binding protein Musashi-1 is known to be allosterically inhibited by unsaturated fatty acids that eventually results in the transcriptional inhibition of stearoyl-CoA desaturase, a fatty acid desaturase [Wegner et al., 2015]. Moreover, it was reported that metabolite-sensing RNA elements, namely riboswitches, regulate the gene expression in bacteria, algae, fungi and higher plants [Garst et al., 2011]. In the presence of a metabolic ligand riboswitches form alternative secondary structures that interfere with the transcriptional and/or translational machinery.

The transcriptional control via metabolites is either achieved by allosteric inhibition of transcription factors, e.g., inhibition of carbohydrate-responsive element-binding protein by xylulose 5-phosphate, or by chromatin remodeling [Wegner et al., 2015]. Wellen et al. [2009] provided evidence that histone acetylation is dependent on the enzyme ATP citrate lyase (ACLY) that catalyzes the conversion of citrate into acetyl coenzyme A (acetyl-
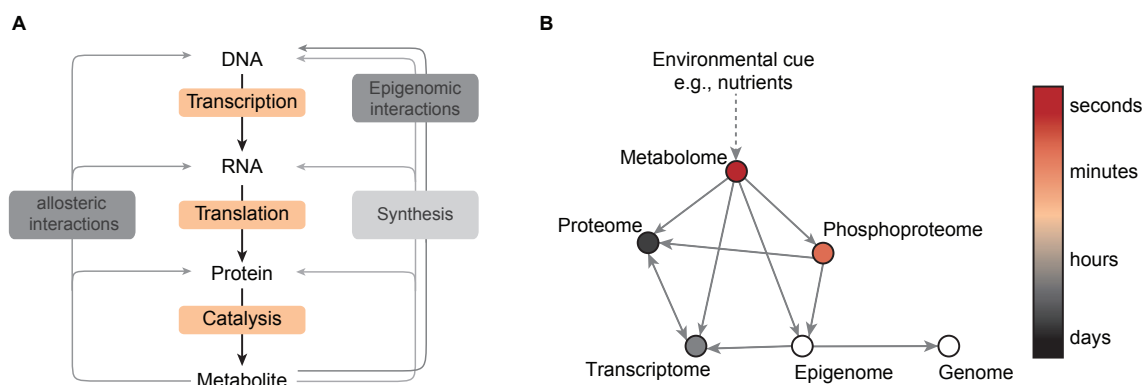
Figure 1.1.: Metabolomics in systems biology. (A) Regulation of omics levels (grey arrows) via metabolites beyond the central dogma of molecular biology. Adapted and modified from Buescher and Driggers [2016]. (B) Time-resolved trans-omics interactions in response to a nutritional cue. Adapted and modified from Yugi and Kuroda [2018].

CoA), which is the major substrate of histone acetyltransferases (HATs). HATs transfer the acetyl group of acetyl-CoA to lysine residues of histones, allowing the transcriptional access to the DNA and thereby the epigenetic control of gene expression.

1.1.2. Time-resolved omics studies

The expression of genes, transcripts and proteins reflect mainly the genotype of a cell, while metabolites transmit the phenotype. The regulation of metabolism is dependent on control processes that occur on each regulatory level, starting with the gene that encodes for different enzyme isoforms, the transcriptional activation via transcription factors, followed by the the control of alternative splicing, mRNA stability as well as translation and protein degradation processes [Wegner et al., 2015]. These gene expression-dependent regulations are time- and energy-consuming processes that are not easily reversible and therefore executed upon chronic environmental alterations. In contrast, the response to acute environmental cues is a gene expression independent process and thereby flexible and fast since it is based on allosteric regulation or post-translational modifications of enzymes [Wegner et al., 2015; Yugi and Kuroda, 2018].

Accordingly, the maintenance of the cellular homeostasis upon environmental stress is assured by a two-dimensional regulation: different omics levels which act on defined time scales [Yugi and Kuroda, 2018]. The time-based delimitation is further discernible in the averaged half lives of cellular metabolite (1 min), mRNA (10 hrs) and protein pools (24 hrs) estimated in HeLa cells [Yugi and Kuroda, 2018].

The cellular function of each omics regime is defined by a inherent time scale allowing the dissection of sequential cellular processes in response to a stimulus. Upon a nutritional alteration the metabolome adapts first, within seconds, signaling reactions via kinases take seconds to minutes, whereas gene expression-dependent regulations are detectable after minutes, but rather hours (*figure* 1.1B) [Buescher and Driggers, 2016; Shaw et al., 2014; Yugi and Kuroda, 2018]. Thus, the recording of changing events on each omics layer over time provides information about the directionality of cellular processes that are induced upon a stimulus [Buescher and Driggers, 2016].

Time-resolved experiments require frequent sampling in short intervals to monitor the response of the system. Each cellular response has a specific dynamic. The comparison of these inherent dynamics give information about the sequential interactions within the network [Buescher and Driggers, 2016]. Especially in the field of cancer research the integrative multi-omics approach provides the opportunity to: (i) uncover bypass reactions leading to drug resistance, (ii) identify biomarkers, (iii) and predict the most beneficial therapy for patients [Werner et al., 2014].

1.1.3. Required tools for metabolism-centric systems biology

In order to conduct systems-level analyses, highly multivariate data sets are required. Advances in microarray and high-throughput methods enable the comprehensive analysis of all omics regimes. Genomics, transcriptomics and epigenomics analyses are predominately based on DNA and RNA sequencing, whereas proteomics and metabolomics approaches rely on mass spectrometry (MS)-based methods that allow the direct identification of subjected molecules [Buescher and Driggers, 2016].

Chromatographic methods, such as liquid and gas chromatography (LC and GC), are usually connected upstream of mass spectrometers performing the pre-separation of biological compounds on the basis of their chemical properties. Proteins are usually subjected to LC-MS, while metabolites are analyzed with both methods. GC-MS is less sensitive than LC-MS, instead it enables the separation of structural isomers, such as glucose and fructose, and is thereby a suitable tool to examine the central carbon metabolism [Pietzke and Kempa, 2014].

Recently, metabolism-centric systems biology gained attention, because it links the biological phenotypes to environmental information. The metabolic adaptation in response to environmental cues might remain undetected due to interconnected, parallel and circular pathways that balance the metabolic homeostasis [Pietzke et al., 2014]. Differences in the abundance of metabolites are only detectable upon clear impairments of metabolic pathways as seen for knockdowns of key metabolic enzymes [Zasada, 2017]. The application of stable isotope substrates overcomes this limitation as it allows to trace the isotope flow throughout the metabolic network [Lane et al., 2011; Wittmann and Heinzle, 1999; Metallo et al., 2009]. A single GC-MS measurement provides the simultaneous analysis of metabolite abundance and isotope incorporation [Zasada, 2017].

Usually, stationary incorporation patterns are observed as a result of long labeling times that might reflect steady-state changes on the genome, transcriptom and proteome level. In contrast, the dynamic characterization of sequential metabolic events upon altered environmental conditions requires the application of stable isotopes in an instationary manner. Accurate kinetic studies require short sampling intervals and the uninterrupted supply of essential nutrients to minimize metabolic and mechanic stress that might affect nutrient conversion rates [Chokkathukalam et al., 2014]. Accordingly, the experimental handling is technically challenging regarding the rapid replacement of carbon sources and the terminal quenching of metabolism. These vulnerabilities were overcome as Pietzke et al. [2014] developed an optimized work flow for stable-isotope incorporation in cell culture, termed pulsed stable isotope-resolved metabolomics (pSIRM). The method, optimized to reduce any kind of perturbation, allows a time- and atom-resolved tracing of the routing of ^{13}C- or ^{15}N-labeled nutrients within the central carbon metabolism (CCM) by GC-MS (*figure* 1.2).
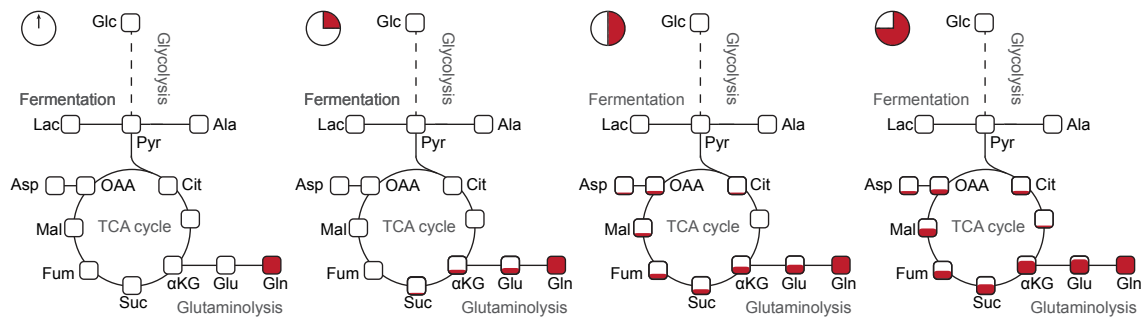
Figure 1.2.: Pulsed stable isotope-resolved metabolomics (pSIRM). Dynamics of ^{13}C-incorporation (red) are shown for the application of u-^{13}C-labeled glutamine. Time-resolved pulsed labeling enables the monitoring of the turnover-dependent replacement of carbon-12 with carbon-13 (red) of each single metabolite pool. The comparison of these dynamics allows the estimation about the preferential routing of applied substrates in different conditions.

Abbreviations – Ala: Alanine, αKG: α-Ketoglutarate, Asp: Aspartate, Cit: Citrate, Fum: Fumarate, Gln: Glutamine, Glu: Glutamate, Lac: Lactate, Mal: Malate, OAA: Oxaloacetate, Pyr: Pyruvate, Suc: Succinate.

1.2. The transcription factor MYC

The proto-oncogene *c-MYC* (*MYC*) encodes for a multifunctional transcription factor, which plays a pivotal role in proliferation, cell growth, differentiation, metabolism and apoptosis. MYC, a basic region/helix-loop-helix/leucine zipper (bHLHZip) protein, forms a heterodimer with the related transcription factor MAX. This complex recognizes consensus sequences within the DNA, namely enhancer boxes (E-boxes), and thereby activates/represses the transcription of specific target genes [Poole and van Riggelen, 2017]. The activation of MYC and its target genes are under tight control in normal cells, while MYC expression is frequently deregulated in human cancer, which contributes to the initiation and the progression of the disease [Kalkat et al., 2017]. The exploratory urge to investigate how MYC expression is regulated and how it regulates target gene expression renders MYC to one of the most studied proteins in the field of cancer research.

1.2.1. Regulation of MYC expression

In normal cells MYC expression is tightly controlled by the intrinsic cell cycle control and through extrinsic signals, such as growth factors and extracellular matrix contacts. MYC expression levels are low in quiescent cells, while they rapidly rise upon cell cycle entry and subsequently decline to remain at a basal level in cycling cells [Vita and Henriksson, 2006]. In contrast, the uncontrolled activation of MYC, that occurs in 60-70% of all human cancer, is driven through various mechanisms that affect MYC expression during transcription and translation or MYC activity via post-translational regulation (*figure* 1.3) [Poole and van Riggelen, 2017; Kalkat et al., 2017].

Transcriptional control of MYC expression

Deregulated expression of MYC originate from alterations that occur in the *MYC* gene itself, such as single point mutations, copy number alterations and chromosomal translocations or as a consequence of increased enhancer activity (*figure* 1.3) [Meyer and Penn, 2008].
The excessive expression of MYC in Burkitt's lymphoma was linked to a chromosomal translocation that juxtapose the *MYC* locus on chromosome 8 to immunoglobin (*Ig*) enhancers on chromosome 2, 14 or 22. The *Ig* enhancers stimulate the constitutive high expression of *MYC* mRNA and subsequently of MYC protein. This recombination occurs in 100% of Burkitt's lymphoma, while chromosomal rearrangements of similar nature are found in a variety of lymphomas, leukemias and myelomas [Vita and Henriksson, 2006; Meyer and Penn, 2008].
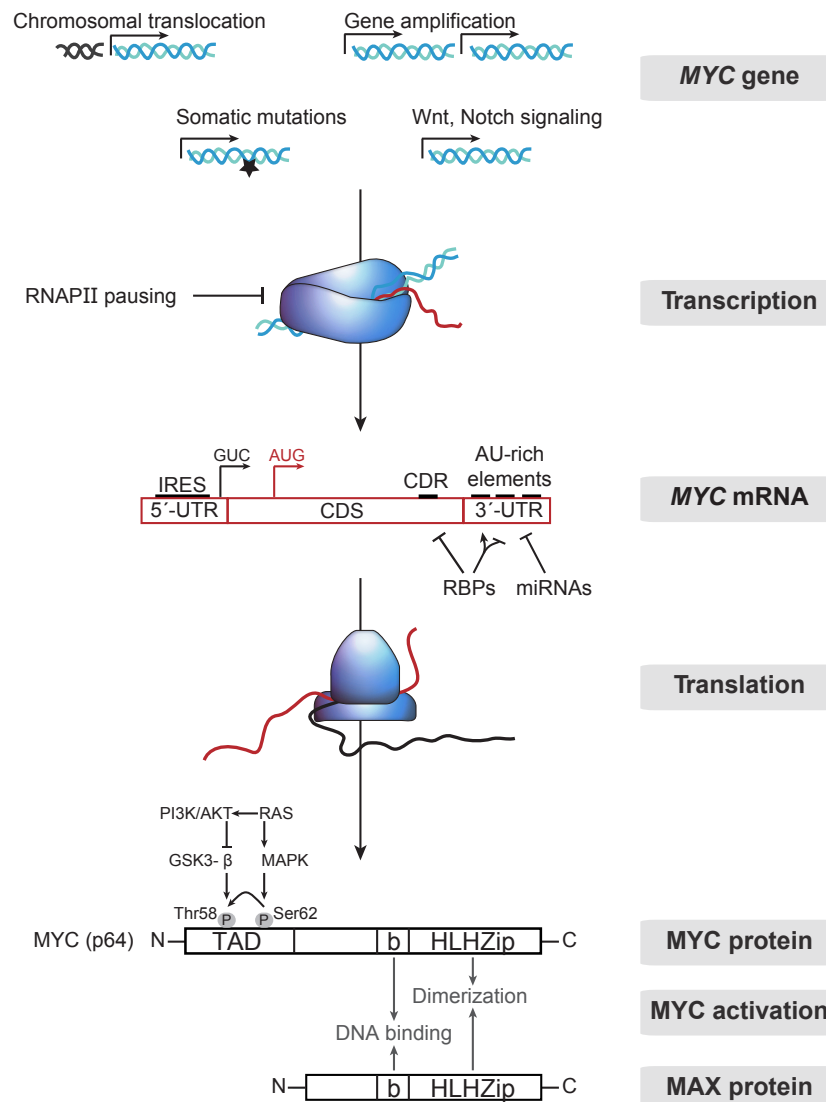
Figure 1.3.: Regulatory elements of MYC expression and activation. MYC, the master regulator of cell growth and proliferation, is tightly regulated at each regulatory level. Genomic alterations and unrestrained upstream Wnt and Notch signaling increase *MYC* transcript levels. Paused RNA polymerase II (RNAPII) contributes to the transcriptional control of *MYC*. Additionally, *MYC* is post-transcriptionally regulated via adenosine and uridine (AU)-rich elements within the 3'-untranslated region (3'-UTR) of the mRNA, that are targets of microRNAs (miRNAs) and RNA-binding proteins (RBPs). The stability of *MYC* mRNA is further determined via the coding region instability determinant (CRD), located at the 3'-terminus of the *MYC* coding sequence (CDS), which is a target for endonucleases. *MYC* mRNA translation occurs either via cap- or internal ribosome entry site (IRES)-dependent mechanisms. Alternative translation start sites give rise to different MYC isoforms (here shown p64 protein via AUG codon). On the protein level, MYC is regulated by several post-translational modifications including phosphorylation. Phosphorylation of Ser62 by RAS stabilizes and activates MYC protein. Once phosphorylated at Ser62, Thr58 becomes a substrate for GSK3-β, which marks MYC for ubiquitination and subsequent proteasomal degradation. In order to act as a transcription factor MYC associates with the protein MAX to bind to target genes. The transactivation domain (TAD) of MYC is located at the N-terminus, containing highly conserved elements that are required for MYC regulation and co-factor recruitment. Figure inspired by Vervoorts et al. [2006]; Meyer and Penn [2008]; Dejure [2017].

In contrast to chromosomal translocations in haematopoietic cancer, the common mode of MYC upregulation via genetic modification in solid tumors is gene amplification. Increased copy numbers of *MYC* are detected in 60% of nodular melanomas, 40% of ovarian cancer and in 30-50% of prostate cancer. However, aberrant copy numbers do not always give rise to deregulated MYC expression, instead have been shown to be associated with aggressiveness, metastasis and poor outcome [Vita and Henriksson, 2006; Meyer and Penn, 2008; Tansey, 2014].

Additionally, somatic mutations within the coding sequence (CDS) of *MYC* can result in elevated MYC expression as it has been reported for Thr58 of MYC. Mutation of Thr58 to alanine or another non-phosphorylatable amino acid increases MYC protein stability, because the transcription factor cannot be marked for ubiquitination and subsequently directed towards protein degradation anymore [Dang, 2012; Tansey, 2014].

Genetic modifications uncouple MYC expression from upstream signaling processes that usually keep *MYC* transcript levels under surveillance. However, in cancer cells these signaling pathways, including Wnt and Notch pathways, are frequently activated and contribute to elevated *MYC* mRNA levels as well [Dang, 2012].

The *MYC* transactivator β-catenin is strictly controlled in normal cells via the so called β-catenin destruction complex. The phosphorylation of β-catenin leads to proteasomal degradation in the absence of Wnt signal. Components of the destruction complex such as APC[1] and GSK3-β[2] are frequently mutated in cancer cells, especially in colon cancer cells, resulting in the accumulation of β-catenin. Once translocated to the nucleus, β-catenin binds the T-cell factor/lymphoid enhancer factor (TCF/LEF) and stimulates the constitutive expression of *MYC* transcripts [Tansey, 2014].

The list of possible mechanisms, including super enhancers, nucleotide polymorphism and retroviral insertion mutagenesis, which play a role in the control of *MYC* mRNA levels is continually extended and cannot be discussed to the full extent at this place [Meyer and Penn, 2008; Tansey, 2014].

Four *MYC* promoter were identified that are assumed to be regulated independently. *MYC* mRNA is transcribed from the weak promoter P1 and the stronger P2 promoter, which contribute to 75-90% of total *MYC* steady-state mRNA levels in normal cells [Strobl and Eick, 1992]. *MYC* is an immediate early gene, that is rapidly and transiently activated upon distinct cellular stimuli. Kelly et al. [1983] documented an increase of *MYC* mRNA by 10- to 40-fold within two hours after stimulation. The transcription of *MYC* and other immediate early genes was shown to be regulated by promoter-proximal paused RNA polymerase II (RNAPII). After transcriptional initiation elongation is paused and transcriptionally engaged RNAPII accumulates 35-50 nucleotides downstream from the transcription start site (TSS). Transcription is paused until a certain trigger releases RNAPII into the elongation mode [Levens, 2013; Liu et al., 2015b].

---

[1]adenomatosis polyposis coli
[2]glycogen synthase kinase 3β

Post-transcriptional and translational control of MYC expression

MYC mRNA is characterized by a short half-life of 15-30 min, that varies in response to different cell growth conditions [Herrick and Ross, 1994]. The cytoplasmic mRNA pool is determined by a complex interplay between transcription rates and mRNA decay. The latter allows the elimination of mutant mRNAs as well as the rapid adaptation of mRNA pools in response to environmental changes. Determinants of mRNA decay are typically located within the 3'-UTR of mRNAs [Shen and Malter, 2015]. The best characterized sequences, so called adenosine/uridine (AU)-rich elements (AREs), are commonly found within the 3'-UTR of several short-lived mRNAs that code for oncoproteins such as MYC [Wu and Brewer, 2012]. These elements contain multiple copies of the pentanucleotide 'AUUUA', which are embedded within U-rich regions and recognized by microRNA (miRNA) and RNA binding proteins (RBP) [Brennan and Steitz, 2001].

Such binding proteins determine fate and function of transcripts as they are involved in nuclear splicing, defect surveillance, cytoplasmic transport, mRNA stability and translation. So far approximately 20 ARE binding proteins (AUBP) have been identified, whereby five are known to bind to *MYC* mRNA (*table* 1.1) [Shen and Malter, 2015]. Among these five proteins, three promote mRNA degradation as they recruit the degradation machinery to mRNAs for their destruction, while ARE/poly(U)-binding protein (AUF-1) and Human antigen R (HuR) stabilize MYC mRNA [Liao et al., 2007; Liu et al., 2009; Wu and Brewer, 2012]. Although predominantly nuclear, HuR shuttles back and forth between the nucleus and the cytoplasm in order to accompany and protect mRNAs from the degradation machinery during cytoplasmic export [Brennan and Steitz, 2001]. Cytoplasmic localization or overexpression of HuR was reported to be associated with several cancer types [Wurth and Gebauer, 2015]. Next to its primary stabilizing function, HuR has been identified as an enhancer of translational repression as it recruits the miRNA let-7 [Gunzburg et al., 2015].

miRNAs are single stranded, non-coding RNAs of approximately 22 nucleotides that function in RNA silencing and post-transcriptional regulation of gene expression. Several *MYC*-targeting miRNAs have been described such as let7, miR-34 and miR-145 [Dang, 2012]. The latters are mediators of the tumor suppressor p53 and directly repress MYC expression. Both miRNAs are frequently silenced in variety of tumor entities pointing towards the importance of miRNA in cancer [Sachdeva et al., 2009; Rokavec et al., 2014]. The coding region instability determinant (CRD) has been described as an additional element that influence *MYC* mRNA stability, that functions independently of AU-rich elements. The CRD, which is located at the 3'-terminus of the *MYC* coding sequence, is susceptible for endoribonuclease cleavage, but is protected via the CRD-binding protein (CRD-BP) [Doyle et al., 1998].

Table 1.1.: *MYC* RNA binding protein (RPB) functions and their mechanisms.
Abbreviations – AUF-1: ARE/poly(U)-binding protein, HuR: Human antigen R, TIAR: TIA-1 related protein, TTP: Tristetraprolin. Table adopted from Dejure [2017].

RBP	Function	Mechanism	Reference
AUF-1	Stabilizer	AUF-1 promotes *MYC* translation by antagonizing TIAR and likely by interacting with translation initiating factors.	Liao et al. [2007]
HUR	Destabilizer	3'-UTR conformational change induced by HuR binding allows binding of miRNA let-7 and repression of translation.	Gunzburg et al. [2015]
		HuR cleavage product (HuR-CP1) associates with *MYC* 3'-UTR, blocking its translation after prolonged hypoxia.	Talwar et al. [2011]
	Stabilizer	HuR protects *MYC* mRNA from degradation in presence of polyamines.	Liu et al. [2009] Liu et al. [2015a]
TIAR	Destabilizer	TIAR represses *MYC* translation following UV-C irradiation and antagonizes AUF-1.	Mazan-Mamczarz et al. [2006] Liao et al. [2007]
TTP	Destabilizer	TTP mediates mRNA decay following rapamycin treatment.	Marderosian et al. [2006]

MYC mRNA gives rise to two main MYC protein isoforms, which differ in their amino-terminus and arise from alternative translational initiation (*figure* 1.3). The predominant p64 isoform (439 amino acids) is the product of a translation initiated from an AUG open reading frame present within exons 2 and 3, whereas the p67 (454 amino acids) originates from a CUG initiation within exon 1. While p64 is highly synthesized in proliferating cells, generation of p67 increases upon cell-to-cell contact [Batsché and Crémisi, 1999; Tansey, 2014]. A third one, known as the MYCS (339 amino acids), is initiated from a conserved downstream AUG codon [Spotts et al., 1997].

Once transcribed, the *MYC* mRNA is accompanied by several RNA binding proteins. One of them, the eukaryotic translation initiation factor 4E (eIF4E), which is under direct control of mitogenic signals, binds *MYC* mRNA already during the transcriptional process, convoys it to the cytosol and initiates cap-dependent translational machinery [Tansey, 2014]. *MYC* mRNA translation occurs either via cap- or internal ribosome entry site (IRES)-dependent mechanisms. The IRES of *MYC*, placed within the 5'-UTR upstream of the alternative translation initiation codon CUG, ensures steady state *MYC* mRNA levels throughout the cell cycle. The suppression of eIF4E and subsequent inhibition of cap-dependent translation during mitosis does not agree with the constant demand of the inherently stable MYC protein, for which reason IRES-dependent translation is taking over [Nanbru et al., 1997]. A study, investigating multiple myeloma in patients, revealed that a single point mutation in the *MYC*-IRES results in increased MYC protein levels driven by aberrant translational regulation [Chappell et al., 2000].

Post-translational control of MYC expression

The MYC protein has a short half-life of 15-20 min and is regulated by several posttranslational processes, including phosphorylation, ubiquitination, glycosylation and acetylation [Dang, 2012; Tansey, 2014]. The stability of MYC protein is predominantly determined by interdependent and sequential phosphorylation events on two highly conserved residues in the N-terminus (Ser62 and Thr58), which allow ubiquitin-mediated degradation of the protein (*figure* 1.3). The phosphorylation of the Ser62 residue by RAS-activated kinases (ERK) activates and stabilizes MYC as a transcription factor. Once Ser62 is phosphorylated, the residue Thr58 becomes a substrate for GSK3-β. GSK3-β is negatively regulated via AKT-mediated inhibition, which is induced upon RAS mitogenic signaling as well. Once RAS and AKT drop due to a missing mitogenic signal, Thr58 is phosphorylated and allows the recognition by the multi-protein ubiquitin ligase complex SCF[3] that stimulates polyubiquitination and subsequent proteasomal degradation. The consecutive phosphorylation ensures the transient stability of MYC protein levels during cell cycle progression. However, MYC protein stabilization does not require cell cycle progression, though mitogen-activated protein kinase (MAPK) signaling, that is frequently deregulated in human cancer. As described earlier, Ser62 and Thr58 are located within a mutational hot spot on the *MYC* gene rendering cells into MYC-overexpressing cells, when mutated [Sears, 2004; Vervoorts et al., 2006].

1.2.2. Regulation of MYC activation

The MYC protein dimerizes with its partner protein MAX via their N-terminal bHLHZip domains in order to act as a transcription factor. MYC competes with other bHLHZip transcriptional regulators of the Mxd family (e.g., MAD) to bind MAX, providing an additional mechanism to regulate MYC activity. The MYC/MAX heterodimer binds with high affinity to DNA enhancer boxes (E-Boxes) and induces or represses gene expression. The transactivation domain of MYC is located at the N-terminus, containing highly conserved elements that are required for MYC regulation and co-factor recruitment [Adhikary and Eilers, 2005; Meyer and Penn, 2008].

1.2.3. MYC-induced cellular signatures

MYC is estimated to bind to 25,000 sites in the human genome and thereby regulates a major proportion of genes, that are associated with various cellular functions, such as the regulation of cell cycle, differentiation, apoptosis and metabolism [Adhikary and Eilers, 2005; Boxer and Dang, 2001]. Two point of views have emerged trying to answer the question how deregulated MYC accounts for the global gene regulation. The specifier

---

[3]Skp, Cullin, F-box containing complex

model arose from the identification of distinct sets of target genes that were shown to be regulated in response to oncogenic MYC expression. However, the identification of a defined and consistent set of genes failed [Lin et al., 2012; Levens, 2013]. The new amplifier model assumes that MYC globally invades promoters and thereby amplifies the same pre-existing set of genes upon enhanced MYC activation [Rahl and Young, 2014]. The distinct gene expression pattern is in turn provoked indirectly by regulatory feedback and feedforward loops [Benary et al., 2017].

MYC coordinately enhances the transcriptional and translational capacity of cancer cells in order to master the oncogene-induced cellular program [Elkon et al., 2015]. MYC recruits a multitude of transcriptional regulators and co-factors that participate in chromatin structure control and histone acetylation. Additionally, MYC activates all three RNA polymerases and thereby controls transcription of coding (mRNA) and non-coding RNAs (miRNA, transfer RNA (tRNA), ribosomal RNA (rRNA)). The transcription factor also enhances protein biosynthesis by collaborating with mTOR, a major positive regulator of protein biosynthesis and cell growth [Adhikary and Eilers, 2005; Vervoorts et al., 2006; Tansey, 2014].

The cellular signature induced by MYC is dependent on the expression level of the transcription factor [Levens, 2013]. Low levels lead to quiescent cells, while moderate MYC expression promotes cell growth and proliferation and inhibits differentiation. It has been reported that quiescent cells enter cell cycle in the absence of growth factor signaling when MYC expression is forced. Enhanced expression of MYC is associated with unrestrained cell proliferation, metastasis, genomic instability and angiogenisis and thereby crucial for tumorigenesis and tumor progression [Adhikary and Eilers, 2005]. While deregulated MYC levels induce hyperproliferation, excessive MYC expression triggers apoptosis. This is understood as a fail-safe mechanism for cells that potentially express oncogenic MYC levels [Adhikary and Eilers, 2005; Levens, 2013]. This program is mostly governed by the environment, the genetic background and the distinctly set MYC activity threshold per cell type [Di Giacomo et al., 2017; Murphy et al., 2008]. Additionally, MYC-driven apoptosis was reported for cells that are coerced to express high MYC levels in the absence of survival factors or stress signals [Adhikary and Eilers, 2005]. Molecular mechanisms that control MYC-induced apoptosis are intensively examined, aiming for therapeutic approaches that transform MYC's pro-proliferative into pro-apoptotic effects [McMahon, 2014].

1.3. Metabolism in cancer

The metabolic program of normal differentiated cells is considerably different to that of cancer cells. While a resting cell needs to meet its energetic demands via the production of ATP to maintain the cellular homeostasis, proliferating cells require additional energy and macromolecules. In order to effectively support cell growth and proliferation, metabolic pathways need to be rewired, so that biosynthetic processes, ATP production and the restriction of co-occurring reactive oxygen species (ROS) are balanced [Cantor and Sabatini, 2012; Vander Heiden, 2011].

Escalated cell growth and proliferation are unifying features of cancer cells, although of the high diversity of underlying metabolic programs. The achievement of a proliferation supportive metabolic program is shelled out for metabolic dependencies and thereby vulnerabilities [Cantor and Sabatini, 2012]. For example, whereas the metabolic program of normal cells relies almost exclusively on glucose, cancer cells require glutamine as an additional source of carbon to satisfy their demands [Amoêdo et al., 2013]. The interconnection of glucose and glutamine metabolism in cancer cells has been intensively studied in the past and examined for therapeutic purposes.

1.3.1. An introduction into glucose metabolism

Glucose is the most abundant sugar in the blood stream and the primary source of energy in the body. The breakdown of glucose in a series of ten cytosolic reactions, that are oxygen independent, is defined as glycolysis. The pathway is the main provider of energy and building blocks for synthetic reactions. In glycolysis one molecule of glucose is converted into two molecules of pyruvate, two molecules of ATP and two molecules of NADH (*figure* 1.4). During the first five steps, the so called 'preparatory phase', ATP is invested in order to generate 3-carbon sugar phosphates, e.g., glyceraldehyde 3-phosphate. These energy-rich trioses compensate for the loss of energy when they are introduced to the 'pay-off-phase'. As one molecule glucose is converted into two molecules of glyceraldehyde 3-phosphate, the degradation of the latter into pyruvate yields four molecules of ATP and two molecules of NADH [Berg et al., 2007].

Glycolysis is highly conserved due to its pivotal role in central carbon metabolism. Hexokinase (HK), phosphofructokinase (PFKM) and pyruvate kinase M (PKM) catalyze irreversible reactions and thereby balance the generation and outflow of glycolytic intermediates that feed several adjacent metabolic pathways, including tricarboxylic acid (TCA) cycle, pentose phosphate pathway and one-carbon metabolism. Moreover, allosteric inhibition of enzymes in the presence of high ATP levels (e.g., phosphofructokinase, pyruvate kinase) or central metabolites, such as citrate and acetyl-CoA, enable a rapid re-direction of carbon-flow upon altering conditions [Berg et al., 2007].

Glc

Cytosol

Glc
ATP
1
ADP
G6P ———— R5P ——→ Nucleotides
Pentose Phosphate Pathway
2
F6P
ATP
3
ADP
FBP
4   4
DHAP   5   GA3P
Lipids ←——
NAD⁺
6
NADH+H⁺
1,3BPG
ADP
7
ATP
3-PGA
8   **One carbon metabolism**
2-PGA ———— Ser ——→ Amino acids
9
PEP
ADP
10
ATP
Fermentation
Lac ———— 11   Pyr ———— Ala ——→ Amino acids

Glycolysis

Mitochondrium

Pyr
NAD⁺
12
NADH+H⁺   Acetly-CoA
Asp
Amino acids,   OAA   13   Cit ——→ Fatty acids
Nucleotides
NADH+H⁺
20   14
NAD⁺
Mal   **TCA cycle**   Isocit
19   NAD⁺
15
Fum   NAD⁺   NADH+H⁺
18   NADH+H⁺ 16   αKG ——→ Amino acids,
FADH₂   Nucleotides
FAD   Suc   17   Succinyl-CoA
GTP GDP

ETC   H⁺   ATP
ADP ↑
+Pi
OXPHOS
I   II   III   IV   V   inner mitochondrial membrane
H⁺ H⁺ H⁺ H⁺ H⁺   H⁺ H⁺ H⁺   outer mitochondrial membrane

Metabolic enzymes
1: Hexokinase
2: Phosphoglucose isomerase
3: Phosphofructokinase
4: Aldolase
5: Triosephosphate isomerase
6: Glyceraldehyde 3-phosphate dehydrogenase
7: Phosphoglycerate kinase
8: Phosphoglycerate mutase
9: Enolase
10: Pyruvate kinase
11: Lactate dehydrogenase
12: Pyruvate dehydrogenase complex
13: Citrate synthase
14: Aconitase
15: Isocitrate dehydrogenase
16: α-Ketoglutarate dehydrogenase complex
17: Succinyl-CoA synthase
18: Succinate dehydrogenase (complex II)
19: Fumarase
20: Malate dehydrogenase

Metabolic intermediates
Glc: Glucose
G6P: Glucose 6-phosphate
R5P: Ribose 5-phosphate
F6P : Fructose 6-phosphate
FBP: Fructose bisphosphate
GA3P: Glyceraldehyde 3-phosphate
DHAP: Dihydroxyacetone phosphate
1,3BPG: 1,3-Bisphosphoglycerate
3-PGA: 3-Phosphoglycerate
2-PGA: 2-Phosphoglycerate
Ser: Serine
PEP: Phosphoenolpyruvate
Pyr: Pyruvate
Lac: Lactate
Ala: Alanine
Acetyl-CoA: Acetyl coenzyme A
Cit: Citrate
Isocit: Isocitrate
αKG: α-Ketoglutarate
Succinyl-CoA: Succinyl coenzyme A
Suc: Succinate
Fum: Fumarate
Mal: Malate
OAA: Oxaloacetate
Asp: Aspartate

Figure 1.4.: Central carbon metabolism – Glycolysis and TCA cycle. In glycolysis one molecule of glucose is converted into two molecules of pyruvate, ATP and NADH. Pyruvate is transported to the mitochondria and the TCA cycle, where it is converted into acetyl-CoA. The step-wise oxidation of acetyl-CoA into CO_2 concomitantly forms three equivalents of NADH, one equivalent of FADH₂ and one equivalent GTP. The reducing agent NADH and FADH₂ are used by the electron transport chain (ETC) and subsequent oxidative phosphorylation (OXPHOS) to generate ATP. In addition glycolysis and TCA cycle provide building blocks, such as amino acids, fatty acids and nucleotides for biosynthesis.

The aerobic processing of glucose occurs subsequent of gylcolysis via the transport of pyruvate to the mitochondria. The glucose derivative is completely oxidized into carbon dioxide in eight enzymatic steps known as the TCA cycle (*figure* 1.4). Pyruvate enters the TCA cycle, where it is decarboxylated to acetyl-CoA via pyruvate dehydrogenase. Acetyl-CoA provides two carbons in form of the acetyl group and forms together with oxaloacetate

the metabolite citrate. In the following, the six-carbon molecule is decarboxylated twice, once into α-ketoglutarate and another time to form the four-carbon body succinate, which is regenerated into oxaloacetate [Berg et al., 2007].

The complete oxidation of acetyl-CoA into two molecules of CO_2 facilitates the transfer of three pairs of electrons to three molecules of NAD^+ and one pair to one molecule of FAD, while an additional molecule GTP is generated. The reduced electron carriers (NADH, FADH2) habour a high electron transfer potential and are thereby oxidized by a series of four membrane proteins (complex I-IV), termed as the electron transport chain (ETC) (*figure* 1.4). The ETC forwards electrons from donors to acceptors such as oxygen or succinate and transports protons across the inner mitochondrial membrane generating a potential. The protein complex V, also known as ATPase, couples the force to equalize the membrane potential to the energetically unfavorable reaction converting ADP and P_i to ATP. In total 36 molecules of ATP are generated from one molecule glucose via this process called oxidative phosphorylation (OXPHOS). Accordingly, the degradation of glucose via TCA cycle coupled to OXPHOS provides the majority of energy for the cell [Berg et al., 2007].

The TCA cycle is the central metabolic hub of the cell as it is an amphibolic pathway, combining catabolic and anabolic reactions. The oxidation of fatty acids into acetly-CoA fuels the TCA cycle, next to amino acids and carbohydrates (*figure* 1.4). The main amino acid suppliers are glutamine and aspartate, which enter the TCA cycle via α-ketoglutarate and oxaloacetate, respectively. Since the TCA cycle is fueled from various entry points it becomes clear that this metabolic pathway is an important supplier for the synthesis of amino acids, fatty acids and ATP [Berg et al., 2007].

1.3.2. An introduction into glutamine metabolism

Glutamine is the most abundant amino acid in the human body. The majority of dietary glutamine is absorbed through the gut and liver, while skeletal muscle, lung and adipose tissue primarily provide glutamine to the blood stream that is synthesized from glucose. Accordingly, glutamine is considered a non-essential amino acid at the organismal level [Oehler and Roth, 2003; Altman et al., 2016].

On the cellular basis, glutamine is a readily available source of nitrogen and carbon. Specifically, glutamine is an indispensable donor of (i) nitrogen for *de novo* purine and pyrimidine nucleotide biosynthesis, (ii) carbon to fuel anaplerotic reactions and (iii) both nitrogen and carbon to support glutathione biosynthesis to assure the cellular redox homeostatsis (*figure* 1.5). In order to assist in all these pathways the amino acid is converted into glutamate, another non-essential amino acid and source of carbon and nitrogen. The deamination of glutamine is either achieved by the enzyme glutaminase (GLS) that releases free ammonia or by aminotransaminases, e.g., asparagine synthetase (ASNS), glutamate oxaloacetate transaminase (GOT) and glutamate pyruvate transaminase (GPT).

Transaminases exchange the amine group of glutamine with the keto group of a donor substrate as ASNS is catalyzing the reaction from aspartate and glutamine to asparagine and glutamate [Zhang et al., 2017a; Yang et al., 2017].

Additional glutamine-dependent transaminases are known that catalyze for instance the synthesis of NAD or glucosamine 6-phosphate (GlcN6P) or that are involved in the *de novo* nucleotide biosynthesis. Although the majority of glutamine-converting enzymes are transaminases, it is assumed that the GLS-dependent reaction is the main contributor to the intracellular glutamate pools [Zhang et al., 2017a; Yang et al., 2017].

TCA cycle anaplerosis

The carbon backbone of glutamine enters the TCA cycle when glutamate is further de-aminased to α-ketoglutarate (*figure* 1.5). The oxidation of the 5-carbon body generates bioenergetic NADH and FADH2 equivalents, which can be either devoted to maintain the cellular redox homeostasis or used to generate ATP via the ETC coupled to OXPHOS. Additionally, the TCA cycle generates diverse biosynthetic precursor such as aspartate and citrate, which support amino acid, nucleotide and fatty acid synthesis (*figure* 1.4) [Berg et al., 2007; Zhang et al., 2017a]. In order to support the formation of fatty acids as well as acetylation processes, glutamine-derived α-ketoglutarate also produces acetyl-CoA via reductive carboxylation. First, α-ketoglutarate is carboxylated into citrate, which is exported to the cytosol, where it is cleaved into oxaloacetate and acetyl-CoA by ACLY. Acetyl-CoA is subsequently used for fatty acid synthesis [D'Adamo and Dugan Tobin, 1979].

The conversion of glutamate into α-ketoglutarate is facilitated by glutamate dehydrogenase (GLUD) or aminotransaminases such as GOT, GPT and phosphoserine aminotransferase (PSAT). Glutamate-dependent transaminases primarily contribute to the synthesis of other amino acids (e.g., serine, alanine, aspartate) and are – similarly to glutamine-dependent transaminases – superior in numbers compared to deaminases (*figure* 1.5) [Yang et al., 2017].

***De novo* glutathione biosynthesis**

Glutamate is a building block of the primary cellular antioxidant glutathione, which is produced in two enzymatic reactions that require ATP. Firstly, cysteine is ligated to glutamate via glutamate cysteine ligase (GCL) before glycine is joined to the peptide by glutathione synthetase (GS) (*figure* 1.5) [Berg et al., 2007].

Glutathione acts as a detoxifying agent as it combats reactive oxygen species (ROS) that are generated concomitant in the ETC. The redox-active thiol group – a cysteine residue in the backbone of the tripeptide – donates reducing equivalents (proton and electrons) to

neutralize electrophiles, oxidants and protein cysteines. Once oxidized, glutathione itself becomes reactive and forms dimer structures, which can be reduced via NADPH [Deponte, 2013].

De novo nucleotide biosynthesis

Nucleotides are the building blocks of DNA and RNA and therefore involved in a variety of biological processes. Although salvage pathways and assimilation contribute to the cellular pools of nucleotides, the molecules are incessantly synthesized *de novo*. The formation of nucleotides is a highly energy-consuming process and depends on several carbon and nitrogen sources since a nucleotide is composed of a 5-carbon sugar, a nitrogen base and at least one phosphate. Glutamine is one indispensable nitrogen donor for *de novo* nucleotide biosynthesis next to aspartate. In total five reactions, three within purine and two within pyrimidine synthesis pathways, are dependent on transaminases that transfer the amine group from glutamine to a nucleotide or precursor [Lane and Fan, 2015; Christopherson, 2006].

Nucleotide biosynthesis starts with the the preparation of the activated ribose 5-phosphoribosepyrophosphate (PRPP). The ribose sugar that fuels purine as well as pyrimidine anabolism is build from glucose via ribose 5-phosphate under the consumption of one glutamine-derived nitrogen and three molecules of ATP [Lane and Fan, 2015].

Purine synthesis is based on the further conversion of PRPP to inosine monophosphate (IMP) – the precursor of adenosine and guanosine derivates. In eight enzymatic steps three nitrogen molecules originating from glutamate, aspartate and glycine are incorporated, while other four molecules of ATP are invested. The subsequent synthesis of GMP requires an additional molecule of ATP and the incorporation of another glutamine-derived nitrogen, while the generation of AMP is only dependent on GTP. The modification of nucleotide monophosphates to nucleotide di- and triphosphates is performed by nucleotide kinases [Lane and Fan, 2015].

Two molecules of ATP are invested to generate dihydroorotate from glutamine, aspartate and CO_2 during the first three reactions of pyrimidine biosynthesis. These reactions are performed by a multifunctional protein consisting of carbamoyl phosphate synthetase, aspartate transcarbamylase and dihydroorotase (CAD). Afterwards, dihydroorotate is further modified to orotate. The produced pyrimidine is joined to PRPP resulting in the formation of UMP that is sequentially phosphorylated to UDP and UTP. Subsequently, CTP is generated by CTP synthetase (CTPS) that transfers a nitrogen from glutamine to UTP [Lane and Fan, 2015; Christopherson, 2006].

The synthesis of deoxyribonucleotides is based on the reduction of ribonucleoside diphosphates into deoxyribonucleoside diphosphates and their subsequent phosphorylation. The generation of deoxythymidine triphosphate (dTTP) is more complex as it is generated by the thymidylate synthesis cycle [Christopherson, 2006; Mathews, 2015].
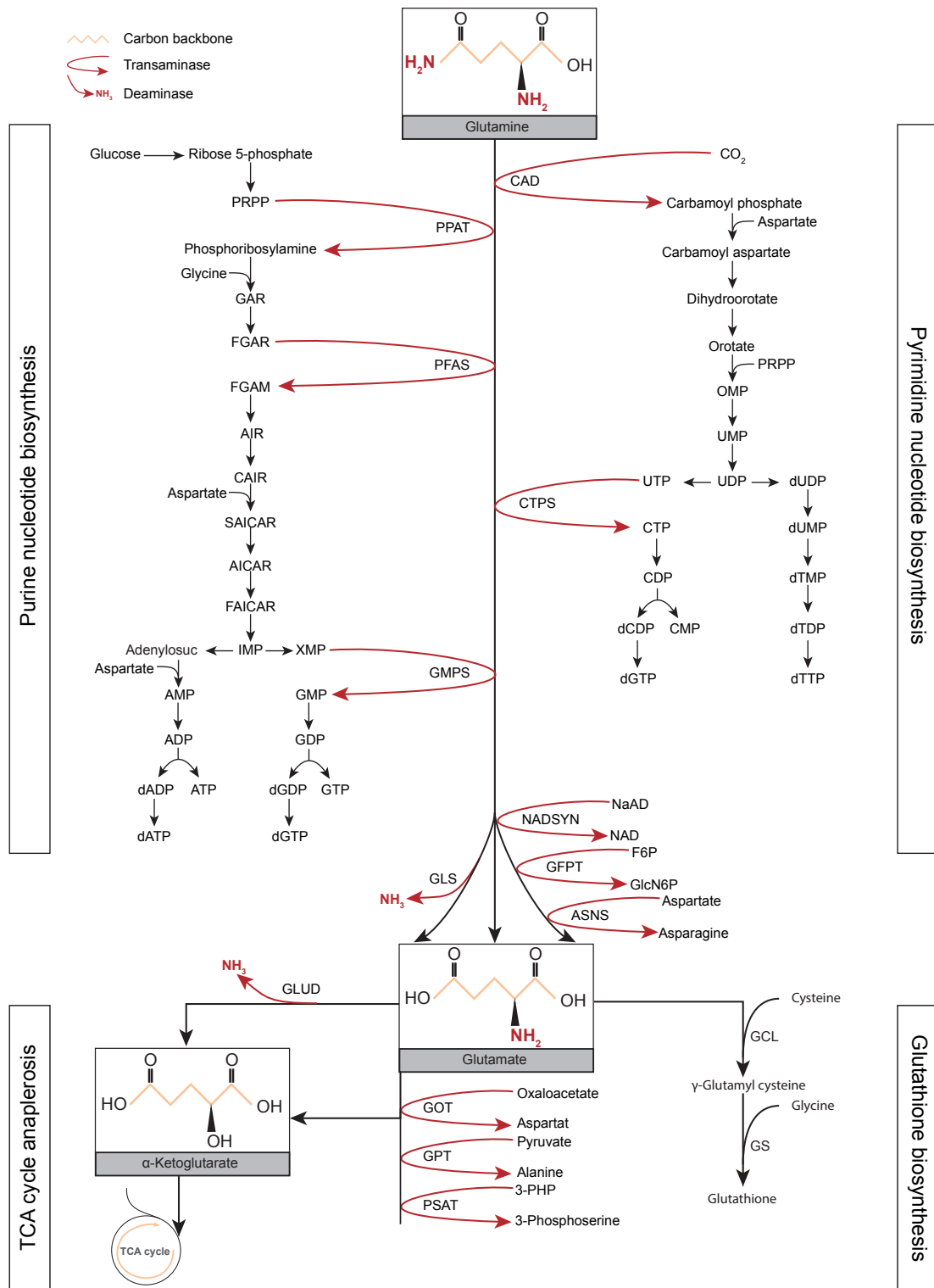
Figure 1.5.: Glutamine's role as a nitrogen (red) and carbon donor (orange) in *de novo* nucleotide biosynthesis, TCA cycle anaplerosis and glutathione biosynthesis. Glutamine is converted into glutamate by either glutaminase accompanied by the release of free ammonia (NH_3) or transaminases that transfer the cleaved nitrogen to donor substrates. Five reactions in the *de novo* nucleotide biosynthesis pathway require glutamine as a nitrogen donor. The support of anaplerotic reactions via glutamine is dependent on its carbon backbone that is introduced to the TCA cycle via α-ketoglutarate. The biosynthesis of glutathione is dependent on both nitrogen and carbon provided by glutamine. Figure inspired by Cluntun et al. [2017]. *Continued on the next page.*

Figure 1.5.: *Continued from previous page.* Abbreviations – ASNS: Asparagine synthetase, CPS: Carbamoyl phosphate synthetase, CTPS: Cytidine triphosphate synthetase, GCL: Glutamate cysteine ligase, GFPT: Glucosamine-fructose 6-phosphate aminotransferase, GLS: Glutaminase, GLUD: Glutamate dehydrogenase, GMPS: Guanosine monophosphate synthetase, GOT: Glutamate oxaloacetate transaminase, GPT: Glutamate pyruvate transaminase, GS: Glutathione synthetase, NADSYN: NAD synthetase, PFAS: Phosphoribosyl formylglycinamidine synthetase, PPAT: Phosphoribosyl pyrophosphate amidotransferase, PSAT: Phosphoserine aminotransferase. For the complete metabolite names refer to the list of abbreviations.

1.3.3. MYC-induced metabolic reprogramming in cancer cells

Metabolic reprogramming defines the concerted deregulation of nutrient consumption in order to drive energy and biomass production and subsequent cell growth [Zasada, 2017]. Already in the early 1930's Otto Warburg postulated that tumor cells prefer to convert glucose into lactate even in the presence of sufficient oxygen supply as a consequence of impaired mitochondria. This unconventional routing of glucose is referred as aerobic glycolysis or the Warburg effect and was observed in a variety of cancer types [Warburg et al., 1924, 1927; Ward and Thompson, 2012b].

In contrast to Warburg's original hypothesis, the aerobic glycolysis is not an indirect result of deficient mitochondria, though an oncogene-induced metabolic program. The majority of proto-oncogenes and tumor suppressor genes encode for signaling proteins that are traditionally linked to the regulation of cell growth and proliferation or inhibition of apoptosis. In the context of carcinogenesis these master regulators, including RAS, PI3K, MYC, p53 and HIF-1α; affect metabolic enzymes in order to support the high demand of building blocks and energy in cancer cells [Ward and Thompson, 2012b; Cantor and Sabatini, 2012]. The oncoprotein MYC is among the master inducers of cancer glycolysis (*figure* 1.6). The transcription factor enhances the activity of several glycolytic enzymes, especially those catalyzing rate-limiting steps (e.g., HK2, PFKM). Additionally, MYC promotes the alternative splicing of *PKM*, resulting in the expression of PKM2. In contrast to PKM1, PKM2 is allosterically inhibited and thereby impedes the formation of pyruvate from phosphoenolpyruvate allowing for glycolytic intermediates to be directed into biosynthetic pathways. Furthermore, MYC upregulates lactate dehydrogenase A (LDHA) that redirects pyruvate away from mitochondria [Dang, 2013].

The conversion of glucose into lactate may seem contradictory, since aerobic glycolysis is inefficient regarding ATP production compared the complete oxidation of glucose via OXPHOS (glycolysis: 2 ATP, mitochondrial respiration: 36 ATP). However, the oncogene-induced transactivation of glucose transporters (GLUT1, GLUT2, GLUT4) and other glycolytic enzymes contribute to a 10-100 times faster conversion of glucose into lactate compared to normal cells [Ward and Thompson, 2012b; Cantor and Sabatini, 2012; Liberti and Locasale, 2016].

TCA cycle intermediates, such as citrate, are continuously depleted under limited pyruvate availability due to aerobic glycolysis. In order to maintain the mitochondrial integrity and TCA cycle function, MYC-driven cancer become dependent on glutamine as an anaplerotic fuel [Chen and Cui, 2015]. This phenotype, termed glutamine addiction, is most likely induced due to the MYC-dependent upregulation of glutamine transporters (SLC1A5, SLC38A5) and glutaminase (GLS) (*figure* 1.6) [Altman et al., 2016]. While SLC1A5 and SLC38A5 are direct targets of MYC, the elevated expression of GLS is a consequence of transcriptional suppression of miRNAs – miR-23a and miR-23b – which bind the 3'-UTR of GLS leading to its degradation [Gao et al., 2009]. The enhanced uptake of glutamine and its conversion via GLS replenish the TCA cycle leading to the production of NADH, FADH2 and macromolecules. For the cell this is a win-win situation as it gains benefits from both pathways, glycolysis and glutaminolysis, resulting in a much higher overall synthesis of energy, building blocks and reducing equivalents that are required for enhanced cell growth and division [Lukey et al., 2013].

Additionally, MYC completes the metabolic reprogramming by enhancing proteins that are rate-limiting in nucleotide, fatty acid and amino acid synthesis (*figure* 1.6) [Stine et al., 2015].
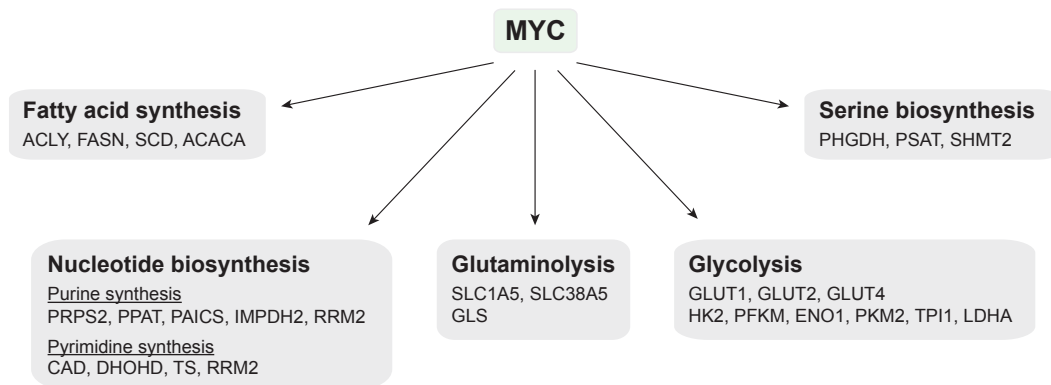
Figure 1.6.: MYC targets involved in metabolic pathways. MYC-induced metabolic reprogramming is driven by the upregulation of metabolic enzymes, which are involved in glycolysis, glutaminolysis, nucleotide biosynthesis, fatty acid biosynthesis and serine biosynthesis.
Abbreviations – ACACA: Acetyl-CoA carboxylase α, ACLY: ATP citrate lyase, CAD: Carbamoyl phosphate synthetase 2 - Aspartate transcarbamylase - Dihydroorotase, DHODH: Dihydroorotate dehydrogenase, ENO1: Enolase 1, FASN: Fatty acid synthase, GLUT: Glucose transporter, GLS: Glutaminase, HK2: Hexokinase 2, IMPDH2: Inosine-5'-monophosphate dehydrogenase 2, LDHA: Lactate dehydrogenase A, PAICS: Phosphoribosylaminoimidazole carboxylase, PFKM: Phosphofructokinase, PHGDH: Phosphoglycerate dehydrogenase, PKM2: Pyruvate kinase isozyme M2, PPAT: Phosphoribosyl pyrophosphate amidotransferase, PRPS2: Phosphoribosyl pyrophosphate synthetase 2, PSAT: Phosphoserine aminotransferase, RRM2: Ribonucleoside-diphosphate reductase, SHMT2: Serine hydroxymethyltransferase, SCD: Stearoyl-CoA desaturase, SLC1A5: Neutral amino acid transporter B(0), TPI1: Triosephosphate isomerase, TS: Thymidylate synthase.

1.3.4. Glutamine addiction as a therapeutic target

The deregulated expression of MYC induces a metabolic signature leading to aerobic glycolysis and concomitant to glutamine addiction in cancer cells. This metabolic program runs unrestrained by negative feedback loops and therefore being most beneficial for the excessive cell growth [Dang, 2013]. However, such specialization always increases vulnerabilities to therapeutic strategies that target metabolism.

Glutamine starvation has been shown to significantly induce apoptosis in hepatoma, leukemia, myeloma and hybridoma cells [Chen and Cui, 2015]. Especially, MYC-over-expressing human cells were found to be dependent on glutamine as the oncogene enhances the expression of genes involved in glutamine metabolism [Yuneva et al., 2007; Wise et al., 2008; Gao et al., 2009; Nieminen et al., 2013]. Several strategies for targeting these acquired features are conceivable, including the restriction of glutamine uptake, the depletion of glutamine pools in the blood stream, the use of glutamine mimetics and the specific inhibition of glutamine synthesizing or converting enzymes [Chen and Cui, 2015; Cluntun et al., 2017].

Glutaminase, the enzyme converting glutamine into glutamate, is the gatekeeper of glutaminoylsis and has been proposed as a biomarker for glutamine-dependent cancer cells. Thus, therapeutic approaches addressing the inhibition of glutaminase have been extensively researched [Chen and Cui, 2015].

In mammals glutaminase is encoded by two genes, *GLS* and *GLS2*. *GLS*, originally termed as the kidney-type glutaminase (*KGA*), is alternatively spliced to *GAC*, a truncated version of *KGA*. In healthy individuals, both GLS isoforms are ubiquitously expressed in cell tissues, but highest in the kidney, while GLS2 is found predominately in liver. KGA and GAC expression are frequently upregulated in human cancer due to oncogenic activation by MYC. In contrast, GLS2 is considered a tumor suppressor as *GLS2* transcript levels are regulated by p53, the master tumor suppressor. The frequently occurring disruption of p53 function in cancer cells is accompanied by reduced GLS2 expression that makes GLS2 a less attractive target compared to KGA and GAC [Katt and Cerione, 2014; Chen and Cui, 2015; Cluntun et al., 2017].

KGA and GAC are allosterically activated by inorganic phosphate that stimulates the transformation of inactive dimers into active tetramers. The promotion of GLS activity by phosphate *in vitro* requires a minimal concentration of 40 mM, while phosphate levels in the human blood were reported to be ≈1 mM. Since little is known about the phosphate-dependent glutaminase regulation *in vivo*, these differences suggest that GLS activity *in vivo* is most likely induced by additional mechanisms [Katt and Cerione, 2014].

To date several mechanism have been investigated by which glutaminase activity is modified by pharmacological agents. The earliest described compound – 6-Diazo-5-oxo-L-norleucine (DON) – a substance isolated from a species of *Streptomyces* by Coffey et al.

[1956], targets GLS directly. DON is a glutamine analogue that acts as an irreversible, glutamine-competitive inhibitor as it covalently binds to the active site of GLS leading to the formation of an enzyme-inhibitor complex. DON as a glutamine mimetic inhibits several glutamine-converting enzymes – including ASNS, CAD, CTPS, guanosine monophosphate synthetase (GMPS), NAD synthetase (NADSYN), phosphoribosyl pyrophosphate amidotransferase (PPAT) and phosphoribosyl formylglycinamidine synthetase (PFAS). Although DON was evaluated to have potent antitumor activity *in vitro* and *in vivo*, the substance did not enter phase III trials as its nonspecificity caused various toxic side effects such as nausea, vomiting and diarrhea [Cervantes-Madrid et al., 2015].

During the last decades novel small molecules have been discovered that selectively inhibit KGA and GAC. Two main classes of allosteric GLS inhibitors have been identified, that rely on the structural and functional difference of the lead compounds Bis-2-(5-phenylacetamido-1,3,4-thiadiazol-2-yl)ethyl sulfide (BPTES) and Compound 968 (C968). While BPTES binds at the dimer-dimer interface of GLS leading to a stabilization of the inactive tetramer, C968 locates in the hydrophobic pocket within the monomer interface and thereby prevents GLS activation by inorganic phosphate [Lukey et al., 2013]. Both inhibitors have been described to suppress cell growth and induce apoptosis in glutamine-dependent cancer cells and xenografts, and more specifically in MYC-overexpressing cell lines and tumors. Even though theses preclinical results are promising, neither BPTES nor C968 have been examined in clinical trails since both compounds exhibit a low micromolecular potency and poor solubility [Li and Simon, 2013; Chen and Cui, 2015].

Recently, CB839, a BPTES-like compound exhibiting a higher potency and solubility than BPTES, has been discovered. The small molecule has been proven to inhibit cell growth in breast, lung, lymphoma, myeloma, leukemia and non-small lung cancer cell lines, which correlates with sensitivity to glutamine withdrawal. The potency of CB839 to suppress solid and haematopoietic cancer is currently being evaluated in multiple phase II trials conducted by Calithera Biosciences, whereby CB839 is either applied as a single inhibitor or in combination with other agents [Parlati et al., 2014; McDermott, 2017].

2. Aim and Scope of the Thesis

The deregulation of the transcription factor MYC drives the metabolic reprogramming in cancer cells. One of the hallmarks of MYC-driven cancer is an enhanced glutaminolysis, which renders cancer cells dependent on the non-essential amino acid glutamine for survival. Initial experiments revealed that glutamine depletion suppresses MYC protein expression in various cancer cell lines and induces a reversible cell cycle arrest, although not apoptosis. The aim of the thesis was to investigate how limitations on external glutamine supply control MYC protein expression, thereby affecting MYC as a major regulator of cell growth, metabolism and apoptosis. In order to analyze the underlying mechanisms and the biological relevance of the glutamine-mediated MYC regulation, we addressed three different aspects of the metabolic feedback.

Firstly, we characterized the glutamine-dependent MYC regulation at all regulatory levels by time-resolved studies. The comparison of dynamics allowed the dissection of sequential cellular processes in response to glutamine availability.

Secondly, we investigated glutamine's different metabolic tasks in TCA cycle anaplerosis, *de novo* nucleotide and glutathione biosynthesis in regard to glutamine-dependent MYC protein expression. The application of quantitative mass spectrometry approaches in a time-resolved manner aimed for the identification of critical metabolic pathways, that may mediate the glutamine-dependent MYC regulation. Identified pathways were validated for their involvement via rescue or inhibition experiments.

Thirdly, we mimicked glutamine depletion by applying inhibitors against glutaminase activity in order to investigate whether and to what extend the enzyme contributes to MYC regulation. Since glutaminase has been extensively researched as a therapeutic target in the scope of glutamine addiction, we hoped to find evidence whether this strategy is reasonable regarding the glutamine-mediated MYC regulation.

Ultimately, we aimed to identify critical molecular targets that mediate the metabolic feedback, which may elucidate new opportunities in cancer therapy.

3. Materials and Methods

A summary of chemicals, kits, equipment, consumables and additional material is listed in the appendix (*supplement* A).

3.1. Cell biology methods

3.1.1. Cell lines and standard cell culture

Cell culture consumables were purchased from Gibco (Thermo Fisher). Cell lines were maintained in Dulbeccos modified Eagle Medium (DMEM, without glucose, glutamine, phenol red and sodium pyruvate) supplemented with 10% fetal bovine serum (FBS, v/v), 2 mM glutamine and 2.5 g/L glucose and cultivated at $37\,^{\circ}$C, 5% CO_2, 21% O_2 and 85% relative humidity. To avoid contact inhibition, cells were passaged on a regular basis (every 2-3 days). Adherent cells at a confluence of 70-80% were washed once with 1x phosphate buffered saline (PBS) and removed from the culture dish surface using TrypLE. When cells detached, fresh medium was added to quench trypsinization. Subsequently, cell suspension was collected and centrifuged (300 x*g*, 2 min). The supernatant was discarded and the cell pellet was resuspended in fresh pre-warmed media. A fraction of the cell suspension, depending on the cell line's doubling time, was transferred into a new dish.

The cell lines A549, Cos7, GEO, HCT116, HeLa, HEPG2, HT29, MCF7, MDAMB231, RKO, SW480 and U2OS were obtained from ATCC. HEK293 cells were a gift by Prof. Dr. Markus Landthaler (BIMSB/MDC, Berlin-Germany).
HCT116 cells, that were transduced with either MYC estrogen receptor chimera (MYC-ER) or empty vector (EV) to achieve stable overexpression in the presence of 100 nM 4-hydroxytamoxifen (OHT), were provided by Francesca Dejure (Julius-Maximilian University Würzburg, Würzburg-Germany) [Dejure, 2017]. In order to ensure a homogenous cell population, cells carrying a vector were selected via continuous puromycine treatment (1 µg/mL).
CaCO2-empty vector (CaCO2 WT), CaCO2-BRAF^{V600E} (CaCO2 BRAF) and CaCO2-KRAS^{G12V} (CaCO2 KRAS) cells were described previously and were a kind gift by Tilman Brummer (Institute of Molecular Medicine and Cell Research, Center of Biochemistry and Molecular Cell Research (ZBMZ), Freiburg-Germany) [Fritsche-Guenther et al., 2016].

Following selection with 5 µg/mL blasticidine and 5 µg/mL puromycine, stable overexpression of KRAS and BRAF were achieved by the application of 2 µg/mL doxycycline. Cell lines were routinely tested for mycoplasma contamination. Additionally, cells were frequently checked for phenotype transformation. Culture duration was kept below 30 passages after cell thawing.

3.1.2. Cell freezing

Cells were collected as described in *section* 3.1.1. The cell pellet was resuspended in 10% dimethyl sulfoxide (DMSO, v/v) diluted in FBS to lower the freezing temperature. Cell suspension (2-4e+6 cells/mL) was transferred into cryovials and stored in a cell freezing chamber at $-80\,^{\circ}$C. The next day cryovials were moved to the liquid nitrogen tank.

3.1.3. Cell thawing

Immediately after removal from liquid nitrogen cryovials were placed in a $37\,^{\circ}$C water bath. As soon as the cell suspension started to thaw, it was transferred into a falcon tube containing pre-warmed media. After a centrifugation step (300 x*g*, 2 min) the supernatant was discarded, the cell pellet was resuspended in fresh media and transferred into a new dish. Twenty four hours after thawing, media was replaced to remove remaining DMSO.

3.1.4. Cell number determination

Cells were trypsinized and harvested as described in *section* 3.1.1. Numbers of viable cells were determined using trypan blue exclusion. A hundred microliter cell suspension and 100 µL 0.4% trypan blue solution (w/v) were mixed and 10 µL were loaded onto a cell counting slide. Viability and cell number were monitored using the TC20 automated cell counter (Biorad). Each sample was measured in technical duplicates.

3.1.5. Cell transfection

In a 6-well plate 2e+5 cells/well were plated in standard cell culture media and incubated for 24 hrs. Per single well a mixture of 250 µL Opti-MEM and 7.5 µL Lipofectamine2000 was prepared and incubated for 5 min at room temperature. 100 pmol of small interfering RNA (siRNA), diluted in 250 µL Opti-MEM, were added to diluted Lipofectamine2000, mixed by gentle pipetting and incubated for another 20 min at room temperature. Cell culture media was renewed and 500 µL of formed DNA-lipid complexes were added dropwise. After 6-16 hrs transfection was repeated in the same manner. Forty-eight hours post first transfection glutamine starvation and re-addition experiments were performed.

3.1.6. Glutamine starvation and re-addition experiments

Cells were plated in standard cell culture media and cultured for at least 24 hrs. In order to starve cells for glutamine, cells were washed once with 1x PBS and glutamine-free media was added. If not indicated differently glutamine was added to the media in a final concentration of 2 mM after 16 hrs of starvation. The following substances, corresponding abbreviations and concentrations are shown in brackets, were added instead of glutamine in separate experiments: Glutamate (E, 2 mM), Dimethyl α-ketoglutarate (DMαKG, 7 mM), Dimethyl succinate (DMSuc, 7 mM), Dimethyl fumarate (DMFum, 200 µM), Dimethyl malate (DMMal, 200 µM), Aspartate (Asp, 2 mM), Asparagine (Asn, 2 mM), Adenosine (Ado, 150 µM), Guanosine (Guo, 150 µM), Uridine (Urd, 150 µM), Thymidine (Thd, 150 µM), Cytidine (Cyd, 150 µM), N-acetyl cysteine (NAC, 10 mM) and Forskolin (10 µM).

Inhibitor studies were performed after inhibitor was applied for 16 hrs with either starvation media or standard cell culture media. *Table* 3.1 lists all inhibitors in the applied concentrations as well as their targets.

Table 3.1.: Inhibitors applied in *in vitro* experiments.
Abbreviations – 2',5'-dd-Ado: 2',5'-dideoxy Adenosine, BPTES: Bis-2-(5-phenylacetamido-1,3,4-thiadiazol-2-yl)ethyl sulfide, C968: Compound 968, DON: 6-Diazo-5-oxo-L-norleucine, ETC: Electron transport chain, mTORC1: mTOR complex 1, TTFA: Thenoyltrifluoroacetone.

Inhibitor	$[c]_{final}$	Target	Reference
2',5'-dd-Ado	50 µM	Adenylyl cyclase	Laux et al. [2004]
DON[*]	10 µM	Glutaminase 1&2	Chen and Cui [2015]
AZD4226	1 µM	MEK	Huang et al. [2013]
BPTES	10 µM	Glutaminase 1	Chen and Cui [2015]
CB839	10 µM	Glutaminase 1	Chen and Cui [2015]
C968	10 µM	Glutaminase 1	Chen and Cui [2015]
LY294002	10 µM	PI3K	Gharbi et al. [2007]
MDL-12,330A	50 µM	Adenylyl cyclase	Boettcher et al. [2014]
Oligomycin	10 µM	ATP synthase	Hao et al. [2010]
PKAi, 14-22 Amide	10 µM	Protein kinase A	Glass et al. [1989]
Rapamycin	20 nM	mTORC1	Ballou and Lin [2008]
SB203580	10 µM	p38	Cuenda and Rousseau [2007]
TTFA	500 µM	Complex II of ETC	Kluckova et al. [2013]

[*] glutamine structural analogue, inhibition of enzymes that use glutamine as a substrate

3.1.7. Cell harvest

Media was discarded, cells were washed once with 1x PBS, scratched and transferred to a 1.5 mL reaction tube. Cells were pelleted by centrifugation (2 min, 300 xg, 4 °C) and the supernatant was removed. Afterwards, cell pellets were snap-frozen in liquid nitrogen and stored at −20 °C until further processing. Samples were used to generate RNA or protein extracts.

3.2. Molecular biological methods

In order to avoid any nuclease activity, nuclease-free H_2O, nuclease-free reaction tubes and pipetting tips were used during all procedures.

3.2.1. Quantification of nucleic acids

The concentration of nucleic acids in solutions was determined spectrophotometrically using the Nanophotometer Classic (Implen) by detecting the absorbance at $\lambda = 260$ nm. Before measurement the photometer was calibrated with the blank solvent. In order to validate the purity of nucleic acid solution the ratio to the absorption at the wavelength at $\lambda = 280$ nm (pure DNA: ≈ 1.8, pure RNA: ≈ 2.0) was determined.

3.2.2. Nucleic acid electrophoresis

In order to validate synthesized DNA and RNA fragments 0.4-1 µg of nucleic acids diluted in 6x loading dye were loaded onto a pre-casted 3% TAE gel containing ethidium bromide. RNA samples were denatured for 5 min at 70 °C followed by a snap cooling step before the gel run. Nucleic acid separation was carried out at 75 V for one hour in an electrophoresis chamber containing 1x TAE buffer (40 mM TrisBase, 1 mM ethylenediaminetetraacetic acid (EDTA, pH 8), 20 mM acetic acid, diluted in H_2O). Either DNA or RNA ladder was used to predict the size of nucleic acid fragments. The UV transillumination imaging was carried out using the ImageQuant LAS4000 system (GE Healthcare) at a wavelength of $\lambda = 312$ nm.

3.2.3. Extraction of RNA

Isolation of total RNA

RNA extraction was performed using the QIAGEN RNeasy Mini Kit in combination with the QIAGEN cell-lysate homogenizer QIAshredder according to the manufacturer's instructions. Briefly, total RNA was extracted by the resuspension of cells in 350 µL RLT lysis buffer. Cell lysates were transferred to QIAshredder columns and centrifuged at maximal speed for 2 min. The flow-through was mixed with an equal volume of 70% EtOH (v/v) and immediately transferred to the RNeasy Mini spin column and centrifuged for 15 s at maximal speed followed by three washing steps to exclude contaminants. The isolated RNA was eluted with 30 µL nuclease-free H_2O and stored at -20 °C.

Phenol-chloroform extraction of RNA

To purify RNA, generated by *in vitro* transcription, the preparation mixture was homogenized with three volumes of TRIzol LS Reagent, vortexed and incubated for 5 min at room temperature. The extraction of RNA was carried out by the addition of 0.2 mL chloroform per 0.75 mL TRIzol LS, followed by 15 min incubation at room temperature and subsequent centrifugation (maximum speed, 15 min, 4 °C) to allow phase separation. The upper clear aqueous layer, containing the RNA, was mixed with an equal volume of isopropanol to precipitate the RNA. Finally, the RNA pellet was washed with 75% EtOH (v/v) and air-dried before it was resuspended in 50 µL nuclease-free H_2O and stored at -20 °C.

Phenol-isoamyl alcohol extraction of biotinylated RNA

To purify RNA from biotinylation reaction, the preparation mixture was diluted in an equal volume of chloroform-isoamyl alcohol (24:1, v/v), vortexed and centrifuged (max. speed, 3 min, 4 °C) to allow phase separation. RNA was precipitated by the addition of 10 µL of 5 M NaCl, 1 µL glycogen and 300 µL ice-cold EtOH followed by an overnight incubation at -80 °C. RNA pellet was washed with 75% EtOH (v/v), air-dried and finally dissolved in 20 µL nuclease-free H_2O. Purified biotinylated RNA was used directly for pull-down experiments.

3.2.4. Polymerase chain reaction (PCR)

PCR amplification of DNA fragments

PCR was performed to amplify *MYC* 3'-UTR from a plasmid DNA template and to introduce the RNA polymerase promoter site (T3 promoter) upstream of the sequence to enable *in vitro* transcription. In order to guarantee fidelity of amplified DNA fragments the Platinum SuperFi PCR Master Mix (Thermo Scientific), which uses a proofreading DNA polymerase, was applied. The PCR reaction setup is shown in *table* 3.2 and *table* 3.3.

Table 3.2.: Components and preparation of single PCR reaction

Component	Volume
Nuclease free H_2O	19 µL
2x Platinum Superfi PCR MasterMix	25 µL
10 µM forward primer	3 µL
10 µM reverse primer	3 µL
50 ng/µL DNA template	1 µL
Total	**50 µL**

Table 3.3.: PCR thermal cycler program

Step	Temperature	Time	
Initial denaturation	98 °C	30 s	
Denature	98 °C	10 s	
Anneal	63 °C	10 s	**35 cycles**
Extend	72 °C	30 s	
Final Extension	72 °C	5 min	
Cooling	4 °C	-	

Forward and reverse primers were designed to have approximately the same melting temperature (T_m). The calculation of annealing temperature was done using the online T_m calculator tool of Thermo Scientific[1]. Primer sequences are summarized in the appendix (*supplemental table* A.5). Amplified DNA was stored at -20 °C.

Reverse transcription PCR (RT-PCR)

Single stranded complementary DNA (cDNA) was synthesized from 1 µg of RNA using the High-Capacity cDNA Reverse Transcription Kit (Thermo Scientific). RNA was diluted in 10 µL of nuclease-free H_2O, mixed with an equal volume of reaction mix (*table* 3.4) and incubated for 10 min at 25 °C, followed by 120 min at 37 °C and 5 min at 85 °C, before samples were cooled down to 4 °C. Synthesized cDNA was stored at -20 °C.

Table 3.4.: Components and preparation of single reverse transcription reaction

Component	Volume
Nuclease-free H_2O	3.2 µL
10x RT buffer	2.0 µL
10x RT random primer	2.0 µL
100 nM dNTP mix	0.8 µL
50 U/µL reverse transcriptase	1.0 µL
RNAse inhibitor	1.0 µL
Total	**10.0 µL**

Quantitative real-time PCR (qPCR)

The expression of mRNA was assessed by an absolute quantitative real time PCR based on a TaqMan assay (Thermo Scientific). Total RNA was isolated and *in vitro* transcribed as described in *section* 3.2.3 and *section* 3.2.4. In total 50 ng of cDNA were used as template. A simultaneous amplification and measurement of two target sequences (*MYC* and *PGK1*) in one reaction, a so called duplex reaction, was set up as indicated in *table* 3.5.

---

[1]https://www.thermofisher.com/de/de/home/brands/thermo-scientific/molecular-biology/molecular-biology-learning-center/molecular-biology-resource-library/thermo-scientific-web-tools/tm-calculator.html

Table 3.5.: Components and preparation of single qPCR

Component	Volume
Nuclease-free H_2O	7.0 µL
2x TaqMan gene expression master mix	2.0 µL
20x *MYC* probe, FAM-labeled	1.0 µL
20x PGK1 probe, VIC-labeled	1.0 µL
50 ng/µL cDNA template	1.0 µL
Total	**20.0 µL**

A non-template control was tested in parallel to ensure proper experimental handling. The housekeeping gene phosphoglycerate kinase 1 (*PGK1*) was used as an endogenous control in order to correct sample preparation related variations. The reaction was performed applying the following protocol on the Applied Biosystems StepOne Real-Time PCR System (*table* 3.6).

Table 3.6.: qPCR thermal cycler program

Step	Temperature	Time	
UDG incubation	50 °C	2 min	
Enzyme activation	95 °C	10 min	
Denature	95 °C	15 s	
Anneal & Extend	60 °C	1 min	**40 cycles**
Cooling	4 °C	-	

The cycle number at which the accumulation of a fluorescent signal crosses the internal set threshold, the so called threshold cycle value (Ct), for every transcript in each sample was determined by the StepOne software (Applied Biosystems). The normalization of data was done by applying the double delta Ct method. Firstly, the difference (ΔCt) between the expression of the reference gene (*PGK1*) and the target gene (*MYC*) was determined and the fold change of expression was calculated as following: fold change $_{mRNA} = 2^{-\Delta\text{CT}}$. Secondly, biological replicates were averaged and the ratio between the glutamine starved and non-starved condition was calculated.

3.2.5. *In vitro* transcription

In vitro transcription was performed using the Thermo Scientific MEGAscript T3 transcription Kit according to the manufacturer's instructions. PCR amplified DNA fragments with upstream RNA polymerase promoter site (T3 promoter) were directly used as template as recommended by the protocol. Reaction mixture was prepared at room temperature as indicated in *table* 3.7 and incubated overnight at 37 °C under constant agitation.

One microliter of Turbo-DNase (2 U/µL) was added to the reaction mixture and incubated for another 15 min at 37 °C to digest the DNA template. Subsequently, the transcription

Table 3.7.: Components and preparation of single *in vitro* transcription reaction

Component	Volume
Nuclease-free H_2O	6.0 µL
10x reaction buffer	2.0 µL
75 mM ATP solution	2.0 µL
75 mM GTP solution	2.0 µL
75 mM CTP solution	2.0 µL
75 mM UTP solution	2.0 µL
0.1 µg/µL DNA template	2.0 µL
T3 RNA polymerase	2.0 µL
Total	**20.0 µL**

prep was diluted with 115 µL nuclease-free H_2O. Fifteen microliter of acetate stop solution (5 M ammonium acetate, 100 mM EDTA) were added to the reaction before cRNA was extracted via phenol-chloroform as described in *section* 3.2.3.

3.2.6. Biotinylation of RNA

The biotinylation of nucleic acids is a powerful tool to study protein-RNA interactions due to its high affinity and specificity to streptavidin. In order to identify interaction partners of the *MYC* 3'-UTR, the RNA fragment was covalently coupled to biotin using Pierce RNA 3'-end Desthiobiotinylation Kit according to the manufacturer's protocol. Briefly, the end labeling was carried out by a T4-RNA ligase, which is able to attach biotinylated cytidine bisphosphate to the 3'-terminus of a RNA strand. *In vitro* transcribed cRNA was purified via phenol-chloroform extraction to remove proteins and free nucleotides prior to ligation. In order to relax the secondary structure, RNA required heating (85 °C, 5 min) followed by a slow cool down to room temperature before reaction mixture was set up in a 0.5 mL nuclease-free reaction tube as given in *table* 3.8.

The reaction was incubated for 16 hrs at 16 °C under constant agitation (300 rpm). Eventually, the reaction was stopped by the addition of 70 µL nuclease-free H_2O before biotinylated RNA was isolated via phenol-isoamyl alcohol and precipitated in EtOH as described in *section* 3.2.3.

The bioinylation efficiency was evaluated via dot blots. Dilution series of sample RNA and 100% biotinylated control RNA were prepared and 2 µL of each dilution were spotted onto a positively charged nylon membrane. After absorption nucleic acids were immediately UV crosslinked to the membrane using the UV crosslinker XLE-1000 (Spectroline). The detection of biotinylated RNA was carried out using the Thermo Scientific Chemoluminescent Nucleic Acid Detection Module Kit. Briefly, the membrane was blocked, incubated with streptavidin coupled horseradish peroxidase (HRP), developed using an enhanced luminol substrate and imaged by the ImageQuant LAS4000 system (GE Healthcare).

Table 3.8.: Components and preparation of single RNA ligation reaction

Component	Volume
Nuclease-free H_2O	6.0 µL
10x RNA ligase reaction buffer[*]	3.0 µL
1 nmol/µL biotinylated cytidine bisphosphate	1.0 µL
40 U/µL RNase inhibitor	1.0 µL
40 U/µL T4-RNA ligase	2.0 µL
25 pmol/µL RNA	2.0 µL
PEG 30%	15.0 µL
Total	**30.0 µL**

[*] 500 mM TrisHCl, 100 mM $MgCl_2$, 100 mM DTT, 10 mM ATP, pH 7.8

3.2.7. Single-molecule RNA fluorescence *in situ* hybridization (smFISH)

Cell culture and sample preparation

Acid washed, circular cover slips (Ø18 mm) were placed into individual wells of a 12-well plate and incubated with 600 µL of coating solution (33 µg/mL poly-D-lysine, 2 µg/mL laminin, diluted in 1x PBS) for 10 min at room temperature. Coating solution was removed and cover slips were washed twice with 600 µL of 1x PBS to remove excess coating or preservatives. Per well 1e+5 cells were plated in standard culture media. After 24 hrs of incubation, cells were washed once with 1x PBS and media containing 2 mM or 0 mM glutamine was added for 16 hrs.

Fixation and permeabilization

Cells were placed immediately on ice and washed with ice-cold 1x PBS containing 100 µM $MgCl_2$ and 100 µM $CaCl_2$. In order to fixate cells on cover slips, cells were incubated with 600 µL fixation solution (4% formaldehyde (v/v), 100 µM $MgCl_2$, 100 µM $CaCl_2$, diluted in 1x PBS) for 10 min at room temperature. Afterwards, cells were washed with 1x PBS, placed on ice and 1 mL ice-cold 70% EtOH (v/v) was added to permeabilize cells at 4 °C overnight.

Hybridization

To prepare samples for hybridization EtOH was aspired and the fixed cells were incubated for 5 min with 1 mL of washing buffer (10% formamide (v/v), 2x saline-sodium citrate buffer (SCC)). Stellaris probes against *MYC* and cyclin A2 (*CCNA2*) (Biosearch Technologies) were hybridized at a concentration of 50 nM with a stringency of 10% formamide at 37 °C overnight. Samples were washed with 1 mL of washing buffer for at least 30 min

at 37 °C in the dark. Subsequently, nuclei were stained by applying 1 mL of DAPI solution (5 ng/mL in washing buffer). After staining for at least 30 min at 37 °C in the dark, DAPI solution was removed and samples were washed twice with 1 mL of 2x SCC buffer.

Imaging

In order to avoid photo-bleaching cover slips were equilibrated for 2 min in 1 mL of GLOX buffer (2x SCC, 0.4% glucose (w/v), 10 mM TrisHCl (pH 8), diluted in nuclease-free H_2O), before 15 µL of GLOX buffer supplemented with glucose oxidase and catalase were added to the cover slips that were immediately mounted on a glass slide and sealed. Images were acquired on an inverted Nikon Ti microscope with a Hamatsu ORCA R2 CCD camera, a 60x NA 1.4 oil objective and Nikon NIS-Elements Ar software (version 4), using an exposure time of 40 ms for DAPI and 1 s for Quasar 670. Groups of cells were chosen in the DAPI channel; Z-stacks were acquired in the Quasar 670 channel using 0.3 µm spacing of 31 layers [Memczak et al., 2013]. Images were processed with the image processing program Fiji [Schindelin et al., 2012]. Monochrome images were stacked and merged using maximum intensity. Eventually, color overlays were generated.

3.3. Biochemical methods

3.3.1. Preparation of whole cell lysates

Cell pellets were thawed on ice. According to the size of the cell pellet, RIPA buffer (50 mM TrisHCl (pH 7.9), 140 mM NaCl, 1 mM ETDA, 1% Triton x-100 (v/v), 0.1% Na-deoxycholate (v/v), 0.1% sodium dodecyl sulfate (SDS, w/v)) supplemented with protease and phosphatase inhibitor was added to the samples. Cells were resuspended intensively before they were chilled on ice for 10 min. Afterwards, samples were sonificated for 25 s (Bandelin Sonorex Digitec DT 100) and vortexed for 10 s. In total three cycles of incubation on ice, sonification and vortexing were performed. Cell debris was removed by centrifugation (maximal speed, 5 min, 4 °C). The protein concentration of cleared lysates was determined as described before (*section* 3.3.2). In total 40 µg of protein were diluted in 2x SDS sample buffer (50 mM TrisBase (pH 6.8), 100 mM dithiothreitol (DTT), 2% SDS (w/v), 10% glycerol (v/v), 10 g/L bromphenol blue, diluted in H_2O), snap-frozen and stored at −20 °C for later sodium dodecyl sulfate polyacrylamide gel electrophoresis (SDS-PAGE) analysis.

3.3.2. Quantification of proteins

The determination of protein concentration was carried out with the colorimetric Pierce BCA Protein Assay Kit (Thermo Scientific). As given by the manufacturer 2 µL of cell lysate and bovine serum albumin (BSA) standard dilution (50-10,000 µg/mL, diluted in 1x PBS) were mixed with 100 µL of working solution and incubated for 30 min at room temperature. The color development was detected at a wavelength of $\lambda = 562$ nm (Infinite2000, Tecan). Each sample was measured in technical duplicates. A negative control (1x PBS) was treated in parallel to correct for the background signal.

3.3.3. SDS-PAGE

SDS-PAGE was performed according to Laemmli [Laemmli, 1970]. Forty micrograms of protein were diluted in 2x SDS sampling buffer and denatured for 5 min at 95 °C under constant agitation. Samples were chilled on ice, spun down and loaded onto a self-casted SDS polyacrylamide gel (*supplemental table* A.11), suitable for the separation of proteins of interest. The PageRuler pre-stained protein ladder (Thermo Scientific) was used as a molecular weight marker. The discontinuous electrophoresis was carried out at 60-135 V in the Biorad Mini Protean system filled with 1x SDS running buffer (25 mM TrisBase, 190 mM glycine, 0.1% SDS (w/v), diluted in H_2O, pH 8.3).

3.3.4. Western blot

After separation proteins were transferred onto a polyvinylidene difluoride (PVDF) membrane for 30 min (25 V, 1 A) by using the Biorad Trans-Blot Turbo Transfer system – a semi-dry blotting system. For proteins of high molecular weight ($\geq$ 150 kDa) the procedure was prolonged to 60 min. In order to guarantee a sufficient transfer, the PVDF membrane was activated in MeOH, subsequently washed in H_2O and equilibrated as well as the gel and the filter paper in blotting buffer (48 mM TrisBase, 40 mM glycine, 0.075% SDS (w/v), 20% MeOH (v/v), diluted in H_2O) prior to western blot assembly. Afterwards, the membrane was blocked with 5% milk or 1-5% BSA (w/v) in TBS-T (1x TBS (20 mM TrisBase, 137 mM NaCl), 0.1% Tween-20 (v/v)) for 30-60 min at room temperature. Probing with the primary antibody was performed overnight at 4°C. The next day, membrane was washed three times for 10 min in TBS-T and probed with a HRP-coupled secondary antibody, according to the species of the primary one, for another hour at room temperature. Three additional washing steps with TBS-T, each 10 min, were performed before the antibodies were exposed on the ImageQuant LAS4000 system (GE Healthcare) using Amersham ECL Western Blotting detection solution (GE Healthcare) according to the manufacturer's protocol. For the relative quantification of protein expression the image processing program ImageJ was used [Schneider et al., 2012]. Expression levels were normalized to a loading control.

In case several proteins needed to be investigated, membranes were stripped for reprobing. Therefore membranes were incubated with stripping buffer (200 mM glycine, 0.1% Tween-20 (v/v), diluted in H_2O, pH 2.5) for 30 min at room temperature, followed by three washing steps using 1x TBS. Subsequently, membranes were blocked and reprobed with a different primary antibody.

3.3.5. Multiplex bead-based immunoassay

The high-throughput Bio-Plex method was used to simultaneously examine multiple phosphorylation events of various cellular signaling pathways. The multiplexed bead-based approach combines properties of enzyme-linked immunosorbant assays (ELISA) and flow cytometry. In a single sample various analytes are identified as they are recruited to Multiplex Assay Beads that harbor different spectral addresses for their identification. The abundance of analytes is determined via streptavidin reporters coupled to biotin-labeled antibodies against the target epitope.

The assay was carried out using the Bio-Plex Cell Lysis Kit and the Bio-Plex ProCell Signaling Assay (Biorad) according to the manufacturer's protocol with modifications. Briefly, glutamine starvation and re-addition experiments were performed as end-point experiments in 24-well plates. After media removement, 30 µL of Bio-Plex lysis buffer, supplemented with 1x factor QG and 2 mM phenylmethylsulfonyl fluoride (PMSF), were

added per well. Plates were sealed and stored for at least 30 min at $-80\,^{\circ}$C to lyse the cells. Afterwards, protein concentration was determined as described in *section* 3.3.2 and 15 µg of sample were diluted in 50 µL of cell lysis buffer. A selection of 15 beads, each coupled to antibodies against different epitopes, were prepared in a light-protected 96-well plate and washed twice with wash buffer before diluted cell lysates were added to the beads. Plate was sealed and incubated overnight in the dark under constant agitation (450 rpm). The next day beads were washed three times with 100 µL washing buffer to remove non-binding molecules. Afterwards, beads were incubated with 25 µL of 1x biotin-labeled detection antibodies (diluted in antibody diluent), specific for a secondary epitope on each target for 30 min. After three washing steps with 100 µL washing buffer, beads were mixed with 25 µL of 1x fluorescently labeled streptavidin reporter (diluted in antibody diluent) for 10 min and rinsed as explained before. After the resuspension of beads in 75 µL assay buffer the bead signature as well as the intensity of the reporter signal per bead were simultaneously detected via the Bio-Plex array reader 200 (Biorad).

3.4. Proteomics

3.4.1. Preparation of whole protein lysates

For shotgun proteome analysis cells were lysed in 300 µL urea buffer (8 M Urea, 100 mM TrisHCl (pH 8.5)) followed by sonification and centrifugation for 5 min at max. speed at 4 °C. Lysates used in RNA pull-down analysis were prepared by the addition of nuclease-free, ice-cold IP lysis buffer (25 mM TrisHCl (pH 7.4), 150 mM NaCl, 1 mM EDTA, 1% NP-40 (v/v), 5% glycerol (v/v)) supplemented with protease and phosphatase inhibitor cocktails. Afterwards, samples were incubated for 10 min at 4 °C under constant shaking, followed by a 10 min centrifugation at maximum speed at 4 °C. Cleared supernatants were transferred into new reaction tubes and subsequently protein concentrations were determined as described in *section* 3.3.2.

3.4.2. Sample preparation for RNA pull-down analysis

Natural binding partners of the *MYC* 3'-UTR were identified via a RNA pull-down assay. As illustrated in *figure* 3.1 the biotin end-labeled RNA template was generated first. Briefly, the 3'-UTR of *MYC*, that was available on a plasmid, was amplified and extended by the T3 RNA polymerase promoter site upstream of the sequence via PCR as described in *section* 3.2.4. The *in vitro* transcription and following biotinylation of the 3'-terminus of the RNA strand were performed as indicated in *section* 3.2.5 and *section* 3.2.6, respectively.

The RNA pull-down assay was carried out using the Pierce Magnetic RNA-Protein Pull-Down Kit (Thermo Scientific). In order to avoid any nuclease activity, nuclease-free H_2O and nuclease-free reaction tubes and pipetting tips were used during all procedures. Fifty microliters of streptavidin magnetic bead solution (10 mg/mL) were transferred into a 1.5 mL reaction tube and washed three times with 20 mM Tris (pH 7.5). Afterwards, 50 µL capturing buffer (20 mM Tris (pH 7.5), 1 M NaCl, 1 mM EDTA) and in total 50 pmol of end-labeled RNA were incubated with streptavidin magnetic beads for 30 min at room temperature under constant agitation (500 rpm). Three additional washing steps with 20 mM Tris (pH 7.5) were performed. Immobilized RNA was equilibrated with 1x RNA-protein binding buffer (20 mM Tris (pH 7.5), 50 mM NaCl, 2 mM $MgCl_2$, 0.1% Tween-20 (v/v)) before the RNA-protein binding reaction (*table* 3.9) was incubated for 60 min at 4 °C at 500 rpm. RNA-binding protein complexes were washed three times with an equal volume of washing buffer (20 mM Tris (pH 7.5), 10 mM NaCl, 0.1% Tween-20 (v/v)) to remove non-interacting proteins and eluted with 50 µL elution buffer (37 °C, 500 rpm). Eluates were diluted in 200 µL 8 M Urea (2.4 g in 3.2 mL 100 mM TrisHCl (pH 8.5)) to continue with the digestion of proteins as described in *section* 3.4.3. Prepared peptide
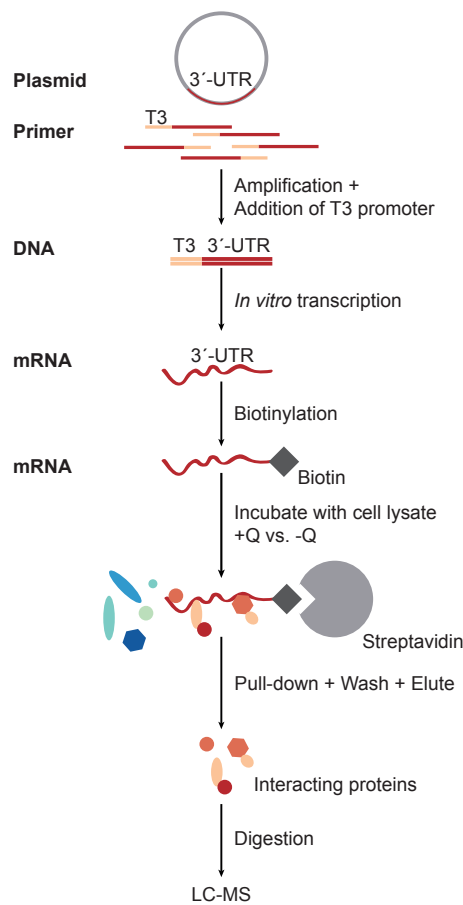
Figure 3.1.: Experimental work flow of RNA pull-down. *MYC* 3'-UTR was amplified and extended upstream by the T3 promoter via PCR to enable *in vitro* transcription. Afterwards, cRNA was biotinylated using T4 RNA ligase. In order to identify RNA interacting proteins the mRNA of *MYC* 3'-UTR was incubated with lysates from HCT116 cells either starved (-Q) or non-starved (+Q) for glutamine. Immobilized streptavidin beads were used to capture biotinylated RNA and to pull-down interacting proteins that were eluted, digested and subjected to LC-MS.

mixtures were measured by liquid chromatography-mass spectrometry (LC-MS) to identify specific RNA-binding proteins (*section* 3.4.4).

An unrelated negative control (poly(A)$_{25}$ RNA) was biotinylated and treated in parallel during the pull-down procedure as well as a bead-control (H$_2$O instead of end-labeled RNA) to exclude unspecific binders. Each sample was incubated with lysates of HCT116 cells that were either cultured in the absence or presence of glutamine for 16 hrs as described in *section* 3.1.6.

3.4.3. Protein digestion

Prior to digestion the denaturation and alkylation of proteins were performed by treating samples with 2 mM DTT (30 min at 25 °C), followed by 11 mM iodoacetamide (20 min at room temperature in the dark). Maximal 100 µg of protein were digested using Lys-C

Table 3.9.: Components and preparation of single RNA binding reaction

Component	Volume
Nuclease-free H_2O	22.5 µL
10x RNA-protein binding buffer[*]	10.0 µL
20 U/µL RNase inhibitor	2.5 µL
2 µg/µL cell lysate	25.0 µL
50% glycerol	30.0 µL
10 mM ATP	10.0 µL
Total	**100.0 µL**

[*] 0.2 M Tris (pH 7.5), 0.5 M NaCl, 20 mM $MgCl_2$, 1% Tween-20 detergent (v/v)

(Wako, 1:40 (w/w), overnight under gentle shaking, 30 °C) and immobilized trypsin beads (Applied Biosystem, 5-10 µL, 4 hrs under rotation, 30 °C). Lys-C digestion products were diluted four times with 50 mM ammonium bicarbonate before continuing the tryptic digestion that was stopped through acidification with 5 µL of triflouracetic acid. For shotgun proteome analysis the corresponding volume of 15 µg of protein was processed further, whereas the whole digestion preparation was used for the pull-down analysis. Peptide mixtures were desalted on Stage Tips, the eluates were dried and reconstituted in 15 µL of 0.5% acetic acid (v/v) [Rappsilber et al., 2007].

3.4.4. LC-MS analysis

Five microliters of each peptide digest were injected in two technical replicates to a liquid chromatography coupled to tandem mass spectrometry system (LC-MS/MS; NanoLC 400 (Eksigent) coupled to Q Exactive Plus (Thermo Scientific)), using a 240 min gradient ranging from 5% to 40% of solvent B (80% acetonitrile, 0.1% formic acid) in solvent A (5% acetonitrile, 0.1% formic acid). For the chromatographic separation 100 cm long MonoCap C18 HighResolution 2000 column (GL Sciences) was used. The nanospray source was operated with spray voltage of 2.4 kV and ion transfer tube temperature of 260 °C. Data were acquired in data dependent mode, with a top10 method (one survey MS scan with resolution 70,000 at m/z 200, followed by up to 10 MS/MS scans on the most intense ions, intensity threshold 5,000). Once selected for fragmentation, ions were excluded from further selection for 45 s, in order to increase the identification rate of lower abundant peptides.

3.4.5. Data analysis

Raw data were analyzed using the MaxQuant proteomics pipeline (version 1.5.3.30) and the built in Andromeda search engine with the human Uniprot database [Cox et al., 2011]. Carbamidomethylation was set as a fixed modification, oxidation of methionine as well as

acetylation of N-terminus as variable modifications. The search engine peptide assignments were filtered at 1% FDR, other parameters were set as default. Peptides with a minimum length of seven amino acids and a maximum of two miscleavages were further processed. The match between runs option was enabled in case of shotgun proteome analysis, but disabled as RNA pull-down data were processed. Label-free quantification, using razor peptides for calculation, has just been performed for shotgun proteome analysis.

The software Perseus (version 1.5.6.0) was used to reveal non-random associations between categories by Fisher exact test, setting the threshold p-value to 0.05 [Tyanova et al., 2016].

3.5. Metabolomics

The method called pulsed stable isotope resolved metabolomics (pSIRM), developed by the group of Dr. Stefan Kempa, was applied due to the fact that short labeling times with ^{13}C-substrates enable time-resolved studies of the central carbon metabolism (CCM) in an instationary manner [Pietzke et al., 2014]. Absolute quantification and isotope incorporation rates were determined for intermediates of the glycolysis, tricarboxylic acid cycle (TCA cycle) and amino acid synthesis by gas chromatography mass spectrometry (GC-MS). Furthermore, a method first described by P. Lorkiewicz and colleagues was adapted and modified to enable the detection of nucleotides besides central carbon metabolites from the same cell culture sample [Lorkiewicz et al., 2012]. The experimental work flow of the method is depicted in *figure* 3.2.
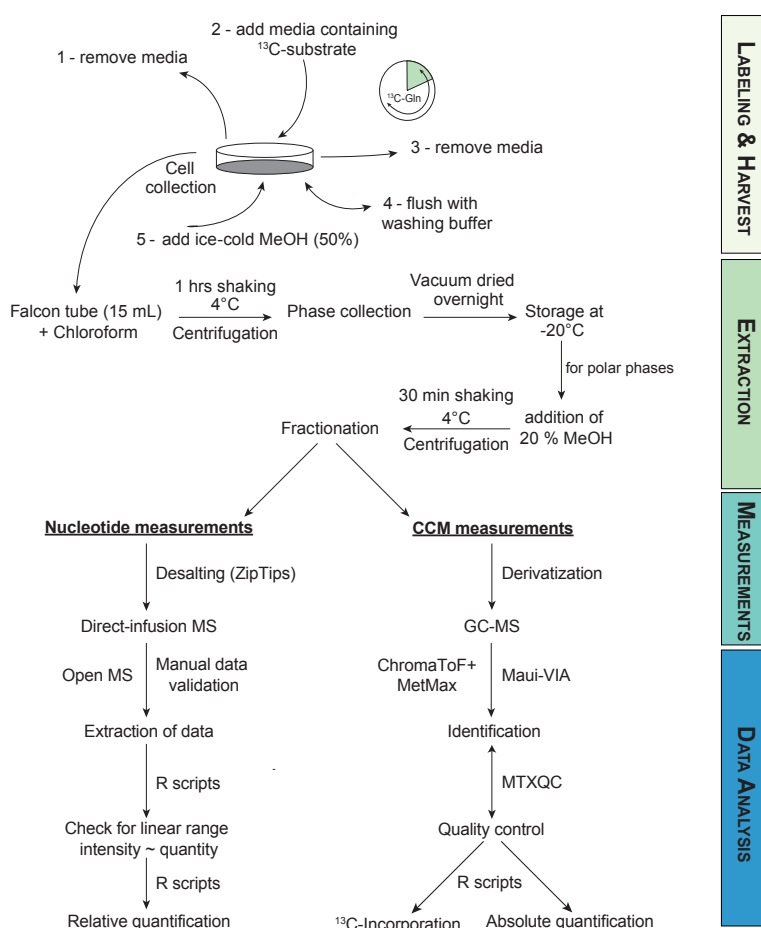
Figure 3.2.: Work flow of mass spectrometry based metabolomics procedures. Cells were incubated with media containing ^{13}C-substrates (e.g.u-^{13}C-glutamine) for distinct short times and their metabolism was quenched subsequently. As metabolites were extracted via methanol-chloroform-water extraction, samples were either derivatized to measure CCM metabolites via GC-MS or desalted to be subjected to direct-infusion MS to detect nucleotides. Data analysis was performed in three steps: (i) data extraction, (ii) quality control of data and (iii) visualization of data by self-written R-scripts.

3.5.1. Cell culture and sample preparation

Adherent cells were plated with a beforehand determined cell number to reach a similar confluence (70-80%) at the time point of harvest. Media was renewed 16 hrs and 4 hrs prior to harvest. Cell culture media was replaced by media containing u-^{13}C-glutamine for experiment-specific time ranges. Cells were quickly washed with buffer (140 mM NaCl, 5 mM HEPES, pH 7.4, supplemented with major carbon sources) to remove extracellular metabolites, but not the main carbon sources. Cells that were not incubated with u-^{13}C-glutamine, but shortly washed with buffer containing ^{12}C-glutamine, were used for the correction of natural isotope abundance. Immediately, cells were quenched with 5 mL ice-cold 50% MeOH supplemented with 2 µg/mL cinnamic acid as an internal extraction standard.

The cells were scratched, collected, transferred into a 15 mL falcon and stored at $-20\,^{\circ}$C until proceeding with metabolite extraction.

3.5.2. Extraction of intracellular metabolites

One milliliter chloroform was added to 5 mL of methanolic cell extracts before samples were shaken for 60 min at $4\,^{\circ}$C and centrifuged at maximum speed for 15 min at $4\,^{\circ}$C for phase separation (methanol-chloroform-water extraction). Equal volumes of polar phases were collected. Each polar phase was split into two aliquots, dried under vacuum and subjected to direct-infusion electrospray ionization (ESI)-MS and to gas chromatography (GC)-MS in order to measure nucleotides and central carbon metabolites from the same sample. The cell extracts were stored at $-20\,^{\circ}$C until preparation for GC-MS or direct-infusion MS measurements.

3.5.3. Measurements of central carbon metabolites via GC-MS

Sample preparation for GC-MS

A quantification dilution series and an identification mixture were treated in parallel with extracts [Pietzke et al., 2014]. Derivatization was carried out as described with modifications [Kempa et al., 2009]. Briefly, cell extracts were resuspended in 20 µL of methoxyamine hydrochloride solution (40 mg/mL MeOx in pyrimidine) and incubated for 60 min at $30\,^{\circ}$C with constant agitation followed by a quick spin down. Eighty microliter of N-methyl-N-[trimethylsilyl] trifluoroacetamide (MSTFA, containing an alkane mixture) were added and incubated at $37\,^{\circ}$C for 90 min with constant shaking. The extracts were centrifuged for 15 min at maximal speed and aliquots of 30 µL were transferred into glass vials for GC-MS measurement.

GC-MS measurements

Metabolite analysis was performed on a gas chromatography coupled to time of flight mass spectrometer (GC-ToF-MS, Pegasus IV-ToF-MS-System, LECO), complemented with an auto-sampler (MultiPurpose Sampler 2 XL, Gerstel). The samples were injected in split mode (split 1:5, injection volume 1 µL) in a temperature-controlled injector (CAS4, Gerstel) with a baffled glass liner (Gerstel). The following temperature program was applied during sample injection: initial temperature of 80 °C for 30 s followed by a ramp with 12 °C/min to 120 °C, a second ramp with 7 °C/min to 300 °C and final hold for 2 min. Gas chromatographic separation was carried out on an Agilent 78903, equipped with a VF-5 ms column of 30 m length, 250 µm inner diameter and 0.25 µm film thickness (Varian). Helium was used as carrier gas with a flow rate of 1.2 mL/min. Gas chromatography was performed with the following temperature gradient: 2 min heating at 70 °C, first temperature gradient with 5 °C/min up to 120 °C and hold for 30 s; subsequently, a second temperature increase of 7 °C/min up to 350 °C with a hold time of 2 min. The spectra were recorded in a mass range of m/z = 60 to 600 mass units with 20 spectra/s at a detector voltage of 1650 V.

Analysis of GC-MS data

The GC-MS chromatograms were processed with the ChromaTOF software (LECO). The Kováts retention index method was applied to transfer retention time into retention index (RI), a unit and system independent constant [Kováts, 1958]. For unambiguous identifications of metabolites of interest identification mixtures were used in order to compare RIs and mass isotopic fingerprints (MIF). Mass spectra data were extracted using the software tool MetMax[2] or the in-house software Maui-VIA [Kuich et al., 2015]. GC-MS measurements were evaluated with the MTXQC script, an in-house developed tool to estimate the quality of machine performance and sample preparation [Zasada, 2017]. Mass isotope distribution of unlabeled metabolites were used for the correction of the natural abundance of isotopes. The theory behind the calculation of label incorporation is described in detail in Pietzke et al. [2014]. Mass fragments that were chosen to calculate the ^{13}C-incorporation are listed in the appendix (*supplemental table* A.13). Absolute quantities were determined by the examination of the peak area in the GC-MS-derived chromatograms and their comparison to quantification standards. Acquired data were normalized to the internal standard cinnamic acid and cell count and calculated in pmol/1e+6 cells.

---

[2]http://gmd.mpimp-golm.mpg.de/apps/metmax/

3.5.4. Measurements of nucleotides via direct-infusion MS

Sample preparation for direct-infusion MS

For the nucleotides extraction, the protocol described by Lorkiewicz et al. [2012] was applied with modifications. Briefly, ZipTips (Millipore) were conditioned by aspirating five times 10 µL of MeOH and then five times 10 µL of buffer A (5 mM hexylamine, pH adjusted to 6.3 with acetic acid). Ten microliters of sample (equivalent to 3e+5 cells) were loaded on the solid phase by eight cycles of aspirating and dispensing, followed by four cycles of washing with 10 µL of buffer A. Elution was performed by aspirating and dispensing twelve times 10 µL of elution buffer (70% buffer A, 30% buffer B (90% MeOH, 10% NH_4AC, pH adjusted to 8.5 with NH_4OH)). The eluted nucleotides were diluted with 20 µL of MeOH before the analysis.

Direct-infusion MS measurements

Direct-infusion mass spectrometry analysis was performed on a TSQ Quantiva triple quadrupole mass spectrometer (Thermo Scientific) coupled to a Triversa Nanomate nanoESI ion source (spray voltage set at 1.5 kV and the head gas pressure at 0.5 psi). Data were acquired in negative mode and the two best transitions for each nucleotide were monitored. The transitions monitored are listed in the supplement (*supplemental table* A.14). On the TSQ Quantiva, argon was used as collision gas at a pressure of 1.5 mTorr. FWHM Resolution for both Q1 and Q3 was set at 0.7. Data were acquired for three minutes, using a cycle time of 3.3 s, resulting in the acquisition of 55 SRM scans for each nucleotide.

Analysis of direct-infusion MS data

Data were manually checked for the quality and processed with the OpenMS package and in-house developed R-scripts. Standard mixtures, containing all monitored nucleotides in a dilution series, were measured with each sample batch to ensure the quantification of nucleotides to be in the quantitative range of detection.

3.6. Statistics

Statistical analysis were performed using the RStudio Desktop software (version 1.1.383). All data are presented as mean $\pm$ SD (standard deviation). Sample sizes are indicated in the figure legends. To test significance between groups two-tailed Students t-tests were executed. The significance levels were set at * $0.01 < p \leq 0.05$; ** $0.001 < p \leq 0.01$; *** $p \leq 0.001$.

4. Results

The main part of this chapter presents work originating from a cooperation with Francesca Romana Dejure and Martin Eilers from the Julius-Maximilian University Würzburg that was published under the title "The *MYC* mRNA 3'-UTR couples RNA polymerase II function to glutamine and ribonucleotide levels" in the EMBO Journal in 2017 [Dejure and Royla et al., 2017]. The majority of the following experiments were performed in parallel in the Eilers laboratory and in the Kempa laboratory, confirming the herein described results.

4.1. Characterization of cellular adaptation to alterations in external glutamine supply

In contrast to normal cells, cancer cells depend on a high conversion rate of glucose into lactate, known as the Warburg effect, in order to provide energy and macromolecules for their enhanced growth and survival. Paradoxically, several studies reported that oncogenic transformed cells additionally rely on the supply of external glutamine, although the non-essential amino acid can be synthesized from glucose. Furthermore, it is known that *c-MYC* (*MYC*) transformed cells upregulate their glutamine metabolism with the consequence of glutamine addiction [Wise et al., 2008; Yuneva et al., 2007]. The following experiments were performed to investigate the dependencies of glutamine supply on MYC and cell growth in cancer cells.

4.1.1. Cell growth and MYC expression depend on glutamine supply

In order to evaluate the effects of external glutamine supply, the colon cancer cell line HCT116 was cultured in media containing different glutamine concentrations (0-6 mM). After 24 hrs media was renewed to avoid nutrient limitation. Viable cell count as well as MYC protein expression were examined after 48 hrs (*figure* 4.1).
HCT116 cells did not proliferate in the absence of glutamine, but continuously increased cell numbers upon glutamine supplementation up to the physiological levels of the amino acid (0.6-0.9 mM) [Hensley et al., 2013]. Above this concentration range cell growth remained constant and slightly declined at high glutamine levels (2-6 mM).
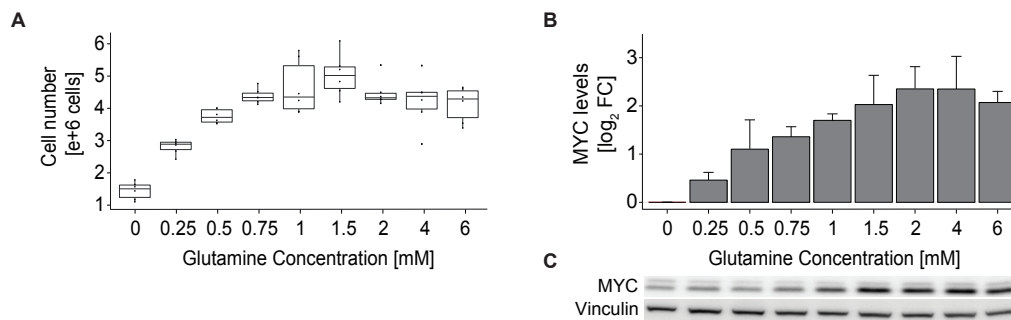
Figure 4.1.: Effects of glutamine availability on cellular growth and MYC protein expression. (A) Viable cell numbers per Ø10 cm dish and (B) quantification of MYC protein expression in HCT116 cells that were cultured for 48 hrs in media containing indicated glutamine concentrations. 1.5e+6 cells were plated per Ø10 cm dish. Results represent mean + SD of at least four independent experiments. (C) Representative immunoblot shows MYC protein levels in HCT116 cells cultured as described before. Data confirm recently published results shown in figure 1E in Dejure and Royla et al. [2017].

Similar effects were observed for MYC protein expression as MYC was drastically down-regulated upon glutamine starvation. MYC protein levels increased with the elevated supply of glutamine in the cell culture media, but remained stable in the presence of high glutamine.

4.1.2. Time-resolved analysis of MYC protein expression upon glutamine starvation and re-addition

A kinetic experiment was performed to characterize the dependency of MYC protein expression on external glutamine availability. HCT116 cells plated in standard cell culture media were starved of glutamine for 16 hrs, followed by re-addition of the amino acid for up to 4 hrs. The experimental setup has been described in greater detail in *section* 3.1.6. During the time course samples were collected frequently as indicated in *figure* 4.2 and analyzed by western blot.

Quantification of protein expression revealed a continuous and pronounced decline of MYC over time in the absence of glutamine (*figure* 4.2 A). An eleven fold decrease in MYC protein was observed following 16 hrs of starvation. Interestingly, after one hour of glutamine supplementation MYC protein increased seven fold. Already within 30 min MYC protein levels were doubled (*figure* 4.2 B). The potential to rapidly recover MYC was shown to be independent of the time cells lack glutamine prior to re-addition (*figure* 4.2 C). HCT116 cells were starved for 40 and 64 hrs before glutamine was replenished. The MYC recovery kinetics based on longer periods of glutamine deprivation were similar to the one of 16 hrs starvation.
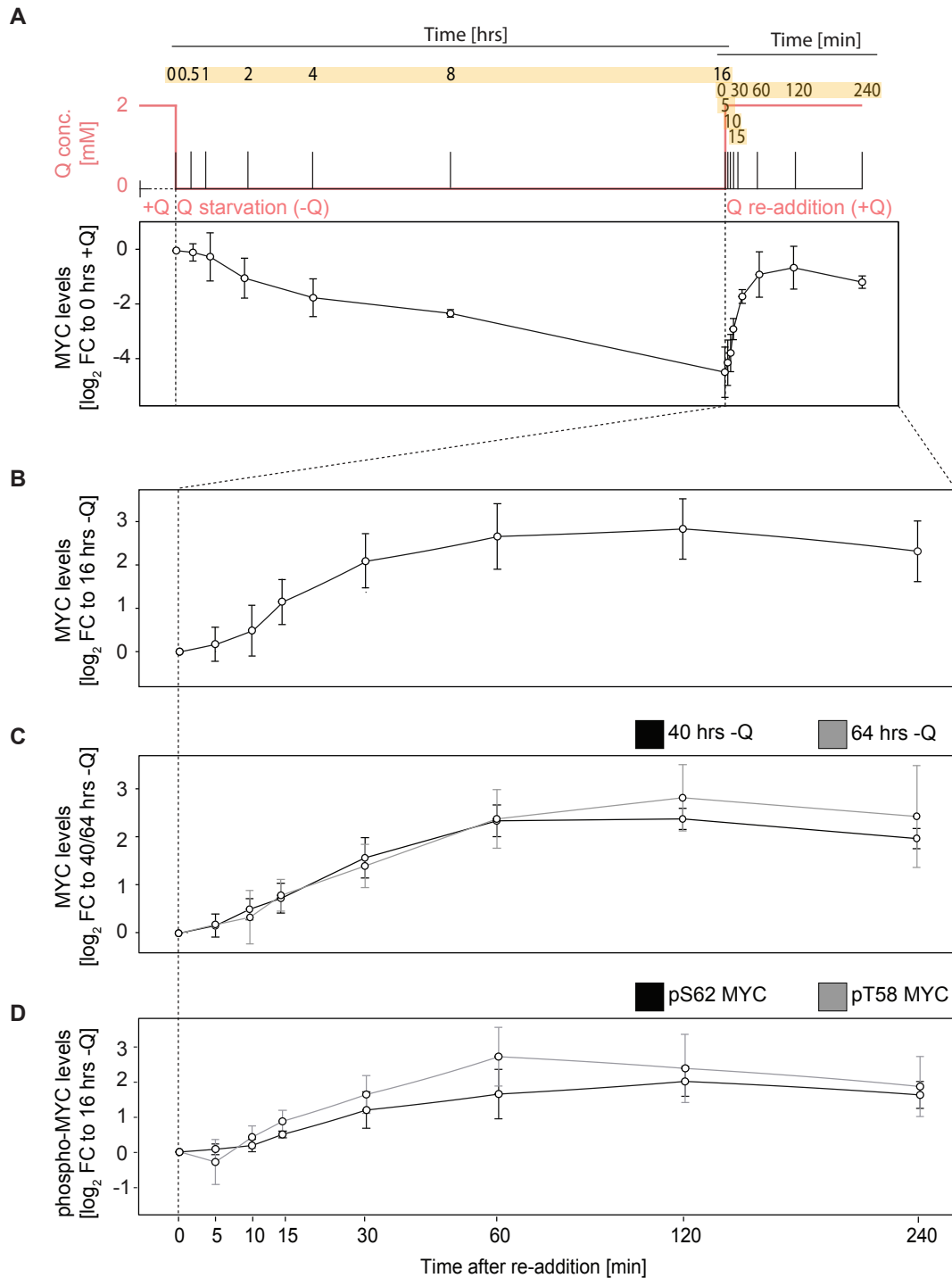
Figure 4.2.: Time-resolved analysis of glutamine starvation and re-addition.
(A) Experimental setup and quantification of MYC protein levels in HCT116 cells starved for 16 hrs (-Q), followed by re-addition of glutamine (+Q) at the indicated time points (yellow). Each value was normalized to +Q at time point 0 hrs (n=4). (B) Kinetic of quantified MYC protein expression after re-addition of glutamine upon starvation for 16 hrs (n=4) and (C) glutamine starvation for 40 hrs or 64 hrs (n=3). Each value was normalized to -Q. (D) Quantification of MYC phosphorylation sites Ser62 and Thr58 over re-addition time course after glutamine starvation. Each value was normalized to -Q at time point 16 hrs (n=3). Protein expression was normalized to Vinculin levels. Results represent mean $\pm$ SD of indicated number of independently performed experiments. Data of panel (B) were published in figure 1F in Dejure and Royla et al. [2017].

Starvation and re-addition experiments were performed using a glutamine concentration of 2 mM, that is above the physiological glutamine concentration in human plasma (0.6-0.9 mM) [Hensley et al., 2013]. In addition, a time course analysis applying 0.5 mM glutamine was executed in order to examine the physiological impact (*supplemental figure* B.1). MYC levels declined with a shallow gradient when cells were deprived for glutamine. The diminished effect was seen as well for the re-addition of the amino acid. Nevertheless, experiments demonstrated the ability to downregulate and to recover MYC protein levels in response to glutamine alterations. In order to further investigate the rapid MYC regulation, experiments were performed at 2 and 0 mM glutamine and 16 hrs glutamine starvation. Short-time effects were analyzed using read-outs obtained 5, 10, 15 min after re-addition of glutamine, while the investigation of long-time effects was based on measurements 30, 60, 120 and 240 min after glutamine re-addition.
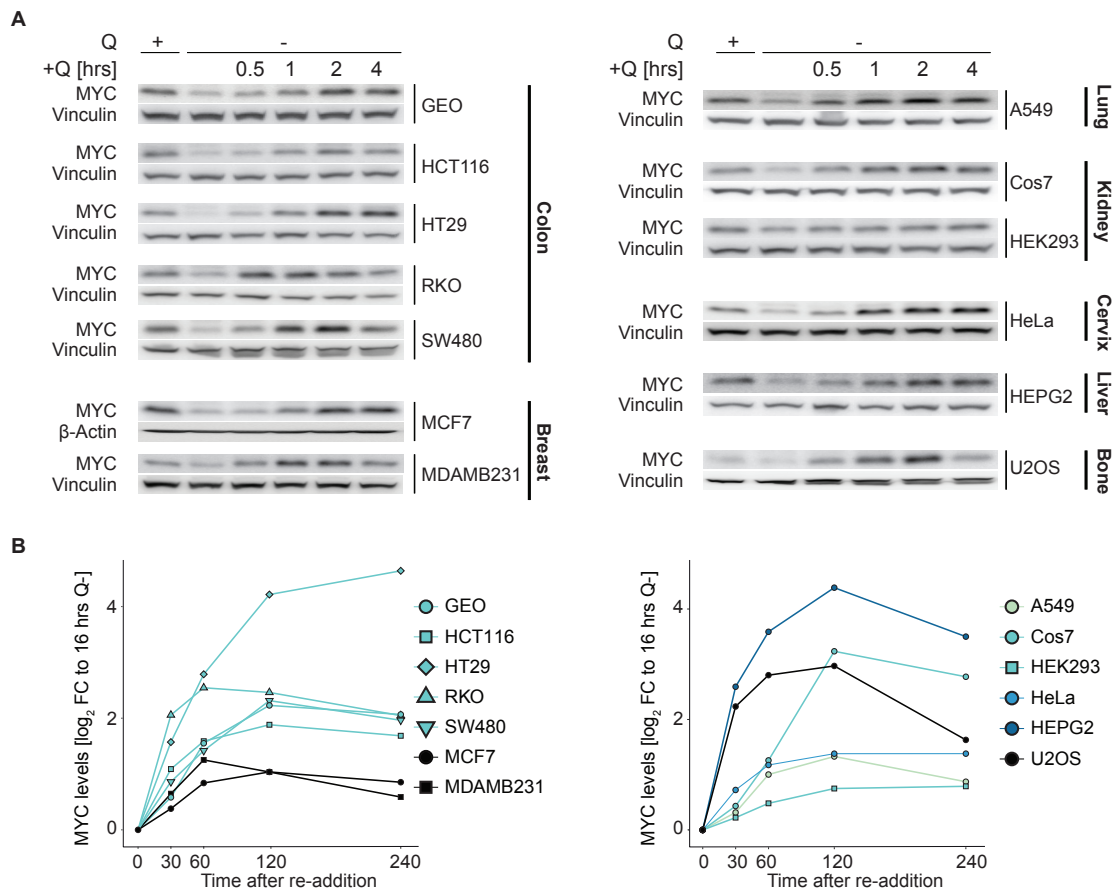
Figure 4.3.: Time-resolved analysis of MYC protein after glutamine re-addition in various cell lines. (A) Representative immunoblots illustrate MYC regulation upon glutamine starvation for 16 hrs and subsequent re-addition of glutamine in various cell lines. (B) Quantification of MYC protein expression of at least two independent experiments. MYC levels were normalized to protein levels of the loading control. Each value was normalized to -Q at time point 16 hrs. Cell lines are colored according to their tissue origin as indicated in panel A.

A number of excellent reviews illustrated MYC's functional significance in diverse cellular processes such as apoptosis, cell cycle progression and cellular growth and differentiation. MYC's ability to regulate a tremendous number of genes is accompanied by the requirement to be tightly regulated in normal cells [Vervoorts et al., 2006; Dang, 2012]. The capability of glutamine – one of the main carbon sources fueling the central carbon metabolism (CCM) – to control MYC protein expression adds another layer to the regulatory network of MYC.

The previously described experimental setup was applied to eleven cancerous and two non-cancerous cell lines of seven tissue origins of two different organisms (*Homo sapiens, Cercopithecus aethiops*) to verify if the glutamine-adjustable MYC expression is a cell line-, entity- or cancer-specific phenomenon. Glutamine deprivation suppressed MYC protein expression in all tested cell lines with the exception of HEK293, a non-cancerous kidney cell line, that showed a moderate repression but overall sustained MYC levels. All cell lines restored MYC expression levels upon glutamine re-addition, although with a cell line-specific kinetic. One could classify A549, HeLa, HEK293, MCF7 and MDAMB231 as slow/weak responders, because MYC protein levels seldom increased by 2-fold over the 4 hrs time course (*figure* 4.3). The cell lines HEPG2, HT29, RKO and U2OS were categorized as fast/strong responders as they increased MYC levels by at least a factor of four within 60 min. Surprisingly, the osteosarcoma cell line U2OS, which showed an initial low MYC expression even in the presence of glutamine, markedly raised MYC levels by the factor of five within 30 min after glutamine supplementation in comparison to levels at starvation.

4.1.3. Effects of glutamine starvation on cell growth

In order to evaluate the effect of glutamine starvation on cell growth, five colon cancer cell lines and HEK293 cells were starved for glutamine for in total 96 hrs. Cell proliferation was monitored every 24 hrs. The cell culture media was renewed every 24 hrs to sustain a sufficient supply of nutrients.

Glutamine starvation suppressed MYC expression and cell growth in all five colon cancer cell lines (*figure* 4.4). Cell numbers remained constant over the whole time course. In contrast, HEK293 cells continued growing, while the MYC protein expression remained constant in the absence of glutamine (*figure* 4.4).
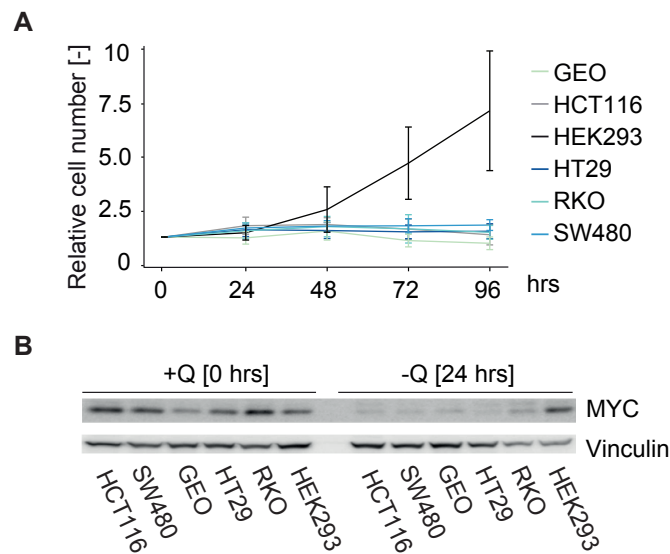
Figure 4.4.: Effects of glutamine starvation on cell growth. (A) Cell proliferation upon glutamine starvation in the indicated cell lines. Cells were starved for 96 hrs. Cell number was normalized to 0 hrs. Results represent mean $\pm$ SD (n=4, each measurement performed in technical duplicates). (B) Representative immunoblot documents MYC protein expression in the indicated cell lines at 0 hrs (+Q) and after 24 hrs of starvation (-Q). Data were published in figure S1B in Dejure and Royla et al. [2017].

4.2. Analysis of post-transcriptional mechanisms of glutamine-dependent MYC regulation

The discovery of the fine-tuned feedback control that coordinates expression of MYC in response to external glutamine supply raised the question how this effect might be mediated. Since MYC protein levels are tightly controlled at the level of transcription, messenger RNA (mRNA) stability, translation, and protein stability; these regulatory levels were examined in response to glutamine starvation and re-addition.

4.2.1. Transcription

In order to successfully transcribe a gene into a mRNA numerous processes have to happen that include transcription, pre-mRNA processing steps such as polyadenylation, splicing, capping, and translocalization of mature mRNA to the cytoplasm; where the translation itself is taking place. All of these processes are managed by multi-component machineries, therefore the synthesis of a protein from scratch requires time [Ben-Ari et al., 2010]. *Figure* 4.2 illustrates the rapid increase of MYC protein in response to glutamine re-addition in deprived cells. The graphically determined doubling time of MYC protein $t_{2xMYC} = 13.75$ min revealed a synthesis rate that cannot be realized by the transcription and subsequent translation machinery (*figure* 4.5).

4.2.2. *MYC* mRNA stability

Changes in protein levels might reflect changes in the corresponding mRNA levels. *MYC* transcript levels were determined via qPCR in HEK293 cells and the colon cancer cell line panel cultured in the absence (-Q) or presence (+Q) of glutamine for 24 hrs. *MYC* mRNA level did not decrease in the absence of glutamine as protein level did (*figure* 4.6).
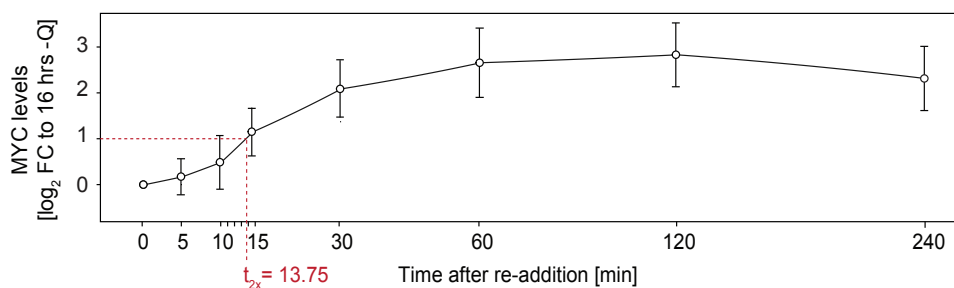
Figure 4.5.: Graphical determination of MYC protein doubling time. Quantification of MYC protein over re-addition time course after glutamine starvation (-Q) in HCT116 cells. Each value was normalized to -Q at time point 16 hrs. Protein expression was normalized to Vinculin levels. Results represent mean ± SD of four independently performed experiments.
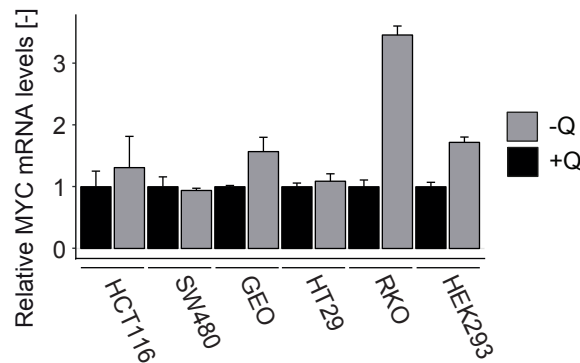
Figure 4.6.: Effects of glutamine starvation on *MYC* transcript level. Shown are qPCR obtained MYC transcript levels of indicated cell lines cultured in the absence (-Q) and presence (+Q) of glutamine for 24 hrs. *MYC* mRNA levels were normalized to *PGK1*. mRNA levels are shown relative to +Q. Bars represent mean + SD (*n*=3). Data were published in figure S1B in Dejure and Royla et al. [2017].

Transcript levels in SW480 and HT29 were unaffected by glutamine deprivation, whereas the other cell lines increased *MYC* mRNA. Transcript analysis showed 3.5 times higher *MYC* mRNA levels during glutamine deprivation in comparison to glutamine supplementation in RKO cells (*figure* 4.6).

There are several determinants that coordinate the stabilization and degradation of mRNA. Specific sequences and/or secondary structures within the mRNA are recognized by RNA binding proteins (RBP) or microRNA (miRNA), which either recruit or exclude the mRNA degradation machinery [Jiang and Coller, 2012]. One prominent RNA binding protein is human antigen R (HuR) that binds to cis-acting elements, more specifically to adenosine/uridine-rich elements (AREs) that are present in the untranslated regions of mRNAs [Brennan and Steitz, 2001].

To address the importance of HuR in regard to glutamine-dependent MYC expression a siRNA[1]-mediated knockdown of the RBP was performed. HCT116 cells were transfected with siRNA against HuR. After 48 hrs, when HuR was uniformly inhibited, cells were starved for 16 hrs and glutamine was re-added. The elimination of HuR did not impede MYC downregulation upon glutamine starvation or decelerate upregulation after glutamine re-addition (*figure* 4.7).

4.2.3. Translation

Once a mRNA is transcribed it is accompanied by complexes of proteins which determine its fate. Some of these components, namely messenger ribonucleoprotein complexes (mRNPs), are tightly bound to the mRNA while others bind dynamically in response to

---

[1]Small interfering RNA
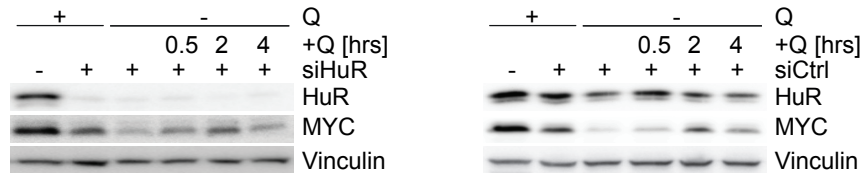
Figure 4.7.: Effect of HuR inhibition on MYC protein levels in response to glutamine availability. HCT116 cells were transfected with a siRNA against human antigen R (HuR) or a nonsense sequence (Ctrl). After 48 hrs, cells were starved for 16 hrs and glutamine was re-added for the indicated time points. The representative immunoblot documents HuR, MYC and Vinculin levels under the described conditions (n=2). Abbreviations – Q: Glutamine.

cellular changes. In addition, mRNPs undergo a series of remodeling events as associated proteins manage mRNA processing steps including transcription, polyadenylation, splicing, capping and translocalization of mature mRNA to the cytoplasm. Eventually, mRNPs recruit enzymes that either initiate translation or induce deadenylation and decapping processes in order to promote mRNA decay [Decker and Parker, 2012; Shyu et al., 2008]. Efficiently decapped mRNAs are marked as nontranslating mRNAs that accumulate in cytoplasmic granules. Two types of nontranslating mRNP granules are known – those that associate with the mRNA decay machinery, called P-bodies and those which assemble transcription initiation components that further recruit ribosomes, called stress granules. The latter were observed to be reversibly induced upon cellular stresses in order to stall translation [Decker and Parker, 2012; Parker and Sheth, 2007].

The rapid glutamine-mediated recovery of MYC protein and the stable/increased *MYC* transcript levels in glutamine-starved cells might be an indication of a reversible translational repression and storage of *MYC* mRNA in stress granules. In order to verify this hypothesis, the localization of *MYC* transcripts were monitored by means of the smFISH[2] approach. HCT116 cells were cultured in the absence (-Q) and presence (+Q) of glutamine for 16 hrs and probes against *MYC* and cyclin A2 (*CCN2A*) transcripts were applied (*figure* 4.8). Cyclin A2, which starts accumulating during S-phase and suddenly degrades before M-phase entry, was chosen as a internal experimental control to validate the cell growth arrest upon glutamine starvation [Yam et al., 2002].
Less *CCN2A* transcripts were present in cells lacking glutamine pointing towards an arrested cell growth that correlates with previous cell growth results (*figure* 4.4). In contrast, *MYC* transcript abundance was not dependent on glutamine availability which is concurrent with previous results (*figure* 4.6). Additionally, no obvious localization of *MYC* mRNA into stress granules was observed in the absence of glutamine as the mRNA was similarly distributed within the cells in both culturing conditions.

---

[2]Single-molecule RNA fluorescence *in situ* hybridization
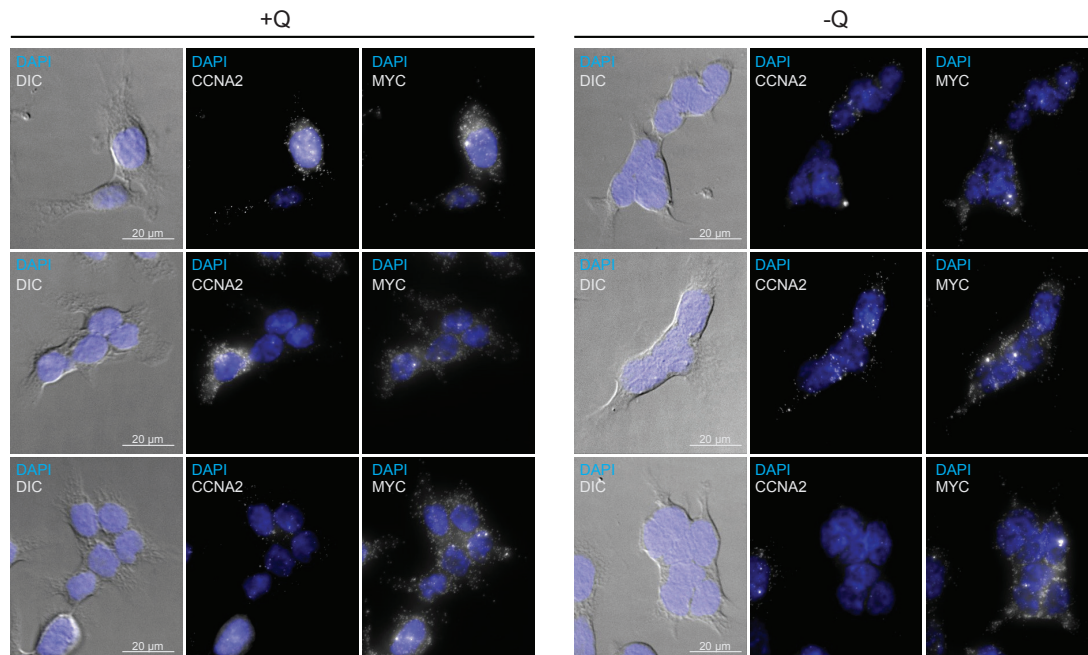
Figure 4.8.: *MYC* **transcript localization detected by smFISH.** *MYC* and *CCN2A* transcripts were monitored in HCT116 cells cultured in the absence (-Q) or presence (+Q) of glutamine for 16 hrs. Merged images of DAPI stained nuclei (blue) and cell phenotype or the maximum intensity projections of smFISH probes (grey) for three representative groups of cells are shown. Sample preparation as well as microscopy were performed by Christine Kocks and Anastasiya Boltengagen (Nikolaus Rajewsky Lab, BIMSB/MDC, Berlin-Germany).

4.2.4. MYC protein stability

The stability of MYC protein is largely affected by the N-terminal phosphorylation sites Ser62 and Thr58. Phosphorylation of Ser62, mediated by the mitogen-activated protein kinase (MAPK) pathway, supports MYC protein stability. Phosphorylation of Thr58 that requires phosphorylated Ser62 and GSK3-β[3] as a mediator, promotes ubiquitination and subsequent protein degradation. The activation of phosphorylation sites during glutamine re-addition upon starvation showed no obvious imbalance that could account for an altered stabilization of MYC protein in the presence of glutamine. The kinetics of both phosphorylation sites followed the one of the total protein, at which Ser62 was slightly more present than Thr58 (*figure* 4.2).

---

[3]glycogen synthase kinase 3β

4.3. The role of signaling pathways in glutamine-dependent MYC expression

4.3.1. Impact of oncogenic mutations

During oncogenesis cells acquire several mutations. BRAF and KRAS are major onco-genic drivers in colorectal cancer. As shown in *figure* 4.4 glutamine deprivation caused suppression of MYC protein expression and cell growth in the panel of colon cancer cell lines that either harbor a *BRAF* or *KRAS* mutation indicated in *table* 4.1.

The role of *BRAF* and *KRAS* mutations in regard to glutamine-dependent MYC expres-sion was evaluated. CaCO2 cells, being naturally not mutated in *BRAF* and *KRAS*, were genetically modified to overexpress either KRAS or BRAF upon doxycycline treatment (*supplemental figure* B.2). Similar to HCT116 cells, CaCO2 cell lines arrested cell growth upon glutamine starvation independently of their mutation status, in line with repressed MYC protein expression (*figure* 4.9).
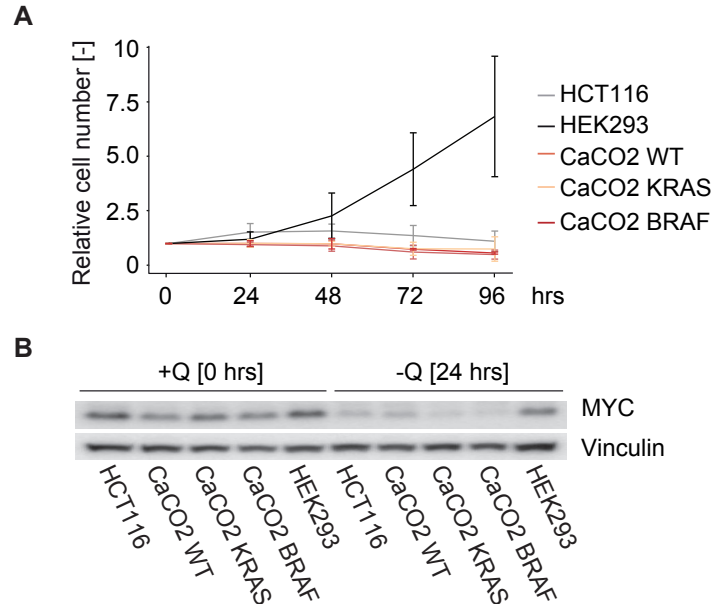
Figure 4.9.: Oncogene-dependent proliferation upon glutamine starvation. (A) Cell proliferation upon glutamine starvation in indicated cell lines. Cells were starved for 96 hrs. Cell number was normalized to 0 hrs. Results represent mean ± SD (*n*=3, each measurement was performed in technical duplicates). (B) Representative immunoblot shows MYC protein expression in the indicated cell lines at 0 hrs (+Q) and after 24 hrs of starvation (-Q).

Table 4.1.: *BRAF* and *KRAS* mutations in colon cancer cell lines

Cell line	Mutation[*]
CaCO2	-
GEO	$KRAS^{G12A}$
HCT116	$KRAS^{G13D}$
HT29	$BRAF^{V600E}$
RKO	$BRAF^{V600E}$
SW480	$KRAS^{G12V}$

[*] https://cansar.icr.ac.uk/cansar/cell-lines

4.3.2. Impact of signaling pathways

Mammalian cells require growth factor receptor-initiated signal transduction for cell growth. Once a cell turns into a tumor cell it acquires the ability to proliferate independently of external growth factor signaling [Ward and Thompson, 2012a]. The integration of external growth signals and nutrient availability is implemented by the protein kinase mTOR, the main coordinator of anabolic and catabolic processes and the guardian of cellular homeostasis [Jewell and Guan, 2013].

Signaling pathways are highly interconnected to efficiently transduce cellular programs via kinases, phosphatases and phospho-binding proteins. Therefore not only the activation/inhibition status of mTOR, but of twelve additional signaling molecules of major signaling pathways were analyzed in response to glutamine starvation in HCT116 cells using the multiplex bead-based Bio-Plex assay. Upon the withdrawal of glutamine all tested signaling molecules were dephosphorylated at their activation sites leading to the conclusion of an overall signaling shutdown (*figure* 4.10). The deactivation of mitogenic RAS/MAPK (ERK, MEK, CREB, p90RSK, cJUN) and survival PI3K/AKT (AKT, mTOR, p70S6) pathways corresponds to the arrested cell growth upon glutamine starvation (*figure* 4.4). Stress response pathways (p38 and JNK) were inhibited as well.

These findings led to the assumption that a signaling molecule that might transmit the information of glutamine availability, should recover its phosphorylation state faster than MYC protein after glutamine re-addition. In order to confirm this hypothesis, the activation states of kinases were monitored 5, 10, 15 and 30 min after re-adding glutamine to starved HCT116 cells. Five signaling molecules showed a faster kinetic than MYC protein after 5 min (*figure* 4.10). Surprisingly, these kinases belong either to the RAS/MAPK pathway or to the PI3K/AKT pathway.

Small molecules, targeting signaling proteins within these pathways, were applied during re-addition to validate their role in glutamine-dependent MYC expression (*figure* 4.11). Additionally, the inhibition of phosphorylation of the kinase p38 was tested.
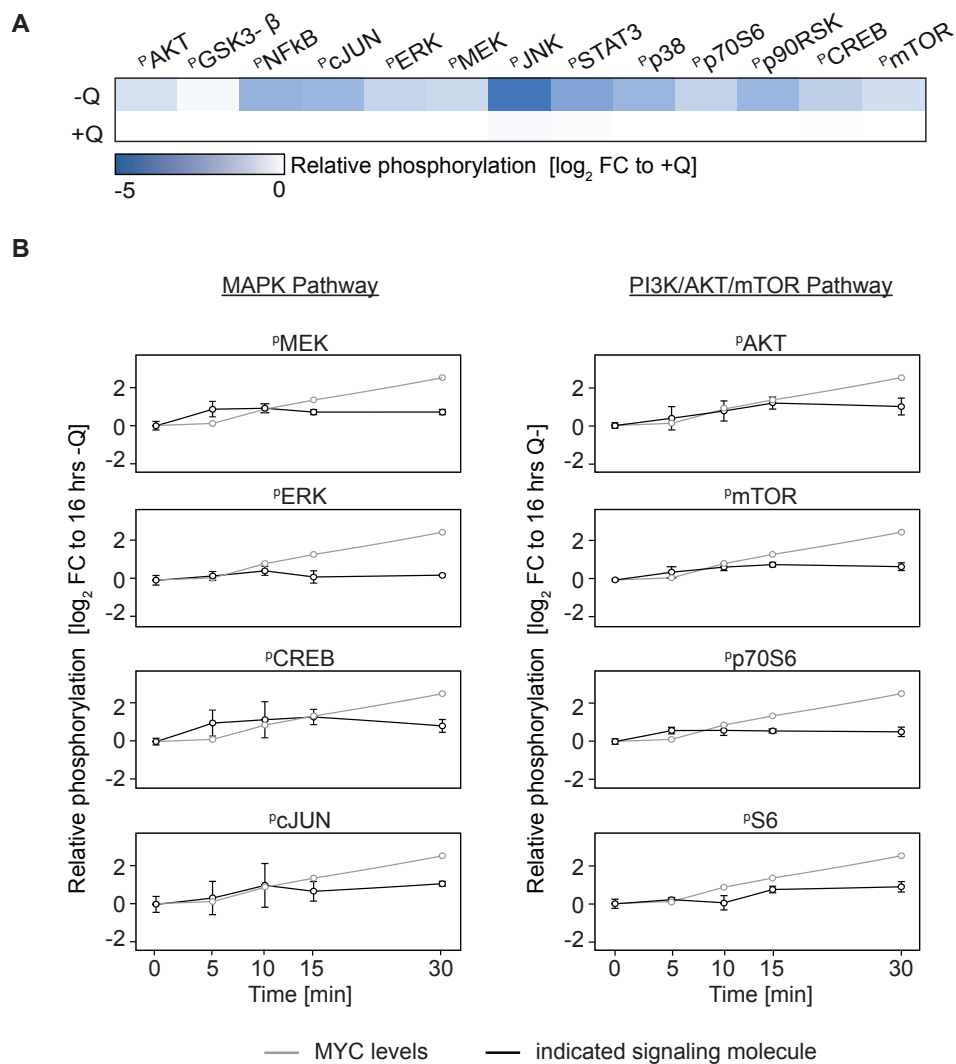
Figure 4.10.: Effects of glutamine starvation and re-addition on major signaling pathways. (A) Phosphorylation of indicated kinases in the absence (-Q) and presence (+Q) of glutamine (16 hrs) in HCT116 cells. Phosphorylation levels are shown relative to +Q and represent the mean of n=3. (B) Kinetic of phosphorylation status of indicated signaling proteins after glutamine re-addition in comparison to MYC protein expression over time. Phosphorylation levels are shown relative to -Q at 16 hrs time point. Results represent mean $\pm$ SD (n=3). Bio-Plex sample preparation and measurements were performed by Raphaela Fritsche (Jennifer Kirwan Lab, Berlin Institute of Health, Berlin-Germany). For the specific phospho-sites that were examined refer to *supplemental table* A.4.

Neither the treatment with the MEK inhibitor AZD4226 nor the inhibition of PI3K using LY294002 altered the speed or the strength of MYC recovery. The verification of the inhibitors failed as the downstream targets phospho-ERK and phospho-4EPB1 were not downregulated upon treatment, most likely because of feedback mechanisms (*supplemental figure* B.3). In comparison, mTOR complex 1 (mTORC1) inhibition via rapamycin resulted in an expected decreased phosphorylation of the downstream target 4EPB1. In addition, the application of SB203580 blocked p38 mediated-signaling resulting in an

accumulation of phospho-p38 and a reduction of phosphoylated HSP27, a protein down-stream of p38. The inhibition of both kinases led to a slightly weaker MYC protein recovery compared to the solvent control (*figure* 4.11).

On the one hand mTOR is activated by amino acids, such as glutamine and leucine, in order to control mRNA translation, while on the other hand mTOR is known to regulate MYC. The role of the kinase in the glutamine-dependent MYC regulation was further investigated by siRNA-mediated inhibition of its subunits mTORC1 and mTORC2 [Bar-Peled and Sabatini, 2014; Goberdhan et al., 2016]. HCT116 cells were transfected with siRNAs against Raptor or Rictor, which are subunits of mTORC1 and mTORC2, respectively. After 48 hrs, cells were starved for 16 hrs and glutamine was re-added. The disruption of mTOR did marginally impede MYC upregulation as it was observed upon rapamycin treatment (*figure* 4.11).
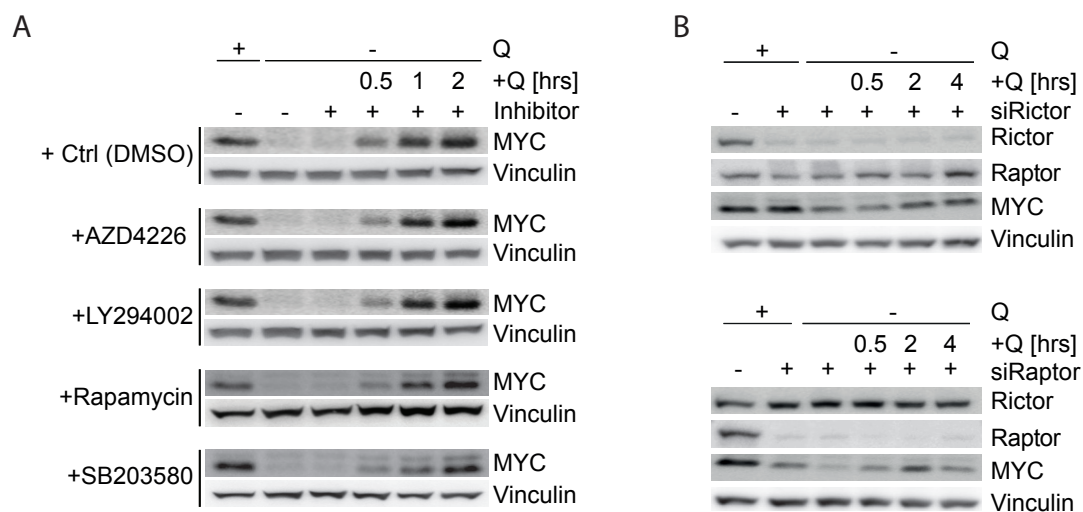
Figure 4.11.: Effects of inhibition of signaling proteins on the glutamine-dependent MYC recovery. (A) Representative immunoblots show MYC protein expression upon starvation and treatment with indicated inhibitors for 16 hrs followed by glutamine re-addition (*n*=2). (B) Effect of mTORC1 and mTORC2 inhibition on MYC protein levels in response to glutamine availability. HCT116 cells were transfected with siRNAs against Raptor or Rictor. After 48 hrs, cells were starved for 16 hrs and glutamine was re-added for the indicated time points. Immunoblots document Raptor, Rictor, MYC and Vinculin levels under the described conditions (*n*=2). Abbreviations – Q: Glutamine. Data of panel (B) were published in figure S2 in Dejure and Royla et al. [2017].

4.4. Identification of metabolic stimuli mediating MYC regulation

4.4.1. Metabolic effects upon glutamine starvation

Glutamine is a non-essential amino acid. Nevertheless, it is involved in several metabolic pathways resulting in the production of macromolecules and bioenergetics which support cell growth. Glutamine's major metabolic tasks are: (i) supply of nitrogen for *de novo* nucleotide biosynthesis, (ii) antagonize oxidative stress by being a precursor of the antioxidant glutathione, (iii) provision of intermediates to fuel anaplerotic reactions, (iv) contribution to the pool of reducing equivalent NADPH [DeBerardinis and Cheng, 2010]. Gas chromatography (GC) and direct-infusion mass spectrometry (MS) approaches, that have been described in detail in *section* 3.5, have been applied in order to investigate the different downstream effects upon glutamine starvation in a time-resolved manner.

Glutamine as nitrogen donor

Nitrogen occurs in the form of free ammonia, when it is released by transaminases or protein degradation processes. The highly toxic ammonium is cleared via urea cycle under the formation of ornithine and eventually excreted. Pronounced decreases in steady-state quantities of ornithine and putrescine, a downstream metabolite of ornithine, were observed in the absence of glutamine indicating an overall reduction in nitrogen metabolism (*figure* 4.12).

De novo nucleotide biosynthesis is an energy-consuming process that uses several sources of carbon and nitrogen. Glutamine serves as a major nitrogen donor because it provides its γ-nitrogen directly and the α-nitrogen indirectly via glycine and aspartate that originate from glutamine [DeBerardinis and Cheng, 2010]. Short- and long-term (2 and 16 hrs)
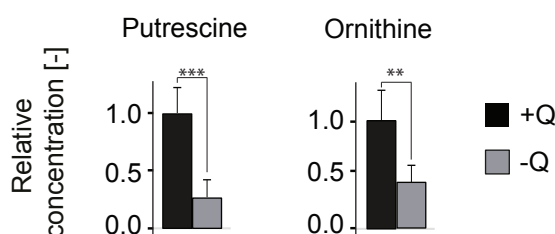
Figure 4.12.: Effects of glutamine starvation on nitrogen metabolism. Relative quantities of putrescine and ornithine, determined by GC-MS, are shown in response to glutamine starvation. HCT116 cell were cultured for 16 hrs either in the presence (+Q) or absence of glutamine (-Q). Quantities were normalized to +Q. Results represent mean + SD (n=3, each measurement performed in technical duplicates). P-values were calculated using a two-tailed student's t-test (* $0.01 < p \leq 0.05$; ** $0.001 < p \leq 0.01$; *** $p \leq 0.001$). Data were published in figure EV3B in Dejure and Royla et al. [2017].
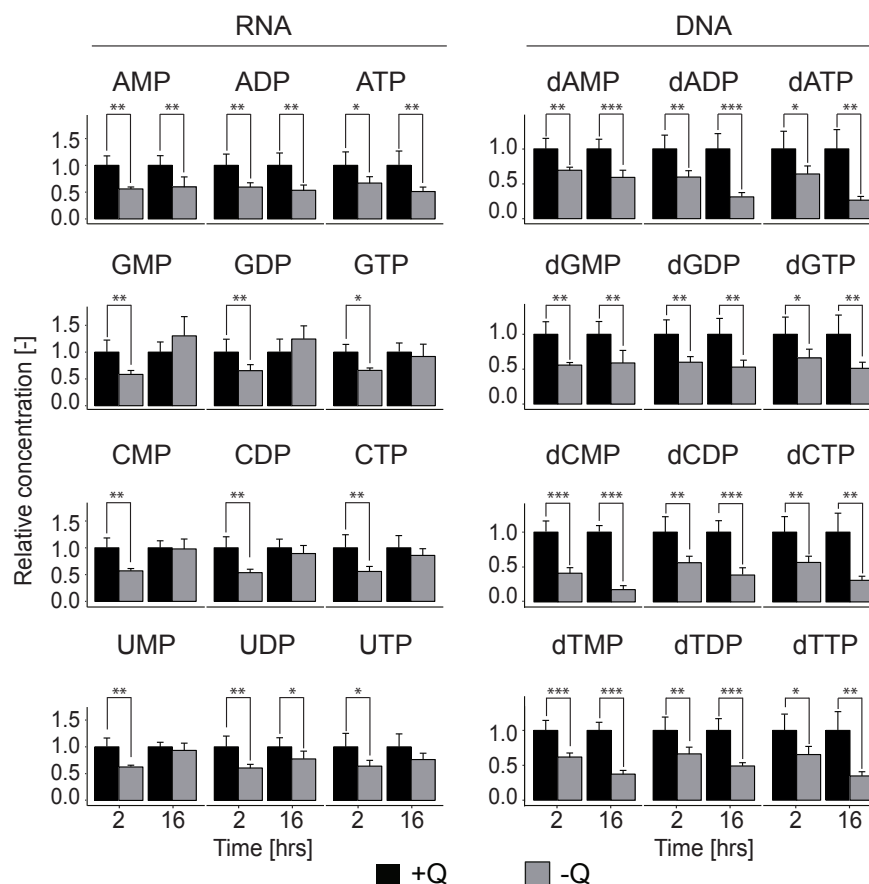
Figure 4.13.: Effects of glutamine starvation on nucleotide levels. Direct-infusion MS acquired quantification of ribonucleotide and deoxyribonucleotide levels are shown in response to short- (2 hrs) and long-term (16 hrs) glutamine starvation. HCT116 cells were cultured for 2 hrs or 16 hrs either in the presence (+Q) or absence of glutamine (-Q). Quantities were normalized to +Q per metabolite and per time. Results represent mean + SD (n=6, each measurement performed in technical triplicates). P-values were calculated using a two-tailed student's t-test (* $0.01 < p \leq 0.05$; ** $0.001 < p \leq 0.01$; *** $p \leq 0.001$). Data were published in figure 4E in Dejure and Royla et al. [2017].

glutamine starvation effects on nucleotide levels were investigated in HCT116 applying direct-infusion MS. Deoxyribonucleotide levels significantly decreased independently of the duration of glutamine depletion (*figure* 4.13). Similarly, ribonucleotide pools were reduced in cells lacking glutamine for 2 hrs. In contrast, RNA building block quantities did not significantly change comparing cells cultured with and without glutamine for 16 hrs except for adenosine-derived ribonucleotides: AMP, ADP and ATP. The pool sizes of the three ribonucleotides were halved within 16 hrs.

Additionally, we compared the abundance of adenosine-derived deoxy- and ribonucleotides in HCT116 and HEK293 cells that were starved for glutamine for 16 hrs. As illustrated in *figure* 4.14 nucleotide pools significantly dropped in both cell lines in the absence of
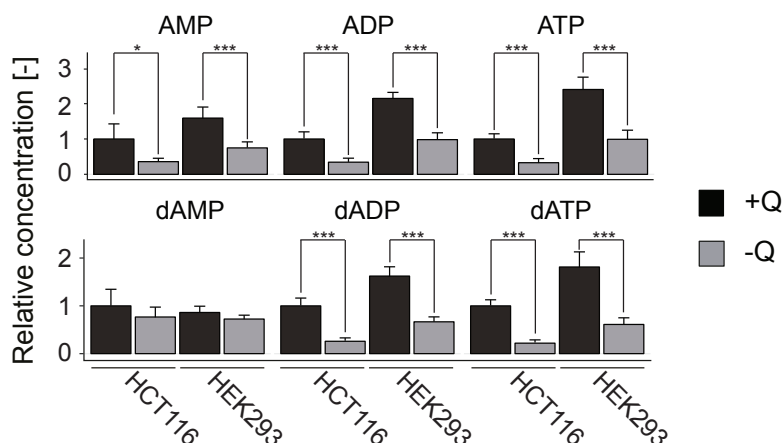
Figure 4.14.: Cell line-dependent effects of glutamine starvation on nucleotide levels.
Direct-infusion MS acquired quantification of ribonucleotide and deoxyribonucleotide levels after
16 hrs of glutamine starvation are shown in HCT116 and HEK293 cells. Cells were cultured 16 hrs
either in the presence (+Q) or absence of glutamine (-Q). Quantities were normalized to +Q
condition in HCT116 cells per metabolite. Results represent mean + SD (n=6, each measurement
performed in technical triplicates). P-values were calculated using a two-tailed student's t-test
(* $0.01 < p \leq 0.05$; ** $0.001 < p \leq 0.01$; *** $p \leq 0.001$).

glutamine. Levels of dAMP remained constant. However, HEK293 cells initially showed
higher nucleotide levels at 2 mM glutamine, which decreased upon glutamine starvation,
but were still in the range of the nucleotide concentrations detected in HCT116 in the
presence of glutamine. ADP and ATP levels in HEK293 cells were reduced by a factor
of two upon glutamine deprivation resulting in the same concentration determined in
HCT116 cells at 2 mM glutamine. The pools of dADP and dATP in HEK293 decreased
to 40% of the non-starved pool sizes of HCT116, while deoxynucleotide levels of starved
HCT116 cells declined to 20-25%.

Glutamine as TCA cycle substrate

A major function of glutamine is the supply of intermediates to fuel anaplerotic reactions
to generate ATP. The conversion into glutamate (Glu) and subsequently α-ketoglutarate
(αKG) allows the introduction of glutamine's carbon skeleton to the TCA cycle. The quan-
tities of glutamine downstream metabolites glutamate, α-ketoglutarate, fumarate (Fum)
and malate (Mal) were measured via GC-MS in HCT116 cells that were cultured with
(+Q) or without (-Q) glutamine for 2 and 16 hrs. As expected, long-term glutamine star-
vation strongly reduced steady-state pool sizes of TCA cycle intermediates (*figure* 4.15).
Surprisingly, rapid decreases in metabolite pools were detected, e.g., glutamate levels were
reduced by 90% after 2 hrs of glutamine depletion. The depletion of downstream metabo-
lite levels in response to short-term glutamine deprivation confirmed that the TCA cycling
is dependent on external glutamine supply in HCT116 cells.
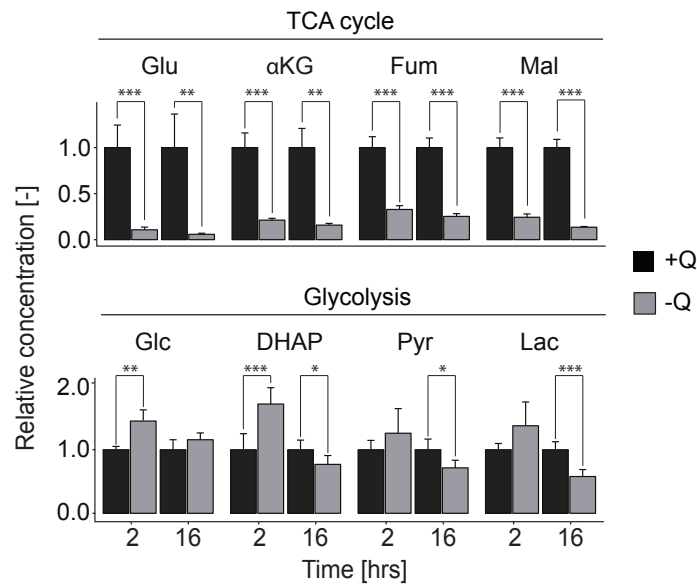
Figure 4.15.: Effects of glutamine starvation on central carbon metabolism. GC-MS determined concentration of glutamine downstream metabolites within the TCA cycle and major glycolysis intermediates are shown in response to short- and long-term glutamine starvation. HCT116 cells were cultured for 2 hrs or 16 hrs either in the presence (+Q) or absence of glutamine (-Q). Quantities were normalized to +Q per metabolite and starvation time. Results represent mean + SD (n=3, each measurement performed in technical duplicates). P-values were calculated using a two-tailed student's t-test (* $0.01 < p \leq 0.05$; ** $0.001 < p \leq 0.01$; *** $p \leq 0.001$). Abbreviations – αKG: α-Ketoglutarate, DHAP: Dihydroxyacetone phosphate, Fum: Fumarate, Glc: Glucose, Glu: Glutamate, Lac: Lactate, Mal: Malate, Pyr: Pyruvate. Data were published in figure 4A in Dejure and Royla et al. [2017].

Glycolytic metabolite levels adapted to the lack of glutamine supply and the consequent reduction in pool sizes of TCA cycle intermediates. After 2 hrs, glucose (Glc), dihydroxyacetone phosphate (DHAP), pyruvate (Pyr) and lactate (Lac) levels increased pointing towards a transient upregulation of glycolysis. An inverted effect was observed after 16 hrs as pool sizes were slightly reduced most likely because cells either balanced glycolysis in response to a less active TCA cycle or directed glycolysis-derived carbons into the TCA cycle in order to maintain oxidative phosphorylation (OXPHOS).

Effects of ectopic MYC expression in response to glutamine starvation

Metabolite and nucleotide pools were significantly depleted upon glutamine starvation (*figure* 4.13, *figure* 4.15). The activation of MYC in the absence of the amino acid was investigated to identify critical metabolite pools that might further decrease in order to sustain MYC functions. HCT116 cells transduced with either the MYC estrogen receptor chimera (MYC-ER) or an empty vector (EV) were treated for eight hours with 100 nM 4-hydroxytamoxifen (OHT) to induce MYC overexpression before cells were incubated for another 16 hrs in the absence or presence of glutamine and OHT. Cells were harvested,

extracted and central carbon metabolites and nucleotides were quantified via GC- and direct-infusion MS, respectively (*section* 3.5).

Figure 4.16 documents the stable overexpression of the artificial MYC-ER upon OHT treatment in the absence and presence of glutamine. The endogenous MYC protein was downregulated in glutamine-deprived MYC-ER and EV cells as it was described earlier (*section* 4.1.1). In line with the results obtained in non-modified HCT116 cells (*figure* 4.15, *figure* 4.13), metabolite abundances were drastically reduced in MYC-ER and EV cells upon glutamine starvation. Surprisingly, expression of ectopic MYC did not alter metabolite levels upon glutamine starvation compared to EV cells (*figure* 4.16).
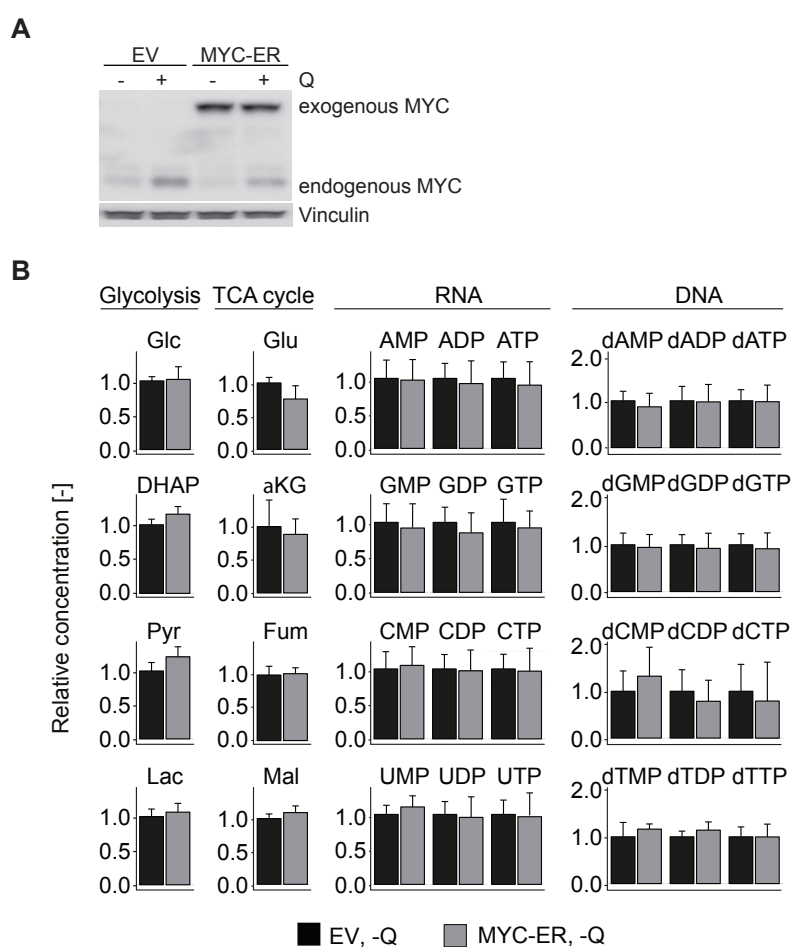
Figure 4.16.: Effects of ectopic MYC expression on the abundance of central carbon metabolites and nucleotides in response to glutamine starvation. (A) Shown are protein levels of HCT116 cells that stably express the indicated MYC estrogen receptor chimera (MYC-ER) construct or an empty vector (EV) as control in response to glutamine starvation (-Q). MYC-ER activity was induced for 8 hrs with 100 nM OHT followed by 16 hrs of glutamine starvation in the presence of OHT. (B) Relative concentrations of the indicated metabolites in glutamine-starved HCT116 cells are shown. Values were normalized to EV. Data represent mean ratios + SD (n=6, direct-infusion MS measurements were carried out in triplicates, GC-MS measurements in duplicates). Abbreviations – αKG: α-Ketoglutarate, DHAP: Dihydroxyacetone phosphate, Fum: Fumarate, Glc: Glucose, Glu: Glutamate, Lac: Lactate, Mal: Malate, Pyr: Pyruvate. Data were published in figure EV7A in Dejure and Royla et al. [2017].

4.4.2. Metabolic short-term effects in response to glutamine re-addition

We hypothesized that the mechanism mediating the glutamine-dependent MYC regulation should respond faster to changes in glutamine concentration than MYC protein levels. The short-term recovery of nucleotide levels was evaluated by determining AMP, ADP and ATP concentrations 5, 10 and 15 min after glutamine re-addition. Upon glutamine depletion nucleotide pools were reduced by 50% verifying the previous results shown in *section* 4.4.1 (*figure* 4.17).

The re-addition of glutamine led to a slight drop in quantities after 5 min that was reversed after 10 min as nucleotide pools increased. The effect was strongest in ATP with an increase by a factor of 1.5 and weakest in AMP. These differences in the recovery dynamic of adenosine-derived nucleotides, which form the energy storage system of the cell, point towards the reanimation of the energy metabolism upon glutamine re-addition.

ATP production is largely driven by the electron transport chain (ETC), a series of complexes that perform the mitochondrial conversion of succinate into fumarate. The pulsed stable isotope resolved metabolomics (pSIRM) approach was applied in order to check if an increase in adenosine-derived nucleotide levels is a result of enhanced TCA cycle activity and concomitant ATP production.

Incubation of cells with media supplemented with stable isotope-labeled substrates, e.g., u-^{13}C-glutamine, instead of the unlabeled one, enables the monitoring of the distribution of carbon-13 along the pathway in dependence of the pathway activity and the incubation time. GC-MS provides the concurrent measurement of metabolite abundance and intensity shifts within isotopomers introduced via carbon-13. The combination of both information allows a dynamic metabolic profiling of cellular metabolism [Pietzke et al., 2014; Zasada and Kempa, 2016].
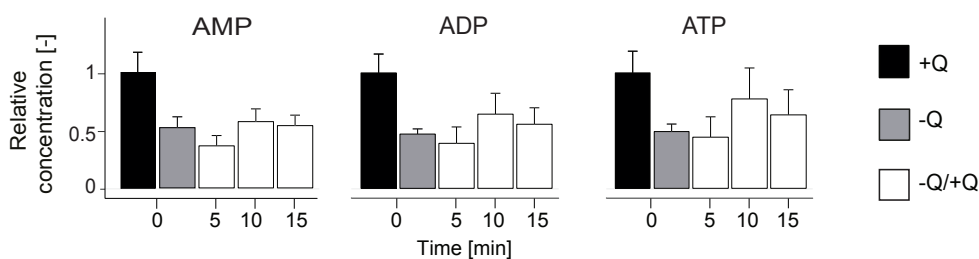
Figure 4.17.: Short-term recovery of adenosine-derived nucleotides. Time-resolved quantification of AMP, ADP and ATP levels is shown in response to glutamine starvation (-Q) followed by re-addition (-Q/+Q) in HCT116 cells. Relative quantities were calculated to time point 0 hrs, when cells were cultured in standard cell culture media (+Q). Results represent mean + SD (*n*=6, each measurement performed in technical triplicates).
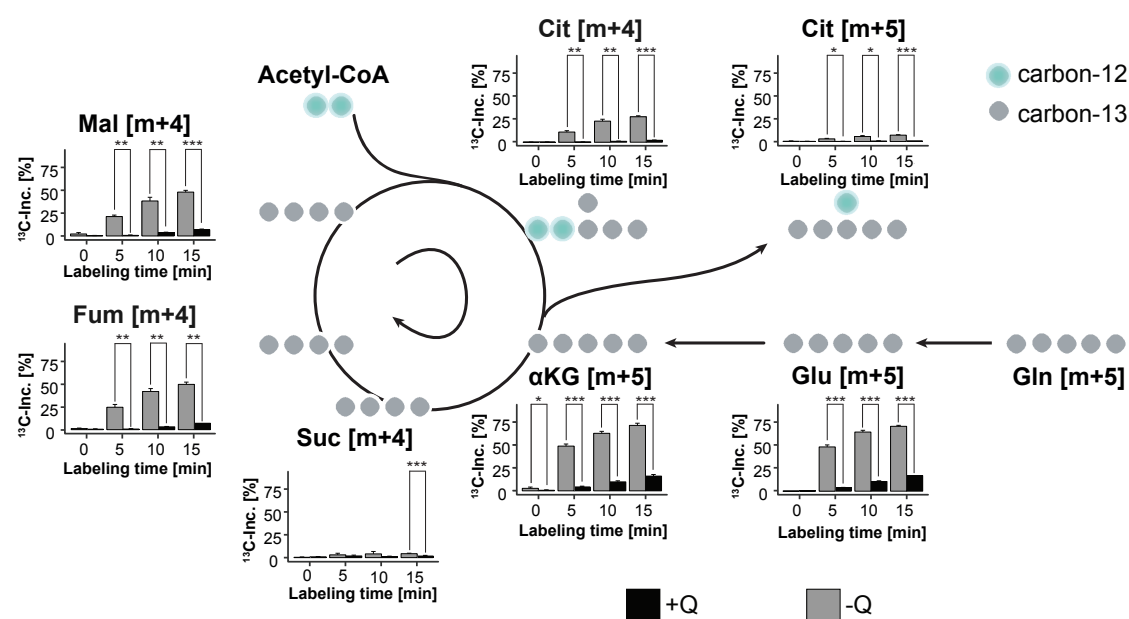
Figure 4.18.: Glutamine-derived ^{13}C-incorporation in response to glutamine availability during pre-treatment. HCT116 cells were cultured in the presence (+Q) and absence (-Q) of glutamine for 16 hrs before incubation for 5, 10 and 15 min with media containing u-^{13}C-glutamine instead of ^{12}C-glutamine. Results represent mean + SD ($n=3$, each measurement performed in technical duplicates). P-values were calculated using a two-tailed student's t-test (* $0.01 < p \leq 0.05$; ** $0.001 < p \leq 0.01$; *** $p \leq 0.001$). Grey circles represent ^{13}C-labeled molecules derived from glutamine, green circles illustrate non-labeled molecules. Numbers of incorporated carbons are shown in brackets. Abbreviations – Acetyl-CoA: Acetyl coenzyme A, αKG: α-Ketoglutarate, Cit: Citrate, Fum: Fumarate, Gln: Glutamine, Glu: Glutamate, Mal: Malate, Suc: Succinate.

HCT116 cells were cultivated in the presence (+Q) and absence (-Q) of glutamine for 16 hrs before they were incubated with media containing completely labeled ^{13}C-glutamine for 5, 10 and 15 min. Additionally, non-labeled cells were harvested in order to normalize for the natural occurring isotopes. Polar metabolites were extracted, derivatized and subjected to the GC-MS in order to trace the carbon routing of glutamine within the TCA cycle.

Figure 4.18 illustrates the ^{13}C-incorporation into TCA cycle metabolites over time. A maximal ^{13}C-incorporation of 3% was detected in non-labeled cells (0 hrs), which correlates with the natural occurrence of carbon-13. With the application of u-^{13}C-glutamine an overall increase in carbon-13 over time was observed in all TCA cycle intermediates. As expected, the glutamine-derived carbon skeleton was directed via glutamate and α-ketoglutarate towards the TCA cycle, where it was further catabolized, indicated by a continuous decrease in carbon-13 throughout the cycle.

Significant less carbon-13 accumulated in cells that were incubated with 2 mM glutamine prior to pSIRM experiment compared to glutamine starved cells. In the latter, ^{13}C-incorporation was ten times higher in glutamate and α-ketoglutarate and seven times

higher in malate and fumarate pools after 5 min leading to the conclusion that TCA cycle activity was stimulated as soon as glutamine was available. This recovery was mainly achieved within the first 5 min as nearly 50% of glutamate and α-ketoglutarate pools were replaced with carbon-13 during this time span. Continued incubation likely led to a saturation indicated by a decelerated ^{13}C-incorporation rate. This argument was underlined by the fact that non-starved cells incorporated carbon-13 constantly over time. The promotion of OXPHOS was additionally verified by the marginal reductive carboxylation of α-ketoglutarate into citric acid, which enables the reductive TCA cycle entering for glutamine's carbon skeleton.

Interestingly, ^{13}C-enrichment in succinate followed the described time-dependent dynamic, but not the pathway-dependent one. One explanation might be a larger cytosolic pool that is not participant to glutamine converting reactions and therefore diluting the smaller mitochondrial labeled pool.

In order to provide a full picture, incorporation data were combined with metabolite abundances (*supplemental figure* B.5). Although some metabolite quantities (fumarate, malate) were clearly increased at 2 mM glutamine, the described dynamics based on the ^{13}C-incorporation could not be overwritten (*supplemental figure* B.4).

4.4.3. Identification of candidates that might mediate glutamine-dependent MYC regulation

The metabolic effects upon glutamine starvation and re-addition were fast and intense, qualifying glutamine-dependent metabolites to potentially mediate MYC regulation. Re-addition experiments with glutamine-derived metabolites were performed to determine which – if any – can restore MYC protein expression upon glutamine starvation (*figure* 4.19).

Glutamate and the membrane-permeable forms of α-ketoglutarate, succinate, fumarate and malate were used to evaluate glutamine's metabolic function as a supplier of TCA cycle intermediates. The addition of glutamate and dimethyl α-ketoglutarate (DMαKG) caused an impaired MYC recovery as well as the further downstream metabolite succinate did, but to a lesser degree (*figure* 4.19). Restoring fumarate and malate pools did not regulate MYC protein levels. These results led to the hypothesis that the production of ATP via the ETC might play a pivotal role. The tempered effect for glutamate, DMαKG and dimethyl succinate (DMSuc) might be explained by the time needed to efficiently transport the substrates in the cell and in the mitochondria, respectively. In order to generate ATP, succinate needs to be converted to fumarate by succinate dehydrogenase, which is part of complex II of the ETC. Since the mitochondrial reaction is nearly irreversible fumarate and malate re-addition can not contribute to OXPHOS.

Besides glutamine, the amino acid aspartate is a major source of nitrogen in the cell. Additionally, aspartate can be deaminated to oxaloacetate and continues cycling in the TCA cycle. Supplementation of aspartate did not recover MYC protein levels upon glutamine starvation. Given that aspartate is a charged molecule, it cannot readily pass through the cell membrane. Therefore the uncharged asparagine was tested, which can be easily converted to aspartate once transported into the cell. Concurrent results were found for both metabolites (*figure* 4.19).

A mixture of the four ribonucleosides and thymidine led to a transient recovery of MYC protein expression 2 hrs after re-addition. In order to narrow down the responsible nucleoside class, mixtures of purine and pyrimidine nucleosides were tested. Surprisingly, the purine mix triggered the transient response, whereas the pyrimidine mix did not increase downregulated MYC protein levels. The separate re-addition analysis of guanosine and adenosine, both purine nucleosides, revealed the latter as the mediator for the temporary recovery of MYC protein.
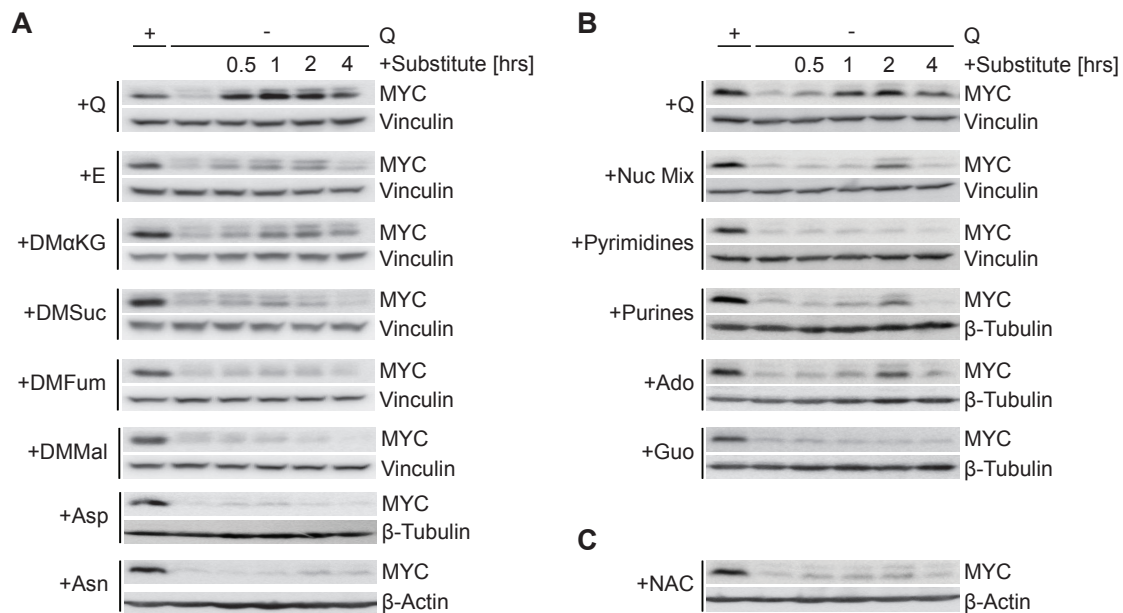
Figure 4.19.: Distinct glutamine-downstream metabolites rescue MYC expression. Representative immunoblots document MYC regulation of glutamine-starved cells after addition of the indicated substrates in HCT116 ($n=2$). Added substitutes should mimic different metabolic functions of glutamine: (A) supplier of TCA cycle intermediates, (B) nitrogen donor for nucleotide biosynthesis and (C) glutathione precursor. Abbreviations – Ado: Adenosine, Asn: Asparagine; Asp: Aspartate, DMαKG: Dimethyl α-ketoglutarate, DMFum: Dimethyl fumarate, DMMal: Dimethyl malate, DMSuc: Dimethyl succinate, E: Glutamate, Q: Glutamine, Guo: Guanosine, NAC: N-acetyl cysteine, Nuc Mix: mix of four ribonucleosides and thymidine, Purines: mix of Ado and Guo, Pyrimidines: mix of cytidine, thymidine and uridine. Data validate results that were recently published in Dejure and Royla et al. [2017] (figure 4C and D).

Reactive oxygen species (ROS) are formed as unavoidable by-products of metabolism by the mitochondrial complexes I and III of the ETC. Cells counterbalance the toxic effects of ROS by supplying antioxidant compounds and enzymes. Glutathione, a substrate of ROS scavenging enzymes, is produced via the formation of γ-glutamylcysteine from glutamate and cysteine [Sun, 2010; Di Meo et al., 2016]. The synthetic N-acetyl cysteine (NAC), a precursor of intracellular cysteine, was re-added to glutamine-deprived HCT116 cells showing no potential to recover MYC protein levels.

4.5. Dissection of MYC regulation in response to adenosine, α-ketoglutarate and glutamine

4.5.1. Metabolite-dependent proliferation effects

In order to evaluate if the cell growth arrest upon glutamine starvation can be reverted by the re-addition of the identified metabolic mediators, HCT116 cells were grown in media deprived for glutamine and/or supplemented with either DMαKG, adenosine, a mixture of both substances or glutamine. Cell numbers and viability were determined after 48 hrs. The arrested cell growth in glutamine starved cells was not reverted upon adenosine addition (*figure* 4.20). In contrast, DMαKG supplementation significantly stimulated cell growth, but not as effectively as glutamine. The combination of both MYC protein stimulating substrates resulted in the same cell numbers as seen for DMαKG alone.

Additionally, it was tested whether the re-addition of the indicated substrates could reverse cell growth arrest in HCT116 cells that were starved for 24 hrs. Cell numbers determined 48 hrs post re-addition were identical to those obtained in the substitution experiment (*supplemental figure* B.6). Thus, the regulation of MYC protein is not a consequence of changes in cell proliferation.
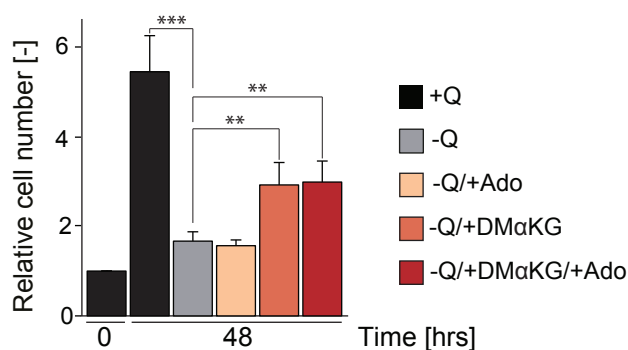
Figure 4.20.: Proliferation effects in response to DMαKG and adenosine supplementation. Cell numbers of HCT116 cells that were grown for 48 hrs in media supplemented with indicated substrates. Cell numbers were determined at 0 and 48 hrs and are shown relative to 0 hrs. Results represent mean + SD (n=5, each measurement performed in technical duplicates). P-values were calculated using a two-tailed student's t-test (* $0.01 < p \leq 0.05$; ** $0.001 < p \leq 0.01$; *** $p \leq 0.001$). Abbreviations – Ado: Adenosine, DMαKG: Dimethyl α-ketoglutarate, Q: Glutamine. Data were published in figure 4F in Dejure and Royla et al. [2017].

4.5.2. Metabolite-dependent effects on nucleotide levels

To further investigate the underlying mechanism of glutamine-dependent MYC regulation, the substrates glutamine, adenosine and DMαKG were tested for their potential to restore ribonucleotide and deoxyribonucleotide levels in deprived HCT116 cells. Samples

were harvested 2 hrs after re-addition because at this time point the strongest MYC expression was observed for all supplements (*section* 4.4.3, *supplemental figure* B.7). Direct-infusion MS measurements confirmed the significant decline in deoxyribonucleotide and adenosine-derived ribonucleotide levels upon glutamine starvation, which was described earlier (*section* 4.4.1, *figure* 4.21). Supplementation of glutamine restored depleted nucleotide levels and even slightly increased non-affected nucleotide quantities (*figure* 4.21). The re-addition of adenosine caused similar effects that were marginally stronger than glutamine-mediated ones. Both substrates induced the strongest alterations in adenosine-derived nucleotide levels. The addition of DMαKG did not have an effect on depleted nucleotide pools except for dTDP, which was significantly elevated.
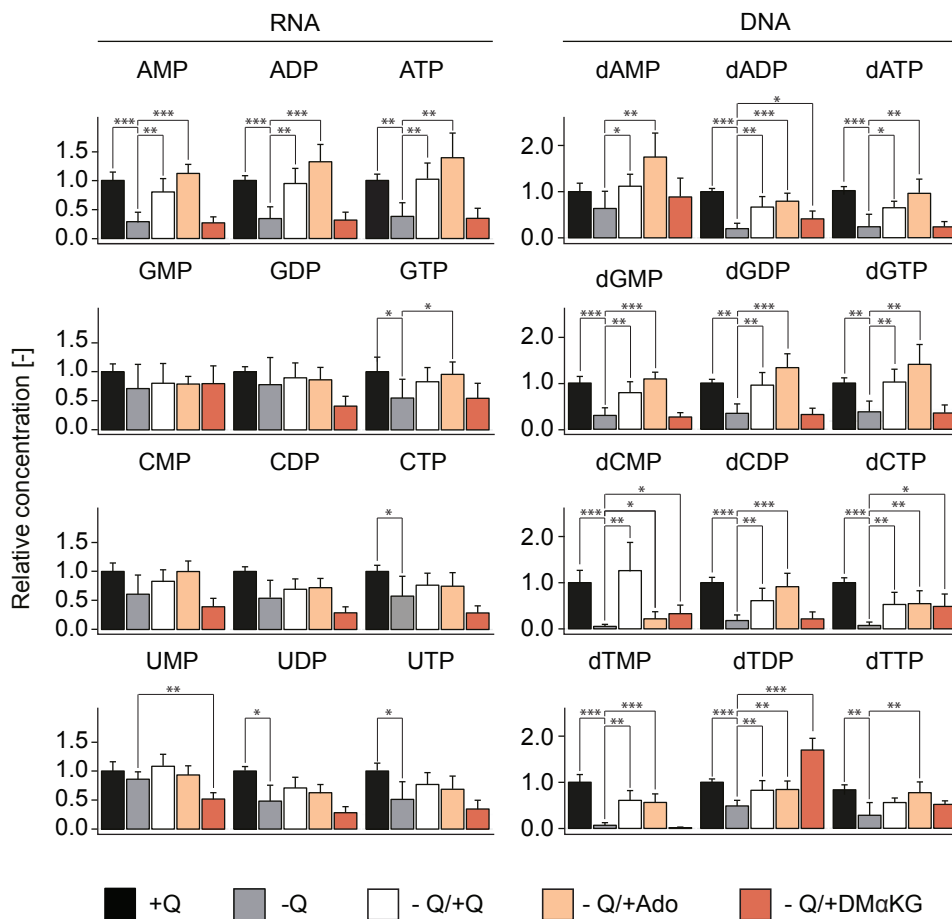
Figure 4.21.: Stimulus-dependent effects on nucleotide levels. Shown are direct-infusion MS acquired nucleotide and deoxynucleotide levels in response to re-addition of indicated substances after 2 hrs upon glutamine starvation (16 hrs) in HCT116 cells. Quantities were normalized to +Q per metabolite. Results represent mean + SD (n=6, each measurement performed in technical triplicates). P-values were calculated using a two-tailed student's t-test (* $0.01 < p \leq 0.05$; ** $0.001 < p \leq 0.01$; *** $p \leq 0.001$). Abbreviations – Ado: Adenosine, DMαKG: Dimethyl α-ketoglutarate, Q: Glutamine. Data were published in figure 4B in Dejure and Royla et al. [2017].

4.5.3. Investigation of energy-generating and -sensing mechanisms

The investigation of the glutamine-dependent MYC expression provided evidences that cellular energy-providing or energy-sensing mechanisms might be involved in the feedback regulation of MYC.

Inhibition of oxidative phosphorylation

The molecule ATP, which is known as the molecular currency of intracellular energy transfer, is generated via the breakdown of carbohydrates, lipids and amino acids. The majority of ATP is produced via OXPHOS. Oxidation/reduction reactions of the ETC release free energy that is ultimately used to produce ATP via the ATPase complex.
The inhibitors oligomycin and thenoyltrifluoroacetone (TTFA), which interfere with the ETC, were tested for their effect on glutamine-dependent MYC regulation (*figure* 4.22). HCT116 cells were cultured for 16 hrs in glutamine-deprived media supplemented with both inhibitors in independent experiments. Both inhibitors neither changed the strength nor the speed of glutamine-mediated MYC protein recovery compared to the solvent control.
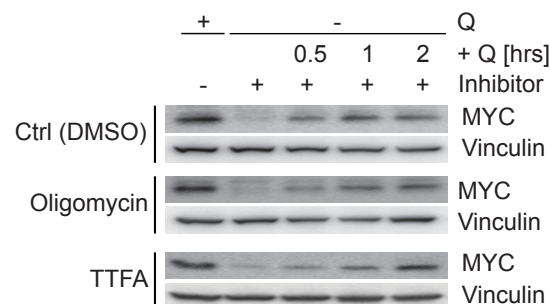
Figure 4.22.: Effects of OXPHOS inhibitors on glutamine-mediated MYC recovery. Representative immunoblots document MYC protein expression upon glutamine starvation and treatment with indicated inhibitors for 16 hrs followed by glutamine re-addition (*n*=3). Applied inhibitor concentrations were based on values that have been reported in literature and were not further validated [Kluckova et al., 2015; Zhang et al., 2017b]. Abbreviations – Q: Glutamine, TTFA: Thenoyltrifluoroacetone.

The role of AMPK activation in glutamine-dependent MYC regulation

Most cellular processes require energy. The key regulator of energy balance in the cell is an enzyme called AMP-activated protein kinase (AMPK), which senses the cells' energy status and promotes ATP-producing catabolic or inhibits ATP-consuming anabolic processes in response. Upon energy stress AMPK is activated as AMP and/or ADP allosterically bind to it inducing the phosphorylation of Thr172 at its α-subunit. Since AMP and ADP compete with ATP to bind AMPK, the enzyme ultimately senses AMP:ATP and/or ADP:ATP ratios [Hardie, 2011; Hardie et al., 2016].

Adenosine-derived nucleotide levels were strongly and rapidly affected upon changes in glutamine availability. Marginal differences in the strength of the response at each single nucleotide level might cause a transient energy imbalance. Therefore, the phosphorylation status of AMPK was investigated over the whole glutamine starvation and re-addition time course (*figure* 4.23A).

Since AMPK is activated upon cellular stresses such as glucose deprivation, the depletion and re-addition of glucose served as a control experiment [Hardie, 2011]. Indeed, glucose removal caused the rapid and pronounced phosphorylation of AMPK at the residue Thr172. The phosphorylation remained constant until glucose was re-added. The supplementation of the carbon source led to a stable deactivation of AMPK (*figure* 4.23A). In contrast, glutamine presence or absence did not influence phosphorylation at Thr172.

It was previously shown that AMP, ADP and ATP levels slightly dropped 5 min after glutamine re-addition before nucleotide pools were re-filled (*section* 4.4.2). At the same time the phosphorylation status of AMPK was slightly increased (*figure* 4.23A). The quantification of AMPK Thr172 revealed no significant AMPK activation peak in comparison to MYC protein recovery (*figure* 4.23B). Moreover, the activation of the phosphorylation site Ser485, which is known to suppress AMPK activation via Thr172, as well as total AMPK levels remained constant upon glutamine re-addition.
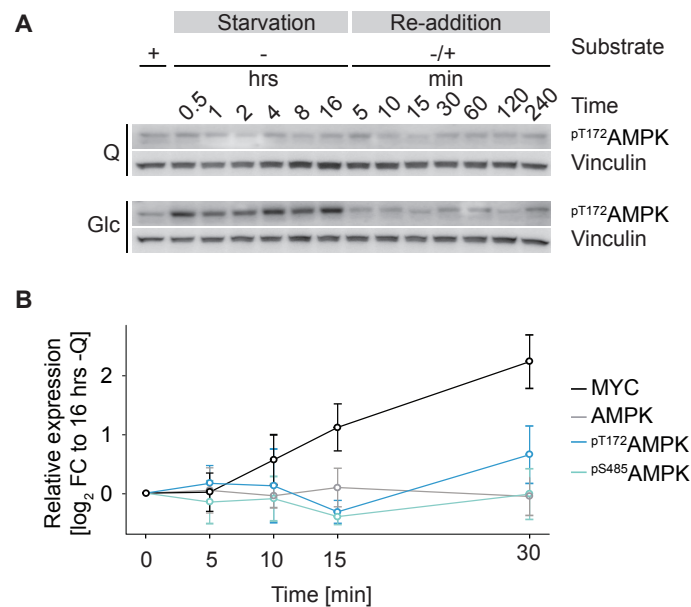
Figure 4.23.: AMPK activation in response to glutamine availability. (A) Representative immunoblots show the time-resolved phosphorylation status of AMPK (Thr172) in response to starvation and re-addition of the major carbon sources glutamine and glucose in HCT116 cells (*n*=3). (B) Quantification of total and phosphorylated AMPK (Thr172 and Ser485) are shown 5, 10 and 15 min after glutamine re-addition in comparison to MYC protein expression. Quantities were normalized to -Q at 16 hrs. Results represent mean ± SD of at least three independent experiments.

Cyclic AMP signaling is dependent on glutamine availability

Direct-infusion MS allowed for the measurement of cyclic AMP (cAMP), a derivative of ATP functioning as a second messenger in signal transduction. The conversion of ATP to cAMP is executed by the enzyme adenylyl cyclase (AC) in response to changes in cellular ATP levels. cAMP activates protein kinase A (PKA), which in turn phosphorylates numerous metabolic enzymes and signaling proteins [Zhang et al., 2016; Sassone-Corsi, 2012].

Levels of cAMP slightly decreased in HCT116 cells that were deprived for glutamine for 16 hrs (*figure* 4.24A). By re-adding glutamine, pools recovered within 10 min and kept constant over the time span of 2 hrs. The re-addition of adenosine caused a faster and stronger effect as cAMP levels were restored after 5 min and they further increased by a factor of two within the next 5 min (*figure* 4.24B). Two hours after supplementation cAMP abundance significantly magnified 4 times compared to starved cells (*figure* 4.24A).

These results led to the hypothesis that cAMP signaling might be a transmitter of glutamine availability. Therefore the inhibitors MDL12-330A, 2',5'-ddAdo and PKAi, 14-22 Amide (PKAi) were used to block cAMP generation and cAMP signaling, respectively. The application of the latter, inhibiting the phosphorylation of cAMP-dependent protein kinase, did not change glutamine-dependent MYC regulation (*figure* 4.25). In contrast, inhibition of AC by MDL12-330A and 2',5'-ddAdo diminished the recovery of MYC protein in response to glutamine re-addition in starved HCT116 cells.

A rescue experiment supplementing forskolin, a stimulator of AC, was performed to further test the impact of cAMP signaling on MYC regulation. Elevated cAMP levels upon
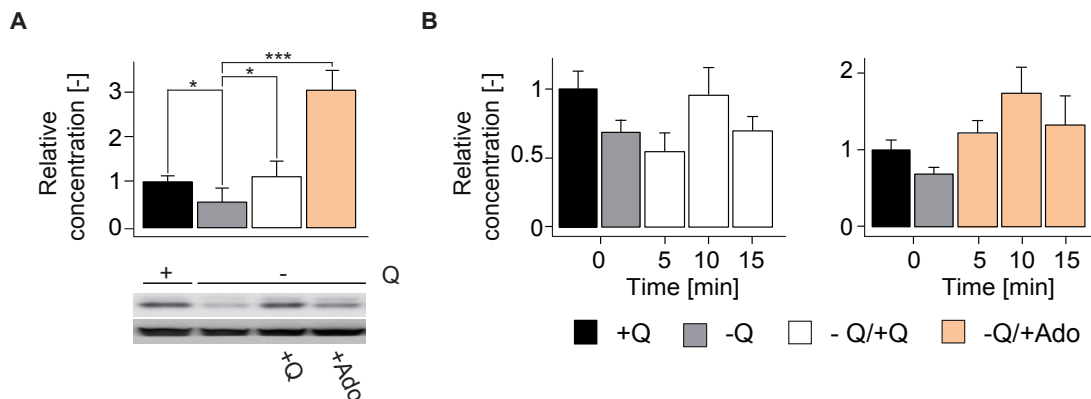
Figure 4.24.: Effects of glutamine and adenosine availability on cAMP signaling.
(A) MYC protein expression and relative concentrations of cAMP are shown in response to re-addition of indicated substances after 2 hrs upon glutamine starvation (16 hrs) in HCT116 cells. (B) Short-term effects (5, 10, 15 min) of glutamine and adenosine re-addition on cAMP abundance are illustrated. Quantities were normalized to +Q. Results represent mean + SD (n=6, each measurement performed in technical triplicates). P-values were calculated using a two-tailed student's t-test (* $0.01 < p \leq 0.05$; ** $0.001 < p \leq 0.01$; *** $p \leq 0.001$). Abbreviations – Ado: Adenosine, Q: Glutamine.

treatment were confirmed by the phosphorylation of the cAMP signaling downstream target CREB at Ser133 (*supplemental figure* B.9). The addition of forskolin to glutamine-deprived cells resulted in a weak MYC protein recovery. These findings led to the conclusion that cAMP signaling might be involved in glutamine-dependent MYC regulation, but further validation is required.
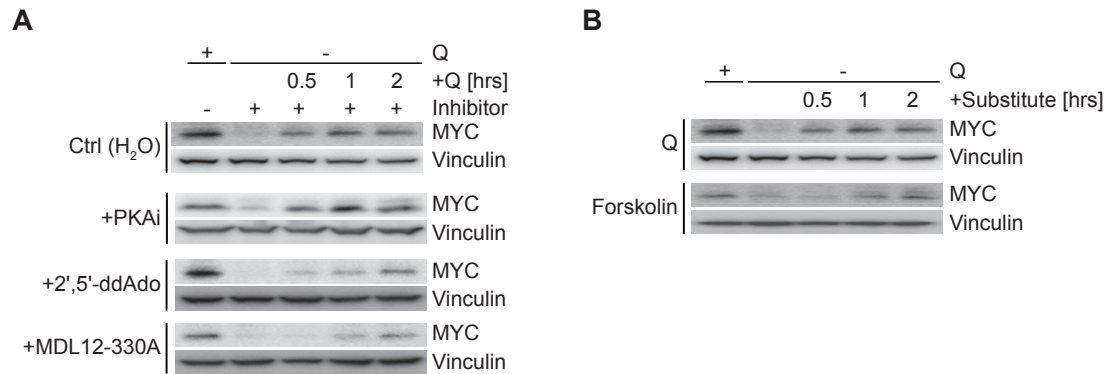
Figure 4.25.: Inhibition and stimulation of cAMP signaling. (A) Immunoblots document MYC protein expression upon starvation and treatment with indicated inhibitors for 16 hrs followed by glutamine re-addition (*n*=2). Applied inhibitor concentrations were based on values that have been reported in literature and were not further validated. (B) MYC protein expression upon glutamine starvation and re-addition of forskolin (*n*=3). Abbreviations – Q: Glutamine.

4.6. Identification of *MYC* 3'-UTR binding proteins

4.6.1. Summary of findings in the Eilers Lab

The MYC-estrogen receptor (MYC-ER) fusion protein system has become a standard tool in the MYC community to identify candidate target genes. The MYC-ER fusion protein is retained in a functionally inactive state in the cytoplasm in the absence of the receptor ligand tamoxifen. However, the supplementation of the ligand triggers a conformational change in the ER leading to the translocation of MYC-ER to the nucleus, where it functions as the normal MYC transcription factor [Eilers et al., 1989; Dang, 1999; Modjtahedi and Clarke, 2008].

The standard cell line HCT116 was transfected with MYC-ER or an empty vector (EV), that served as a control, to analyze the impact of high and stable MYC expression in response to glutamine availability. Experiments performed in the Eilers laboratory confirmed the MYC-induced apoptosis upon glutamine starvation, known as glutamine addiction, in MYC-ER transduced cells [Dejure and Royla et al., 2017]. This result is concordant with a series of studies, that address MYC-driven apoptosis as a result of amino acid or glucose starvation [Shim et al., 1998; Evan et al., 1992; Yuneva et al., 2007; Wise et al., 2008].

The exogenous MYC expression upon tamoxifen treatment was not downregulated in the absence of glutamine contrary to the endogenous one (*figure* 4.16). The questions arising from these results were:

(i) Why did transgenic MYC overexpressing HCT116 cells maintain ectopic MYC levels upon glutamine deprivation, while endogenous levels were suppressed?

(ii) Why did transgenic MYC overexpressing HCT116 cells undergo apoptosis upon glutamine deprivation, while normal HCT116 cells arrested?

Gene expression is ultimately regulated at the post-transcriptional level via regulatory regions that are usually neglected in the process of engineering transgenes. To note, the MYC-ER construct is missing both, the 5'- and 3'-untranslated region (UTR), and so far no aberrations within the regulatory regions of *MYC* are known. Therefore four different *MYC* constructs were expressed in HCT116 cells, which comprised either the coding sequence of *MYC* or the coding sequence plus the 3'-UTR or the 5'-UTR or both regulatory regions (*figure* 4.26). Glutamine presence and absence tests were performed by Francesca Dejure in Würzburg discovering that the presence of the 3'-UTR is essential in order to suppress MYC protein expression in the absence of glutamine (*figure* 4.26).

We further validated the 3'-UTR as the glutamine sensing unit of *MYC* mRNA by including the regulatory region into the MYC-ER construct. In case the 3'-UTR was present,
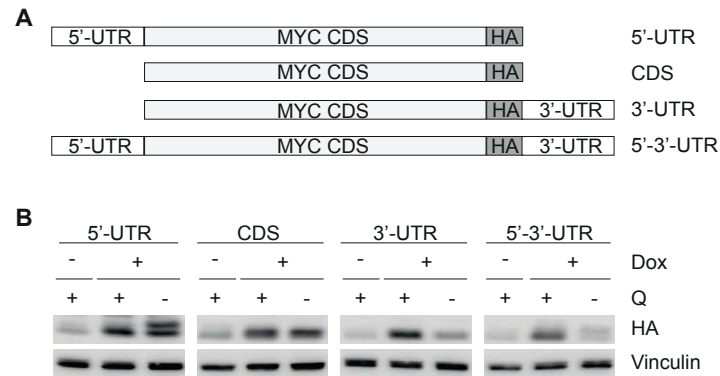
Figure 4.26.: *MYC* 3'-UTR is essential to regulate MYC protein in response to glutamine alterations. (A) Diagram depicts the doxycycline (Dox)-inducible *MYC* constructs used for lentiviral infection of HCT116 cells. All constructs contain a carboxy-terminal HA-tag. (B) Immunoblot documents levels of ectopically expressed MYC. Glutamine starvation was started after 2 hrs of Dox-mediated induction and maintained for 15 hrs in the presence of Dox. Exogenous MYC levels were detected by anti-HA immunoblot (n=3). Abbreviations – CDS: Coding sequence, Q: Glutamine. Figure adopted from Dejure and Royla et al. [2017].

ectopic MYC protein was suppressed upon glutamine starvation, while in the absence stable overexpression was observed [Dejure and Royla et al., 2017]. It was shown that the 3'-UTR is not only sensitive to glutamine, but also to adenosine. Moreover, the decrease of ectopic MYC protein upon glutamine deprivation, enabled by the presence of the 3'-UTR, protected HCT116 cells from apoptosis [Dejure and Royla et al., 2017].

In summary, the MYC protein expression is regulated via the 3'-UTR of *MYC*, which responds to cellular glutamine and adenosine levels to eventually escape apoptosis. The described findings led to the question which proteins might interact with the 3'-UTR leading to the subsequently described experiment.

4.6.2. *MYC* 3'-UTR pull-down to identify RNA binding proteins

The 3'-UTR was found to be the glutamine sensor unit of *MYC* mRNA. A mRNA pull-down experiment was performed in order to identify possible *MYC* 3'-UTR binding proteins that might be involved in the glutamine-mediated MYC regulation. The RNA pull-down assay was carried out as described in *section* 3.4. The 3'-UTR was incubated with lysates of HCT116 cells that were either cultured in the absence (-Q) or presence (+Q) of glutamine for 16 hrs. Next to the 3'-UTR of *MYC*, an unrelated control (poly(A) tail) was treated in parallel to exclude unspecific binders.

In total 764 3'-UTR-specific proteins were identified via LC-MS[4] measurements (*figure* 4.27). The majority of proteins was found in both conditions like the protein HuR

---

[4]Liquid chromatography mass spectrometry
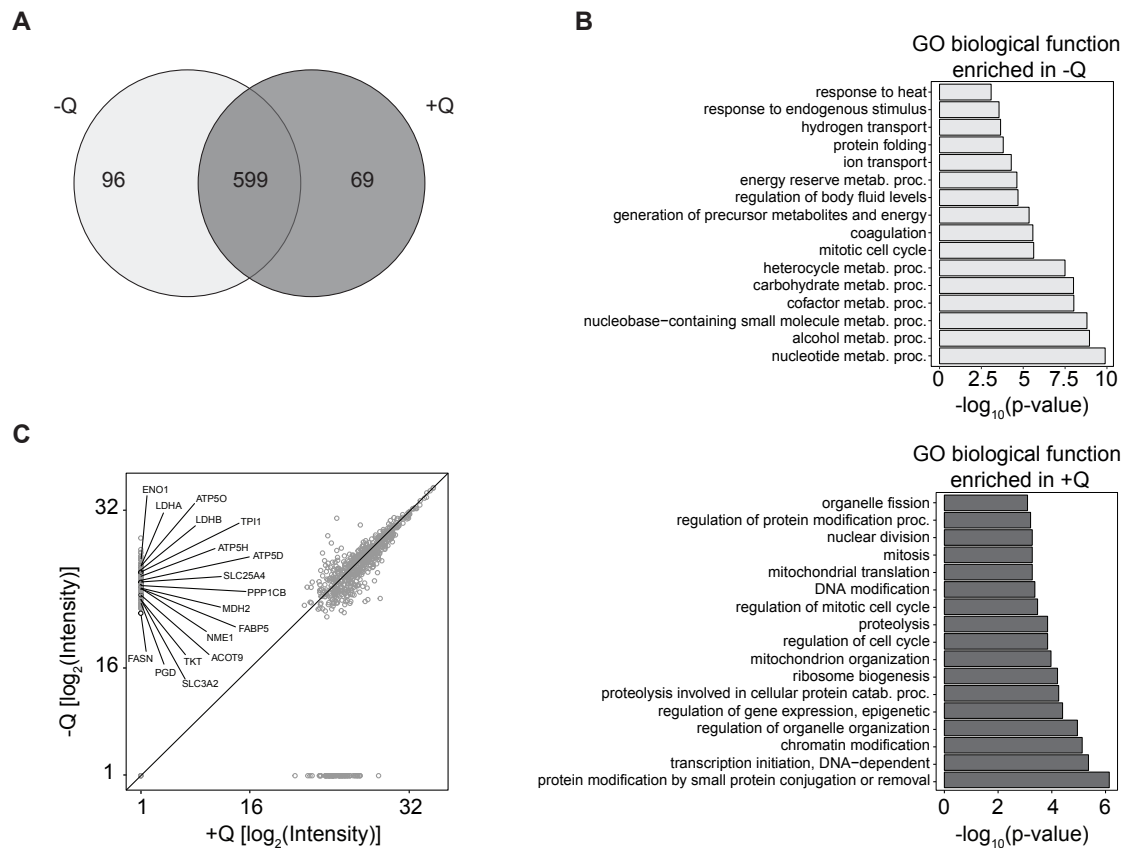
Figure 4.27.: Identification of *MYC* 3'-UTR binding proteins. (A) Venn diagram displays proteins that were identified in *MYC* 3'-UTR pull-down assay comparing absence (-Q) and presence (+Q) of glutamine in the media. Proteins detected via LC-MS with at least one unique peptide that have not been found in the unrelated control are shown. (B) Gene ontology (GO) biological processes analysis of protein clusters enriched either in the presence or absence of glutamine. Bar chart represents classification of GO biological processes and indicates statistical significance (-log$_{10}$(p-value)). (C) Scatter plot of 764 proteins being specific for the 3'-UTR of *MYC* over the unrelated control. The log$_2$ transformed intensities of all proteins are shown comparing the conditions -Q and +Q against one another on the x- and y-axes, respectively. For the complete protein names refer to the list of abbreviations.

that is known to have binding motifs within the sequence of the *MYC* 3'-UTR. Less than 10% of all detected proteins exclusively bound in the presence of glutamine while 96 proteins were only detected under glutamine starvation (*section* 3.4, *supplemental table* B.1, *supplemental table* B.2). Surprisingly, gene ontology (GO) category analysis revealed that proteins of the latter cluster are mainly involved in metabolic and energy generation processes. On the contrary, proteins detected in the presence of glutamine are involved in processes such as transcription initialization, regulation of gene expression, mitochondrial organization and regulation of mitotic cell cycle, which infer to a functioning and dividing cell population (*figure* 4.27).

Previous discussed results have uncovered a link between MYC regulation and the metabolic functions of glutamine. Interestingly, 17 out of 96 proteins, which were found to bind to

the 3'-UTR upon glutamine starvation, are associated with metabolic or energy-providing processes. The glycolytic proteins enolase 1 (ENO1), triosephosphate isomerase (TPI) and the isoforms lactate dehydrogenase A and B (LDHA and LDHB) were identified as interactors next to proteins, that are involved in fatty acid metabolism (fatty acid synthase (FASN), acyl-CoA thioesterase 9 (ACOT9), fatty acid-binding protein 5 (FABP5)). Moreover, three out of these 17 proteins were subunits of the ATP synthase complex (ATP5D, ATP5H, ATP5O). The transporter SLC25A4 shuffling ADP in exchange with ATP from the cytosol into the mitochondria was also identified as a *MYC* 3'-UTR binding protein. The 3'-UTR pull-down assay revealed interesting possible mediators of the glutamine-dependent MYC regulation. Based on the herein presented experiments a list of 100 possible mediators was compiled and forwarded to the Eilers lab, where a siRNA screen will be performed (*supplemental table* B.3)

4.7. Dissection of metabolic bypass reactions in response to glutaminase inhibition

Glutaminase (GLS) is the enzyme catalyzing the conversion of glutamine to glutamate as the first step of glutaminolysis. Numerous studies reported the positive regulation of glutaminolysis by several oncogenic stimuli like those transmitted by MYC [Altman et al., 2016]. The metabolic transformation resulting in glutamine addiction became the focus of various studies that include the inhibition of glutaminase as a possible therapeutic approach [Chen and Cui, 2015].

4.7.1. Characterization of glutaminase inhibitors

Validation of glutaminase inhibitors

GLS inhibitors were applied to mimic glutamine starvation to further validate the role of glutamine as the fuel for anaplerotic reactions. Firstly, the efficiency of the inhibitors was tested in a pSIRM approach applying uniformly labeled ^{13}C-glutamine. The GC-MS based tracing of carbon-13 routing allowed to check for the decrease in ^{13}C-accumulation in glutamine downstream metabolites as the most direct read-out of glutaminase inhibition.

HCT116 cells were exposed to different concentrations of the GLS-specific inhibitors BPTES[5], Compound 968 (C968), CB839 and the glutamine structural analogue 6-Diazo-5-oxo-L-norleucine (DON) for 16 hrs. A solvent control was treated in parallel. Contrary to expectations, no drastic reduction of ^{13}C-incorporation in glutamate (Glu) and α-ketoglutarate (αKG) after 45 min of labeling was observed independently of the applied inhibitors and their concentrations (*figure* 4.28).

The inactivation of glutaminase is achieved via allosteric control by the small molecules BPTES, C968 and CB839, while the glutamine-analogue DON competes with the amino acid to bind glutaminase [Chen and Cui, 2015]. Increasing inhibitor concentrations did not reduce the conversion of glutamine into glutamate and subsequent α-ketoglutarate in the presence of glutamine leading to the assumption that glutaminase might be indeed inhibited, but other bypassing reactions might compensate for the inactivation of the enzyme.

In *section* 4.4.2 it was shown that the usage of glutamine to fuel the TCA cycle is strongly promoted in cells that were starved for the amino acid compared to non-starved cells. This routing is assumed to be mainly driven via glutaminase. Therefore HCT116 cells were starved for glutamine and treated with glutaminase inhibitors for 16 hrs. Afterwards, cells were incubated with u-^{13}C-glutamine for 5, 10 and 15 min in order to monitor inhibitor-controlled retardation of glutamine-derived carbon-13 routing within the TCA cycle.

---

[5]Bis-2-(5-phenylacetamido-1,3,4-thiadiazol-2-yl)ethyl sulfide
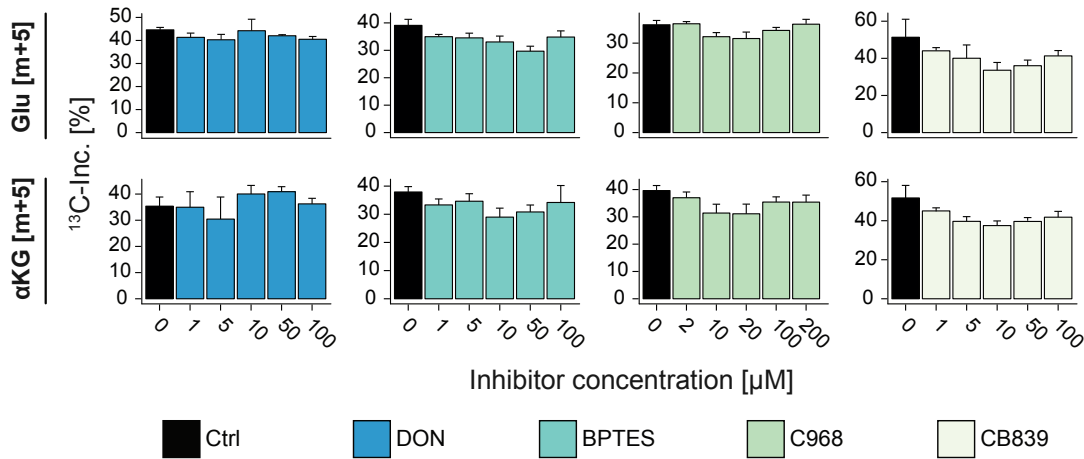
Figure 4.28.: Effects of glutaminase inhibition on ^{13}C-glutamine incorporation. GC-MS-derived ^{13}C-incorporation in glutamate (Glu) and α-ketoglutarate (αKG) after application of u-^{13}C-glutamine for 45 min. HCT116 cells were cultured for 16 hrs in the presence of glutamine and several glutaminase inhibiting substances in the indicated concentrations. Results represent mean + SD (n=3, each measurement performed in technical duplicates). Numbers of incorporated carbons are shown in brackets.

Figure 4.29A compares the inhibition-dependent ^{13}C-incorporation in glutamate and TCA cycle intermediates induced by either the glutamine-starved and therefore dynamic system or the previously described stable glutamine setup (stable Q), which is defined by a constant glutamine concentration of 2 mM throughout the experiment. GLS inhibitors were applied in a working concentration of 10 µM, because numerous studies reported reduced cell growth at this concentration (C968: [Wang et al., 2010; Son et al., 2013]; BPTES: [Le et al., 2012; Shanware et al., 2014]; DON: [Huang et al., 2014]; CB839: [Xiang et al., 2015]). In order to evaluate the inhibitory effects, solvent controls were treated in parallel. In general, cells that were exposed to constant glutamine supply (stable Q) showed less ^{13}C-accumulation in all glutamine downstream metabolites than cells that were deprived for glutamine before labeling (dynamic Q), although labeling time was longer. Here, the earlier proposed promotion of OXPHOS after glutamine re-addition upon starvation was validated (*figure* 4.18). The application of the glutamine-antagonist DON significantly suppressed the dynamic and fast incorporation of carbon-13 in glutamate and malate, while incorporation of the stable glutamine setup after 45 min was not affected by the inhibitor. After 5 min ^{13}C-incorporation was reduced to 40% in glutamate and to 30% in malate compared to the non-treated control. Differences between the ^{13}C-incorporation in treated and non-treated HCT116 cells reduced over time, most likely due to the solvent control reaching steady-state sooner. Similar observations were made for the inhibitors BPTES and CB839, while the degree of dynamic inhibition caused by BPTES was less and the degree caused by CB839 was greater compared to DON. Both small inhibiting molecules
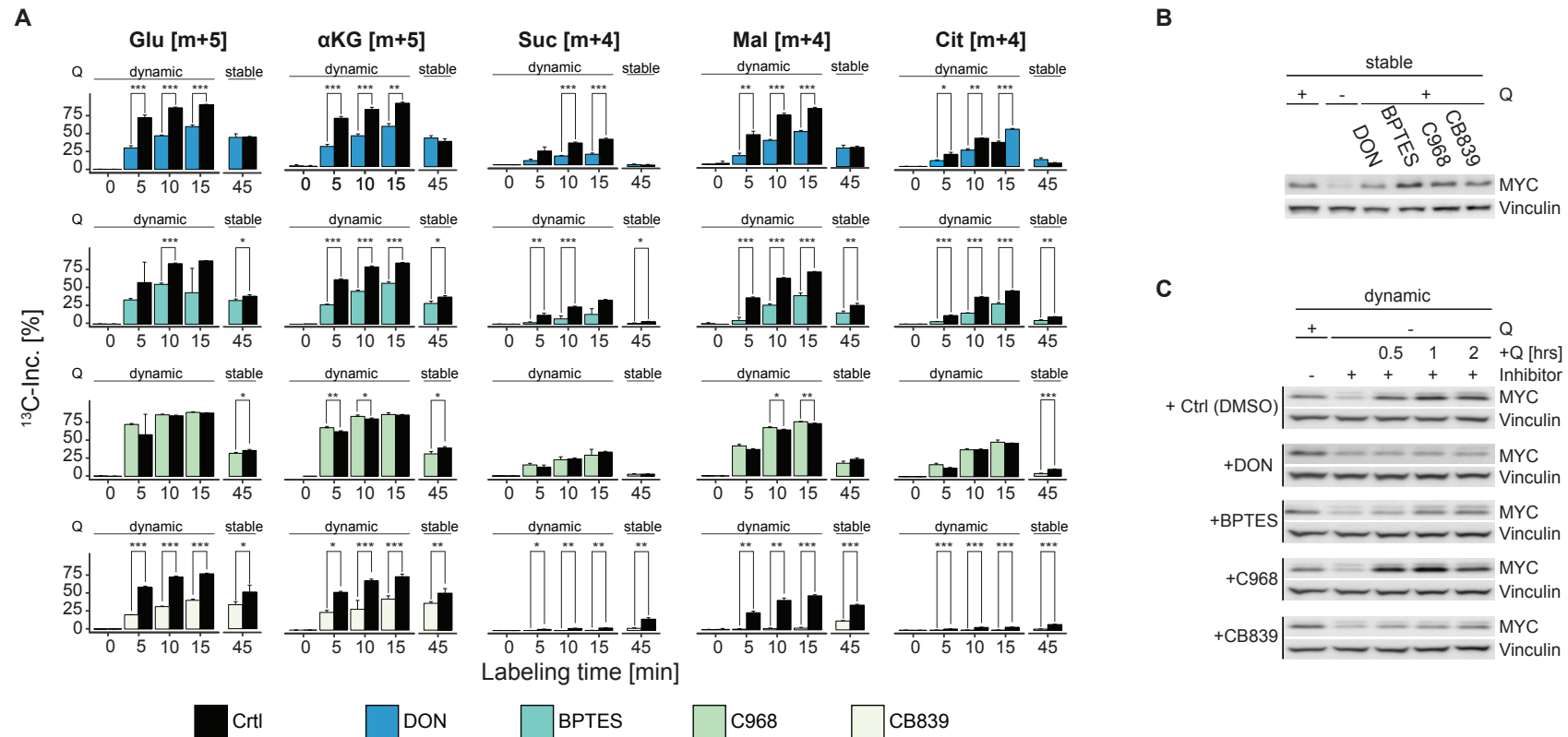
Figure 4.29.: Validation of glutaminase inhibitors and their effects on MYC protein levels (A) ^{13}C-incorporation in glutamine-starved (dynamic Q) and non-starved (stable Q) HCT116 cells are shown. Cells were treated with 10 µM of indicated GLS inhibitors for 16 hrs. The re-addition of u-^{13}C-glutamine to starved cells in a short time frame (5, 10, 15 min) enabled the dynamic tracing of carbon-13 in glutamine downstream metabolites. The effect of the inhibitors in the stable glutamine setup was achieved while replacing ^{12}C-glutamine with u-^{13}C-glutamine for 45 min. Inhibitors were applied during the ^{13}C-glutamine labeling as well. Numbers of incorporated carbons are shown in brackets. All results are shown in comparison to the solvent control. Results represent mean + SD (n=3, each measurement performed in technical duplicates). P-values were calculated using a two-tailed student's t-test (* $0.01 < p \leq 0.05$; ** $0.001 < p \leq 0.01$; *** $p \leq 0.001$). (B) Representative immunoblot of MYC protein expression in HCT116 cells cultured for 16 hrs in the presence of GLS inhibitors and glutamine. A control for glutamine starvation was included. (C) Immunoblots document the dynamic recovery of MYC protein expression after re-addition of glutamine upon starvation in response to simultaneously applied GLS inhibitors (16 hrs). Data were published in figure EV5A and EV5B in Dejure and Royla et al. [2017].

significantly reduced the carbon-13 proportion in glutamine downstream metabolites in the stable glutamine setup. Interestingly, BPTES application resulted in a maximal reduction of 10% whereas the accumulation of carbon-13 upon CB839 treatment led to a decrease of 15-22% (*figure* 4.29A).

Similarly to BPTES, the inhibitor C968 significantly, albeit slightly, reduced ^{13}C-incorporation in glutamate and TCA cycle intermediates upon constant glutamine supply (stable Q). A constant reduction – as it was verified for the other substances in the dynamic system – has not been observed for C968. Surprisingly, the small molecule significantly increased the proportion of carbon-13 in α-ketoglutarate and malate after 5 and 10 min and 10 and 15 min, respectively (*figure* 4.29A).

The ^{13}C-labeled quantities – providing the indirect measurement of the metabolic flux – confirmed the partial inhibition of carbon-13 influx to the TCA cycle upon DON, BPTES and CB839 application in cells starved for glutamine prior re-addition (*supplemental figure* B.8). In the presence of the amino acid, glutaminase inhibitors did not block the transport of glutamine-derived carbons to the TCA cycle. These findings supported the hypothesis of bypassing reactions that compensate for the inhibited glutaminase activity in the presence of glutamine.

Impact of glutaminase inhibition on MYC protein levels

In addition to previous experiments, it was examined if inhibitor-dependent changes in TCA cycle intermediates determined changes in MYC recovery. MYC protein expression was analyzed in the system with constant glutamine supply and the dynamic system induced by glutamine re-addition upon starvation. HCT116 cells were treated as described before.

MYC levels were sustained upon inhibitor treatment with BPTES, C968 and CB839 in the presence of glutamine, while levels decreased upon DON treatment and completely disappeared in the absence of glutamine as illustrated in *figure* 4.29B. In the dynamic system MYC levels decreased upon deprivation of glutamine independent of the applied glutaminase inhibitors (*figure* 4.29C). Glutamine re-addition induced MYC protein recovery in C968-treated cells as observed for the solvent control. Surprisingly, a diminished MYC recovery was observed upon BPTES and CB839 application compared to the untreated control. In addition, glutamine re-addition did not restore MYC levels in the presence of the glutamine analogue DON.

Interestingly, the ability to regulate MYC protein levels in response to glutamine supply depends on the phenotype that glutaminase inhibitors provoke. BPTES, DON and CB839 partially inhibited glutaminase activity in the dynamic system and, likewise, decelerated MYC recovery kinetics upon glutamine re-addition. These inhibitors applied in the same manner did not control MYC levels in the presence of glutamine as their inhibitory effects were not verifiable in the stable glutamine setup.
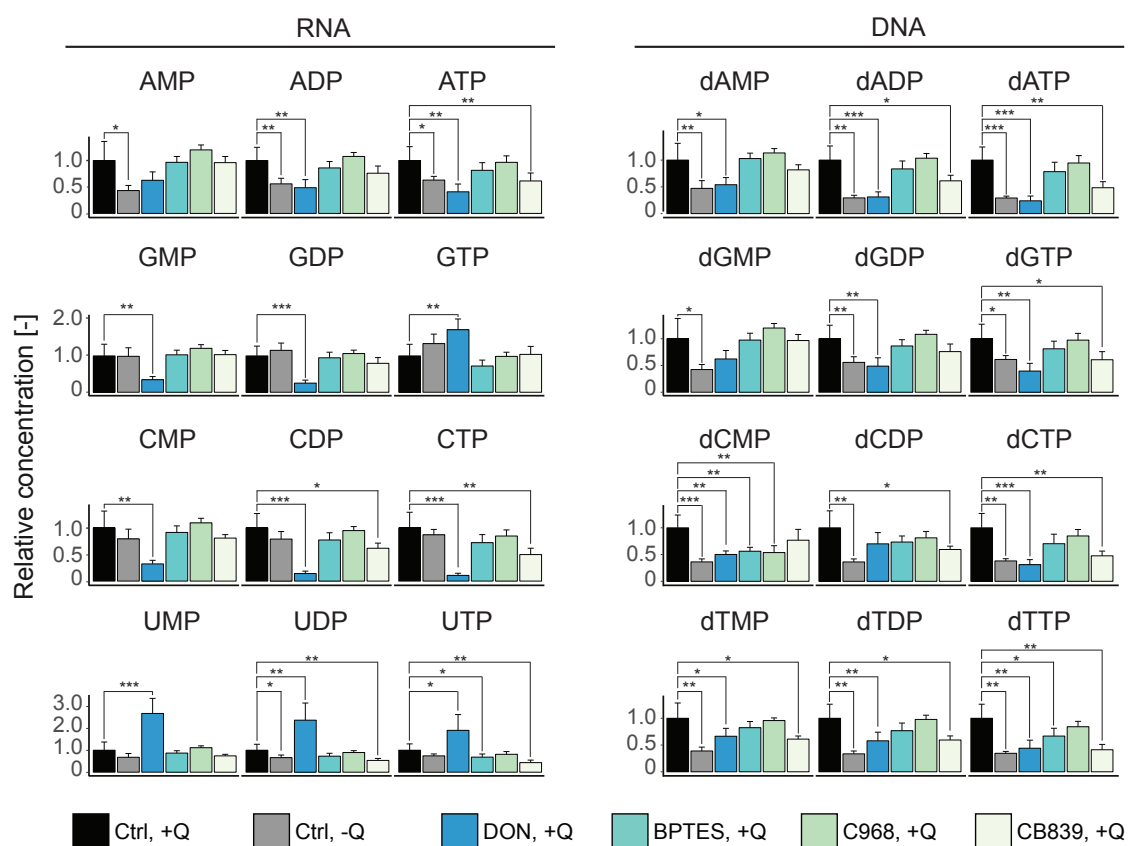
Figure 4.30.: Effects of glutaminase inhibition on nucleotide abundance. Shown are nucleotide concentrations of HCT116 cells cultured in the presence of indicated glutaminase inhibitors and standard cell culture media for 16 hrs. Non-treated, glutamine-starved (Ctrl, -Q) and non-treated, non-starved cells (Ctrl, +Q) served as controls. Results represent mean + SD (n=6, each measurement performed in technical triplicates). P-values were calculated using a two-tailed student's t-test (* $0.01 < p \leq 0.05$; ** $0.001 < p \leq 0.01$; *** $p \leq 0.001$). Data were published in figure EV5C in Dejure and Royla et al. [2017]

Effects of glutaminase inhibitors on nucleotides

Direct-infusion MS measurements were performed to examine the potential of glutaminase inhibitors to mimic glutamine deprivation effects on nucleotide levels. Briefly, HCT116 cells were treated with glutaminase inhibitors for 16 hrs in the presence of glutamine. Glutamine-starved and non-starved cells supplemented with DMSO served as controls. Significant decreases of deoxyribonucleotide and adenosine-derived ribonucleotide levels were detected for DON-treated cells similar to those observed upon glutamine starvation (*figure* 4.30). The quantities of guanosine- and cytidine-derived ribonucleotides diminished upon DON application while uridine-derived ribonucleotide levels significantly increased. Interestingly, nucleotide pools did not change in response to BPTES and C968 treatment. The addition of the inhibitor CB839 to non-starved cells caused a reduction in the abundance of several nucleotides, especially deoxyribonucleotides. However, the observed decline was less pronounced than the one observed upon the withdrawal of glutamine.

4.7.2. Cell growth upon glutaminase inhibition

A proliferation analysis upon glutaminase inhibition was performed in HCT116 and RKO cells. The small molecules BPTES, C968 and CB839 as well as the glutamine analogue DON were supplemented to cells cultivated in the presence of glutamine for in total 96 hours. Every 24 hrs media was renewed to prevent nutrient limitation. Viable cell numbers were determined 96 hrs and MYC protein expression 24 hrs post inhibitor supplementation.

The absence of glutamine caused a pronounced cell growth arrest in the colon cancer cell lines HCT116 and RKO (*figure* 4.31). Cell numbers were diminished by seven- and ten-fold comparing non-treated, glutamine-starved and non-treated, non-starved HCT116 and RKO cells, respectively. The glutamine antagonist DON inhibited cell growth of both cell lines in a similar manner. The application of BPTES and C968 significantly decelerate proliferation in both cell lines. However, the cell growth was reduced by maximal 53% (C968 treatment in RKO cells), which was still significantly elevated compared to glutamine-deprived cells. Surprisingly, the application of the small molecule CB839 partially inhibited cell growth in HCT116 cells, but had no effect on RKO cells in the presence of glutamine.

Additionally, MYC protein levels were analyzed 24 hrs post inhibitor supplementation (*figure* 4.31). This time point was chosen in order to determine the MYC status that drove the exponential proliferation throughout the experiment rather than to determine levels after 96 hrs that might be affected by cell-to-cell contact. As described earlier, the inhibition of glutaminase did not impair MYC protein levels in HCT116 cells. These
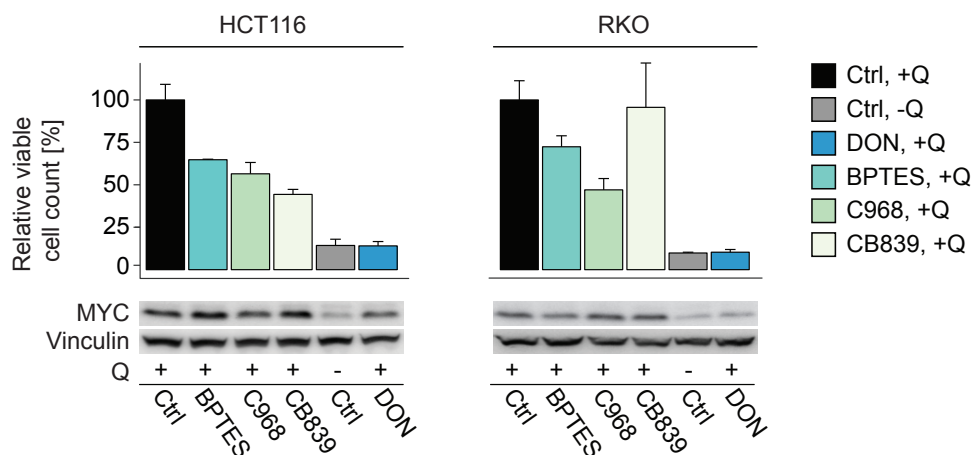
Figure 4.31.: Effects of glutaminase inhibition on cell growth. The colon cancer cell lines HCT116 and RKO were grown for 96 hrs in media supplemented with indicated inhibitors. Cell numbers were determined at 0 and 96 hrs and are shown relative to 0 hrs. MYC protein expression was investigated after 24 hrs. Results represent mean + SD ($n=3$, each measurement performed in technical triplicates). P-values are shown in the *supplemental table* B.4. Cell number determination of RKO cells was performed by Şafak Bayram (Master student in the Lab of Stefan Kempa, BIMSB/MDC, Berlin-Germany) under the supervision of the author.

results were concordant with those of RKO cells, except for DON-treatment. Upon the application of the non-standard amino acid DON MYC protein levels were reduced.

DON as a structural analogue of glutamine, does not only inhibit glutaminase but all glutamine-converting enzymes, e.g., carbamoyl phosphate synthase (CAD), CTP synthase (CTPS), guanosine monophosphate synthetase (GMPS) and asparagine synthetase (ASNS) [Pinkus, 1977]. Since DON is competing with glutamine to bind these enzymes, a sufficient supply of the antagonist should mimic glutamine deprivation effects. The different impacts of DON on MYC levels in the colon cancer cell lines brought up two hypotheses. First, glutamine-converting enzymes mediating the MYC control might be less abundant in RKO compared to HCT116 cells. Therefore they are more efficiently blocked in the presence of DON. In turn, the blockage of the activity of these enzymes might mimic the effect of glutamine starvation on MYC levels. Second, HCT116 cells might have an additional bypassing reaction that could take over the supply of necessary intermediates of certain pathways, which eventually control MYC protein levels.

4.7.3. Analysis of glutamine-consuming enzymes

The shotgun LC-MS proteomics approach and MaxQuant label-free quantification were applied to evaluate the protein expression profile of enzymes that use glutamine as a substrate. The colon cancer cell lines HCT116 and RKO were cultured 24 hrs in standard cell culture media, harvested, digested, desalted and subjected to the LC-MS. The experiments were assisted by Şafak Bayram (Master student in the Lab of Stefan Kempa, BIMSB/MDC, Berlin-Germany) under the supervision of the author.

The list of identified proteins in each cell line was filtered for enzymes that either (i) use glutamine or glutamate as a substrate, (ii) generate glutamine or glutamate as a product, (III) or execute the transport of both metabolites through the plasma or mitochondrial membrane. In total 28 proteins involved in glutamine/glutamate metabolism were detected. *Figure* 4.32 illustrates the compartment-specific reactions catalyzed by the proteins and their abundance in RKO and HCT116 cells normalized to the latter.

Both subunits of the glutamine transporter LAT1 (SLC3A2, SLC7A5), responsible for glutamine uptake, were found to be elevated in RKO cells compared to HCT116 cells. In contrast, the expression of mitochondrial glutamate transporters SLC25A12 and SLC25A13 were 2-fold and 20-fold increased in HCT116 cells, respectively. Proteins, that transport glutamine via the mitochondrial membrane, are not known.

Interestingly, the abundance of mitochondrial proteins were higher in RKO cells, except for glutamine synthase (GLUL) that could only be detected in HCT116 cells. Furthermore, the opposite effect was observed for cytoplasmic enzymes catalyzing transamination reactions involving other amino acids, e.g., GLUL, ASNS, aspartate aminotransferase (GOT1), phosphoserine aminotransferase (PSAT). In both colon cancer cell lines

quantities were similar for enzymes involved in purine and pyrimidine *de novo* nucleotide biosynthesis - carbamoyl-phosphate synthetase (CAD), CTP synthase 1 and 2 (CTPS1 and CTPS2), guanosine monophosphate synthetase (GMPS), phosphoribosyl pyrophosphate amidotransferase (PPAT), phosphoribosyl formylglycinamidine synthase (PFAS) (*figure 4.32*).
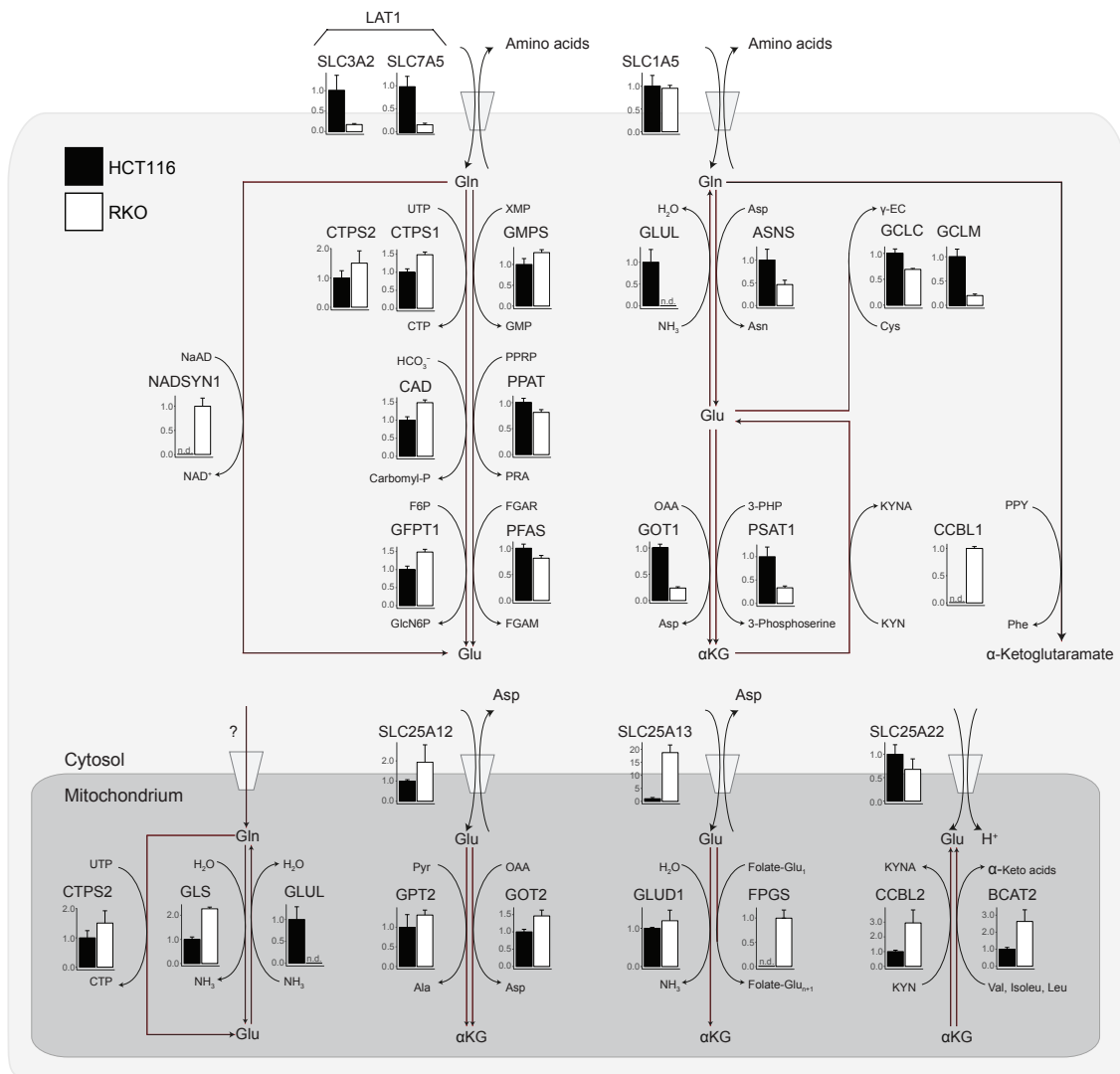
Figure 4.32.: Protein expression of enzymes involved in glutamine/glutamate metabolism. LC-MS obtained quantities of selected enzymes are shown for HCT116 and RKO cells cultivated for 24 hrs in standard cell culture media. Values were normalized to those of HCT116 cells. Results represent mean + SD (n=3). The experiment was performed by Şafak Bayram (Master student in the Lab of Stefan Kempa, BIMSB/MDC, Berlin-Germany) under the supervision of the author. Abbreviations – n.d.: not determined. For the complete protein and metabolite names refer to the list of abbreviations.

Compartment-specific diversity in protein expression observed for HCT116 and RKO cells led to the assumption that the cell lines might prefer different reactions and pathways to generate glutamate and α-ketoglutarate from glutamine. The protein quantities per subcellular localization (cytosol, plasma membrane, mitochondria, mitochondrial membrane) were summed up and divided by the sum of quantities of all 28 identified proteins per cell line. These ratios were determined to identify if the colon cancer cell lines rely on compartment-specific reactions (*figure* 4.33). The analysis suggests an elevated glutamine import to HCT116 cells and an increased glutamate import to the mitochondria of RKO cells. In line with these results is the high expression of mitochondrial enzymes that generate glutamine downstream metabolites in RKO cells.

To further address the question of cell line-specific reactions that efficiently provide glutamine downstream metabolites, additional experiments, e.g., a pSIRM-based approach upon inhibitor treatment in both cell lines, need to be performed.
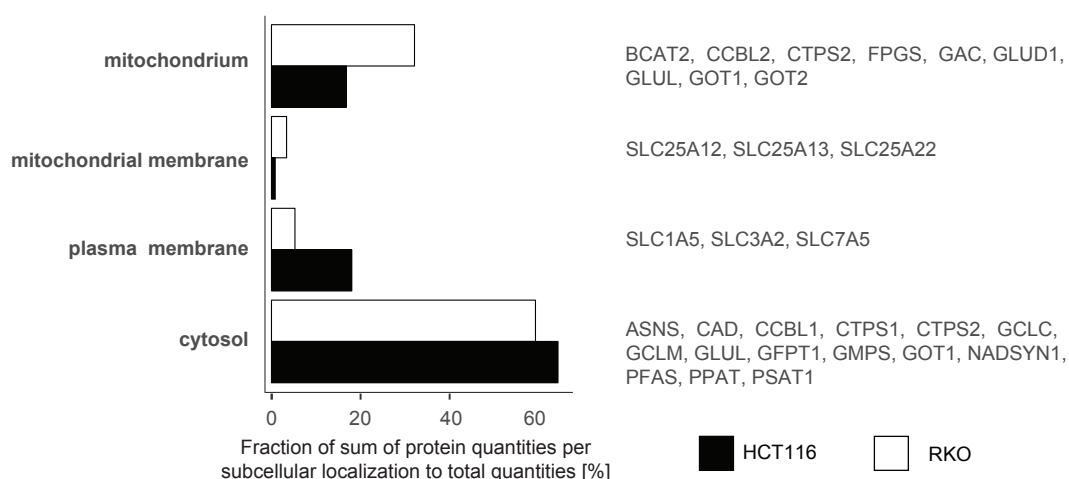
Figure 4.33.: Analysis of compartment-specific expression of proteins involved in glutamine/glutamate metabolism. Protein quantities per subcellular compartment were summarized and divided by the total sum of quantities per cell line (HCT116 and RKO). Compartment-specific proteins are shown. For the complete protein and metabolite names refer to the list of abbreviations.

5. Discussion

Reprogrammed metabolism is considered a hallmark of cancer, due to atypical metabolic characteristics observed frequently across several tumor types [Hanahan and Weinberg, 2011]. Common features are increased glycolysis and glutaminolysis, in order to meet bioenergetic and biosynthetic needs required for an invasive cell growth. Although, this specialization increases the vulnerability to therapies that focus on targeting these mostly oncogene-driven alterations [Moscat et al., 2015].

Sufficient nutrient supply is an important requirement to continuously promote proliferation and survival. Cells of solid tumors that exhibit a great heterogeneity in the accessibility to nutrients, run alternative metabolic programs in order to adjust to the specific microenvironments [DeBerardinis and Chandel, 2016]. The flexibility to rewire oncogene-driven metabolic programs implies that cells possess the ability to adapt the expression of oncogenes in regard to low nutrient conditions. On the contrary, the oncogene *c-MYC* (*MYC*) is known to induce a metabolic program that renders tumor cells to be dependent on the non-essential amino acid glutamine for survival [Wise et al., 2008].

In this study we addressed whether limitations on external glutamine supply affect MYC as a transcription factor in regard to glutamine addiction. In the following I will discuss how (i) we revealed a sequential dependency of MYC protein expression on glutamine supply; (ii) we dissected the dependency by time-resolved studies on different omic levels; (iii) we investigated the contribution of glutamine-converting enzymes to MYC regulation.

5.1. The *MYC* mRNA 3'-UTR suppresses MYC protein levels in the absence of glutamine to escape apoptosis

The colon cancer cell line HCT116 is a suitable cell culture model to address nutrient-dependent MYC regulation because it expresses high levels of MYC, a consequence of a point mutation in the *β-catenin* gene [Kaler et al., 2012]. Mutated β-catenin cannot be marked for ubiquitin-mediated proteasomal degradation via GSK3-β[1], which results in a constitutive activation of its downstream target MYC [Kaler et al., 2012].

MYC along with other oncogenes like *KRAS* and *PI3K*, which are also deregulated in HCT116 cells, drive the metabolic reprogramming in the colon cancer cell line [Ahmed

---

[1]glycogen synthase kinase 3-β

et al., 2013]. Each oncogene is involved in rewiring glucose and glutamine metabolism on a large scale, resulting in an enhanced import and utilization of glucose and glutamine – the main metabolic fuels of the central carbon metabolism in cancer cells [Tarrado-Castellarnau et al., 2016; Kawada et al., 2017]. A multitude of studies focused on how oncogenes regulate metabolism, whereby less effort was made to understand how these re-wiring processes work upon nutrient stress. Accordingly, we were interested in how nutrient availability affects the oncogenic transcription factor MYC, which is a main driver of metabolic reprogramming in cancer cells.

5.1.1. Glutamine availability regulates MYC protein expression

Changes of glutamine levels in the cell culture media revealed a dependency of MYC protein expression on external glutamine availability. High glutamine concentrations (2-6 mM), usually supplemented in cell culture experiments, caused high and stable MYC levels, whereas in the absence of glutamine protein expression was suppressed (*figure* 4.1). Gradual rise of glutamine concentration proportionally increased MYC protein levels up to the physiological range of the amino acid in human plasma (0.6-0.9 mM) [Hensley et al., 2013]. Additionally, MYC protein expression was restored upon the re-addition of glutamine subsequently after starvation (*figure* 4.2).

The herein presented data reveal a feedback between external glutamine supply and MYC protein expression that is precisely responding to variations between no and physiological glutamine supply. Interestingly, the concentration range coincides with the regional heterogeneity of glutamine accessibility observed in solid tumors [Pan et al., 2016]. A recent study demonstrated region-specific differences in glutamine availability in xenograft tumors, as significantly lower quantities of glutamine were detected in the tumor core compared to the tumor periphery. At the edge of the tumor glutamine levels were slightly below the physiological concentration of human plasma, whereas levels in the core tumor areas were in the range of 0.1-0.25 mM [Pan et al., 2016]. Based on the presented data and their physiological relevance, we imputed a high significance to the regulation of glutamine-dependent MYC expression in tumor cells.

The feedback was verified in ten cell lines derived from different entities and organisms (*figure* 4.4). The non-cancerous kidney cell line Cos7 showed, similar to various cancerous cell lines, alleviated MYC protein levels upon glutamine starvation leading to the assumption that the glutamine-dependent regulation of MYC is not only a cancer-dependent phenomenon. Nevertheless, the ability of HEK293 cells – an embryonic kidney cell line – to sustain MYC protein levels in the absence of glutamine demonstrates that the MYC control is not an universal valid mechanism.

5.1.2. Glutamine deprivation induces a reversible cell cycle arrest, not apoptosis

As shown, changes in glutamine availability revealed similar trends in proliferation and MYC protein expression, since MYC is known to be a transcriptional master regulator of cell growth (*figure* 4.1) [Dang, 2013]. MYC is targeting and amplifying a multitude of genes that are involved in cell cycle progression, DNA replication, as well as energy production and macromolecular biosynthesis. The interplay of all genes causes the simultaneous production of biomass and DNA, thus MYC is considered the nexus of cell division and growth [Kress et al., 2015; Dang, 1999].

In this context we investigated the proliferation of colon cancer cells in response to glutamine depletion. HCT116, RKO, GEO, SW480, HT29 and HEK293 cells were exposed to glutamine-deprived medium resulting in a halted proliferation and downregulated MYC protein levels in all colon cancer cell lines (*figure* 4.4). In contrast, HEK293 cells, showing sustained MYC protein expression in the absence of glutamine, maintained proliferation. These results confirm MYC's role as a major regulator of cell growth and proliferation.

Glutamine is the most abundant amino acid in the blood and in cell culture. Amino acid uptake experiments identified glutamine as the most highly consumed amino acid *in vitro* [Still and Yuneva, 2017]. Interestingly, not all cancer cell lines require glutamine for proliferation and survival [Timmerman et al., 2013; van den Heuvel et al., 2012]. However, multiple cancer cell lines do so, showing a glutamine dependency or glutamine addiction. Whether glutamine starvation causes decreased cell proliferation or increased cell death differs between cell types [Timmerman et al., 2013].

In line with our findings, two studies analyzing cell growth of non-small cell lung cancer and breast cancer cell lines revealed different phenotypes in response to glutamine starvation. Timmerman et al. [2013] identified cultures that (i) enhanced, (ii) decreased or (iii) suppressed cell growth in the absence of the amino acid. The suppressed and reduced proliferation phenotypes were linked to S-phase stalling. Additionally, they confirmed increased apoptosis in the cultures with diminished cell numbers.

Kung et al. [2011] uncovered differences in the response to glutamine starvation according to the tumor subtypes in a panel of seven breast cancer cell lines. Basal-type cells showed reduced viability and cell growth indicating glutamine addiction, while luminal-type cells did not.

In this context we addressed whether glutamine starvation causes decreased cell proliferation or increased cell death that could account for the observed cell growth arrest in colon cancer cell lines. FACS analysis of bromodeoxyuridine-labeled or annexin V/propidium iodide-stained HCT116 cells, enabling the discrimination of different types of cell death and cell cycle phases, were performed by Francesca Dejure.

In contrast to our expectations, glutamine-deprivation did not result in a high degree of apoptosis, but induced a cell cycle arrest in both the G1- and in the late S-phase of the cell cycle [Dejure and Royla et al., 2017]. Re-addition experiments showed that the cell cycle arrest is fully reversible. Interestingly, we observed pronounced apoptosis in glucose starvation experiments, demonstrating the ability of HCT116 cells to induce acute cell death. Seventy-five percent of the culture underwent apoptosis in the absence of glucose underlining the distinct impact of glutamine. [Dejure and Royla et al., 2017]. We concluded that human colon carcinoma cells are not addicted to glutamine as expected for MYC-driven tumor cells.

In line with our results, Cetinbas et al. [2016] identified 25% of glutamine-deprived HCT116 cells to be apoptotic [Dejure and Royla et al., 2017]. Contradictory to these findings, a study focusing on PI3K-driven glutamine addiction, observed glutamine deprivation-induced cell death in HCT116 cells [Hao et al., 2016]. Cell numbers were reduced by 2-fold within five days of glutamine starvation and 45% apoptotic cells were detected 72 hrs post deprivation [Hao et al., 2016]. While the exact reason for the discrepancies remains unclear, differences in media composition may explain the inconsistency in the results.

5.1.3. The 3'-UTR of *MYC* protects tumor cells from glutamine addiction

Comparison of concepts: glutamine addiction versus the physiological significance of the 3'-UTR of *MYC*

In addition to its profound role in stimulating cell growth, MYC is able to trigger cell-autonomous apoptosis. At first glance this might seem surprising and counterintuitive, but the capability of inducing cell death in cells expressing extreme levels of MYC is obviously a beneficial protection mechanism [McMahon, 2014]. Moderate MYC levels promote cell growth, while excessive MYC expression can lead to apoptosis which is in turn mostly governed by the environment, the genetic background and the distinct MYC threshold per cell type [Di Giacomo et al., 2017; Murphy et al., 2008]. It has been reported that cells expressing high MYC levels, experiencing the limitation of growth factors or nutrients, rapidly undergo apoptosis [Yuneva et al., 2007; Nieminen et al., 2013].

In Yuneva et al. [2007] immortalized human kidney epithelial cells were either transduced with MYC estrogen receptor chimera (MYC-ER) or a control vector in order to compare effects of abnormal and normal MYC expression upon glutamine and glucose deprivation. Interestingly, the limitation of glutamine availability, not glucose, induced apoptosis selectively in cells with acutely activated MYC-ER. Cells without an ectopic expression remained unaffected. Five years later they reported a synthetic lethal interaction between

Table 5.1.: *In vivo* and *in vitro* studies focusing on MYC-induced glutamine addiction.
MYC overexpression is achieved via transgenes that put MYC expression under the control of the tetracycline regulated promoter (TRE-MYC) or the estrogen receptor (ER-MYC/MYC-ER).

	Experimental system	References
in vitro	Breast epithelial cell line (MYC-ER)	Nieminen et al. [2013]
	Human fibroblasts (MYC-ER)	Yuneva et al. [2007]
	Human fibroblasts (ER-MYC) Human kidney epithelial cells (MYC-ER)	Yuneva et al. [2012]
in vivo	B-cell lymphoma (TRE-MYC)	Le et al. [2012]
	Hepatocellular carcinoma (TRE-MYC)	Xiang et al. [2015]
	Renal cell adenocarcinoma (MYC-ER)	Shroff et al. [2015]

MYC and the glutaminase inhibitors BPTES[2] and DON[3] in human lung fibroblast and human kidney epithelial cells expressing ER-MYC or MYC-ER, respectively [Yuneva et al., 2012].

Another study showed increased activity of caspase 3 and 7 in the absence of glutamine comparing MYC-ER-induced and normal human mammary epithelial cells confirming MYC-induced addiction to glutamine [Nieminen et al., 2013].

The ectopic expression of the oncogene *MYC* that sensitizes cells to diverse stimuli and stress is a common feature of these publications and other MYC-induced apoptosis studies (*table* 5.1). Adhikary and Eilers [2005] presented several hypotheses about the mechanism behind this phenomenon. They proposed the p53-independent release of cytochrome c and an overwriting mechanism of the DNA damage check point, resulting in the continued proliferation in the presence of unrepaired DNA breaks. Despite, the precise mechanism remains unclear.

Glutamine addiction was verified in several cell culture systems overexpressing *MYC* transgenes. In this context we addressed whether the induced MYC-ER overexpression in the herein investigated colon cancer cell lines drives glutamine-dependency into lethal glutamine-addiction. Glutamine starvation experiments in MYC-ER transduced HCT116 cells confirmed MYC-induced apoptosis, similar to what was seen in Yuneva et al. [2007]. Cells expressing ectopic MYC showed a three times increased rate of cell death than control cells in the absence of the amino acid [Dejure and Royla et al., 2017]. At the same time endogenous MYC levels were suppressed in both cell lines, leading to the conclusion that transgenic *MYC* overexpression is overwriting the regulatory capacity of endogenous MYC upon glutamine deprivation, which finally results in MYC-induced apoptosis.

Intriguingly, the MYC-ER as well as other *MYC* transgene constructs (e.g., tetracycline regulatable promoter (TRE)-MYC) are missing both regulatory regions since they comprise only the *MYC* coding sequence. Hence, regulatory features mediated by either the

---

[2]Bis-2-(5-phenylacetamido-1,3,4-thiadiazol-2-yl)ethyl sulfide
[3]6-Diazo-5-oxo-L-norleucine

3'- or 5'-untranslated region (UTR) are neglected in *MYC* transgenes.

It is well known that the 3'-UTR of *MYC* is targeted by a large number of microRNAs (miRNAs). The expression of those, in particular the expression of the miR-34 family that negatively regulates *MYC* via its 3'-UTR, is regulated by the FOXO transcription factor [Myant and Sansom, 2011]. FOXO is activated upon several stress stimuli by kinases such as JNK, MK5 and AMPK. The latter is phosphorylated and thereby activated upon energetic stress, which finally couples endogenous MYC expression to the cellular energy status [Chiacchiera and Simone, 2010].

In this framework we investigated the role of both UTRs in regard to glutamine-mediated MYC regulation. In order to do so, Francesca Dejure designed four doxycycline-inducible *MYC* constructs that comprised: (i) only the coding sequence of *MYC*, (ii) the coding sequence plus either the 3'-UTR, (iii) the 5'-UTR, (iv) or both regulatory regions and transduced them into HCT116 cells. Glutamine starvation experiments revealed that MYC protein suppression strictly depends on the presence of the 3'-UTR [Dejure and Royla et al., 2017]. Cells expressing only the coding sequence or the coding sequence plus the 5'-UTR exhibited high MYC levels in the absence of glutamine, similar to those detected upon sufficient glutamine supply. In the presence of the 3'-UTR MYC protein levels were suppressed when glutamine was depleted as observed for non-modified HCT116 cells [Dejure and Royla et al., 2017].

We further validated this result as Francesca Dejure performed a Dual-Luciferase reporter assay. HCT116 cells were transfected with either the double luciferase reporter vector containing the 3'-UTR of *MYC* or the empty vector. Luciferase activity decreased following glutamine starvation in a 3'-UTR-dependent manner confirming the specificity of the *MYC* 3'-UTR regarding the glutamine-mediated MYC regulation [Dejure, 2017].

We concluded that the incorporation of the 3'-UTR into the MYC-ER construct alleviates MYC-dependent apoptosis under glutamine-starved conditions. We have tested and confirmed this hypothesis by expressing a MYC-ER construct that contains the 3'-UTR in the absence and presence of glutamine. We detected suppressed MYC protein levels, enhanced cell growth and rescued apoptosis upon glutamine starvation compared to MYC-ER cells that lacked the 3'-UTR [Dejure and Royla et al., 2017].

These data confirm that the *MYC* 3'-UTR suppresses MYC protein levels in the absence of glutamine in order to escape glutamine addiction.

Importance of including regulatory regions in transgene studies

The 3'-UTR-mediated MYC protein suppression upon glutamine starvation adds another layer of complexity to MYC's role in metabolic regulation that questions the concept of glutamine addiction. In line with herein discussed *in vitro* studies, transgenes that lack the *MYC* 3'-UTR were commonly used to exploit MYC's pro-apoptotic properties regarding glutamine addiction *in vivo* (*table* 5.1).

Considering our finding in this context, we assume a possible overvaluation of the pro-apoptotic behavior of MYC-driven experimental systems. *In vivo* systems, in particular, might be affected as many tumors are challenged with the limitations of nutrient and oxygen supply [DeBerardinis and Chandel, 2016]. Thus, the inclusion of the 3'-UTR to *MYC* transgenes is advisable in order to mimic physiological responses in artificial systems.

Nevertheless, characteristic phenotypes identified in *in vitro* studies are not always retrievable in the corresponding *in vivo* models [Davidson et al., 2016]. Davidson et al. [2016] reported *ex vivo* cultured KRAS-driven non-small cell lung cancer cells, that exhibited a vulnerability to glutaminase inhibition, while the same cells lost the phenotype when grown *in vivo* in mice.

So far, we can only speculate about the role of the 3'-UTR in *in vivo* studies using *MYC* transgenes. The concept of escaping glutamine addiction via the 3'-UTR needs to be further investigated in MYC-inducible *in vivo* models.

Inducing synthetic lethality by triggering glutamine addiction?

The concept of glutamine addiction implies that MYC-induced apoptosis can be provoked by the disruption of the mechanism leading to glutamine-dependent MYC regulation. Glutaminolyis can be disturbed in several ways, including the blockade of glutamine uptake and the inhibition of enzymes that catabolize or synthesize the amino acid. The most popular approach is the inhibition of glutaminase via small molecules, that will be discussed in more detail in *section* 5.3.

According to the 3'-UTR-mediated MYC suppression in the absence of glutamine, the inclusion of the 3'-UTR should erase lethal glutamine addiction and therefore invalidate the effect of glutaminase inhibitors. However, the combination of glutaminase inhibitors with a targeted disruption of the 3'-UTR-mediated feedback might induce synthetic lethality. This is especially of value since MYC is not directly druggable as it lacks any enzymatic activity or structural properties that can be targeted by small molecules [Koh et al., 2016]. Efforts to identify a novel class of molecular targets that regulate MYC's metabolic feedback are discussed in more detail in *section* 5.2.

5.1.4. RNA polymerase II stalls global transcription in response to glutamine starvation

MYC-induced transcriptional alterations contribute to almost every aspect of tumor cell biology since the transcription factor MYC binds promoters of about 15% of genes in the human genome [Dang, 2012].

Sequencing analysis identified 18,912 genes that are in total expressed in HCT116 cells [Dejure and Royla et al., 2017]. Upon glutamine starvation 47% of all expressed genes were significantly up- or downregulated. MYC-ER expression differentially regulated 21% of all genes compared to empty vector (EV) cells, confirming MYC's role as the transcriptional master regulator [Dejure, 2017].

Since increased MYC occupancy at genes results in enhanced RNA polymerase II (RNAPII) pause release, we globally determined the RNAPII occupancy at the transcriptional start site, the gene body and the transcriptional end site of genes [Rahl and Young, 2014]. Indeed, the metagene analysis confirmed that RNAPII stalls transcription in the presence of low glutamine [Dejure and Royla et al., 2017]. We observed decreased RNAPII loading of promoters and subsequently slowed down transcriptional elongation and termination in glutamine depleted cells. The induction of ectopic MYC upon glutamine starvation restored RNAPII promoter binding and increased transcriptional initiation events. We concluded that glutamine availability has global effects on RNAPII function that are dependent on the 3'-UTR of *MYC*.

Additionally, coerced transcriptional elongation in the absence of glutamine caused R-loop formation, which is an indicator for transcriptional stress [Dejure and Royla et al., 2017]. We concluded that RNAPII stalling and R-loop formation induced apoptosis in cells that expressed high MYC in the absence of glutamine.

5.1.5. Summary

The oncoprotein MYC drives the accelerated glutamine metabolism by the transcriptional and post-transcriptional regulation of glutaminolysis enzymes in cancer cells. Contrary to MYC's known function to regulate glutamine metabolism, we found MYC protein expression to be controlled by glutamine availability as a feedback mechanism in various cancer cell lines. We showed that the 3'-UTR of *MYC* senses glutamine and adjusts MYC protein levels in order to escape MYC-driven glutamine addiction (*figure* 5.1). However, how the glutamine signal might be mediated to the 3'-UTR is discussed in *section* 5.2.

The activation of MYC in the absence of glutamine causes RNAPII stalling, that correlates with R-loop formation and subsequent DNA damage. This finding underscores the critical role of the *MYC* 3'-UTR to obstruct MYC-driven apoptosis. Thus, this study highlights the need to include regulatory sequences into transgenes in *in vivo* and *in vitro* studies. We further speculate that the transcriptional stress caused by the disruption of the 3'-UTR-mediated process might sensitize MYC-driven tumors to pro-apoptotic therapies.
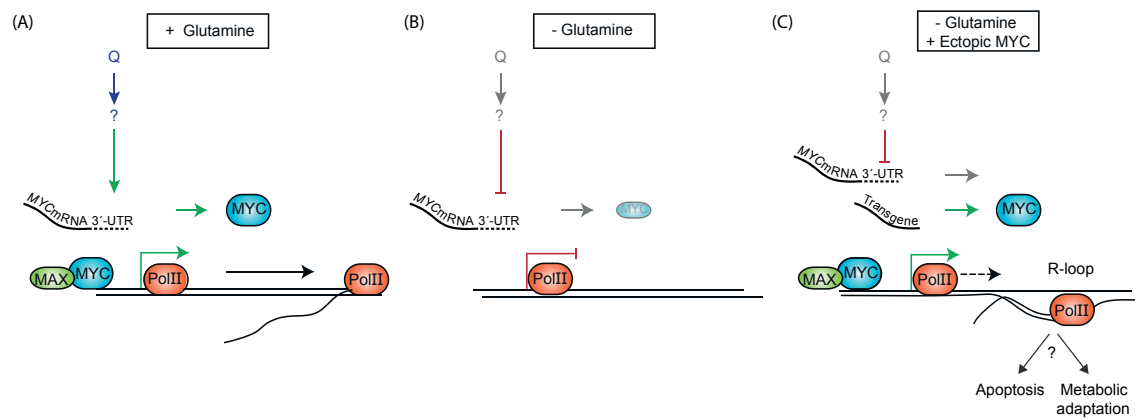
Figure 5.1.: Model summarizing the major findings. (A) The presence of glutamine is sensed via the 3'-UTR of *MYC* allowing MYC protein expression, which induces global transcription via RNAPII. (B) Glutamine limitation suppresses MYC protein and stalls RNAPolII resulting in cell growth arrest (S-/G1-phase). (C) The presence of ectopic MYC, lacking the glutamine-sensing 3'-UTR, forces RNAPII to initiate translation leading to transcriptional stress and induced apoptosis in the absence of glutamine. Figure is adopted and slightly modified from Dejure and Royla et al. [2017].

5.2. Identification of molecules mediating glutamine-dependent MYC regulation

The 3'-UTR-mediated mechanism to escape apoptosis in the absence of glutamine offers great potential for novel therapeutic approaches as already discussed in *section* 5.1. Therefore, molecules that mediate the 3'-UTR-dependent MYC control need to be identified. MYC is regulated on all omic levels by various mechanisms (see introduction). The regulatory levels are in the broadest sense separated by the time they need to respond to an alteration in the cellular environment. Upon a change in nutrient availability metabolism responds within seconds, signaling within minutes and transcription as well as translation within minutes or rather hours. Here, we applied time-resolved molecular biological, biochemical analyses as well as metabolomics and proteomics approaches to examine how fast the discovered feedback control reacts to changes in glutamine supply.

Alterations of glutamine availability resulted in rapid adaptations of MYC protein levels. The abundance of MYC protein was halved within 2 hrs of glutamine starvation, while the re-addition of the amino acid subsequent of starvation accounted for doubled MYC protein levels after 13.75 min (*figure* 4.2). Suppressed MYC levels upon starvation completely recovered one hour post glutamine re-addition. How and in what extend the regulation of *MYC* transcription and translation might affect the feedback is discussed in the following paragraphs.

5.2.1. Transcriptional and translational regulation of MYC in response to glutamine availability

Transcriptional regulation

MYC is an early immediate gene, which is rapidly and transiently activated upon distinct cellular stimuli. There are three studies revealing *MYC* transcription to be extremely fast and/or coupled to nutrient supply. First, Röhrs et al. [2009] reported that Wnt pathway activates *MYC* in less than one hour upon a stimulus. Second, in a series of elegant experiments Sethi and Vidal-Puig [2010] revealed the pivotal role of Wnt/β-catenin signaling in integrating cellular responses to metabolic stress. The third study published by Kelly et al. [1983] documented an increase of *MYC* mRNA by 10- to 40-fold 2 hrs after mitogenic stimulation that was proven to be independent of cell growth.

Opposing to the introduced studies, the glutamine-mediated feedback is not driven by transcription. Transcriptional suppression of *MYC* should be accompanied by reduced mRNA levels. On the contrary, we observed unaffected or elevated *MYC* mRNA levels in the absence of glutamine in several colon cancer cell lines providing indications against the suppression of transcription (*figure* 4.6). Therefore, we concluded that the glutamine-dependent feedback is controlled at the post-transcriptional level.

Post-transcriptional regulation

Once transcribed, mRNA is regulated during all mRNA maturation processes, including polyadenylation, decapping, splicing and nucleo-cytoplasmic transport [Wu and Brewer, 2012]. The degradation and stabilization of mRNA is mainly driven by the involvement of miRNAs and RNA binding proteins (RBPs).

Stable or increased *MYC* mRNA levels were observed upon glutamine starvation arguing against a severe degradation mechanism (*figure* 4.6). Nevertheless, we evaluated the involvement of eleven miRNAs that are known to interact with the 3'-UTR of *MYC*, thereby causing translational inhibition or mRNA degradation. We applied anti-miRs, oligonucleotides which are complementary to selected miRNAs, to impair miRNA activities. The application of anti-miRs did not affect MYC protein suppression upon glutamine starvation leading to the conclusion that miRNAs might not be involved in the 3'-UTR-dependent MYC regulation [Dejure and Royla et al., 2017].

There are several determinants that coordinate stabilization and degradation of mRNA, along with miRNAs. We assumed that RBPs might account for the imbalance of elevated *MYC* mRNA and suppressed MYC protein levels observed in glutamine-deprived colon cancer cell lines (RKO, HCT116, HT29 and GEO) (*figure* 4.4, *figure* 4.6).

Two *MYC* mRNA-stabilizing proteins are known: AUF1[4] and HuR[5]. Both enhance *MYC* mRNA stability as they bind to AU-rich elements within the *MYC* 3'-UTR [Yaman et al., 2002; Liao et al., 2007]. The role of HuR in the glutamine-mediated MYC control was evaluated, due to indications that HuR increases mRNA stability during amino acid starvation published by Yaman et al. [2002]. The knockdown of HuR did not rescue MYC protein levels upon glutamine starvation and did not affect the protein recovery kinetic upon re-addition (*figure* 4.7). According to this, HuR is not involved in the feedback control of MYC. However, the role of AUF-1, which is competing with the translational suppressor TIAR[6] to bind MYC, still needs to be investigated in additional siRNA experiments [Liao et al., 2007].

We provided evidence that the regulation of mRNA stability via HuR or miRNAs is not involved in the glutamine-dependent MYC regulation. We concluded that the suppression of MYC protein expression is induced via a paused translation of *MYC* in the absence of glutamine.

Translational regulation

Translational regulation is dictated by the competition of translational initiation and decapping processes leading to mRNA degradation [Wu and Brewer, 2012]. The initiation of mRNA decay requires the recruitment of specific enzyme complexes that remove the

---

[4] adenosine/uridine (AU)-rich element RNA-binding protein 1
[5] Human antigen R
[6] TIA-1 related protein

5'-cap structure from the RNA [Decker and Parker, 2012]. Efficiently decapped mRNAs are marked as nontranslating and accumulate in cytoplasmic granules. Two types of non-translating mRNA granules are known – those that are associated with the mRNA decay machinery, called P-bodies and those which assemble transcription initiation components that further recruit ribosomes, called stress granules. The latters were observed to be reversibly induced upon cellular stresses in order to stall translation [Decker and Parker, 2012; Parker and Sheth, 2007]

As the process of translation initiation is stalled in stress granules, they typically contain translational initiation factors, e.g., 40S ribosomal subunits, the eukaryotic translation initiation factors eIF3, eIF2, eIF4E, eIF4G, eIF4A, eIF4B; and Poly(A) binding protein [Buchan and Parker, 2009]. Surprisingly, we identified eIF4B, eIF4E, 40S ribosomal protein S30 as well as the serine-, histidine- and phenylalanine-tRNA[7] ligases to be associated with the 3'-UTR of *MYC* in the absence of glutamine (*supplemental table* B.2).

Applying the smFISH[8] approach we did not observe a re-localization of *MYC* transcripts in glutamine-deprived cells (*figure* 4.8). However, we detected slightly weaker *MYC* mRNA signals in absence of glutamine leading to the speculation that mRNA might be masked by a protein complex, that stalls translation, as described for *β-actin* in Buxbaum et al. [2014]. Moreover, Buxbaum et al. [2014] showed that the unmasking event correlated with an increase in β-actin protein synthesis. Since we observed a profound MYC protein kinetic (doubling time = 13.75 min) after glutamine re-addition we assume that *MYC* mRNA is similarly inaccessible for the translation machinery upon glutamine starvation. Therefore, we propose a protease digestion prior to microscopy analysis as done in Buxbaum et al. [2014] in order to verify this hypothesis.

Post-translational regulation

The MYC protein comprises several domains that control the stability as well as the activity of the MYC transcription factor [Vervoorts et al., 2006]. We investigated two post-transcriptional modifications, phosphorylation of the Ser62 and Thr58, that account for MYC's short protein half-life of $\approx$20 min [Farrell and Sears, 2014]. The phosphorylation of the Ser62 residue activates and stabilizes MYC as a transcription factor. Once Ser62 is phosphorylated, the residue Thr58 becomes a substrate for GSK3-β, which in turn marks MYC for degradation by the ubiquitin-proteasome system [Farrell and Sears, 2014]. The consecutive phosphorylation ensures the tight regulation of MYC levels as it is expected of a transcription factor with pleiotropic functions [Vervoorts et al., 2006].

An imbalance in the activation of both phosphorylation sites indicates a disruption of this fine-tuned mechanism. However, phosphorylation of Ser62 and Thr58 displayed similar kinetics as seen for total MYC protein after the re-addition of glutamine following star-

---

[7]transfer RNA

[8]Single-molecule RNA fluorescence *in situ* hybridization

vation (*figure* 4.2). These results lead to the conclusion that post-translational activation and degradation of MYC is under tight control and not affected by glutamine availability.

5.2.2. The role of cellular signaling in glutamine-dependent MYC regulation

Nutrient sensing via signaling pathways

Signaling pathways coordinate cell actions in response to the cellular microenvironment via kinases, phosphatases and phospho-binding proteins [Martin, 2003]. Once a cell receives a signal from growth factors, the cell matrix or cell-to-cell contacts, this information is integrated and distributed in order to manage various processes, including cell growth, differentiation, apoptosis, metastases and angiogenesis [Martin, 2003; Wu et al., 2013]. In order to determine a cell's fate, signaling pathways are highly interconnected via feedback and crosstalk mechanisms [Wu et al., 2013].

We investigated the effect of glutamine starvation on global signaling as it was reported that amino acids, including glutamine, glutamate, proline and arginine; activate cellular signaling pathways [Wu, 2013]. The analysis of a panel of 13 signaling molecules of various pathways documented a severe suppression of overall signaling in glutamine-deprived HCT116 cells (*figure* 4.10). Furthermore, we identified molecules of the MAPK and PI3K/AKT/mTOR pathway as possible candidates mediating the MYC feedback by a re-addition time course experiment (*figure* 4.10). Simultaneous glutamine re-addition and inhibition of mTOR, PI3K and MEK were performed with the expectation to impede MYC protein recovery if they are involved in the glutamine-mediated MYC control.

The inhibition of MEK and PI3K did not interfere with MYC protein suppression in the absence of glutamine or the recovery kinetic upon glutamine re-addition (*figure* 4.11). The inhibition of MEK and PI3K could not be validated, most likely due to feedback and crosstalk mechanisms triggered by the applied small molecules, AZD4226 and LY294002, respectively (*figure* 4.11) [Fritsche-Guenther et al., 2011; Klinger et al., 2013]. Therefore, the involvement of both proteins in the glutamine-mediated MYC control remains unclear and needs to be further investigated, e.g., via the combinatorial inhibition of both signaling pathways.

The master regulator of growth, mTOR, is known to balance anabolic and catabolic processes in response to nutrient availability that can account for its deactivation upon glutamine starvation (*figure* 4.10). The kinase mTOR is the core component of two complexes, termed mTORC1 and mTORC2. Both complexes respond to growth factors, whereas mTORC1 is additionally sensitive to nutrients such as glucose and amino acids [Jewell and Guan, 2013]. Moreover, mTOR signaling controls MYC translation and subsequently MYC protein turnover [Csibi et al., 2014]. Contradictory to expectations, inhibiting mTORC1 function or assembly by applying the inhibitor rapamycin or siRNA-mediated knockdown of Raptor, respectively, did not disturb the MYC control (*figure* 4.11).

Two main amino acid sensing mechanisms are known in mammalian cells: (i) via mTOR that has already been discussed and (ii) via the eIF2α kinase (GCN2), which is part of the integrated stress response. The latter is activated in the presence of uncharged tRNAs and thereby senses indirectly depleted amino acid pools [Efeyan et al., 2015]. Afterwards, GCN2 phosphorylates the eukaryotic initiator factor2α (eIF2α), which in turn loses its activity as the key early activator of translation initiation [Efeyan et al., 2015]. Accordingly, this signaling cascade is preventing cells to initiate translation when single or global amino acid pools are depleted in order to safe bioenergetics. Here, the phosphorylation status of the mediating molecules GCN2 and eIF2α in response to glutamine starvation and re-addition needs to be examined. Additionally, these proteins were chosen to be tested as possible mediators in the siRNA screen that will be performed by our cooperation partners in Würzburg (*supplemental table* B.3).

Mutation of KRAS or BRAF is not crucial in the glutamine-mediated MYC regulation

We verified glutamine-mediated MYC regulation in several colon cancer cell lines harboring either a KRAS or a BRAF mutation. In contrast, the CaCO2 cell line, which is wild-type for KRAS and BRAF, responded similarly to changes in glutamine compared to the investigated colon cancer panel (*figure* 4.4). We concluded that a mutation in the *KRAS* or *BRAF* oncogene is not crucial in the glutamine-mediated MYC regulation.

5.2.3. MYC responds to changes in cellular adenosine and α-ketoglutarate

Glutamine has several metabolic functions: (i) supply of nitrogen for *de novo* nucleotide biosynthesis, (ii) antagonize oxidative stress by being a precursor of the antioxidant glutathione, (iii) provision of intermediates to fuel anaplerotic reactions, (iv) contribution to the pool of reducing equivalent NADPH [DeBerardinis and Cheng, 2010].
In order to evaluate whether and how each metabolic fate of glutamine is involved in the 3'-UTR-mediated MYC regulation, we first examined how the levels of glutaminolysis intermediates, nucleotides and reactive oxygen species (ROS) respond to glutamine starvation. We observed that the quantities of glutamate and tricarboxylic acid (TCA) cycle intermediates as well as nucleotide and deoxynucleotide levels significantly decreased in the absence of glutamine (*figure* 4.13, *figure* 4.15). Additionally, Francesca Dejure detected elevated ROS levels, so we assumed glutathione and NADPH production – both providing reducing power – to be reduced as well [Dejure and Royla et al., 2017]. Thus, the 3'-UTR of *MYC* might indirectly sense decreased glutamine levels via changes in one or more glutamine downstream metabolites.
Furthermore, we tested whether and which intermediates of glutaminolysis and *de novo* nucleotide biosynthesis responded as fast as MYC protein levels to glutamine re-addition.

We applied u-^{13}C-glutamine in the pSIRM[9] set up in order to narrow down possible mediator candidates of the TCA cycle by tracing the time-dependent increase of carbon-13 throughout the pathway. Interestingly, glutamate and TCA cycle metabolite pools did not replenish as fast as expected, most likely due to high turnover rates indicated by a strong accumulation of carbon-13 within 5 and 10 minutes (*figure* 4.18). Surprisingly, the pool sizes of nucleotides also raised in the same time scale, so that all nucleotide and TCA cycle related intermediates could be assumed as mediator metabolites (*figure* 4.17).

MYC is known to induce metabolic changes by transcriptional control of metabolic enzymes such as glutaminase and aspartate transcarbamylase. We aimed to address critical metabolites by inducing MYC expression upon glutamine starvation in MYC-ER transduced HCT116 cells. Interestingly, we observed that metabolic changes driven by glutamine depletion were not distinguishable between cells with high or suppressed MYC expression (*figure* 4.16).

In summary, we identified NADPH, glutathione, metabolites of the TCA cycle and *de novo* nucleotide biosynthesis as possible candidates mediating alterations in glutamine supply to the 3'-UTR of *MYC*. In follow-up experiments, summarized in *figure* 5.2, we supplemented membrane-permeable analogues of selected intermediates to glutamine-deprived HCT116 cells in order to test for their potential to rescue MYC protein expression.

Electron transport chain and glutathione biosynthesis do not contribute to MYC regulation

The addition of glutamate and dimethyl α-ketoglutarate (DMαKG), but not dimethyl fumarate (DMFum) and dimethyl malate (DMMal) caused an alleviated MYC recovery in glutamine-starved HCT116 cells. These findings suggest that the production of ATP via the electron transport chain (ETC) might play a pivotal role in the glutamine-mediated feedback control (*figure* 4.19). We applied the OXPHOS inhibitors TTFA[10] and oligomycin that interfered with either complex II or ATP synthase activity, respectively, for experimental validation. Both inhibitors neither altered the strength nor the speed of MYC protein recovery after glutamine re-addition in starved HCT116 cells. Accordingly, the energy-providing mechanism via ETC coupled to OXPHOS was excluded as a part and parcel of MYC regulation (*figure* 4.22). This argument was underlined by the missing activation of the energy-sensing enzyme AMPK in response to changed glutamine levels (*figure* 4.23). The kinase that is activated upon unbalanced AMP:ATP and ADP:ATP ratios was unaffected upon glutamine starvation and re-addition. Since the efficiency of the inhibitors oligomycin and TTFA were not verified, enzymes involved in the ETC and ATPase complex were added to the siRNA list that was forwarded to our cooperation partners in Würzburg to validate the discussed results (*supplemental table* B.3).

Cellular α-ketoglutarate can be converted by glutamate dehydrogenase (GLUD) or other

---

[9]pulsed stable isotope resolved metabolomics
[10]Thenoyltrifluoroacetone
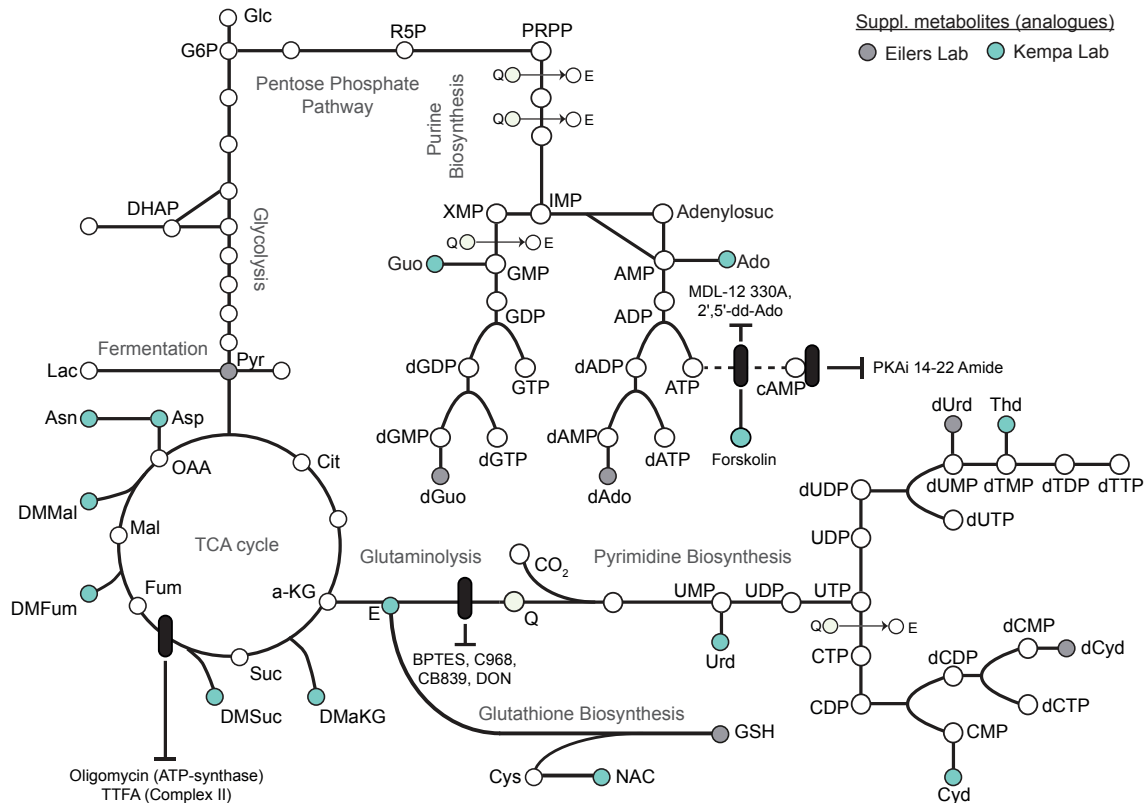
Figure 5.2.: Glutamine-dependent metabolic pathways. The diagram summarizes the main glutamine-dependent metabolic pathways. Dots indicate the metabolites/analogues applied in rescue experiments that were performed in the Eilers and/or the Kempa laboratory. Black rectangles indicate inhibited metabolic enzymes via the indicated substances. A modified figure was published as figure EV3A in Dejure and Royla et al. [2017]. For full metabolite names refer to the list of abbreviations.

amino transferases (e.g., GPT, GOT) into glutamate and finally via glutamine synthetase (GLUL) into glutamine in order to contribute to the glutamine-mediated MYC feedback [Ratnikov et al., 2015]. Although appearing contradictory, there is evidence that glutamine-consuming tumor cells secrete glutamate [Ratnikov et al., 2015]. Further it was reported for breast cancer cells that GLUL levels were upregulated upon glutamine starvation supporting the supposition of the backwards conversion of α-ketoglutarate and glutamate into glutamine [Kung et al., 2011]. In order to validate this hypothesis, the fate of u-^{13}C-labeled DMαKG should be investigated in additional GC-MS measurements. Tracing the routing of carbon-13 in either glutamate, glutamine or into downstream metabolites of the TCA cycle might help to gain insights into the conversion routes of supplemented DMαKG.

Furthermore, glutathione biosynthesis was excluded as a possible mediator pathway since the supplementation of the membrane-permeable form of glutathione and its precursor N-acetyl cysteine showed no effects on MYC protein levels upon glutamine starvation (*figure* 4.19) [Dejure and Royla et al., 2017].

The role of NADPH as a reducing equivalent was not investigated so far. Its involvement

in the glutamine-mediated MYC regulation needs to be reviewed in the future.

The 3'-UTR of *MYC* senses cellular adenosine levels and links RNAPII function to ribonucleotide levels

Rescue experiments in glutamine-deprived HCT116 cells revealed the potential of ribonucleosides to recover MYC protein expression (*figure* 4.19). A deeper analysis uncovered the single ribonucleoside adenosine as a specific metabolic mediator of the glutamine-dependent MYC regulation. Adenosine supplementation triggered MYC protein expression in the absence of glutamine. In line with our previous results, we validated this mechanism to be dependent on the 3'-UTR of *MYC* [Dejure and Royla et al., 2017].

Additionally, we analyzed ribonucleotide and deoxyribonucleotide levels in response to adenosine supplementation in glutamine-deprived HCT116 cells. We observed a similar increase in nucleotide levels, especially in deoxyribonucleotides and the adenosine-derived ribonucleotides, as monitored for glutamine re-addition (*figure* 4.21). Interestingly, the membrane-permeable forms of deoxyribonucleotides failed to recover MYC protein levels, although all deoxyribonucleotide pools were fully replenished upon adenosine addition [Dejure and Royla et al., 2017]. Among all ribonucleotides AMP, ADP and ATP levels are exclusively recovered upon glutamine and adenosine supplementation (*figure* 4.21). Therefore we assumed that the 3'-UTR of *MYC* is sensing changes in ribonucleotide - levels, specifically adenosine-derived ribonucleotides, rather than changes in glutamine availability.

These findings are of special interest since we observed that the addition of adenosine to glutamine-deprived cells restored binding of RNAPII to the promoters of three tested genes (*ACTB*, *NCL*, *GLN3*) [Dejure and Royla et al., 2017]. We concluded that variations of global transcriptional elongation by RNAPII are caused most likely due to changes in ribonucleotide levels.

Based on these new insights, we compared nucleotide levels in HEK293 and HCT116 cells in regard to glutamine availability. We hypothesized that nucleotide levels are less affected in HEK293 than HCT116 cells upon glutamine depletion. In turn, sufficient ribonucleotide abundance causes sustained MYC protein expression in the absence of glutamine. Indeed, we observed decreased AMP, ADP and ATP pool sizes in HEK293 cells that were still in the range of the nucleotide concentration detected in non-starved HCT116 cells. We assumed that nucleotide concentrations below a distinct threshold suppress MYC protein expression. Additional experiments need to be performed to prove this hypothesis. We suggest to determine the abundance of nucleotides in cell lines, which showed the glutamine-mediated MYC regulation, upon varying glutamine concentrations.

De novo purine biosynthesis does not exclusively contribute to MYC regulation

To note, the potential of adenosine to rescue MYC was transient as MYC protein expression was restored two hours after adenosine supplementation, but suppressed again two additional hours later. We speculate that adenosine addition triggers MYC regulation as it induces the translation of *MYC*, while later on translation is repressed again as other essential components, that originate from glutamine, are missing. These missing components might derive from glutamate and α-ketoglutarate since we observed that supplemented DMαKG restored MYC protein levels similar to adenosine and glutamine. However, DMαKG was not able to replenish overall nucleotide levels (*figure* 4.21).
Interestingly, the *de novo* biosynthesis of purine nucleotides is dependent on glutamine in two ways. Firstly, two molecules of glutamine donate their γ-nitrogen to produce IMP from phosphoribosyl pyrophosphate (PRPP) via phosphoribosylamine (see introduction). Secondly, the α-nitrogen is transferred from glutamate to oxaloacetate via GOT to form aspartate and α-ketoglutarate. Aspartate in turn provides the nitrogen to IMP which is finally converted into AMP. However, the herein described link between the two fates of glutamine that meet at the step of AMP generation does not explain the MYC regulation upon glutamate and α-ketoglutarate supplementation. We hypothesized, that the addition of glutamate or α-ketoglutarate provides aspartate which in turn contributes to the production of adenosine-derived ribonucleotides via AMP. However, ribonucleotide levels cannot be recovered without the donation of the γ-nitrogen from glutamine since it is essential for PRPP generation and therefore MYC protein levels can not be restored. This is in line with the inability of aspartate and asparagine to recover MYC protein levels in glutamine-deprived cells (*figure* 4.19). We concluded that the MYC regulation upon glutamate and α-ketoglutarate supplementation is not driven by their indirect contribution to *de novo* purine biosynthesis via aspartate.
As we speculate that both substrates – adenosine and DMαKG – induce different cellular mechanisms, we tested whether their combination mirrors glutamine's functions. We addressed this hypothesis with a proliferation assay in HCT116 cells that were either supplemented with adenosine, DMαKG or both substrates instead of glutamine. Interestingly, DMαKG partially restored proliferation, while adenosine did not (*figure* 4.20). The combination of both showed effects similar to the single application of DMαKG, leading to the assumption that another factor remains still unidentified.

Adenosine and its role in the moonlighting function of RNA binding proteins

The majority of studies concerning adenosine in cancer metabolism focus on its feature as an immunosuppressor, whereas very little is known about its regulatory potential similar to what we discovered [Ohta, 2016]. This permits a line of inquiry regarding possible mechanisms. The most exiting hypothesis is based on the discovery of multifunctional

Table 5.2.: *MYC* 3'-UTR binding moonlighting proteins. Common proteins that were identified as *MYC* 3'-UTR binding proteins and confirmed as RNA binding proteins (RBPs) in RNA interactome studies in either mouse embryonic stem cells (mESC), HeLa or HEK293 cells (indicated with x). Table was adapted from Castello et al. [2015].

		RNA interactome of		
RBP	**Pathway**	**HeLa**	**HEK293**	**mESC**
ENO1	Glycolysis	x	-	x
FASN	Fatty acid synthesis	x	x	-
MDH2	TCA cycle	x	x	-
NME1	Synthesis of nucleoside triphosphates	x	-	-
TPI1	Glycolysis and gluconeogenesis	-	-	x

proteins which moonlight RBP functions that are fully unrelated to their catalytic functions [Castello et al., 2015]. In the presence of the substrate the enzyme is catalytic active, while in the absence of the substrate its catalytic activity is reversibly paused, which in turn enables the protein to bind the mRNA. Castello et al. [2015] reported larger assemblies of consecutive enzymes of one pathway, that are held together in a so-called metabolon, providing superior metabolic flux features [Castello et al., 2015].

Characterized moonlighting proteins are highly conserved enzymes, such as those involved in glucose metabolism (e.g., HK2, PKM2, ENO1) [Huberts and van der Klei, 2010]. In addition, several metabolic proteins that are related to glutamine and nucleotide metabolism have been identified to exhibit moonlighting functions, including nucleoside diphosphate kinase A (NME1), mitochondrial deoxyuridine 5'-triphosphate nucleotidohydrolase (DUT) and NAD(P)H dehydrogenase 1 (NQO1) [Castello et al., 2015]. Interestingly, the enzyme adenylate kinase (ADK) catalyzing the interconversion of adenosine-derived ribonucleotides is also listed among moonlighting proteins. Accordingly, we suspect that ADK might bind *MYC* mRNA in the absence of its substrates AMP, ADP and ATP.

In order to uncover *MYC* 3'-UTR interacting proteins, we performed a RNA pull-down assay in HCT116 cells. We identified 17 metabolic enzymes to interact with the 3'-UTR in the absence of glutamine (*figure* 4.27). Five out of these 17 enzymes have been previously reported as RBPs (*table* 5.2).

None of the detected proteins has a direct link to glutamine and nucleotide metabolism except for the protein NME1. This protein synthesizes nucleoside triphosphates from nucleoside diphosphates – other than ATP – by utilizing ATP. In order to check for the role of the identified possibly moonlighting enzymes in MYC regulation, inhibition or knockdown experiments have to be performed in future.

Additionally, we propose to repeat the RNA pull-down with the crucial sequence of the *MYC* 3'-UTR that enables the regulation of the glutamine-dependent MYC expression. Francesca Dejure identified the region between the nucleotides 2127 and 2261 of the *MYC* mRNA by deletion mapping [Dejure and Royla et al., 2017]. We suggest simultaneous RNA pull-downs applying both; the full length mRNA and the mRNA sequence up to the

nucleotide 2261, in order to allow formation of secondary RNA structures to which moon-lighting proteins might bind. Interacting proteins should be identified in the presence and absence of glutamine as well as under adenosine supplementation in glutamine-deprived cells. Overlapping RBPs should be region-specific, so that the panel of possible mediator enzymes downsizes.

Evaluation of cAMP signaling pathway

The secondary messenger cAMP might be an additional component of the mediating mechanism that controls glutamine-dependent MYC regulation. We found cAMP levels to be reduced in the absence of glutamine and rapidly restored after the re-addition of the amino acid (*figure* 4.24). The supplementation of adenosine to glutamine-deprived HCT116 cells induced a similar trend in cAMP levels, although to a higher degree. These observations indicated that cAMP levels respond rapidly to changes in cellular adenosine and glutamine levels.

In follow-up experiments we investigated the involvement of cAMP in the glutamine-mediated feedback by either inhibiting cAMP generation via adenylate cyclase (AC) or its downstream signaling via protein kinase A (PKA). The inhibition of AC, but not of PKA, drastically alleviated the recovery of MYC protein expression after glutamine re-addition to deprived HCT116 cells (*figure* 4.25). We observed this effect upon the applica-tion of two inhibitors namely 2'5'-dideoxyadenosine (2'5'-ddAdo) and the small molecule MDL12-330A. Furthermore, we confirmed the role of AC in the MYC feedback via the supplementation of forskolin, a direct stimulator of AC, that slightly recovered MYC pro-tein expression in the absence of glutamine (*figure* 4.25). Since we did not follow-up on the inhibitor verification, we added AC as well as PKA to the list of possible mediators that was forwarded to our cooperation partners in Würzburg in order to perform a siRNA screen (*supplemental table* B.3).

cAMP is generated from the highly energetic molecule ATP. Therefore, we assume that changes in cAMP levels upon glutamine availability contribute to the MYC feedback, rather than being a read-out of a side effect. Classically, cAMP is known to provoke PKA activation as it binds to its regulatory subunits which in turn triggers the dissociation of its catalytic subunits [Sassone-Corsi, 2012]. Once activated the kinase PKA phosphorylates numerous targets, including metabolic enzymes such as GSK3-β and acetyl-CoA carboxy-lase (ACC). However, PKA-mediated cAMP signaling was shown to be not involved in the glutamine-mediated MYC regulation. Given this, we propose to examine the role of the two other main effectors of cAMP, termed the guanine-nucleotide-exchange factor and cyclic-nucleotide-gated ion channels [Sassone-Corsi, 2012].

5.2.4. Summary

Time-resolved studies revealed that the transcription factor MYC is not only highly regulated on the transcriptional level, but also at the level of translation via its 3'-UTR. We showed that the translational inhibition of MYC in the absence of glutamine is independent of mTOR, miRNAs, HuR and the re-localization of *MYC* mRNA, but dependent on the depletion of ribonucleotide levels. We linked the global transcriptional response via RNAPII to ribonucleotide levels as we identified the small metabolite adenosine to specifically restore MYC protein level in glutamine-deprived cells. We proposed that nucleotide concentrations below a distinct threshold suppress MYC protein expression. Additionally, we provided evidence that the levels of ribonucleotides do not exclusively contribute to MYC regulation since glutamate and α-ketoglutarate supplementation also restored MYC protein expression in the absence of glutamine.

5.3. Dissection of glutaminase bypass reactions by aminotransferases

A hallmark of MYC-driven cancer is the reprogrammed metabolism, that is defined by the enhancement of glycolytic enzyme activity and an elevated glutamine uptake and utilization. Although, this specialization increases the vulnerability to therapies that target especially these dependencies.

One approach addresses the pivotal function of glutaminase in glutamine metabolism. Several compounds that inhibit the conversion of glutamine into glutamate via glutaminase have been described, including the structural glutamine analogue DON and the allosteric inhibitors BPTES, C968 and CB839. We investigated whether the inhibition of glutaminase activity by these four compounds contributes to a suppression of MYC protein expression in the presence of glutamine similar to the one observed upon glutamine depletion. If so, this would support our hypothesis to induce synthetic lethality in glutamine-dependent cells by a combinatorial treatment targeting the mediator of the 3'-UTR-dependent MYC regulation and glutamine metabolism via glutaminase.

5.3.1. Verification of glutaminase inhibitors

Firstly, we examined the efficiency of the glutaminase inhibitors via the application of ^{13}C-glutamine. HCT116 cells were exposed to different concentrations of the inhibitors in the presence of glutamine and the distribution of the glutamine-derived carbon-13 was monitored in glutamate and further glutamine downstream metabolites. Surprisingly, no reduction of ^{13}C-incorporation was observed independently of the applied inhibitors and their concentration in the presence of glutamine (stable Q, *figure* 4.28). The inhibitory effects for DON, BPTES and CB839 were validated in HCT116 cells that were starved for glutamine before the ^{13}C-labeled glutamine was applied, but not for C968 (dynamic Q, *figure* 4.28). We observed reduced incorporation rates of carbon-13 in glutamate and TCA cycle intermediates upon DON, BPTES and CB839 treatment, while the distribution of carbon-13 was not affected by C968.

Katt et al. [2012] reported the ineffectiveness of C968 to inhibit glutaminase activity, which is dependent on inorganic phosphate as an allosteric activator. C968 binds to a hydrophobic pocket of the enzyme preventing phosphate to bind and activate glutaminase [Lukey et al., 2013]. Therefore the small compound cannot interfere with glutaminase once it is activated, instead stabilizes the inactive conformation by blocking the association with phosphate. An *in vivo* study documented that C968 retained the inactive state of glutaminase when treatment with the inhibitor occurred prior to the addition of inorganic phosphate [Lukey et al., 2013]. Nevertheless, the small molecule is commonly used in glutaminase inhibition studies as it negatively affects cell proliferation due to its ability

to bind to the inactive conformation of glutaminase in the process of protein turnover [Lukey et al., 2013]. Since we performed all experiments in DMEM media, which contains sodium phosphate, we expect glutaminase to be active when C968 was applied. This assumption elucidates the unaffected carbon-13 distribution upon the supplementation of ^{13}C-glutamine (*figure* 4.29). Furthermore, the potential of C968 to retain glutaminase inactivity during protein turnover is very unlikely as the inhibitor treatment was performed for 16 hrs, while the glutaminase half-life in the bacterium *A. aeolicus* was determined to 25 hrs [Bera et al., 2000].

In contrast, the molecules DON, BPTES and CB839 are known to inhibit phosphate-activated glutaminase [Lukey et al., 2013]. BPTES and CB839 interfere with the enzyme activity of glutaminase by inducing a conformational change of the catalytic site leaving it inactive. We observed that CB839, which is a BPTES analogue, repressed the incorporation of glutamine stronger than BPTES most likely because it exhibits a higher affinity to glutaminase as well as a higher irreversibility (*figure* 4.29) [Thangavelu et al., 2012].

The glutamine antagonist DON binds to the catalytic site of glutaminase resulting in the formation of an enzyme-inhibitor complex that is inaccessible for glutamine [Thangavelu et al., 2015]. Although the glutamine analogue inhibits glutaminase activity irreversibly, it competes with glutamine to bind to the enzyme. Since we applied DON for 16 hrs to glutamine-deprived cells before re-adding the amino acid, we assumed the glutaminase activity to be completely inhibited. Contrary to our expectations, DON treatment decelerated the ^{13}C-incorporation partially upon glutamine-addition (*figure* 4.29). We concluded that (i) DON may have a low binding affinity to glutamine and/or (ii) glutamine-converting enzymes, mainly transaminases, might compensate for the inhibition of glutaminase.

5.3.2. The potential of glutamine-dependent transaminases to balance glutaminolysis and nucleotide biosynthesis intermediate levels

Several transaminases that convert glutamine into glutamate are known, e.g., GMPS, CTPS, ASNS, CAD, PPAT, PFAS and GFPT (for full protein names refer to the list of abbreviation). Due to this repertoire, there are numerous possible bypass reactions how glutamine-derived carbon-13 might circumvent a blockade in glutaminase activity resulting in high ^{13}C-incorporation rates in glutamate. Transaminases might account for the unaffected ^{13}C-incorporation upon glutaminase inhibitor treatment in the presence of glutamine (stable Q, *figure* 4.29). Specifically, we assume that the inhibition of glutaminase in the presence of glutamine is negligible since transaminases compensate for the emerging deficit in glutamate.

Additionally, decelerated ^{13}C-incorporation was detected in all glutamine-downstream metabolites in cells that were deprived in advance and treated with either DON, BPTES,

or CB839 to inhibit glutaminase activity compared to the non-treated control (dynamic Q, *figure* 4.29). We speculate that the impaired accumulation of carbon-13 is mainly driven by the inhibition of glutaminase. Glutamine-deprived cells replenished the TCA cycle intermediate pools rapidly after glutamine re-addition (*figure* 4.18). We assume that this process is mainly driven by the glutaminase as this reaction, in contrast to transaminase reactions, is not dependent on the availability of other substrates that might be limited upon glutamine starvation. However, the ability to convert glutamine into glutamate by transaminases might account for the partial reduction of ^{13}C-incorporation. Thus, the potential of transaminases to compensate for glutaminase inhibition should be considered in regard to therapeutic approaches in future.

Numerous transaminases that utilize glutamine as a substrate are also involved in the *de novo* nucleotide biosynthesis like CTPS and GMPS. We examined nucleotide levels upon glutaminase inhibition as we aimed to address whether nucleotide biosynthesis and glutaminolysis are interconnected via these transaminases. Surprisingly, pool sizes of deoxyribonucleotides and adenosine-derived ribonucleotides correlated with the inhibitor-driven changes in glutaminolysis intermediates. Specifically, DON and CB839 with the highest glutaminase inhibition efficiencies caused strong reductions in these specific nucleotides in the presence of glutamine similar to those detected upon glutamine starvation (*figure* 4.29, *figure* 4.30). Furthermore, nucleotide levels of C968-treated cells were in the same concentration range of the non-treated control, while glutamine conversion was not impeded in both conditions. BPTES that exhibited a moderate glutamine inhibition capacity, caused moderate suppression of nucleotide pool sizes in the presence of glutamine. Here, we speculate that glutaminolysis and nucleotide biosynthesis are interconnected in order to balance their levels in response to glutamine conversion or even glutamate abundance.

We reinforced this hypotheses by linking UTP, CTP and GTP levels to the conversion of glutamine in cells treated with the glutamine antagonist DON. Upon the inhibitor treatment UTP levels rose while CTP levels decreased (*figure* 4.30). This anti-correlation might occur due to the inhibition of the glutamine utilizing transaminase CTPS as DON as a glutamine analogue has the potential to inhibit all glutamine-consuming enzymes [Pinkus, 1977].

CTPS transfers the γ-nitrogen from glutamine to UTP generating glutamate and CTP under the usage of ATP. In the absence of glutamine UTP and uridine-ribonucleotide levels increase since the reaction cannot be proceeded, while CTP and cytidine-ribonucleotide levels drop. Interestingly, GTP was identified as a direct effector of this reaction in enzymatic assays and can be further linked to the activation of glutaminase via Rho GTPases [Pinkus, 1977; Erickson and Cerione, 2010]. These proteins are activated when they bind to GTP and inhibited when associated with GDP [Orgaz et al., 2014]. The reciprocal correlation between GTP and GDP as well as GMP upon DON treatment support the hypothesis of a signal transduction from nucleotides to glutaminase. The regulation of

UTP, CTP and GTP levels upon DON treatment partially recur in glutamine-depleted cells (*figure* 4.30). However, how this finding could be linked to the adenosine- and α-ketoglutarate-mediated rescue of MYC protein levels upon glutamine starvation remains unclear.

Transaminase-dependent nucleotide levels regulate MYC protein levels

Furthermore, we investigated the potential of glutaminase inhibitors (i) to retard MYC protein recovery in response to glutamine re-addition in prior starved cells and (ii) to suppress MYC protein expression in the presence of the amino acid.

Interestingly, MYC protein recovery was only retarded in response to inhibitors that were validated to interfere with glutaminase activity (*figure* 4.29C). The application of DON, CB839 and BPTES negatively affected the recovery of MYC protein and, likewise, the ^{13}C-incorporation of glutamate after ^{13}C-glutamine re-addition (*figure* 4.29A&C). In contrast, C968-treated cells, that showed no inhibitory effect on glutaminase, recovered MYC protein in the same manner as seen for non-treated cells. Here, we observed that MYC protein expression is dependent on the conversion of glutamine into glutamate via glutaminase.

Surprisingly, the dependency was abrogated in cells that were continuously cultivated in the presence of glutamine. MYC protein levels sustained upon inhibitor treatment with BPTES, C968 and CB839, while the application of DON caused a reduction in MYC protein expression in the presence of glutamine (*figure* 4.29B). We proposed that transaminases might contribute to the diversity in MYC protein regulation. Since several glutamine-converting transaminases are involved in the *de novo* nucleotide biosynthesis, nucleotide levels are sustained to a certain degree upon glutaminase inhibition. DON as a glutamine antagonist inhibits glutamine-utilizing transaminases next to glutaminase. We speculate that DON mimics glutamine starvation effects in TCA cycle, nucleotide and MYC protein levels in the presence of glutamine as it blocks all glutamine-dependent reactions. Contrary to expectations, DON treatment did not suppress MYC levels completely most likely because it competes with glutamine to bind enzymes (*figure* 4.29B). The other three substances, which specifically inhibit glutaminase, might sustain nucleotide levels and, likewise, MYC protein expression upon glutaminase inhibition due to transaminases (*figure* 4.29B, *figure* 4.30).

These data provide additional evidence that nucleotide concentrations below a distinct threshold might suppress MYC protein expression as it was discussed before (*section* 5.2). In this context the question how rapidly nucleotide levels recover after glutamine re-addition in cells treated with DON, BPTES and CB839 rose. MYC protein recovery was decelerated upon these inhibitor treatments assuming a decelerated recovery of nucleotide levels after the re-addition of the amino acid (*figure* 4.29C, *figure* 4.30). Follow-

up experiments addressing the inhibitor-dependent nucleotide abundance during the re-addition time course may answer this question.

With the evidence available to us we only can speculate about the mechanism of the glutamine-dependent MYC regulation. Nevertheless, we have found evidence that MYC protein expression is metabolically regulated by two pathways, glutaminolysis (via α-ketoglutarate and glutamate) and *de novo* nucleotide biosynthesis (via adenosine), that may be linked via the bilateral functions of transaminases.

5.3.3. Summary

The inhibition of glutaminase via the three allosteric inhibitors BPTES, C968 and CB839 and the glutamine analogue DON stressed the complexity of metabolic interconnections in regard to glutamine-dependent MYC regulation. We highlighted that the combination of innovative MS-based approaches gives new insight into the mode of action of glutaminase inhibitors. We propose delaying clinical trials in order to focus on the clarification of inhibitor effectiveness in different experimental settings.

Moreover, we speculated that glutamine-utilizing transaminases may play a pivotal role in the double-sided MYC regulation via glutamine/glutamate/α-ketoglutarate and adenosine. However, if and how transaminases are involved remains unclear and needs to be evaluated in follow-up experiments.

6. Conclusion and Future Perspectives

This dissertation describes recent efforts to investigate MYC's role as a nexus in metabolic regulation by addressing the concept of glutamine addiction, one of the fundamental links between the MYC oncoprotein and cellular metabolism.

We showed that the suppression of MYC protein expression in the absence of glutamine is mediated by its 3'-untranslated region (3'-UTR), which senses glutamine-dependent changes in adenosine nucleotide levels. The metabolic feedback protects cells from lethal glutamine addiction, while the activation of ectopic MYC in the absence of glutamine causes RNA polymerase II stalling, which is associated with R-loop formation and DNA damage, inducing MYC-driven apoptosis.

We questioned the concept of glutamine addiction, since it has been described in experimental systems, that are predominantly based on use of *MYC* transgenes, which usually lack the regulatory regions of *MYC* mRNA. Thus, this study underscores the need to include regulatory sequences into transgene in *in vivo* and *in vitro* studies.

We speculate that the transcriptional stress caused by a disruption of the 3'-UTR-mediated feedback might sensitize MYC-driven tumors to pro-apoptotic therapies. In order to identify possible mediators, we examined the glutamine-dependent MYC regulation in extensive time-resolved studies addressing MYC's complexity at its various regulatory levels. The holistic approach provided evidence that the suppression of MYC protein expression in the absence of glutamine is a consequence of paused *MYC* translation. We assume the regulation to be associated with a formation of a protein complex, which renders mRNA inaccessible for the translation machinery, rather than the complex induces mRNA re-localization or mRNA decay via microRNAs. We propose to perform a smFISH[1] approach with an included protease digestion step as done by Buxbaum et al. [2014] in order to verify this hypothesis.

A RNA pull-down identified several *MYC* 3'-UTR binding proteins (e.g., enolase 1, lactate dehydrogenase A) as possible complex components, next to translation initiation factors, that will be validated in a siRNA screen by our cooperation partners in Würzburg. The list of 100 proteins comprises the most promising 3'-UTR binding proteins as well as manually selected proteins that (i) are assumed to be involved in the feedback, but so far were not investigated (e.g., eIF2α kinase (GCN2)) or (ii) have been examined but require further validation (e.g., adenylyl cyclases, protein kinase A, electron transport chain components).

---

[1]Single-molecule RNA fluorescence *in situ* hybridization

The identification of molecular targets, that mediate the glutamine-dependent MYC regulation, may elucidate novel combinatorial treatments inducing synthetic lethality on the principle of glutamine addiction.

In this framework, we investigated whether glutaminase inhibitors induce MYC protein suppression in the presence of glutamine. Glutaminase inhibitors failed to reduce MYC protein expression and glutamine to glutamate conversion rates, leading to the hypothesis that glutamine-utilizing transaminases compensate for the perturbation. We propose to delay clinical trials and focus on the clarification of inhibitor effectiveness upon different experimental settings.

Firstly, Şafak Bayram, a master student under the author's supervision, is currently setting up a comprehensive data matrix, combining cell growth and metabolic conversion data of glutaminase-inhibited HCT116, RKO and HEK293 cells in order to test for correlations. We further determine the protein abundance of transaminases in these cell lines with the aim to match them to the different proliferation phenotypes that have been observed.

Secondly, we will focus on the time-dependent incorporation of nitrogen-15 in nucleotide precursors by applying ^{15}N-glutamine in a pSIRM[2] experiment. This approach will reveal to which extend transaminases contribute to the glutamine to glutamate conversion, especially when analyzed in combination with glutaminase and/or transaminase inhibitors (e.g., aminooxyacetic acid).

---

[2]pulsed stable isotope resolved metabolomics

7. Publications

F. R. Dejure*, **N. Royla***, S. Herold, J. Kalb, S. Walz, C. P. Ade, G. Mastrobuoni, J. T. Vanselow, A. Schlosser, E. Wolf, S. Kempa, and M. Eilers. The MYC mRNA 3'-UTR couples RNA polymerase II function to glutamine and ribonucleotide levels. *The EMBO Journal*, 36 (13):1854-1868, 2017. ISSN 0261-4189. doi: 10.15252/embj.201796662.

*Contributed equally

N. Royla and S. Kempa. The answer's in the tail: MYC mRNA has a metabolic sensor that supports cancer chemoresistance. *Molecular & Cellular Oncology*, 4(4):e1338209, 2017. ISSN 2372-3556. doi: 10.1080/23723556.2017.1338209.

B. von Eyss, L. A. Jaenicke, R. M. Kortlever, **N. Royla**, K. E. Wiese, S. Letschert, L. A. McDuffus, M. Sauer, A. Rosenwald, G. I. Evan, S. Kempa, and M. Eilers. A MYC-Driven Change in Mitochondrial Dynamics Limits YAP/TAZ Function in Mammary Epithelial Cells and Breast Cancer. *Cancer Cell*, 28(6):743-757, 2015. ISSN 18783686. doi: 10.1016/j.ccell.2015.10.013.

B. Kuropka, **N. Royla**, C. Freund, and E. Krause. Sortase A mediated site-specific immobilization for identification of protein interactions in affinity purification-mass spectrometry experiments. *PROTEOMICS*, 15(7):1230-1234, 2015. ISSN 16159853. doi: 10.1002/pmic.201400395.

8. Bibliography

S. Adhikary and M. Eilers. Transcriptional regulation and transformation by Myc proteins. *Nature Reviews Molecular Cell Biology*, 6(8):635–645, 2005. ISSN 14710072. doi: 10.1038/nrm1703.

D. Ahmed, P. W. Eide, I. A. Eilertsen, S. A. Danielsen, M. Eknæs, M. Hektoen, G. E. Lind, and R. A. Lothe. Epigenetic and genetic features of 24 colon cancer cell lines. *Oncogenesis*, 2(9): e71–e71, 2013. ISSN 2157-9024. doi: 10.1038/oncsis.2013.35.

B. J. Altman, Z. E. Stine, and C. V. Dang. From Krebs to clinic: Glutamine metabolism to cancer therapy. *Nature Reviews Cancer*, 16(10):619–634, 2016. ISSN 14741768. doi: 10.1038/nrc.2016.71.

N. D. Amoêdo, J. P. Valencia, M. F. Rodrigues, A. Galina, and F. D. Rumjanek. How does the metabolism of tumour cells differ from that of normal cells. *Bioscience Reports*, 33(6):865–873, 2013. ISSN 0144-8463. doi: 10.1042/BSR20130066.

L. M. Ballou and R. Z. Lin. Rapamycin and mTOR kinase inhibitors. *Journal of Chemical Biology*, 1(1-4):27–36, 2008. ISSN 1864-6158. doi: 10.1007/s12154-008-0003-5.

L. Bar-Peled and D. M. Sabatini. Regulation of mTORC1 by amino acids. *Trends in Cell Biology*, 24(7):400–406, 2014. ISSN 18793088. doi: 10.1016/j.tcb.2014.03.003.

E. Batsché and C. Crémisi. Opposite transcriptional activity between the wild type c-myc gene coding for c-Myc1 and c-Myc2 proteins and c-Myc1 and c-Myc2 separately. *Oncogene*, 18(41): 5662–5671, 1999. ISSN 09509232. doi: 10.1038/sj.onc.1202927.

Y. Ben-Ari, Y. Brody, N. Kinor, A. Mor, T. Tsukamoto, D. L. Spector, R. H. Singer, and Y. Shav-Tal. The life of an mRNA in space and time. *Journal of Cell Science*, 123(10):1761–1774, 2010. ISSN 0021-9533. doi: 10.1242/jcs.062638.

U. Benary, E. Wolf, and J. Wolf. Mathematical modelling of promoter occupancies in MYC-dependent gene regulation. *Genomics and Computational Biology*, 3(2):54, 2017. ISSN 2365-7154. doi: 10.18547/gcb.2017.vol3.iss2.e54.

A. K. Bera, S. Chen, J. L. Smith, and H. Zalkin. Temperature-dependent function of the glutamine phosphoribosylpyrophosphate amidotransferase ammonia channel and coupling with glycinamide ribonucleotide synthetase in a hyperthermophile. *Journal of Bacteriology*, 182(13): 3734–3739, 2000. ISSN 00219193. doi: 10.1128/JB.182.13.3734-3739.2000.

J. M. Berg, J. L. Tymoczko, and L. Stryer. *Stryer Biochemie*. Springer Berlin Heidelberg, Berlin, Heidelberg, 2007. ISBN 978-3-8274-2988-9. doi: 10.1007/978-3-8274-2989-6.

M. Boettcher, A. Lawson, V. Ladenburger, J. Fredebohm, J. Wolf, J. D. Hoheisel, C. Frezza, and T. Shlomi. High throughput synthetic lethality screen reveals a tumorigenic role of adenylate cyclase in fumarate hydratase-deficient cancer cells. *BMC Genomics*, 15(1):158, 2014. ISSN 1471-2164. doi: 10.1186/1471-2164-15-158.

L. M. Boxer and C. V. Dang. Translocations involving c- myc and c- myc function. *Oncogene*, 20 (40):5595–5610, 2001.

C. M. Brennan and J. a. Steitz. HuR and mRNA stability. *Cellular and molecular life sciences : CMLS*, 58(2):266–277, 2001. ISSN 1420-682X. doi: 10.1007/PL00000854.

J. R. Buchan and R. Parker. Eukaryotic Stress Granules: The Ins and Outs of Translation. *Molecular Cell*, 36(6):932–941, 2009. ISSN 10972765. doi: 10.1016/j.molcel.2009.11.020.

J. M. Buescher and E. M. Driggers. Integration of omics: more than the sum of its parts. *Cancer & Metabolism*, 4(1):4, 2016. ISSN 2049-3002. doi: 10.1186/s40170-016-0143-y.

A. R. Buxbaum, B. Wu, and R. H. Singer. Single -Actin mRNA Detection in Neurons Reveals a Mechanism for Regulating Its Translatability. *Science*, 343(6169):419–422, 2014. ISSN 0036-8075. doi: 10.1126/science.1242939.

J. R. Cantor and D. M. Sabatini. Cancer cell metabolism: One hallmark, many faces. *Cancer Discovery*, 2(10):881–898, 2012. ISSN 21598274. doi: 10.1158/2159-8290.CD-12-0345.

A. Castello, M. W. Hentze, and T. Preiss. Metabolic Enzymes Enjoying New Partnerships as RNA-Binding Proteins. *Trends in Endocrinology and Metabolism*, 26(12):746–757, 2015. ISSN 18793061. doi: 10.1016/j.tem.2015.09.012.

D. Cervantes-Madrid, Y. Romero, and A. Dueñas-González. Reviving Lonidamine and 6-Diazo-5-oxo-L-norleucine to Be Used in Combination for Metabolic Cancer Therapy. *BioMed Research International*, pages 1–13, 2015. ISSN 2314-6133. doi: 10.1155/2015/690492.

N. M. Cetinbas, J. Sudderth, R. C. Harris, A. Cebeci, G. L. Negri, Ö. H. Yllmaz, R. J. Deberardinis, and P. H. Sorensen. Glucose-dependent anaplerosis in cancer cells is required for cellular redox balance in the absence of glutamine. *Scientific Reports*, 6(February):1–12, 2016. ISSN 20452322. doi: 10.1038/srep32606.

S. A. Chappell, J. P. LeQuesne, F. E. Paulin, M. L. DeSchoolmeester, M. Stoneley, R. L. Soutar, S. H. Ralston, M. H. Helfrich, and A. E. Willis. A mutation in the c-myc-IRES leads to enhanced internal ribosome entry in multiple myeloma: a novel mechanism of oncogene de-regulation. *Oncogene*, 19(38):4437–4440, 2000. ISSN 0950-9232. doi: 10.1038/sj.onc.1203791.

L. Chen and H. Cui. Targeting glutamine induces apoptosis: A cancer therapy approach. *International Journal of Molecular Sciences*, 16(9):22830–22855, 2015. ISSN 14220067. doi: 10.3390/ijmsl60922830.

F. Chiacchiera and C. Simone. The AMPK-FoxO3A axis as a target for cancer treatment. *Cell Cycle*, 9(6):1091–1096, 2010. ISSN 15514005. doi: 10.4161/cc.9.6.11035.

A. Chokkathukalam, D.-h. Kim, M. P. Barrett, R. Breitling, and D. J. Creek. Stable isotope-labeling studies in metabolomics: new insights into structure and dynamics of metabolic networks. *Bioanalysis*, 6(4):511–524, 2014. ISSN 1757-6180. doi: 10.4155/bio.13.348.

R. I. Christopherson. *Encyclopedic Reference of Genomics and Proteomics in Molecular Medicine.* Springer Berlin Heidelberg, 2006. ISBN 978-3-540-44244-8. doi: 10.1007/3-540-29623-9.

A. A. Cluntun, M. J. Lukey, R. A. Cerione, and J. W. Locasale. Glutamine Metabolism in Cancer: Understanding the Heterogeneity. *Trends in Cancer*, 3(3):169–180, 2017. ISSN 24058033. doi: 10.1016/j.trecan.2017.01.005.

G. L. Coffey, J. Ehrlich, M. W. Fisher, A. B. Hillegas, D. L. Kohberger, H. E. Machamer, W. A. Rightsel, and F. R. Roegner. 6-Diazo-5-oxo-L-norleucine, a new tumor-inhibitory substance. I. Biologic studies. *Antibiotics & chemotherapy (Northfield, Ill.)*, 6(8):487–97, 1956. ISSN 0570-3123.

J. Cox, N. Neuhauser, A. Michalski, R. A. Scheltema, J. V. Olsen, and M. Mann. Andromeda: A peptide search engine integrated into the MaxQuant environment. *Journal of Proteome Research*, 10(4):1794–1805, 2011. ISSN 15353893. doi: 10.1021/pr101065j.

F. Crick. Central dogma of molecular biology. *Nature*, 227(5258):561–3, 1970. ISSN 0028-0836.

A. Csibi, G. Lee, S.-O. Yoon, H. Tong, D. Ilter, I. Elia, S.-M. Fendt, T. M. Roberts, and J. Blenis. The mTORC1/S6K1 Pathway Regulates Glutamine Metabolism through the eIF4B-Dependent Control of c-Myc Translation. *Current Biology*, 24(19):2274–2280, 2014. ISSN 09609822. doi: 10.1016/j.cub.2014.08.007.

A. Cuenda and S. Rousseau. p38 MAP-Kinases pathway regulation, function and role in human diseases. *Biochimica et Biophysica Acta (BBA) - Molecular Cell Research*, 1773(8):1358–1375, 2007. ISSN 01674889. doi: 10.1016/j.bbamcr.2007.03.010.

A. F. D'Adamo and K. Dugan Tobin. The oxoglutarate reductive carboxylation pathway: A review. *Life Sciences*, 24(22):2011–2022, 1979. ISSN 00243205. doi: 10.1016/0024-3205(79)90073-0.

C. V. Dang. c-Myc Target Genes Involved in Cell Growth, Apoptosis, and Metabolism. *Molecular and Cellular Biology*, 19(1):1–11, 1999. ISSN 0270-7306. doi: 10.1128/MCB.19.1.1.

C. V. Dang. MYC on the path to cancer. *Cell*, 149(1):22–35, 2012. ISSN 00928674. doi: 10.1016/j.cell.2012.03.003.

C. V. Dang. MYC, Metabolism, Cell Growth, and Tumorigenesis. *Cold Spring Harbor Perspectives in Medicine*, 3(8):a014217–a014217, 2013. ISSN 2157-1422. doi: 10.1101/cshperspect.a014217.

S. M. Davidson, T. Papagiannakopoulos, B. A. Olenchock, J. E. Heyman, M. A. Keibler, A. Luengo, M. R. Bauer, A. K. Jha, J. P. O'Brien, K. A. Pierce, D. Y. Gui, L. B. Sullivan, T. M. Wasylenko, L. Subbaraj, C. R. Chin, G. Stephanopolous, B. T. Mott, T. Jacks, C. B. Clish, and M. G. Van Der Heiden. Environment impacts the metabolic dependencies of ras-driven non-small cell lung cancer. *Cell Metabolism*, 23(3):517–528, 2016. ISSN 19327420. doi: 10.1016/j.cmet.2016.01.007.

R. J. DeBerardinis and N. S. Chandel. Fundamentals of cancer metabolism. *Science advances*, 2 (5):e1600200, 2016. ISSN 23752548. doi: 10.1126/sciadv.1600200.

R. J. DeBerardinis and T. Cheng. Q's next: the diverse functions of glutamine in metabolism, cell biology and cancer. *Oncogene*, 29(3):313–24, 2010. ISSN 1476-5594. doi: 10.1038/onc.2009.358.

C. J. Decker and R. Parker. P-Bodies and Stress Granules: Possible Roles in the Control of Translation and mRNA Degradation. *Cold Spring Harbor Perspectives in Biology*, 4(9):1–17, 2012. ISSN 1943-0264. doi: 10.1101/cshperspect.a012286.

F. R. Dejure. *Investigation of the role of MYC as a stress responsive protein*. PhD thesis, Julius-Maximilians-Universität Würzburg, 2017.

F. R. Dejure, N. Royla, S. Herold, J. Kalb, S. Walz, C. P. Ade, G. Mastrobuoni, J. T. Vanselow, A. Schlosser, E. Wolf, S. Kempa, and M. Eilers. The MYC mRNA 3'-UTR couples RNA polymerase II function to glutamine and ribonucleotide levels. *The EMBO Journal*, 36(13): 1854–1868, 2017. ISSN 0261-4189. doi: 10.15252/embj.201796662.

M. Deponte. Glutathione catalysis and the reaction mechanisms of glutathione-dependent enzymes. *Biochimica et Biophysica Acta - General Subjects*, 1830(5):3217–3266, 2013. ISSN 03044165. doi: 10.1016/j.bbagen.2012.09.018.

S. Di Giacomo, M. Sollazzo, S. Paglia, and D. Grifoni. MYC, cell competition, and cell death in cancer: The inseparable triad. *Genes*, 8(4):1–11, 2017. ISSN 20734425. doi: 10.3390/genes8040120.

S. Di Meo, T. T. Reed, P. Venditti, and V. M. Victor. Harmful and Beneficial Role of ROS. *Oxidative Medicine and Cellular Longevity*, 2016:1–3, 2016. ISSN 1942-0900. doi: 10.1155/2016/7909186.

G. A. Doyle, N. A. Betz, P. F. Leeds, A. J. Fleisig, R. D. Prokipcak, and J. Ross. The c-myc coding region determinant-binding protein: a member of a family of KH domain RNA-binding proteins. *Nucleic acids research*, 26(22):5036–44, 1998. ISSN 0305-1048.

A. Efeyan, W. C. Comb, and D. M. Sabatini. Nutrient-sensing mechanisms and pathways. *Nature*, 517(7534):302–310, 2015. ISSN 0028-0836. doi: 10.1038/nature14190.

M. Eilers, D. Picard, K. R. Yamamoto, and J. M. Bishop. Chimaeras of Myc oncoprotein and steroid receptors cause hormone-dependent transformation of cells. *Nature*, 340(6228):66–68, 1989. ISSN 0028-0836. doi: 10.1038/340066a0.

R. Elkon, F. Loayza-Puch, G. Korkmaz, R. Lopes, P. C. van Breugel, O. B. Bleijerveld, A. M. Altelaar, E. Wolf, F. Lorenzin, M. Eilers, and R. Agami. Myc coordinates transcription and translation to enhance transformation and suppress invasiveness. *EMBO reports*, 16(12):1723–1736, 2015. ISSN 1469-221X. doi: 10.15252/embr.201540717.

J. J. W. Erickson and R. a. R. Cerione. Glutaminase: a hot spot for regulation of cancer cell metabolism? *Oncotarget*, 1(8):734–740, 2010. ISSN 1949-2553. doi: 10.1016/j.bbi.2008.05.010.

G. I. Evan, A. H. Wyllie, S. Gilbert, T. D. Littlewood, H. Land, M. Brooks, C. M. Waters, L. Penn, and D. C. Hancock. Induction of Apoptosis by c-myc Protein in Fibroblasts. *Cell*, 69:119–128, 1992. ISSN 00928674. doi: 10.1074/jbc.270.48.28797.

A. S. Farrell and R. C. Sears. MYC Degradation. *Cold Spring Harbor Perspectives in Medicine*, 4 (3), 2014. ISSN 2157-1422. doi: 10.1101/cshperspect.a014365.

R. Fritsche-Guenther, F. Witzel, A. Sieber, R. Herr, N. Schmidt, S. Braun, T. Brummer, C. Sers, and N. Blüthgen. Strong negative feedback from Erk to Raf confers robustness to MAPK signalling. *Molecular Systems Biology*, 7(489):1–13, 2011. ISSN 17444292. doi: 10.1038/msb.2011.27.

R. Fritsche-Guenther, F. Witzel, S. Kempa, T. Brummer, C. Sers, and N. Blüthgen. Effects of RAF inhibitors on PI3K/AKT signalling depend on mutational status of the RAS/RAF signalling axis. *Oncotarget*, 7(7):7960–7969, 2016. ISSN 1949-2553. doi: 10.18632/oncotarget.6959.

P. Gao, I. Tchernyshyov, T.-C. Chang, Y.-S. Lee, K. Kita, T. Ochi, K. I. Zeller, A. M. De Marzo, J. E. Van Eyk, J. T. Mendell, and C. V. Dang. c-Myc suppression of miR-23a/b enhances mitochondrial glutaminase expression and glutamine metabolism. *Nature*, 458(7239):762–765, 2009. ISSN 0028-0836. doi: 10.1038/nature07823.

A. D. Garst, A. L. Edwards, and R. T. Batey. Riboswitches: Structures and Mechanisms. *Cold Spring Harbor Perspectives in Biology*, 3(6):a003533–a003533, 2011. ISSN 1943-0264. doi: 10.1101/cshperspect.a003533.

S. I. Gharbi, M. J. Zvelebil, S. J. Shuttleworth, T. Hancox, N. Saghir, J. F. Timms, and M. D. Waterfield. Exploring the specificity of the PI3K family inhibitor LY294002. *Biochemical Journal*, 404(1):15–21, 2007. ISSN 0264-6021. doi: 10.1042/BJ20061489.

D. B. Glass, H. C. Cheng, L. Mende-Mueller, J. Reed, and D. A. Walsh. Primary structural determinants essential for potent inhibition of cAMP-dependent protein kinase by inhibitory peptides corresponding to the active portion of the heat-stable inhibitor protein. *Journal of Biological Chemistry*, 264(15):8802–8810, 1989. ISSN 00219258.

D. C. Goberdhan, C. Wilson, and A. L. Harris. Amino Acid Sensing by mTORC1: Intracellular Transporters Mark the Spot. *Cell Metabolism*, 23(4):580–589, 2016. ISSN 19327420. doi: 10.1016/j.cmet.2016.03.013.

M. J. Gunzburg, A. Sivakumaran, N. R. Pendini, J. H. Yoon, M. Gorospe, M. C. Wilce, and J. A. Wilce. Cooperative interplay of let-7 mimic and HuR with MYC RNA. *Cell Cycle*, 14(17): 2729–2733, 2015. ISSN 15514005. doi: 10.1080/15384101.2015.1069930.

D. Hanahan and R. A. Weinberg. The hallmarks of cancer. *Cell*, 100(1):57–70, 2000. ISSN 0092-8674.

D. Hanahan and R. A. Weinberg. Hallmarks of cancer: The next generation. *Cell*, 144(5):646–674, 2011. ISSN 00928674. doi: 10.1016/j.cell.2011.02.013.

W. Hao, C. P. B. Chang, C. C. Tsao, and J. Xu. Oligomycin-induced bioenergetic adaptation in cancer cells with heterogeneous bioenergetic organization. *Journal of Biological Chemistry*, 285 (17):12647–12654, 2010. ISSN 00219258. doi: 10.1074/jbc.M109.084194.

Y. Hao, Y. Samuels, Q. Li, D. Krokowski, B. J. Guan, C. Wang, Z. Jin, B. Dong, B. Cao, X. Feng, M. Xiang, C. Xu, S. Fink, N. J. Meropol, Y. Xu, R. A. Conlon, S. Markowitz, K. W. Kinzler, V. E. Velculescu, H. Brunengraber, J. E. Willis, T. Laframboise, M. Hatzoglou, G. F. Zhang, B. Vogelstein, and Z. Wang. Oncogenic PIK3CA mutations reprogram glutamine metabolism in colorectal cancer. *Nature Communications*, 7(May), 2016. ISSN 20411723. doi: 10.1038/ncomms11971.

D. G. Hardie. AMP-activated protein kinase-an energy sensor that regulates all aspects of cell function. *Genes and Development*, 25(18):1895–1908, 2011. ISSN 08909369. doi: 10.1101/gad.17420111.

D. G. Hardie, B. E. Schaffer, and A. Brunet. AMPK: An Energy-Sensing Pathway with Multiple Inputs and Outputs. *Trends in Cell Biology*, 26(3):190–201, 2016. ISSN 18793088. doi: 10.1016/j.tcb.2015.10.013.

C. T. Hensley, A. T. Wasti, and R. J. Deberardinis. Review series Glutamine and cancer: cell biology, physiology, and clinical opportunities. *The Journal of Clinical Investigation*, 123(9): 3678–3684, 2013. ISSN 00219738. doi: 10.1172/JCI69600.3678.

D. J. Herrick and J. Ross. The half-life of c-myc mRNA in growing and serum-stimulated cells: influence of the coding and 3' untranslated regions and role of ribosome translocation. *Molecular and cellular biology*, 14(3):2119–2128, 1994. ISSN 0270-7306. doi: 10.1128/MCB.14.3.2119.Updated.

F. Huang, Q. Zhang, H. Ma, Q. Lv, and T. Zhang. Expression of glutaminase is upregulated in colorectal cancer and of clinical significance. *International Journal of Clinical and Experimental Pathology*, 7(3):1093–1100, 2014. ISSN 19362625.

T. Huang, M. Karsy, J. Zhuge, M. Zhong, and D. Liu. B-Raf and the inhibitors: from bench to bedside. *Journal of Hematology & Oncology*, 6(1):30, 2013. ISSN 1756-8722. doi: 10.1186/1756-8722-6-30.

D. H. Huberts and I. J. van der Klei. Moonlighting proteins: An intriguing mode of multitasking. *Biochimica et Biophysica Acta (BBA) - Molecular Cell Research*, 1803(4):520–525, 2010. ISSN 01674889. doi: 10.1016/j.bbamcr.2010.01.022.

J. L. Jewell and K. L. Guan. Nutrient signaling to mTOR and cell growth. *Trends in Biochemical Sciences*, 38(5):233–242, 2013. ISSN 09680004. doi: 10.1016/j.tibs.2013.01.004.

P. Jiang and H. Coller. Functional Interactions Between microRNAs and RNA Binding Proteins. *MicroRNA*, 1(1):70–79, 2012. ISSN 22115366. doi: 10.2174/2211536611201010070.

P. Kaler, L. Augenlicht, and L. Klampfer. Activating Mutations in β-Catenin in Colon Cancer Cells Alter Their Interaction with Macrophages; the Role of Snail. *PLoS ONE*, 7(9):1–9, 2012. ISSN 19326203. doi: 10.1371/journal.pone.0045462.

M. Kalkat, J. De Melo, K. A. Hickman, C. Lourenco, C. Redel, D. Resetca, A. Tamachi, W. B. Tu, and L. Z. Penn. MYC deregulation in primary human cancers. *Genes*, 8(6):2–30, 2017. ISSN 20734425. doi: 10.3390/genes8060151.

W. P. Katt and R. A. Cerione. Glutaminase regulation in cancer cells: A druggable chain of events. *Drug Discovery Today*, 19(4):450–457, 2014. ISSN 18785832. doi: 10.1016/j.drudis.2013.10.008.

W. P. Katt, S. Ramachandran, J. W. Erickson, and R. A. Cerione. Dibenzophenanthridines as Inhibitors of Glutaminase C and Cancer Cell Proliferation. *Molecular Cancer Therapeutics*, 11 (6):1269–1278, 2012. ISSN 1535-7163. doi: 10.1158/1535-7163.MCT-11-0942.

K. Kawada, K. Toda, and Y. Sakai. Targeting metabolic reprogramming in KRAS-driven cancers. *International Journal of Clinical Oncology*, 22(4):651–659, 2017. ISSN 14377772. doi: 10.1007/s10147-017-1156-4.

K. Kelly, B. H. Cochran, C. D. Stiles, and P. Leder. Cell-specific regulation of the c-myc gene by lymphocyte mitogens and platelet-derived growth factor. *Cell*, 35(3 PART 2):603–610, 1983. ISSN 00928674. doi: 10.1016/0092-8674(83)90092-2.

S. Kempa, J. Hummel, T. Schwemmer, M. Pietzke, N. Strehmel, S. Wienkoop, J. Kopka, and W. Weckwerth. An automated GCxGC-TOF-MS protocol for batch-wise extraction and alignment of mass isotopomer matrixes from differential13C-labelling experiments: A case study for photoautotrophic-mixotrophic grown Chlamydomonas reinhardtii cells. *Journal of Basic Microbiology*, 49(1):82–91, 2009. ISSN 0233111X. doi: 10.1002/jobm.200800337.

B. Klinger, A. Sieber, R. Fritsche-Guenther, F. Witzel, L. Berry, D. Schumacher, Y. Yan, P. Durek, M. Merchant, R. Schäfer, C. Sers, and N. Blüthgen. Network quantification of EGFR signaling unveils potential for targeted combination therapy. *Molecular Systems Biology*, 9(1), 2013. ISSN 17444292. doi: 10.1038/msb.2013.29.

K. Kluckova, A. Bezawork-Geleta, J. Rohlena, L. Dong, and J. Neuzil. Mitochondrial complex II, a novel target for anti-cancer agents. *Biochimica et Biophysica Acta (BBA) - Bioenergetics*, 1827(5):552–564, 2013. ISSN 00052728. doi: 10.1016/j.bbabio.2012.10.015.

K. Kluckova, M. Sticha, J. Cerny, T. Mracek, L. Dong, Z. Drahota, E. Gottlieb, J. Neuzil, and J. Rohlena. Ubiquinone-binding site mutagenesis reveals the role of mitochondrial complex II in cell death initiation. *Cell Death and Disease*, 6(5):e1749–13, 2015. ISSN 20414889. doi: 10.1038/cddis.2015.110.

C. M. Koh, A. Sabò, and E. Guccione. Targeting MYC in cancer therapy: RNA processing offers new opportunities. *BioEssays*, 38(3):266–275, 2016. ISSN 15211878. doi: 10.1002/bies.201500134.

E. Kováts. Gas-chromatographische Charakterisierung organischer Verbindungen. Teil 1: Retentionsindices aliphatischer Halogenide, Alkohole, Aldehyde und Ketone. *Helvetica Chimica Acta*, 41(7):1915–1932, 1958. ISSN 0018019X. doi: 10.1002/hlca.19580410703.

P. K. Kreeger and D. A. Lauffenburger. Cancer systems biology: A network modeling perspective. *Carcinogenesis*, 31(1):2–8, 2009. ISSN 01433334. doi: 10.1093/carcin/bgp261.

T. R. Kress, A. Sabò, and B. Amati. MYC: Connecting selective transcriptional control to global RNA production. *Nature Reviews Cancer*, 15(10):593–607, 2015. ISSN 14741768. doi: 10.1038/nrc3984.

P. H. J. L. Kuich, N. Hoffmann, and S. Kempa. Maui-VIA: A User-Friendly Software for Visual Identification, Alignment, Correction, and Quantification of Gas Chromatograph-Mass Spectrometry Data. *Frontiers in Bioengineering and Biotechnology*, 2(January):1–8, 2015. ISSN 2296-4185. doi: 10.3389/fbioe.2014.00084.

H. N. Kung, J. R. Marks, and J. T. Chi. Glutamine synthetase is a genetic determinant of cell type-specific glutamine independence in breast epithelia. *PLoS Genetics*, 7(8), 2011. ISSN 15537390. doi: 10.1371/journal.pgen.1002229.

U. Laemmli. Cleavage of structural proteins during the assembly of the head of bacteriophage T4. *Nature*, 227:680–685, 1970.

A. N. Lane and T. W. Fan. Regulation of mammalian nucleotide metabolism and biosynthesis. *Nucleic Acids Research*, 43(4):2466–2485, 2015. ISSN 1362-4962. doi: 10.1093/nar/gkv047.

A. N. Lane, T. W.-M. Fan, M. Bousamra, R. M. Higashi, J. Yan, and D. M. Miller. Stable Isotope-Resolved Metabolomics (SIRM) in Cancer Research with Clinical Application to NonSmall Cell Lung Cancer. *OMICS: A Journal of Integrative Biology*, 15(3):173–182, 2011. ISSN 1536-2310. doi: 10.1089/omi.2010.0088.

W. H. Laux, P. Pande, I. Shoshani, J. Gao, V. Boudou-Vivet, G. Gosselin, and R. A. Johnson. Pro-nucleotide Inhibitors of Adenylyl Cyclases in Intact Cells. *Journal of Biological Chemistry*, 279(14):13317–13332, 2004. ISSN 00219258. doi: 10.1074/jbc.M309535200.

A. Le, A. N. Lane, M. Hamaker, S. Bose, A. Gouw, J. Barbi, T. Tsukamoto, C. J. Rojas, B. S. Slusher, H. Zhang, L. J. Zimmerman, D. C. Liebler, R. J. Slebos, P. K. Lorkiewicz, R. M. Higashi, T. W. Fan, and C. V. Dang. Glucose-independent glutamine metabolism via TCA cycling for proliferation and survival in B cells. *Cell Metabolism*, 15(1):110–121, 2012. ISSN 15504131. doi: 10.1016/j.cmet.2011.12.009.

D. Levens. Cellular MYCro economics: Balancing MYC function with MYC expression. *Cold Spring Harbor Perspectives in Medicine*, 3(11):1–15, 2013. ISSN 21571422. doi: 10.1101/cshperspect.a014233.

B. Li and M. C. Simon. Molecular Pathways: Targeting MYC-induced Metabolic Reprogramming and Oncogenic Stress in Cancer. *Clinical Cancer Research*, 19(21):5835–5841, 2013. ISSN 1078-0432. doi: 10.1158/1078-0432.CCR-12-3629.

B. Liao, Y. Hu, and G. Brewer. Competitive binding of AUF1 and TIAR to MYC mRNA controls its translation. *Nature Structural and Molecular Biology*, 14(6):511–518, 2007. ISSN 15459993. doi: 10.1038/nsmb1249.

M. V. Liberti and J. W. Locasale. The Warburg Effect: How Does it Benefit Cancer Cells? *Trends in Biochemical Sciences*, 41(3):211–218, 2016. ISSN 09680004. doi: 10.1016/j.tibs.2015.12.001.

C. Y. Lin, J. Lovén, P. B. Rahl, R. M. Paranal, C. B. Burge, J. E. Bradner, T. I. Lee, and R. A. Young. Transcriptional amplification in tumor cells with elevated c-Myc. *Cell*, 151(1):56–67, 2012. ISSN 00928674. doi: 10.1016/j.cell.2012.08.026.

L. Liu, J. N. Rao, T. Zou, L. Xiao, P.-Y. Wang, D. J. Turner, M. Gorospe, and J.-Y. Wang. Polyamines Regulate c-Myc Translation through Chk2-dependent HuR Phosphorylation. *Molecular Biology of the Cell*, 20(23):4885–4898, 2009. ISSN 1059-1524. doi: 10.1091/mbc.E09-07-0550.

L. Liu, M. Ouyang, J. N. Rao, T. Zou, L. Xiao, H. K. Chung, J. Wu, J. M. Donahue, M. Gorospe, and J.-Y. Wang. Competition between RNA-binding proteins CELF1 and HuR modulates MYC translation and intestinal epithelium renewal. *Molecular Biology of the Cell*, 26(10):1797–1810, 2015a. ISSN 1059-1524. doi: 10.1091/mbc.E14-11-1500.

X. Liu, W. L. Kraus, and X. Bai. Ready, pause, go: regulation of RNA polymerase II pausing and release by cellular signaling pathways. *Trends in Biochemical Sciences*, 40(9):516–525, 2015b. ISSN 09680004. doi: 10.1016/j.tibs.2015.07.003.

P. Lorkiewicz, R. M. Higashi, A. N. Lane, and T. W. Fan. High information throughput analysis of nucleotides and their isotopically enriched isotopologues by direct-infusion FTICR-MS. *Metabolomics*, 8(5):930–939, 2012. ISSN 15733882. doi: 10.1007/s11306-011-0388-y.

M. J. Lukey, K. F. Wilson, and R. A. Cerione. Therapeutic strategies impacting cancer cell glutamine metabolism. *Future medicinal chemistry*, 5(14):1685–700, 2013. ISSN 1756-8927. doi: 10.4155/fmc.13.130.

M. Marderosian, A. Sharma, A. P. Funk, R. Vartanian, J. Masri, O. D. Jo, and J. F. Gera. Tristetraprolin regulates cyclin D1 and c-Myc mRNA stability in response to rapamycin in an Akt-dependent manner via p38 MAPK signaling. *Oncogene*, 25(47):6277–6290, 2006. ISSN 09509232. doi: 10.1038/sj.onc.1209645.

G. Martin. Cell signaling and cancer. *Cancer Cell*, 4(3):167–174, 2003. ISSN 15356108. doi: 10.1016/S1535-6108(03)00216-2.

I. Martincorena, K. M. Raine, M. Gerstung, K. J. Dawson, K. Haase, P. Van Loo, H. Davies, M. R. Stratton, and P. J. Campbell. Universal Patterns of Selection in Cancer and Somatic Tissues. *Cell*, 171(5):1029–1041.e21, 2017. ISSN 10974172. doi: 10.1016/j.cell.2017.09.042.

C. K. Mathews. Deoxyribonucleotide metabolism, mutagenesis and cancer. *Nature Reviews Cancer*, 15(9):528–539, 2015. ISSN 1474-175X. doi: 10.1038/nrc3981.

K. Mazan-Mamczarz, A. Lal, L. Jennifer, T. Kawai, M. Gorospe, and J. L. Martindale. Translational Repression by RNA-Binding Protein TIAR Translational Repression by RNA-Binding Protein TIAR. *Molecular and cellular biology*, 26(7):2716–2727, 2006. doi: 10.1128/MCB.26.7.2716.

L. McDermott. Kidney-Type Glutaminase Inhibitors for Treating Cancer. An Overview. *Journal of Drug Research and Development*, 3(2):1–6, 2017. ISSN 24701009. doi: 10.16966/2470-1009.133.

S. B. McMahon. MYC and the Control of Apoptosis. *Cold Spring Harbor Perspectives in Medicine*, 4(7):a014407–a014407, 2014. ISSN 2157-1422. doi: 10.1101/cshperspect.a014407.

S. Memczak, M. Jens, A. Elefsinioti, F. Torti, J. Krueger, A. Rybak, L. Maier, S. D. Mackowiak, L. H. Gregersen, M. Munschauer, A. Loewer, U. Ziebold, M. Landthaler, C. Kocks, F. le Noble, and N. Rajewsky. Circular RNAs are a large class of animal RNAs with regulatory potency. *Nature*, 495(7441):333–338, 2013. ISSN 0028-0836. doi: 10.1038/nature11928.

C. M. Metallo, J. L. Walther, G. Stephanopoulos, P. S. Ward, J. Patel, D. R. Wise, O. Abdel-wahab, B. D. Bennett, H. A. Coller, J. R. Cross, V. R. Fantin, C. V. Hedvat, E. Alexander, J. D. Rabinowitz, M. Carroll, S. M. Su, K. A. Sharp, L. Ross, and C. B. Thompson. Evaluation of ^{13}C isotopic tracers for metabolic flux analysis in mammalian cells. *BioTechniques*, 144(3): 167–174, 2009. doi: 10.1016/j.jbiotec.2009.07.010.Evaluation.

N. Meyer and L. Z. Penn. Reflecting on 25 years with MYC. *Nature Reviews Cancer*, 8(12): 976–990, 2008. ISSN 1474-175X. doi: 10.1038/nrc2231.

H. Modjtahedi and A. Clarke. The Immune System. In *The Biology of Cancer*, pages 79–98. John Wiley & Sons Ltd, West Sussex, England, second edition, 2008. doi: 10.1002/9780470988121.ch8.

J. Moscat, A. Richardson, and M. T. Diaz-Meco. Nutrient stress revamps cancer cell metabolism. *Cell Research*, 25(5):537–538, 2015. ISSN 17487838. doi: 10.1038/cr.2015.38.

D. J. Murphy, M. R. Junttila, L. Pouyet, A. Karnezis, K. Shchors, D. A. Bui, L. Brown-Swigart, L. Johnson, and G. I. Evan. Distinct Thresholds Govern Myc's Biological Output In Vivo. *Cancer Cell*, 14(6):447–457, 2008. ISSN 15356108. doi: 10.1016/j.ccr.2008.10.018.

K. Myant and O. J. Sansom. More, More, More: Downregulation of a MK5-FoxO3a-mir34b/c Pathway Further Increases c-Myc Levels in Colorectal Cancer. *Molecular Cell*, 41(4):369–370, 2011. ISSN 10972765. doi: 10.1016/j.molcel.2011.01.028.

C. Nanbru, I. Lafon, S. Audigier, M.-C. Gensac, S. Vagner, G. Huez, and A.-C. Prats. Alternative Translation of the Proto-oncogene c-myc by an Internal Ribosome Entry Site. *Journal of Biological Chemistry*, 272(51):32061–32066, 1997. ISSN 0021-9258. doi: 10.1074/jbc.272.51.32061.

A. I. Nieminen, V. M. Eskelinen, H. M. Haikala, T. A. Tervonen, Y. Yan, J. I. Partanen, and J. Klefstrom. Myc-induced AMPK-phospho p53 pathway activates Bak to sensitize mitochondrial apoptosis. *Proceedings of the National Academy of Sciences*, 110(20):E1839–E1848, 2013. ISSN 0027-8424. doi: 10.1073/pnas.1208530110.

R. Oehler and E. Roth. Regulative capacity of glutamine. *Current Opinion in Clinical Nutrition and Metabolic Care*, 6(3):277–282, 2003. ISSN 13631950. doi: 10.1097/00075197-200305000-00002.

A. Ohta. A metabolic immune checkpoint: Adenosine in Tumor Microenvironment. *Frontiers in Immunology*, 7(MAR):1–11, 2016. ISSN 16643224. doi: 10.3389/fimmu.2016.00109.

J. L. Orgaz, C. Herraiz, and V. Sanz-Moreno. Rho GTPases modulate malignant transformation of tumor cells. *Small GTPases*, 5(4):e983867, 2014. ISSN 2154-1248. doi: 10.4161/sgtp.29019.

M. Pan, M. A. Reid, X. H. Lowman, R. P. Kulkarni, T. Q. Tran, X. Liu, Y. Yang, J. E. Hernandez-Davies, K. K. Rosales, H. Li, W. Hugo, C. Song, X. Xu, D. E. Schones, D. K. Ann, V. Gradinaru, R. S. Lo, J. W. Locasale, and M. Kong. Regional glutamine deficiency in tumours promotes dedifferentiation through inhibition of histone demethylation. *Nature Cell Biology*, 18(10):1090–1101, 2016. ISSN 1465-7392. doi: 10.1038/ncb3410.

R. Parker and U. Sheth. P Bodies and the Control of mRNA Translation and Degradation. *Molecular Cell*, 25(5):635–646, 2007. ISSN 10972765. doi: 10.1016/j.molcel.2007.02.011.

F. Parlati, S. D. Demo, M. I. Gross, J. R. Janes, E. R. Lewis, A. L. MacKinnon, M. L. Rodriguez, P. J. Shwonek, T. Wang, J. Yang, D. Zhang, F. Zhao, and M. K. Bennett. CB-839, a novel potent and selective glutaminase inhibitor, has broad antiproliferative activity in cell lines derived from both solid tumors and hematological malignancies. *Cancer Research*, 74(1416):839, 2014.

M. Pietzke and S. Kempa. Pulsed stable isotope-resolved metabolomic studies of cancer cells. *Methods in Enzymology*, 543:179–198, 2014. ISSN 15577988. doi: 10.1016/B978-0-12-801329-8.00009-X.

M. Pietzke, C. Zasada, S. Mudrich, and S. Kempa. Decoding the dynamics of cellular metabolism and the action of 3-bromopyruvate and 2-deoxyglucose using pulsed stable isotope-resolved metabolomics. *Cancer & Metabolism*, 2(1):9, 2014. ISSN 2049-3002. doi: 10.1186/2049-3002-2-9.

L. M. Pinkus. [45] Glutamine binding sites. *Methods in Enzymology*, 46(I):414–427, 1977. ISSN 00766879. doi: 10.1016/S0076-6879(77)46049-X.

C. J. Poole and J. van Riggelen. MYC–master regulator of the cancer epigenome and transcriptome. *Genes*, 8(5), 2017. ISSN 20734425. doi: 10.3390/genes8050142.

P. B. Rahl and R. A. Young. MYC and transcription elongation. *Cold Spring Harbor Perspectives in Medicine*, 4(1):1–12, 2014. ISSN 21571422. doi: 10.1101/cshperspect.a020990.

J. Rappsilber, M. Mann, and Y. Ishihama. Protocol for micro-purification, enrichment, pre-fractionation and storage of peptides for proteomics using StageTips. *Nature Protocols*, 2(8): 1896–1906, 2007. ISSN 1754-2189. doi: 10.1038/nprot.2007.261.

B. Ratnikov, P. Aza-blanc, Z. A. Ronai, J. W. Smith, A. L. Osterman, D. A. Scott, L. Andrei, and D. A. Scott. Glutamate and asparagine cataplerosis underlie glutamine addiction in melanoma. *Oncotarget*, 6(10):14–18, 2015. ISSN 1949-2553. doi: 10.18632/oncotarget.3132.

S. Röhrs, N. Kutzner, A. Vlad, T. Grunwald, S. Ziegler, and O. Müller. Chronological expression of Wnt target genes Ccnd1, Myc, Cdkn1a, Tfrc, Plf1 and Ramp3. *Cell Biology International*, 33(4):501–508, 2009. ISSN 10656995. doi: 10.1016/j.cellbi.2009.01.016.

M. Rokavec, H. Li, L. Jiang, and H. Hermeking. The p53/miR-34 axis in development and disease. *Journal of Molecular Cell Biology*, 6(3):214–230, 2014. ISSN 1674-2788. doi: 10.1093/jmcb/mju003.

M. Sachdeva, S. Zhu, F. Wu, H. Wu, V. Walia, S. Kumar, R. Elble, K. Watabe, and Y.-Y. Mo. p53 represses c-Myc through induction of the tumor suppressor miR-145. *Proceedings of the National Academy of Sciences*, 106(9):3207–3212, 2009. ISSN 0027-8424. doi: 10.1073/pnas.0808042106.

P. Sassone-Corsi. The Cyclic AMP pathway. *Cold Spring Harbor Perspectives in Biology*, 4(12): 1–4, 2012. ISSN 19430264. doi: 10.1101/cshperspect.a011148.

J. Schindelin, I. Arganda-Carreras, E. Frise, V. Kaynig, M. Longair, T. Pietzsch, S. Preibisch, C. Rueden, S. Saalfeld, B. Schmid, J.-Y. Tinevez, D. J. White, V. Hartenstein, K. Eliceiri, P. Tomancak, and A. Cardona. Fiji: an open-source platform for biological-image analysis. *Nature Methods*, 9(7):676–682, 2012. ISSN 1548-7091. doi: 10.1038/nmeth.2019.

C. A. Schneider, W. S. Rasband, and K. W. Eliceiri. NIH Image to ImageJ: 25 years of image analysis. *Nature Methods*, 9(7):671–675, 2012. ISSN 15487091. doi: 10.1038/nmeth.2089.

R. C. Sears. The life cycle of c-Myc: From synthesis to degradation. *Cell Cycle*, 3(9):1133–1137, 2004. ISSN 15514005. doi: 10.4161/cc.3.9.1145.

J. K. Sethi and A. Vidal-Puig. Wnt signalling and the control of cellular metabolism. *Biochemical Journal*, 427(1):1–17, 2010. ISSN 0264-6021. doi: 10.1042/BJ20091866.

N. P. Shanware, K. Bray, C. H. Eng, F. Wang, M. Follettie, J. Myers, V. R. Fantin, and R. T. Abraham. Glutamine deprivation stimulates mTOR-JNK-dependent chemokine secretion. *Nature Communications*, 5, 2014. ISSN 20411723. doi: 10.1038/ncomms5900.

A. S. Shaw, A. P. Kornev, J. Hu, L. G. Ahuja, and S. S. Taylor. Kinases and Pseudokinases: Lessons from RAF. *Molecular and Cellular Biology*, 34(9):1538–1546, 2014. ISSN 0270-7306. doi: 10.1128/MCB.00057-14.

Z.-J. Shen and J. Malter. Regulation of AU-Rich Element RNA Binding Proteins by Phosphorylation and the Prolyl Isomerase Pin1. *Biomolecules*, 5(2):412–434, 2015. ISSN 2218-273X. doi: 10.3390/biom5020412.

H. Shim, Y. S. Chun, B. C. Lewis, and C. V. Dang. A unique glucose-dependent apoptotic pathway induced by c-Myc. *Proceedings of the National Academy of Sciences*, 95(4):1511–1516, 1998. ISSN 0027-8424. doi: 10.1073/pnas.95.4.1511.

E. H. Shroff, L. S. Eberlin, V. M. Dang, A. M. Gouw, M. Gabay, S. J. Adam, D. I. Bellovin, P. T. Tran, W. M. Philbrick, A. Garcia-Ocana, S. C. Casey, Y. Li, C. V. Dang, R. N. Zare, and D. W. Felsher. MYC oncogene overexpression drives renal cell carcinoma in a mouse model through glutamine metabolism. *Proceedings of the National Academy of Sciences*, 112(21):6539–6544, 2015. ISSN 0027-8424. doi: 10.1073/pnas.1507228112.

A.-B. Shyu, M. F. Wilkinson, and A. van Hoof. Messenger RNA regulation: to translate or to degrade. *The EMBO Journal*, 27(3):471–481, 2008. ISSN 0261-4189. doi: 10.1038/sj.emboj.7601977.

J. Son, C. A. Lyssiotis, H. Ying, X. Wang, S. Hua, M. Ligorio, R. M. Perera, C. R. Ferrone, E. Mullarky, N. Shyh-Chang, Y. Kang, J. B. Fleming, N. Bardeesy, J. M. Asara, M. C. Haigis, R. A. Depinho, L. C. Cantley, and A. C. Kimmelman. Glutamine supports pancreatic cancer growth through a KRAS-regulated metabolic pathway. *Nature*, 496(7443):101–105, 2013. ISSN 00280836. doi: 10.1038/nature12040.

G. D. Spotts, S. V. Patel, Q. Xiao, and S. R. Hann. Identification of downstream-initiated c-Myc proteins which are dominant-negative inhibitors of transactivation by full-length c-Myc proteins. *Molecular and cellular biology*, 17(3):1459–68, 1997. ISSN 0270-7306.

E. R. Still and M. O. Yuneva. Hopefully devoted to Q: Targeting glutamine addiction in cancer. *British Journal of Cancer*, 116(11):1375–1381, 2017. ISSN 15321827. doi: 10.1038/bjc.2017.113.

Z. E. Stine, Z. E. Walton, B. J. Altman, A. L. Hsieh, and C. V. Dang. MYC, metabolism, and cancer. *Cancer Discovery*, 5(10):1024–1039, 2015. ISSN 21598290. doi: 10.1158/2159-8290.CD-15-0507.

L. J. Strobl and D. Eick. Hold back of RNA polymerase II at the transcription start site mediates down-regulation of c-myc in vivo. *The EMBO journal*, 11(9):3307–14, 1992. ISSN 0261-4189.

S.-Y. Sun. N-acetylcysteine, reactive oxygen species and beyond. *Cancer Biology & Therapy*, 9(2):109–110, 2010. ISSN 1538-4047. doi: 10.4161/cbt.9.2.10583.

S. Talwar, J. Jin, B. Carroll, A. Liu, M. B. Gillespie, and V. Palanisamy. Caspase-mediated cleavage of RNA-binding protein HuR regulates c-Myc protein expression after hypoxic stress. *Journal of Biological Chemistry*, 286(37):32333–32343, 2011. ISSN 00219258. doi: 10.1074/jbc.M111.255927.

W. P. Tansey. Mammalian MYC Proteins and Cancer. *New Journal of Science*, 2014:1–27, 2014. ISSN 2356-7740. doi: 10.1155/2014/757534.

M. Tarrado-Castellarnau, P. de Atauri, and M. Cascante. Oncogenic regulation of tumor metabolic reprogramming. *Oncotarget*, 7(38):62726–62753, 2016. ISSN 1949-2553. doi: 10.18632/oncotarget.10911.

K. Thangavelu, C. Q. Pan, T. Karlberg, G. Balaji, M. Uttamchandani, V. Suresh, H. Schuler, B. C. Low, and J. Sivaraman. Structural basis for the allosteric inhibitory mechanism of human kidney-type glutaminase (KGA) and its regulation by Raf-Mek-Erk signaling in cancer cell metabolism. *Proceedings of the National Academy of Sciences*, 109(20):7705–7710, 2012. ISSN 0027-8424. doi: 10.1073/pnas.1116573109.

K. Thangavelu, Q. Y. Chong, B. C. Low, and J. Sivaraman. Structural Basis for the Active Site Inhibition Mechanism of Human Kidney-Type Glutaminase (KGA). *Scientific Reports*, 4:1–7, 2015. ISSN 20452322. doi: 10.1038/srep03827.

L. A. Timmerman, T. Holton, M. Yuneva, R. J. Louie, M. Padró, A. Daemen, M. Hu, D. A. Chan, S. P. Ethier, L. J. Van'tVeer, K. Polyak, F. McCormick, and J. W. Gray. Glutamine Sensitivity Analysis Identifies the xCT Antiporter as a Common Triple-Negative Breast Tumor Therapeutic Target. *Cancer Cell*, 24(4):450–465, 2013. ISSN 15356108. doi: 10.1016/j.ccr.2013.08.020.

S. Tyanova, T. Temu, P. Sinitcyn, A. Carlson, M. Y. Hein, T. Geiger, M. Mann, and J. Cox. The Perseus computational platform for comprehensive analysis of (prote)omics data. *Nature Methods*, 13(9):731–740, 2016. ISSN 15487105. doi: 10.1038/nmeth.3901.

A. P. J. van den Heuvel, J. Jing, R. F. Wooster, and K. E. Bachman. Analysis of glutamine dependency in non-small cell lung cancer. *Cancer Biology & Therapy*, 13(12):1185–1194, 2012. ISSN 1538-4047. doi: 10.4161/cbt.21348.

M. G. Vander Heiden. Targeting cancer metabolism: A therapeutic window opens. *Nature Reviews Drug Discovery*, 10(9):671–684, 2011. ISSN 14741776. doi: 10.1038/nrd3504.

J. Vervoorts, J. Lüscher-Firzlaff, and B. Lüscher. The ins and outs of MYC regulation by post-translational mechanisms. *Journal of Biological Chemistry*, 281(46):34725–34729, 2006. ISSN 00219258. doi: 10.1074/jbc.R600017200.

M. Vita and M. Henriksson. The Myc oncoprotein as a therapeutic target for human cancer. *Seminars in Cancer Biology*, 16(4):318–330, aug 2006. ISSN 1044579X. doi: 10.1016/j.semcancer.2006.07.015.

B. Vogelstein, N. Papadopoulos, V. E. Velculescu, S. Zhou, L. A. Diaz, and K. W. Kinzler. Cancer Genome Lanscapes. *Science*, 339(6127):1546–1558, 2013. ISSN 1095-9203. doi: 10.1126/science.1235122.Cancer.

J. B. Wang, J. W. Erickson, R. Fuji, S. Ramachandran, P. Gao, R. Dinavahi, K. F. Wilson, A. L. B. Ambrosio, S. M. G. Dias, C. V. Dang, and R. A. Cerione. Targeting mitochondrial glutaminase activity inhibits oncogenic transformation. *Cancer Cell*, 18(3):207–219, 2010. ISSN 15356108. doi: 10.1016/j.ccr.2010.08.009.

O. Warburg, K. Possener, and E. Negelein. Über den Stoffwechsel der Carcinomzelle. *Biochemische Zeitschrift*, 152:310–343, 1924.

O. Warburg, F. Wind, and N. Erwin. The Metabolism of Tumors in the Body. *The Journal of General Physiology*, 8(6):519–530, 1927.

P. S. Ward and C. B. Thompson. Signaling in Control of Cell Growth and Metabolism. *Cold Spring Harbor Perspectives in Biology*, 4(7):a006783–a006783, 2012a. ISSN 1943-0264. doi: 10.1101/cshperspect.a006783.

P. S. Ward and C. B. Thompson. Metabolic Reprogramming: A Cancer Hallmark Even Warburg Did Not Anticipate. *Cancer Cell*, 21(3):297–308, 2012b. ISSN 15356108. doi: 10.1016/j.ccr.2012.02.014.

A. Wegner, J. Meiser, D. Weindl, and K. Hiller. How metabolites modulate metabolic flux. *Current Opinion in Biotechnology*, 34:16–22, 2015. ISSN 18790429. doi: 10.1016/j.copbio.2014.11.008.

K. E. Wellen, G. Hatzivassiliou, U. M. Sachdeva, T. V. Bui, J. R. Cross, and C. B. Thompson. ATP-Citrate Lyase Links Cellular Metabolism to Histone Acetylation. *Science*, 324(5930):1076–1080, 2009. ISSN 0036-8075. doi: 10.1126/science.1164097.

H. M. J. Werner, G. B. Mills, and P. T. Ram. Cancer Systems Biology: a peak into the future of patient care? *Nature reviews. Clinical oncology*, 11(3):167–176, 2014. ISSN 1759-4774. doi: 10.1038/nrclinonc.2014.6.

D. R. Wise, R. J. DeBerardinis, A. Mancuso, N. Sayed, X.-Y. Zhang, H. K. Pfeiffer, I. Nissim, E. Daikhin, M. Yudkoff, S. B. McMahon, and C. B. Thompson. Myc regulates a transcriptional program that stimulates mitochondrial glutaminolysis and leads to glutamine addiction. *Proceedings of the National Academy of Sciences of the United States of America*, 105(48):18782–7, 2008. ISSN 1091-6490. doi: 10.1073/pnas.0810199105.

Wittmann and Heinzle. Mass spectrometry for metabolic flux analysis. *Biotechnology and bioengineering*, 62(6):739–750, mar 1999. ISSN 1097-0290.

G. Wu. Physiological Functions of Amino Acids. In *Amino Acids: Biochemistry and Nutrition*, chapter 11, pages 339–391. CRC Press, 2013. ISBN 1439861900.

W. K. K. Wu, X. J. Wang, A. S. L. Cheng, M. X. M. Luo, S. S. M. Ng, K. F. To, F. K. L. Chan, C. H. Cho, J. J. Y. Sung, and J. Yu. Dysregulation and crosstalk of cellular signaling pathways in colon carcinogenesis. *Critical Reviews in Oncology/Hematology*, 86(3):251–277, 2013. ISSN 10408428. doi: 10.1016/j.critrevonc.2012.11.009.

X. Wu and G. Brewer. The regulation of mRNA stability in mammalian cells: 2.0. *Gene*, 500(1):10–21, 2012. ISSN 03781119. doi: 10.1016/j.gene.2012.03.021.

L. Wurth and F. Gebauer. RNA-binding proteins, multifaceted translational regulators in cancer. *Biochimica et Biophysica Acta - Gene Regulatory Mechanisms*, 1849(7):881–886, 2015. ISSN 18764320. doi: 10.1016/j.bbagrm.2014.10.001.

Y. Xiang, Z. E. Stine, J. Xia, Y. Lu, R. S. O'Connor, B. J. Altman, A. L. Hsieh, A. M. Gouw, A. G. Thomas, P. Gao, L. Sun, L. Song, B. Yan, B. S. Slusher, J. Zhuo, L. L. Ooi, C. G. L. Lee, A. Mancuso, A. S. McCallion, A. Le, M. C. Milone, S. Rayport, D. W. Felsher, and C. V. Dang. Targeted inhibition of tumor-specific glutaminase diminishes cell-autonomous tumorigenesis. *Journal of Clinical Investigation*, 125(6):2293–2306, 2015. ISSN 15588238. doi: 10.1172/JCI75836.

C. H. Yam, T. K. Fung, and R. Y. C. Poon. Cyclin A in cell cycle control and cancer. *Cellular and molecular life sciences: CMLS*, 59(8):1317–26, 2002. ISSN 1420-682X.

I. Yaman, J. Fernandez, B. Sarkar, R. J. Schneider, M. D. Snider, L. E. Nagy, and M. Hatzoglou. Nutritional control of mRNA stability is mediated by a conserved AU-rich element that binds the cytoplasmic shuttling protein HuR. *Journal of Biological Chemistry*, 277(44):41539–41546, 2002. ISSN 00219258. doi: 10.1074/jbc.M204850200.

L. Yang, S. Venneti, and D. Nagrath. Glutaminolysis: A Hallmark of Cancer Metabolism. *Annual Review of Biomedical Engineering*, 19(1):163–194, 2017. ISSN 1523-9829. doi: 10.1146/annurev-bioeng-071516-044546.

K. Yugi and S. Kuroda. Metabolism as a signal generator across trans-omic networks at distinct time scales. *Current Opinion in Systems Biology*, 8:59–66, 2018. ISSN 24523100. doi: 10.1016/j.coisb.2017.12.002.

M. Yuneva, N. Zamboni, P. Oefner, R. Sachidanandam, and Y. Lazebnik. Deficiency in glutamine but not glucose induces MYC-dependent apoptosis in human cells. *Journal of Cell Biology*, 178(1):93–105, 2007. ISSN 00219525. doi: 10.1083/jcb.200703099.

M. O. Yuneva, T. W. Fan, T. D. Allen, R. M. Higashi, D. V. Ferraris, T. Tsukamoto, J. M. Matés, F. J. Alonso, C. Wang, Y. Seo, X. Chen, and J. M. Bishop. The metabolic profile of tumors depends on both the responsible genetic lesion and tissue type. *Cell Metabolism*, 15(2):157–170, 2012. ISSN 15504131. doi: 10.1016/j.cmet.2011.12.015.

C. Zasada. *Experimental and mathematical analysis of the central carbon metabolism in cancer and stem cells*. PhD thesis, Humbolt-Universität zu Berlin, 2017.

C. Zasada and S. Kempa. Quantitative Analysis of Cancer Metabolism: From pSIRM to MFA. In *Metabolism in Cancer. Recent Results in Cancer Research*, pages 207–220. Springer International Publishing, 2016. ISBN 978-3-319-42118-6. doi: 10.1007/978-3-319-42118-6.

F. Zhang, L. Zhang, Y. Qi, and H. Xu. Mitochondrial cAMP signaling. *Cellular and Molecular Life Sciences*, 73(24):4577–4590, 2016. ISSN 14209071. doi: 10.1007/s00018-016-2282-2.

J. Zhang, N. N. Pavlova, and C. B. Thompson. Cancer cell metabolism: the essential role of the nonessential amino acid, glutamine. *The EMBO Journal*, 36(10):1302–1315, 2017a. ISSN 0261-4189. doi: 10.15252/embj.201696151.

X. Zhang, A. Mofers, P. Hydbring, M. Hägg Olofsson, J. Guo, S. Linder, and P. D'Arcy. MYC is downregulated by a mitochondrial checkpoint mechanism. *Oncotarget*, 8(52):90225–90237, 2017b. ISSN 1949-2553. doi: 10.18632/oncotarget.21653.

A. Supplementary: Material and Methods

Table A.1.: Cell culture reagents and supplements

Name	Supplier
2',5'-dideoxy adenosine	Calbiochem/Millipore, D - Darmstadt
4-Hydroxytamoxifen	Sigma-Aldrich, D - Darmstadt
6-Diazo-5-oxo-L-norleucine	Sigma-Aldrich, D - Darmstadt
Adenosine	Sigma-Aldrich, D - Darmstadt
Asparagine	Sigma-Aldrich, D - Darmstadt
Aspartate	Sigma-Aldrich, D - Darmstadt
AZD4226	Selleckchem, USA - Houston
BPTES	Sigma-Aldrich, D - Darmstadt
Blasticidine S hydrochloride	AppliChem GmbH, D - Darmstadt
CB839	Selleckchem, USA - Houston
Compound 968	Calbiochem/Millipore, D - Darmstadt
Cytidine	Sigma-Aldrich, D - Darmstadt
Dimethyl alphaketoglutarate	Sigma-Aldrich, D - Darmstadt
Dimethyl fumarate	Sigma-Aldrich, D - Darmstadt
Dimethyl malate	Sigma-Aldrich, D - Darmstadt
Dimethyl succinate	Sigma-Aldrich, D - Darmstadt
Dimethyl sulfoxide	Sigma-Aldrich, D - Darmstadt
DMEM, no glucose, glutamine, phenol red	Gibco, USA - Waltham
Doxycycline	Sigma-Aldrich, D - Darmstadt
Fetal bovine serum	Gibco, USA - Waltham
Forskolin	Sigma-Aldrich, D - Darmstadt
Glucose	Sigma-Aldrich, D - Darmstadt
Guanosine	Sigma-Aldrich, D - Darmstadt
L-Glutamine	Gibco, USA - Waltham
Lipofectamine 2000	Invitrogen, USA - Waltham
LY294002	Alexis Biochemicals, USA - San Diego
MDL-12,330A	Calbiochem/Millipore, D - Darmstadt
N-acetyl cysteine	Sigma-Aldrich, D - Darmstadt
Oligomycine	Sigma-Aldrich, D - Darmstadt
Opti-MEM, Reduced Serum Medium	Gibco, USA - Waltham
Phosphate-buffered saline	Gibco, USA - Waltham
PKAi, 14-22 Amide	Calbiochem/Millipore, D - Darmstadt
Puromycin dihydrochloride	Calbiochem/Millipore, D - Darmstadt
Rapamycin	Calbiochem/Millipore, D - Darmstadt
SB203580	Selleckchem, USA - Houston
Thenoyltrifluoroacetone	Sigma-Aldrich, D - Darmstadt

Table A.1.: Continued from previous page

Name	Supplier
Thymidine	Sigma-Aldrich, D - Darmstadt
Trypan Blue Solution (0.4%)	Gibco, USA - Waltham
TrypLE Express	Gibco, USA - Waltham
u-^{13}C-Glucose	Campro-Scientific, D - Berlin
u-^{13}C-Glutamine	Campro-Scientific, D - Berlin
Uridine	Sigma-Aldrich, D - Darmstadt

Table A.2.: Chemicals

Name	Supplier
Acetic acid	Fluka, D - Darmstadt
Acetonitrile	VWR, USA - Radnor
Acrylamide	Carl Roth, D - Karlsruhe
Ammonium bicarbonate	Fluka, D - Darmstadt
Ammonium persulfate	Sigma-Aldrich, D - Darmstadt
Bromphenol blue	AppliChem GmbH, D - Darmstadt
BSA	SERVA, D - Heidelberg
CaCl$_2$ (1 M), nuclease-free	Sigma-Aldrich, D - Darmstadt
Catalase	Sigma-Aldrich, D - Darmstadt
Chloroform	Sigma-Aldrich, D - Darmstadt
Chloroform-isoamyl alcohol (24:1)	Carl Roth, D - Karlsruhe
Cinnamic acid	Sigma-Aldrich, D - Darmstadt
DAPI	Sigma-Aldrich, D - Darmstadt
DNA loading dye (6x)	Thermo Fisher, USA - Waltham
DTT	Sigma-Aldrich, D - Darmstadt
EDTA	Carl Roth, D - Karlsruhe
EDTA (0.5 M), pH 8, nuclease-freee	Invitrogen, USA - Waltham
Ethanol (EtOH)	LiChrosolv, D - Darmstadt
Formaldehyde (16%)	Polysciences, USA - Warrington
Formamide	AppliChem GmbH, D - Darmstadt
Formic acid	Fluka, D - Darmstadt
Glucose	Sigma-Aldrich, D - Darmstadt
Glucose oxidase	Sigma-Aldrich, D - Darmstadt
Glycogen	Thermo Fisher, USA - Waltham
Glycerol	Carl Roth, D - Karlsruhe
Glycine	Carl Roth, D - Karlsruhe
H$_2$O, nuclease-free	Invitrogen, USA - Waltham
HEPES	Sigma-Aldrich, D - Darmstadt
Hexylamine	Sigma-Aldrich, D - Darmstadt
IAA	Sigma-Aldrich, D - Darmstadt
Isopropanol	Carl Roth, D - Karlsruhe
Laminin	Sigma-Aldrich, D - Darmstadt
Lysyl Endopeptidase	Wako, D - Neuss
MgCl$_2$	Sigma-Aldrich, D - Darmstadt
MeOH	Merck, D - Darmstadt

Table A.2.: Continued from previous page

Name	Supplier
MeOx	Sigma-Aldrich, D - Darmstadt
Skim milk powder	Sigma-Aldrich, D - Darmstadt
MSTFA	VWR, USA - Radnor
NaCl	Sigma-Aldrich, D - Darmstadt
NaCl (5 M), nuclease-free	Invitrogen, USA - Waltham
Na-deoxycholate	Sigma-Aldrich, D - Darmstadt
NaOAc	Thermo Fisher, USA - Waltham
NH_4Ac	Carl Roth, D - Karlsruhe
NH_4OH	Sigma-Aldrich, D - Darmstadt
NP-40	Sigma-Aldrich, D - Darmstadt
Page ruler prestained protein ladder	Bio-Rad, D - München
PBS (10x)	Biochrom, D - Darmstadt
PBS (10x), nuclease-free	Invitrogen, USA - Waltham
Phophatase inhibitor cocktail	Sigma-Aldrich, D - Darmstadt
PMSF	Sigma-Aldrich, D - Darmstadt
Poly-D-lysine	Sigma-Aldrich, D - Darmstadt
Protease Inhibitor Cocktail, EDTA-free	Roche, D - Darmstadt
Pyridine	Sigma-Aldrich, D - Darmstadt
Sodium acetate (3 M), pH 5.5, nuclease free	Invitrogen, USA - Waltham
SDS (20%)	Carl Roth, D - Karlsruhe
SSC (20x), nuclease free	AppliChem GmbH, D - Darmstadt
TEMED	Carl Roth, D - Karlsruhe
Triflouracetic acid	Merck, D - Darmstadt
Tris (1 M), pH 8.0, nuclease-free	Invitrogen, USA - Waltham
TrisBase	Carl Roth, D - Karlsruhe
TrisHCl	Carl Roth, D - Karlsruhe
Triton x-100	Carl Roth, D - Karlsruhe
TRIzol LS reagent	Thermo Fisher, USA - Waltham
Trypsin Beads	Aplied Biosystems, USA - Waltham
Tween-20	Carl Roth, D - Karlsruhe
Urea	Carl Roth, D - Karlsruhe

Table A.3.: Commercial kits

Name	Supplier
ECL Prime Western Blotting Detection Reagent	GE Healthcare, UK - Little Chalfont
Bio-Plex Cell Lysis Kit	Biorad, D - München
Bio-Plex Pro Cell Signalling Reagent Kit	Biorad, D - München
Chemiluminescent Nucleic Acid Detection Module Kit	Thermo Fisher, USA - Waltham
High capacity cDNA Reverse Transcription Kit	Thermo Fisher, USA - Waltham
MEGAscript T3 stranscription Kit	Thermo Fisher, USA - Waltham
MycoAlert Mycoplasma Detection Kit	Lonza, CH - Basel
Pierce BCA Protein Assay Kit	Thermo Fisher, USA - Waltham
Pierce Magnetic RNA-Protein Pull-Down Kit	Thermo Fisher, USA - Waltham
Pierce RNA 3'END Desthiobiotinylation Kit	Thermo Fisher, USA - Waltham

Table A.3.: Continued from previous page

Name	Supplier
Platinum SuperFi PCR Master Mix	Thermo Fisher, USA - Waltham
QIAshredder	Qiagen, D - Hilden
Rneasy Mini Kit	Qiagen, D - Hilden
TaqMan Gene Expression Master Mix	Thermo Fisher, USA - Waltham

Table A.4.: Antibodies

Target	Manufacturer	Cat.-No	Application
4EBP1	Cell Signaling	#9452	IB
β-Actin	Cell Signaling	#2146	IB
β-Tubulin	Sigma	#T3828	IB
CREB	Cell Signaling	#9104	IB
ERK1/2	Cell Signaling	#9102	IB
HSP27	Cell Signaling	#2402	IB
Mouse, horseradish peroxidase-linked	Dako	#P0447	IB
MYC	Millipore	#2506410	IB
p38 MAPK	Cell Signaling	#8690	IB
phospho-4EBP1 (Thr37/46)	Cell Signaling	#9455	IB
phospho-AKT (Ser473)	Biorad	#171-V50001M	Bio-Plex
phospho-cJun (Ser63)	Biorad	#171-V50003M	Bio-Plex
phospho-CREB (Ser133)	Cell Signaling	#9198	IB
phospho-CREB (Ser133)	Biorad	#171-V50028M	Bio-Plex
phospho-ERK1/2 (Thr202/Tyr204)	Cell Signaling	#9106	IB
phospho-ERK1/2 (Thr202/Tyr204, Thr185/Tyr187)	Biorad	#171-V50006M	Bio-Plex
phospho-GSK3α/β (Ser21/Ser9)	Biorad	#171-V50007M	Bio-Plex
phospho-HSP27 (Ser82)	Cell Signaling	#9709	IB
phospho-JNK (Thr183/Tyr185)	Biorad	#171-V50011M	Bio-Plex
phospho-MEK (Ser217/221)	Biorad	#171-V50012M	Bio-Plex
phospho-NFκB p65 (Ser536)	Biorad	#171-V50013M	Bio-Plex
phospho-p38 MAPK (Thr180/Tyr182)	Cell Signaling	#4631	IB
phospho-p70 S6 kinase (Thr421/Tyr424)	Biorad	#171-V50015M	Bio-Plex
phospho-p90 RSK (Ser380)	Biorad	#171-V50035M	Bio-Plex
phospho-S6 ribosomal protein (Ser235/236)	Biorad	#171-V50038M	Bio-Plex
phospho-STAT3 (Ser727)	Biorad	#171-V50021M	Bio-Plex
phospho-TOR (Ser2448)	Biorad	#171-V50033M	Bio-Plex
Rabbit, horseradish peroxidase-linked	Cell Signaling	#7074	IB
Vinculin	Sigma	#V9131	IB

Table A.5.: Primers

Name	Sequence (5'-3')	Manufacturer
T3 MYC 3'-UTR forward	AATTAACCCTCACTAAAGGGGGAAAAGTAAGGAAAACGATTC	TIB-MolBio
MYC 3'-UTR reverse	TTAAGATTTGGCTCAATGATATATTTGC	TIB-MolBio

Table A.6.: Small interfering RNAs

Target	Sequence (5'-3')	Manufacturer	Cat.-No	ID
HuR	GCGUUUAUCCGGUUUGACAtt	Ambion/Life Science	#4390824	s4610
Rictor	GCCCAGCAGUAAAUUAUAUtt	Ambion/Life Science	#AM16708	261571
Raptor	CCAUCGGUGCAAAUUUACAtt	Ambion/Life Science	#4392420	s33216
Non-targeting		Ambion/Life Science	#AM4611	

Table A.7.: Labeled oligonucleotides

Target	Manufacturer	Cat.-No	Label	Application
CCNA2	Stellaris	#VSMF-2447-5	Quasar570	smFish probe
MYC	Stellaris	#VSMF-2231-5	Quasar670	smFish probe
MYC	Thermo Fisher	#4331182-H00153408_m1	FAM	TaqMan probe
PKG1	Thermo Fisher	#4331182-H00943178_g1	VIC	TaqMan probe

Table A.8.: Consumables

Name	Supplier
Cell lifter	Sigma-Aldrich, D - Darmstadt
Counting slides	Biorad, D - München
Gas liner, CI34	Gerstel, D - Mühlheim an der Ruhr
Glas vials	Th.Geyer, D - Berlin
Nytran N Blotting Membrane	GE Healthcare, UK - Little Chalfont
PVDF membrane	GE Healthcare, UK - Little Chalfont
TAE Mini ReadyAgarose Precast Gel (3%)	Biorad, D - München
Whatman Blotting paper	Biorad, D - München

Table A.9.: Equipment

Name	Manufacturer
Autosampler - MPS2XL-Twister	Gerstel, D - Mühlheim an der Ruhr
Autosampler, ESI ion source - TriVersa NanoMate	Advion, D - Ithaca
Balance - CP2202S	Satorius, D - Göttigen
Bio-Plex array reader 200	Bio-Rad, D - München
Blotting device - TransBlot Turbo	Biorad, D - München
Cell counter - TC20	Biorad, D - München
Centrifuge - 5417R	Eppendorf, D - Hamburg
Centrifuge - 5430	Eppendorf, D - Hamburg
Electrophoresis system - ReadySub-Cell	Biorad, D - München
Electrophoresis system - Protean Tetra cell	Biorad, D - München
Gas chromatograph - Agilent 78903	LECO, USA - St. Joseph
Imager - ImageQuant LAS4000	GE Healthcare, UK - Little Chalfont
Magnet - DynaMag2	Thermo Fisher, USA - Waltham

Continued on next page

Table A.9.: Continued from previous page

Name	Manufacturer
Mass Spectrometer - Q Exactive Plus	Thermo Fisher, USA - Waltham
Mass Spectrometer - TSQ Quantiva	Thermo Fisher, USA - Waltham
Mass Spectrometer-TOF - Pegasus IV	LECO, USA - St. Joseph
Microplate reader, Infinite M200	Tecan, CH - Männedorf
Microscope, Inverted Elipse Ti-E	Nikon, D- Düsseldorf
Nano Liquid Chromatograph 400	Eksigent, D - Darmstadt
Nanophotometer - Classic	Implen, D - München
pH meter - VMS C7	VWR, USA - Radnor
Power supply - PowerPac Universal	Biorad, D - München
Real-Time PCR System - StepOne	Applied Biosystems, USA - Waltham
Vacuum concentrator - 2-33 CD plus	Christ, D - Osterode
Sonicator - Sonorex Digitech DT 100	Bandelin, D - Berlin
Thermomixer - comfort	Eppendorf, D - Hamburg
Tube roller - SRT6D	Stuart, UK - Staffordshire
UV crosslinker- XLE-1000	Spectroline, USA - New York City

Table A.10.: Software

Name	Comment
ChromaToF (version 4.51.6.0)	Processing/annotation of GC-MS data (LECO, USA - St. Joseph)
Fuji	smFISH analysis [Schindelin et al., 2012]
Illustrator (version 5.6)	Figure preparation (Adobe, USA - San Jose)
ImageJ	Western blot quantification tool [Schneider et al., 2012]
MAUI-SILVIA (version 1.0.5)	Annotation of GC-MS data [Kuich et al., 2015]
MaxQuant (version 1.5.3.30)	Protein quantification [Cox et al., 2011]
MetMax	ChromaToF data extraction (manual annotation)
MTXQC (version 1.9)	Quality control for GC-MS data [Zasada, 2017]
Open MS	Pipeline for analysis and processing of mass spectrometry data
Perseus (version 1.5.6.0)	LC-MS analysis tool [Tyanova et al., 2016]
RStudio Desktop	Figure preparation/Data processing
StepOnePlus (version 2.3)	Analysis of qPCR data (Applied Biosystems, USA - Waltham)

Table A.11.: SDS-PAGE gel preparation

Component	4%	8%	10%	12%
H_2O	6.1 mL	4.6 mL	4.0 mL	3.3 mL
Acrylamide 30%	1.33 mL	2.7 mL	3.3 mL	4.0 mL
0.5 M Tris (pH 6.8)	2.5 mL	-	-	-
1.5 M Tris (pH 8.8)	-	2.5 mL	2.5 mL	2.5 mL
SDS 10%	100 µL	50 µL	50 µL	50 µL
Ammonium persulfate 10%	50 µL	50 µL	50 µL	50 µL
TEMED	10 µL	6 µL	4 µL	4 µL

Table A.12.: GC-MS masses used for absolute quantification. Peak areas under the indicated masses, specific for the indicated metabolite, were summed up for absolute quantification.

Metabolite	Derivate	Quantification masses [m/z]
Citrate	3TMS	149+273+183+133+211+275+277+278
Dihydroxyacetone phosphate	1MEOX, 3TMS	103+299+142+89+133+400+403
Fumarate	2TMS	143+246+133+115+245+247+249
Glucose	1MEOX, 5TMS	160+117+129+205+103+217+220+162+132+207
Glutamate	3TMS	246+247+100+156+128+250
α-Ketoglutarate	1MEOX, 2TMS	156+112+170+89+198+200+203
Lactate	2TMS	118+190+191+117+133+119+193+219+222
Ornithine	3TMS	86+142+186+100+174
Malate	3TMS	101+133+117+149+233+245+247+249
Putrescine	4TMS	86+130+175+100+174
Pyruvate	1MEOX, 1TMS	100+99+89+174+115+177
Succinate	2TMS	149+247+129+133+172+249+251

Table A.13.: GC-MS fragments used for determination of stable isotope incorporation

Metabolite	Derivate	Mass fragments [m/z]		Mass shift
		Unlabeled [m+0]	u-^{13}C-glutamine	
Citrate	3TMS	273	277(oxidative)	[m+4]
			278 (reductive)	[m+5]
Fumarate	2TMS	245	249	[m+4]
Glutamate	3TMS	246	250	[m+5]
α-Ketoglutarate	1MEOX, 2TMS	198	203	[m+5]
Malate	3TMS	245	249	[m+4]
Succinate	2TMS	247	251	[m+4]

Table A.14.: Direct-infusion MS transition parameters

Compound	Precursor [m/z]	Product [m/z]	Collision Energy [V]	RF Lens [V]
ADP	426.02	134.06	24	92
ADP	426.02	158.92	27	92
AMP	346.06	107.08	47	80
AMP	346.06	134.06	31	80
ATP	505.99	158.96	29	92
ATP	505.99	408.04	20	92
cAMP	328.02	107.08	44	78
cAMP	328.02	134.07	25	78
CDP	402.01	159.03	25	94
CDP	402.01	272.94	23	94
CMP	322.04	79.03	26	72
CMP	322.04	97.01	22	72

Continued on next page

Table A.14.: Continued from previous page

Compound	Precursor [m/z]	Product [m/z]	Collision Energy [V]	RF Lens [V]
CTP	481.98	159.05	29	85
CTP	481.98	383.93	20	85
dADP	410.09	158.94	25	94
dADP	410.09	256.96	24	94
dAMP	330.09	134.12	27	68
dAMP	330.09	194.94	27	68
dATP	490.05	158.94	26	136
dATP	490.05	256.96	29	136
dCDP	86.05	158.96	23	78
dCDP	86.05	177.01	22	78
dCMP	306.08	97.00	23	80
dCMP	306.08	110.11	23	80
dCTP	66.01	158.94	26	111
dCTP	466.01	256.80	28	111
dGDP	426.05	158.96	24	99
dGDP	426.05	176.94	24	99
dGMP	346.09	79.00	22	73
dGMP	346.09	150.07	25	73
dGTP	506.11	159.03	28	120
dGTP	506.11	238.97	26	120
dTDP	401.05	158.94	24	82
dTDP	401.05	256.96	23	82
dTMP	321.11	125.05	22	69
dTMP	321.11	194.95	16	69
dTTP	480.98	158.94	30	90
dTTP	480.98	256.84	15	90
GDP	442.00	158.93	26	105
GDP	442.00	343.96	16	105
GMP	362.05	133.05	40	83
GMP	362.05	150.06	29	83
GTP	522.03	240.96	29	163
GTP	522.03	320.90	26	163
UDP	402.99	158.91	22	95
UDP	402.99	272.89	22	95
UMP	323.03	79.04	28	70
UMP	323.03	97.02	23	70
UTP	482.98	158.93	28	118
UTP	482.98	403.01	24	118

B. Supplementary: Results
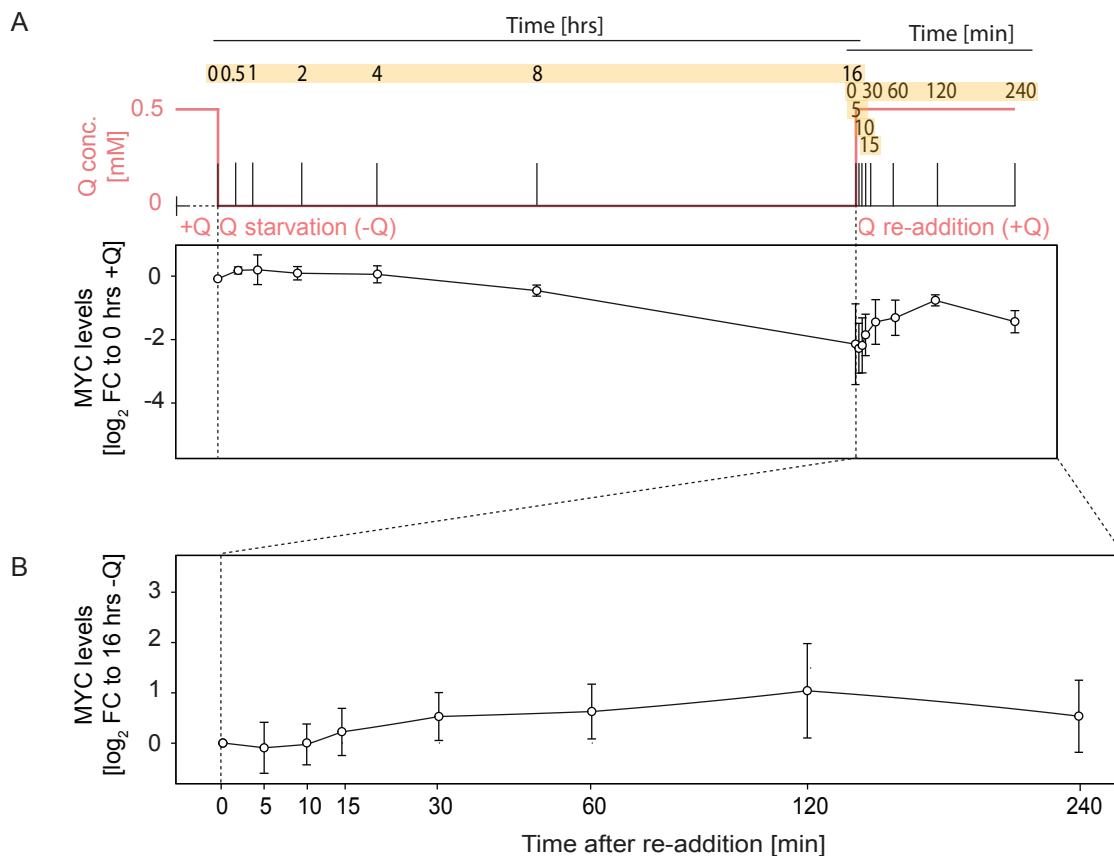
Figure B.1.: Time-resolved analysis of glutamine starvation and re-addition (0.5 mM Gln). (A) Experimental setup of (B) time course of quantified MYC protein levels in cells starved for 16 hrs, followed by re-addition of glutamine at the indicated time points (yellowed-out). Cells have been cultured in media with physiological glutamine concentration as well as the according amount of the amino acid was re-added upon starvation. Each value was normalized to +Q at time point 0 hrs (n=3). Protein expression was normalized to Vinculin levels. Results represent mean $\pm$ SD of indicated number of independently performed experiments.
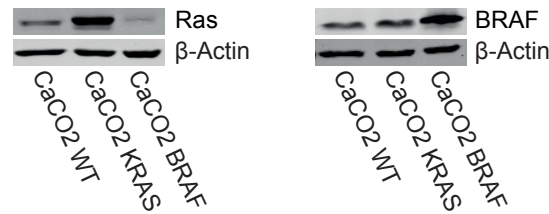
Figure B.2.: BRAF and KRAS overexpression in CaCO2 cells. CaCO2-GFP (CaCO2 WT), CaCO2-BRAF^{V600E} (CaCO2 BRAF) and CaCO2-KRAS^{G12V} (CaCO2 KRAS) cells were induced with doxycycline for two weeks and analyzed with antibodies against BRAF and RAS. β-Actin served as the loading control. Western blot was prepared by Raphaela Fritsche (Jennifer Kirwan Lab, Berlin Institute of Health, Berlin-Germany).
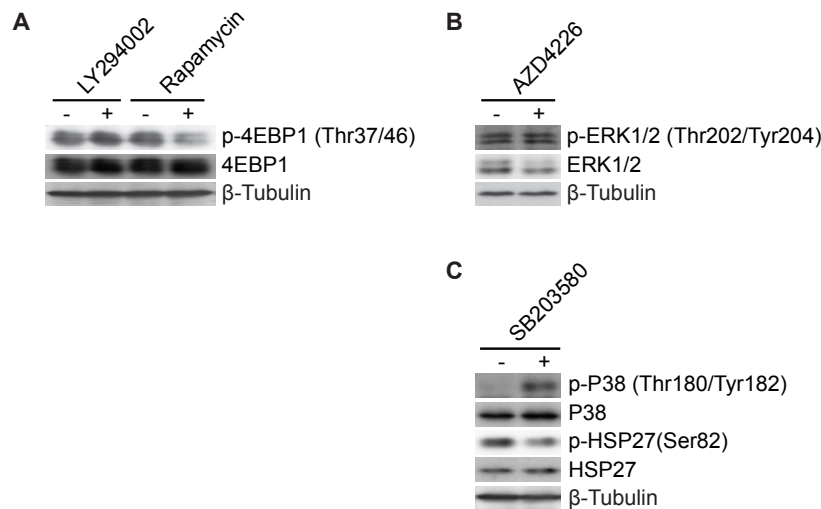
Figure B.3.: Verification of signaling inhibitors. HCT116 cells were treated for 16 hrs with inhibitors blocking (A) PI3K (LY294002), mTOR (Rapamycin), (B) ERK (AZD4226) and (C) p38 (SB203580) signaling at 2 mM glutamine. Immunoblots document indicated downstream targets of inhibited kinases (*n*=2). β-Tubulin served as the loading control.

Note: Inhibitors have been applied with starvation media for 16 hrs to examine the role of indicated kinases in glutamine-dependent MYC expression (*figure* 4.11). Global signaling shutdown was observed upon glutamine starvation, therefore the validation of inhibitor efficacy was performed at 2 mM glutamine in order to detect downregulation of downstream targets of inhibited molecules.
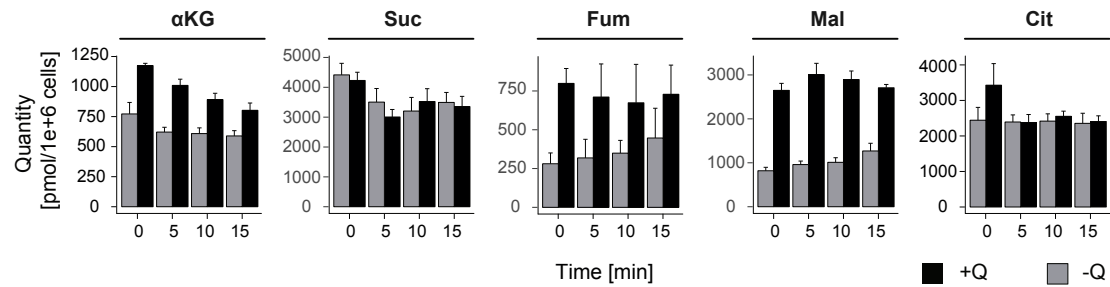
Figure B.4.: Dependence of absolute quantification of glutaminolysis intermediates on glutamine availability. HCT116 cells have been cultured in the presence (+Q) and absence (-Q) of glutamine for 16 hrs before cells have been incubated for 5, 10 and 15 min with media containing u-^{13}C-glutamine instead of ^{12}C-glutamine. Results represent mean + SD (n=3, each measurement performed in technical duplicates).
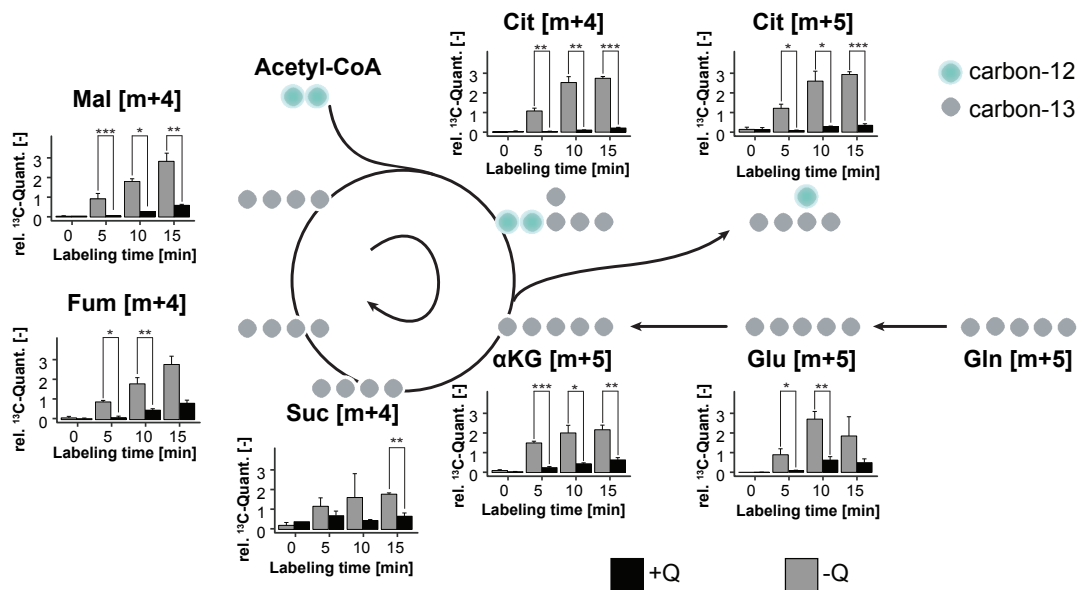
Figure B.5.: Glutamine-derived ^{13}C-quantities in response to glutamine availability during pre-treatment. HCT116 cells have been cultured in the presence (+Q) and absence (-Q) of glutamine for 16 hrs before cells have been incubated for 5, 10 and 15 min with media containing u-^{13}C-glutamine instead of ^{12}C-glutamine. Results represent mean + SD (n=3 each, each measurement performed in technical duplicates). P-values were calculated using a two-tailed Student's t-test (* $0.01 < p \leq 0.05$; ** $0.001 < p \leq 0.01$; *** $p \leq 0.001$). Grey circles represent ^{13}C-labeled molecules derived from glutamine, green circles illustrate non-labeled molecules. Numbers of incorporated carbons are shown in brackets.
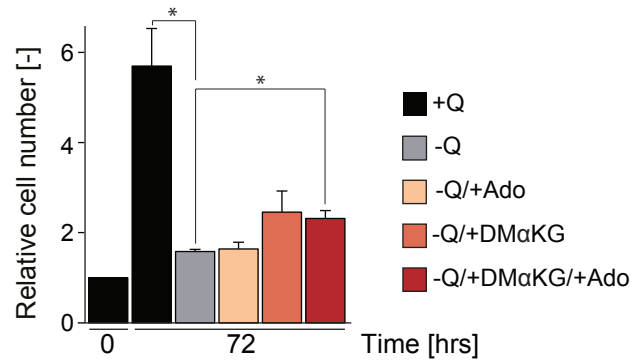
Figure B.6.: Proliferation effects in response to DMαKG and adenosine supplementation. Numbers of HCT116 cells starved for 24 hrs before indicated substrates were re-added for another 48 hrs. Cell numbers were determined at 0 and 72 hrs and are shown relative to 0 hrs. Results represent mean + SD ($n=3$, each measurement performed in technical duplicates). P-values were calculated using a two-tailed student's t-test (* $0.01 < p \leq 0.05$; ** $0.001 < p \leq 0.01$; *** $p \leq 0.001$). Abbreviations – Ado: Adenosine, DMαKG: Dimethyl α-ketoglutarate, Q: Glutamine.
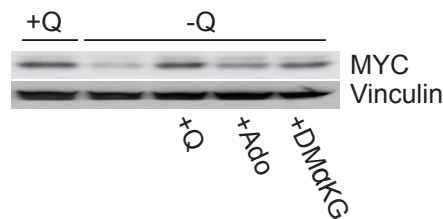
Figure B.7.: MYC protein levels in response to substrate re-addition. HCT116 cells have been deprived for glutamine for 16 hrs before indicated substrate have been re-added for 2 hrs. MYC protein levels have been examined and normalized to Vinculin levels. Abbreviations – Ado: Adenosine, DMαKG: Dimethyl α-ketoglutarate, Q: Glutamine.
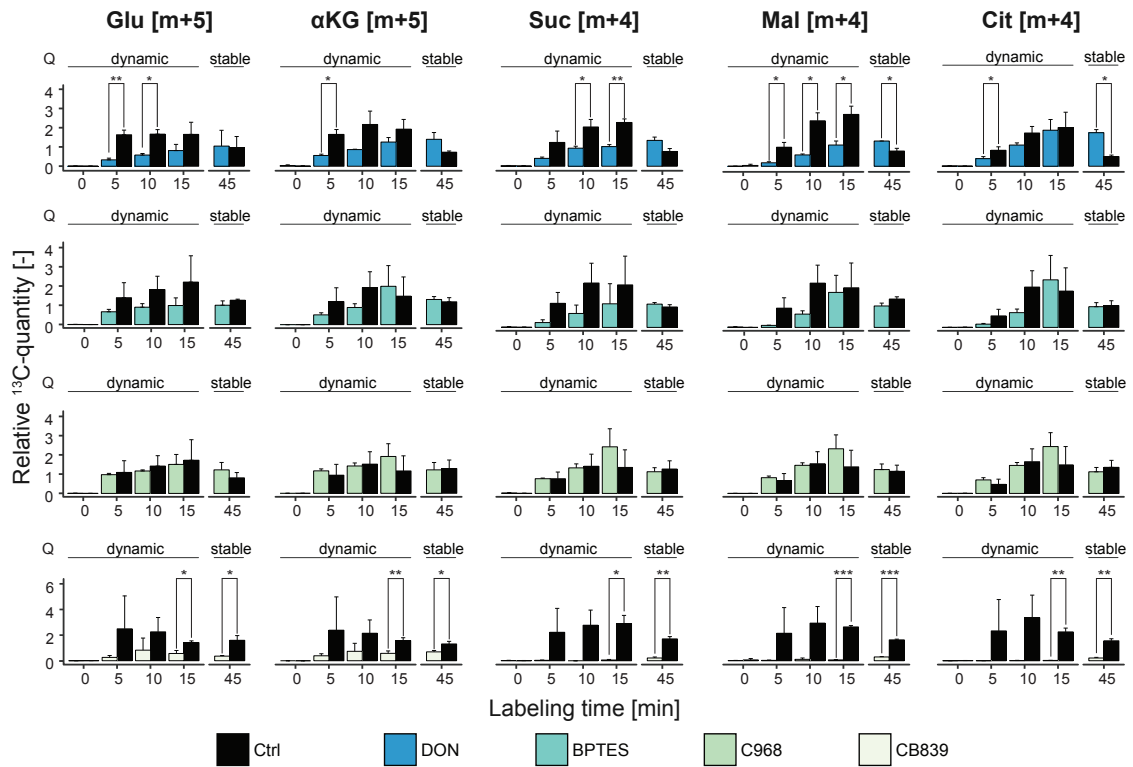
Figure B.8.: Validation of glutaminase inhibitors (^{13}C-quantities) ^{13}C-quantities of glutamine-starved and non-starved HCT116 cells are shown. Cells have been treated with 10 μM of indicated GLS inhibitors for 16 hrs. The re-addition of u-^{13}C-glutamine to starved cells in a short time frame (5, 10, 15 min) enabled the dynamic tracing of carbon-13 in glutamine downstream metabolites. The effect of the inhibitors in a steady glutamine state was achieved by replacing ^{12}C-glutamine with u-^{13}C-glutamine for 45 min. All results are shown in comparison to the solvent control. Numbers of incorporated carbons are shown in brackets. Results represent mean + SD (n=3, each measurement performed in technical duplicates). P-values were calculated using a two-tailed student's t-test (* $0.01 < p \leq 0.05$; ** $0.001 < p \leq 0.01$; *** $p \leq 0.001$).

Figure B.9.: Validation of forskolin. HCT116 cells were cultivated for 16 hrs in the presence of 2 mM glutamine before forskolin was added for 45 min. Immunoblot documents the PKA downstream target p-CREB. Vinculin served as the loading control.

Table B.1.: 3'-UTR interacting proteins detected in the presence of glutamine

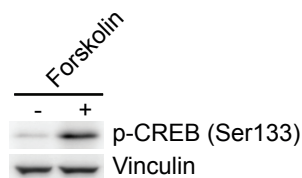| Gene names	Uniprot ID	Protein names
ACTG1	P63261	Actin, cytoplasmic 2
ANAPC7	Q9UJX3	Anaphase-promoting complex subunit 7
BAIAP2	Q9UQB8	Brain-specific angiogenesis inhibitor 1-associated protein 2
BZW1	Q7L1Q6	Basic leucine zipper and W2 domain-containing protein 1
CAPZA1	P52907, P47755	F-actin-capping protein subunit α-1 & -2
CBX3	Q13185, P83916	Chromobox protein homolog 1 & 3
CDC16	Q13042	Cell division cycle protein 16 homolog
CDC23	Q9UJX2	Cell division cycle protein 23 homolog
CDK9	P50750	Cyclin-dependent kinase 9
CNGB3	Q9NQW8	Cyclic nucleotide-gated cation channel β-3
COX5A	P20674	Cytochrome c oxidase subunit 5A
DDB1	Q16531	DNA damage-binding protein 1
DDX18	Q9NVP1	ATP-dependent RNA helicase DDX18
DDX41	Q9UJV9	Probable ATP-dependent RNA helicase DDX41
DDX49	Q9Y6V7	Probable ATP-dependent RNA helicase DDX49
DDX55	Q8NHQ9	ATP-dependent RNA helicase DDX55
DHX8	Q14562	ATP-dependent RNA helicase DHX8
DYNLL1	P63167	Dynein light chain 1
DYNLL2	Q96FJ2	Dynein light chain 2
FAM60A	Q9NP50	Protein FAM60A
GATAD2A	Q86YP4, Q8WXI9	Transcriptional repressor p66-α & -β
GEMIN8	Q9NWZ8	Gem-associated protein 8
GIGYF2	Q6Y7W6	GRB10-interacting GYF protein 2
GNL2	Q13823	Nucleolar GTP-binding protein 2
GNL3L	Q9NVN8	Guanine nucleotide-binding protein-like 3-like protein
HELLS	Q9NRZ9	Lymphoid-specific helicase
HLTF	Q14527	Helicase-like transcription factor
HNRNPU	Q00839	Heterogeneous nuclear ribonucleoprotein U
ILF3	Q12906	Interleukin enhancer-binding factor 3
KTN1	Q86UP2	Kinectin
LENG8	Q96PV6	Leukocyte receptor cluster member 8
MAZ	P56270, Q9HBE1	Myc-associated zinc finger protein
MKRN2	Q9H000	Probable E3 ubiquitin-protein ligase makorin-2
MPP7	Q5T2T1	MAGUK p55 subfamily member 7
MRPL49	Q13405	39S ribosomal protein L49
MRPL53	Q96EL3	39S ribosomal protein L53
MRPS2	Q9Y399	28S ribosomal protein S2
MRPS27	Q92552	28S ribosomal protein S27
MTA2	O94776	Metastasis-associated protein MTA2
NAF1	Q96HR8	H/ACA ribonucleoprotein complex non-core subunit NAF1
NDUFS1	P28331	NADH-ubiquinone oxidoreductase 75 kDa subunit
NELFA	Q9H3P2	Negative elongation factor A
NOA1	Q8NC60	Nitric oxide-associated protein 1
NOL11	Q9H8H0	Nucleolar protein 11
NPM3	O75607	Nucleoplasmin-3

Continued on next page

Table B.1.: Continued from previous page

Gene names	Uniprot ID	Protein names
PFKP	Q01813	ATP-dependent 6-phosphofructokinase
POLR1B	Q9H9Y6	DNA-directed RNA polymerase I subunit RPA2
POLR2H	P52434	DNA-directed RNA polymerases I, II, III subunit RPABC3
PRRC2B	Q5JSZ5	Protein PRRC2B
PRSS3P2	Q8NHM4	Putative trypsin-6
PUS1	Q9Y606	tRNA pseudouridine synthase A
PYCRL	Q53H96	Pyrroline-5-carboxylate reductase 3
RBM5	P52756	RNA-binding protein 5
RNASEH2C	Q8TDP1	Ribonuclease H2 subunit C
RPLP1	P05386	60S acidic ribosomal protein P1
RPP25L	Q8N5L8	Ribonuclease P protein subunit p25-like protein
SCAF4	O95104, Q9UPN6	Splicing factor, arginine/serine-rich 15; Protein SCAF8
SFN	P31947	14-3-3 protein σ
SKP1	P63208	S-phase kinase-associated protein 1
SMC4	Q9NTJ3	Structural maintenance of chromosomes protein 4
SPATS2	Q86XZ4	Spermatogenesis-associated serine-rich protein 2
TCF25	Q9BQ70	Transcription factor 25
TFB2M	Q9H5Q4	Dimethyladenosine transferase 2
TXLNG	Q9NUQ3	Gamma-taxilin
UHRF1	Q96T88	E3 ubiquitin-protein ligase UHRF1
UTP15	Q8TED0	U3 small nucleolar RNA-associated protein 15 homolog
VAPA	Q9P0L0	Vesicle-associated membrane protein-associated protein A
WDR6	Q9NNW5	WD repeat-containing protein 6
ZC3H11A	O75152	Zinc finger CCCH domain-containing protein 11A

Table B.2.: 3'-UTR interacting proteins detected in the absence of glutamine

Gene names	Uniprot ID	Protein names
ACOT9	Q9Y305	Acyl-coenzyme A thioesterase 9
ADARB1	P78563	Double-stranded RNA-specific editase 1
ANKHD1	Q8IWZ3	Ankyrin repeat and KH domain-containing protein 1
AREG	P15514	Amphiregulin
ATP5D	P30049	ATP synthase subunit δ
ATP5H	O75947	ATP synthase subunit d
ATP5O	P48047	ATP synthase subunit O
C12orf29	Q8N999	Uncharacterized protein C12orf29
CALML5	Q9NZT1	Calmodulin-like protein 5
CELA3A	P09093, P08861	Chymotrypsin-like elastase family member 3A & 3B
CLPB	Q9H078	Caseinolytic peptidase B protein homolog
CNTNAP3	Q9BZ76, Q96NU0	Contactin-associated protein-like 3
DBR1	Q9UK59	Lariat debranching enzyme
DCD	P81605	Dermcidin
DNAJB1	P25685	DnaJ homolog subfamily B member 1
EIF4B	P23588	Eukaryotic translation initiation factor 4B
EIF4E	P06730	Eukaryotic translation initiation factor 4E

Table B.2.: Continued from previous page

Gene names	Uniprot ID	Protein names
ENO1	P06733	Enolase 1
FABP5	Q01469	Fatty acid-binding protein, epidermal
FARSA	Q9Y285	Phenylalanine–tRNA ligase α subunit
FASN	P49327	Fatty acid synthase
FAU	P62861	40S ribosomal protein S30
H1F0	P07305	Histone H1.0
HARS	P12081, P49590	Histidine–tRNA ligase
HBS1L	Q9Y450	HBS1-like protein
HDAC2	Q92769, Q13547	Histone deacetylase 1 & 2
HIST2H3A	Q71DI3, Q16695, P84243, P68431, Q6NXT2	Histone H3.1 & H3.2 & H3.3
HMGB1	P09429, B2RPK0	High mobility group protein B1
HSP90AA1	P07900	Heat shock protein HSP 90-α
HSP90B1	P14625	Endoplasmin
HSPA14	Q0VDF9	Heat shock 70 kDa protein 14
HSPA4	P34932	Heat shock 70 kDa protein 4
HSPE1	P61604	10 kDa heat shock protein, mitochondrial
IREB2	P48200	Iron-responsive element-binding protein 2
JUND	P17535	Transcription factor jun-D
KIF2A	O00139	Kinesin-like protein KIF2A
LARP1	Q6PKG0	La-related protein 1
LDHA	P00338	L-lactate dehydrogenase A chain
LDHB	P07195	L-lactate dehydrogenase B chain
LSM12	Q3MHD2	Protein LSM12 homolog
LUC7L2	Q9Y383, Q9NQ29	Putative RNA-binding protein Luc7-like 1 & 2
MCM3	P25205	DNA replication licensing factor MCM3
MCM5	P33992	DNA replication licensing factor MCM5
MCM8	Q9UJA3	DNA helicase MCM8
MDH2	P40926	Malate dehydrogenase
MRM1	Q6IN84	rRNA methyltransferase 1
MRPL11	Q9Y3B7	39S ribosomal protein L11
MRPS18B	Q9Y676	28S ribosomal protein S18b
MRPS9	P82933	28S ribosomal protein S9
NFIB	O00712, P08651, Q14938, Q14938, Q12857	Nuclear factor 1 B-type
NME1	P15531	Nucleoside diphosphate kinase A
NOLC1	Q14978	Nucleolar and coiled-body phosphoprotein 1
PATL1	Q86TB9	Protein PAT1 homolog 1
PCNA	P12004	Proliferating cell nuclear antigen
PFN1	P07737	Profilin-1
PGD	P52209	6-phosphogluconate dehydrogenase
PNN	Q9H307	Pinin
POLR2A	P24928	DNA-directed RNA polymerase II subunit RPB1

Table B.2.: Continued from previous page

Gene names	Uniprot ID	Protein names
PPP1CB	P62140	Serine/threonine-protein phosphatase PP1-beta catalytic subunit
PSMA3	P25788	Proteasome subunit α type-3
PSMD14	O00487	26S proteasome non-ATPase regulatory subunit 14
RNPC3	Q96LT9	RNA-binding protein 40
RPL15	P61313	60S ribosomal protein L15
RPL18	Q07020	60S ribosomal protein L18
RPL19	P84098	60S ribosomal protein L19
RPL27A	P46776	60S ribosomal protein L27a
RPL28	P46779	60S ribosomal protein L28
RPL34	P49207	60S ribosomal protein L34
RPL35	P42766	60S ribosomal protein L35
RPS28	P62857	40S ribosomal protein S28
S100A6	P06703	Protein S100-A6
SAP18	O00422	Histone deacetylase complex subunit SAP18
SARNP	P82979	SAP domain-containing ribonucleoprotein
SARS	P49591	Serine–tRNA ligase
SET	Q01105	Protein SET
SHOC2	Q9UQ13	Leucine-rich repeat protein SHOC-2
SLC25A4	P12235	ADP/ATP translocase 1
SLC3A2	P08195	4F2 cell-surface antigen heavy chain
SNRPB2	P08579	U2 small nuclear ribonucleoprotein B
SNRPC	P09234	U1 small nuclear ribonucleoprotein C
SRRT	Q9BXP5	Serrate RNA effector molecule homolog
SUB1	P53999	Activated RNA polymerase II transcriptional coactivator p15
SUGP2	Q8IX01	SURP and G-patch domain-containing protein 2
THOC2	Q8NI27	THO complex subunit 2
TKT	P29401	Transketolase
TPI1	P60174	Triosephosphate isomerase
TUBA1C	Q9BQE3	Tubulin alpha-1C chain
UNK	Q9C0B0	RING finger protein unkempt homolog
VDAC1	P21796	Voltage-dependent anion-selective channel protein 1
WDR19	Q8NEZ3	WD repeat-containing protein 19
WDR36	Q8NI36	WD repeat-containing protein 36
WDR5	P61964	WD repeat-containing protein 5
YTHDF1	Q9BYJ9	YTH domain-containing family protein 1
YWHAE	P62258	14-3-3 protein ε
ZNF787	Q6DD87	Zinc finger protein 787
ZRSR1	Q15695	U2 small nuclear ribonucleoprotein auxiliary factor 35 kDa subunit-related protein 1 & 2

Table B.3.: Target list for siRNA screen

Gene names	Gene ID	Protein names
HSPE1	3336	10 kDa heat shock protein, mitochondrial
MRPS2	51116	28S ribosomal protein S2, mitochondrial
MRPS27	23107	28S ribosomal protein S27, mitochondrial
MRPS28	28957	28S ribosomal protein S28, mitochondrial
MRPL53	116540	39S ribosomal protein L53, mitochondrial
RPS28	6234	40S ribosomal protein S28
HSPD1	3329	60 kDa heat shock protein, mitochondrial
RPL15	6138	60S ribosomal protein L15
RPL19	6143	60S ribosomal protein L19
RPL30	6156	60S ribosomal protein L30
SLC25A4	291	ADP/ATP translocase 1
SLC25A5	292	ADP/ATP translocase 2
GTP2	84706	Alanine aminotransferase 2
ENO1	2023	Enolase 1
AREG	374	Amphiregulin
ANXA2P1	303	Annexin A2, Putative annexin A2-like protein
ASNS	440	Asparagine synthetase
GOT1	2805	Aspartate aminotransferase, cytoplasmic
GOT2	2806	Aspartate aminotransferase, mitochondrial
ATP5A1	498	ATP synthase subunit α, mitochondrial
ATP5B	506	ATP synthase subunit β, mitochondrial
ATP5H	10476	ATP synthase subunit d, mitochondrial
ATP5D	513	ATP synthase subunit δ, mitochondrial
ATP5O	539	ATP synthase subunit O, mitochondrial
MTHFD1	4522	C-1-tetrahydrofolate synthase
CALML5	51806	Calmodulin-like protein 5
PRKACA	5566	cAMP-dependent protein kinase catalytic subunit α
PRKACB	5567	cAMP-dependent protein kinase catalytic subunit β
SKD3	81570	Caseinolytic peptidase B protein homolog
CDKN2AIP	55602	CDKN2A-interacting protein
CDC16	8881	Cell division cycle protein 16 homolog
CS	1431	Citrate synthase, mitochondrial
CFL1	1072	Cofilin-1
COIL	8161	Coilin
ATF4	468	Cyclic AMP-dependent transcription factor ATF-4
COX5A	9377	Cytochrome c oxidase subunit 5A, mitochondrial
COX5B	1329	Cytochrome c oxidase subunit 5B, mitochondrial
TFB2M	64216	Dimethyladenosine transferase 2, mitochondrial
POLR2B	5431	DNA-directed RNA polymerase II subunit RPB2
POLR3A	11128	DNA-directed RNA polymerase III subunit RPC1
POLRMT	5442	DNA-directed RNA polymerase, mitochondrial
POLR1C	9533	DNA-directed RNA polymerases I & III subunit RPAC1
POLR2H	5437	DNA-directed RNA polymerases I, II, & III subunit RPABC3
POLR2L	5441	DNA-directed RNA polymerases I, II, & III subunit RPABC5
DNAJC13	23317	DnaJ homolog subfamily C member 13

Table B.3.: Continued from previous page

Gene names	Gene ID	Protein names
PIN1	5300	Dynein light chain 1, cytoplasmic
UHRF1	29128	E3 ubiquitin-protein ligase UHRF1
EIF2AK4	440275	eIF-2-α kinase GCN2
NTHL1	4913	Endonuclease III-like protein 1
RBM35B	80004	Epithelial splicing regulatory protein 2
CABP1	9478	Eukaryotic translation initiation factor 6
GEMIN4	50628	Gem-associated protein 4
GLUD1	2746	Glutamate dehydrogenase 1, mitochondrial
GLS	2744	Glutaminase kidney isoform, mitochondrial
GLS2	27165	Glutaminase liver isoform, mitochondrial
GLUL	2752	Glutamine synthetase
AGTPBP1	23287	GTP-binding protein 1
NHP2L1	4809	H/ACA ribonucleoprotein complex subunit 2
NOLA3	55505	H/ACA ribonucleoprotein complex subunit 3
DKC1	1736	H/ACA ribonucleoprotein complex subunit 4
HSPB1	3315	Heat shock protein β-1
KPNA2	3838	Importin subunit α-1
KPNB1	3837	Importin subunit β-1
IMPDH1	3614	Inosine-5-monophosphate dehydrogenase 1
KIF14	9928	Kinesin-like protein KIF14
LDHA	3939	L-lactate dehydrogenase A chain
LDHB	3945	L-lactate dehydrogenase B chain
MPP7	143098	MAGUK p55 subfamily member 7
MDH2	4191	Malate dehydrogenase, mitochondrial
DGCR8	54487	Microprocessor complex subunit DGCR8
MLXIPL	51085	MLX interacting protein like
MLXIP	22877	MLX-interacting protein
NCOA5	57727	Nuclear receptor coactivator 5
HSD17B4	3295	Peroxisomal multifunctional enzyme type 2
WTAP	9589	Pre-mRNA-splicing regulator WTAP
DDX20	11218	Probable ATP-dependent RNA helicase DDX20
HSA9761	27292	Probable dimethyladenosine transferase
SKB1	10419	Protein arginine N-methyltransferase 5
G3BP1	10146	Ras GTPase-activating protein-binding protein 1
RFC1	5981	Replication factor C subunit 1
TARBP2	6895	RISC-loading complex subunit TARBP2
PPP1CC	5501	Serine/threonine-protein phosphatase PP1-γ
STRBP	55342	Spermatid perinuclear RNA-binding protein
TAF15	8148	TATA-binding protein-associated factor 2N
TXN	7295	Thioredoxin
TXNIP	10628	Thioredoxin-interacting protein
JUN	3725	Transcription factor AP-1
JUNB	3726	Transcription factor jun-B
JUND	3727	Transcription factor jun-D
SSR4	6748	Translocon-associated protein subunit δ
TPI1	7167	Triosephosphate isomerase

Table B.3.: Continued from previous page

Gene names	Gene ID	Protein names
TUBG1	7283	Tubulin γ-1 chain
TUBG2	27175	Tubulin γ-2 chain
VARS2	7407	Valine–tRNA ligase
WDR6	11180	WD repeat-containing protein 6
ZCCHC8	55596	Zinc finger CCHC domain-containing protein 8

Table B.4.: P-values for cell growth analysis upon glutaminase inhibition. P-values were calculated using a two-tailed student's t-test (* $0.01 < p \leq 0.05$; ** $0.001 < p \leq 0.01$; *** $p \leq 0.001$).

Treatment	p-value to Ctrl, +Q		p-value to Ctrl, -Q	
	HCT116	RKO	HCT116	RKO
Ctrl, +Q	-	-	***	*
Ctrl, -Q	***	**	-	-
BPTES, +Q	**	*	***	**
C968, +Q	***	**	**	*
CB839, +Q	***	-	***	*
DON, +Q	***	**	-	-